

2011

Structural Behaviour of Dented Pipelines

Abu Naim Md Rafi
University of Windsor

Follow this and additional works at: <http://scholar.uwindsor.ca/etd>

Recommended Citation

Rafi, Abu Naim Md, "Structural Behaviour of Dented Pipelines" (2011). *Electronic Theses and Dissertations*. Paper 89.

This online database contains the full-text of PhD dissertations and Masters' theses of University of Windsor students from 1954 forward. These documents are made available for personal study and research purposes only, in accordance with the Canadian Copyright Act and the Creative Commons license—CC BY-NC-ND (Attribution, Non-Commercial, No Derivative Works). Under this license, works must always be attributed to the copyright holder (original author), cannot be used for any commercial purposes, and may not be altered. Any other use would require the permission of the copyright holder. Students may inquire about withdrawing their dissertation and/or thesis from this database. For additional inquiries, please contact the repository administrator via email (scholarship@uwindsor.ca) or by telephone at 519-253-3000ext. 3208.

Structural Behaviour of Dented Pipelines

By

Abu Naim Md Rafi

A Thesis

Submitted to the Faculty of Graduate Studies
through Civil and Environmental Engineering
in Partial Fulfillment of the Requirements for
the Degree of Master of Applied Science at the
University of Windsor

Windsor, Ontario, Canada

2011

© 2011 Abu Naim Md Rafi

Structural Behaviour of Dented Pipelines

By

Abu Naim Md Rafi

APPROVED BY:

Dr Randy Bowers, Outside Department Reader
Department of Mechanical, Automotive and Materials Engineering

Dr. Shaohong Cheng, Department Reader
Department of Civil and Environmental Engineering

Dr. Sreekanta Das, Advisor
Department of Civil and Environmental Engineering

Dr. Hanna Maoh, Chair of Defense
Department of Civil and Environmental Engineering

April 19, 2011

DECLARATION OF ORIGINALITY

I hereby certify that I am the sole author of this thesis and that no part of this thesis has been published or submitted for publication.

I certify that, to the best of my knowledge, my thesis does not infringe upon anyone's copyright nor violate any proprietary rights and that any ideas, techniques, quotations, or any other material from the work of other people included in my thesis, published or otherwise, are fully acknowledged in accordance with the standard referencing practices. Furthermore, to the extent that I have included copyrighted material that surpasses the bounds of fair dealing within the meaning of the Canada Copyright Act, I certify that I have obtained a written permission from the copyright owner(s) to include such material(s) in my thesis and have included copies of such copyright clearances to my appendix.

I declare that this is a true copy of my thesis, including any final revisions, as approved by my thesis committee and the Graduate Studies office, and that this thesis has not been submitted for a higher degree to any other University or Institution.

ABSTRACT

A dent is a defect in the pipe wall in the form of localized inward plastic deformation. Dents are a matter of serious concern for pipeline operators because they may cause a rupture or a leak in the pipeline. Hence, a reliable strain-based criterion for the assessment of dents is very important. An understanding of the local strain distributions in the dent is very important for the development of a strain-based dent evaluation criterion. Therefore, this study was undertaken using full-scale tests and a parametric study to assess the influence of various parameters on the strain distributions in a dent. Additionally, the ASME strain-based dent evaluation criterion was reviewed.

It was shown that strain distributions and strain values in a dent are significantly influenced by the dent depth, internal pressure, and dent shape. The study also noted that upgrading is required for the ASME criterion.

DEDICATION

To My Parents and Wife

ACKNOWLEDGEMENTS

I am deeply grateful to my supervisor Dr. Sreekanta Das whose help, inspiring suggestions, continuous support and encouragement helped me in all the time of this research work and writing of this thesis. Dr. Das devoted his time and sincere effort to provide all necessary research facilities for this work. I would like to express my appreciation to the committee members: Dr. R Bowers and Dr. S Cheng for their valuable and constructive suggestions. I would also like to express my gratitude to Jeorge, Sara and Hanif for their sincere help.

The assistance of Mr. M. St. Louis, Mr. L. Pop and Mr. P. Seguin in the laboratory works is sincerely acknowledged.

Finally I would like to thank my family members for their love, encouragement and support.

TABLE OF CONTENTS

DECLARATION OF ORIGINALITY	iii
ABSTRACT	iv
DEDICATION	v
ACKNOWLEDGEMENTS	vi
LIST OF TABLES	xi
LIST OF FIGURES	xiii
CHAPTER	
1. INTRODUCTION	
1.1 General	1
1.2 Statement of the Problem	3
1.3 Objectives	4
1.4 Organization of the Thesis	5
2. REVIEW OF LITERATURE	
2.1 General	6
2.2 Dent	6
2.3 Recommendations in Codes and Manuals	8
2.3.1 Depth Based Criteria	8
2.3.1.1 ASME B31.4	9
2.3.1.2 ASME B31.8	9
2.3.1.3 DNV-OS-F101	10
2.3.1.4 CSA Z662-07	11
2.3.1.5 EPRG Methods	11
2.3.1.6 PDAM	13
2.3.2 Strain Based Criteria	14
2.4 Burst Strength of Pipe with Dent	16
2.4.1 Burst Strength of Pipe with Plain-Smooth Dent	16
2.4.2 Burst Strength of Pipe with Plain-Kinked Dent	17
2.5 Fatigue Life of Pipe with Dent	17
2.6 Strain Analysis of a Dent	19
2.6.1 Strain During Pressure Application	20
2.6.2 Strain in a Dented Pipe Wall	21

2.7 Conclusions	28
3. EXPERIMENTAL PROGRAM	
3.1 General	35
3.2 Selection of Specimen Parameters	36
3.3 Preparation of the specimen	36
3.4 Selection of Boundary Conditions.....	37
3.5 Selection of Indenter Shape.....	37
3.6 Internal pressure	38
3.7 Test Variables.....	39
3.8 Designation of Specimen.....	40
3.9 Material Property.....	40
3.10 Experimental Setup	41
3.10.1 Loading Jack and Loadcell.....	41
3.10.2 Fluid Pump and Pressure Transducer.....	42
3.10.3 Linear Voltage Displacement Transducers	42
3.10.4 Electronic Resistance Strain Gauges.....	42
3.10.5 Data Acquisition System.....	43
3.11 Test Procedure	43
3.11.1 Test 1: Specimen LRP20D4	44
3.11.2 Test 2: Specimen LRP40D4	44
3.11.3 Test 3: Specimen SSP20D8.....	45
3.11.4 Tests 4 to 6: Specimen SRP20D10, SRP20D8 and SRP20D12.....	45
3.11.5 Tests 7 to 9: Specimen SDP0D8, SDP20D8 and SDP40D8	47
4. TEST RESULTS	
4.1 General	67
4.2 Load-deformation Behaviour	67
4.2.1 Effect of Internal Pressure.....	68
4.2.2 Effect of Indenter Shape.....	69
4.3 Deformed Shapes and Strain Distributions	70
4.3.1 Specimen LRP20D4	70
4.3.2 Specimen LRP40D4	71
4.3.3 Specimen SSP20D8.....	72
4.3.4 Specimen SRP20D10	74
4.3.5 Specimen SRP20D8	75
4.3.6 Specimen SRP20D12	76
4.3.7 Specimen SDP0D8	77
4.3.8 Specimen SDP20D8	78

4.3.9 Specimen SDP40D8	79
4.4 Effect of Different Parameters on Strain Distributions	80
4.4.1 Effect of Internal Pressure	80
4.4.2 Effect of Dent Shape	82
4.4.3 Effect of Dent Depth	82
4.5 Conclusions	84
5. DEVELOPMENT OF FINITE ELEMENT MODEL	
5.1 General	126
5.2 Finite Element Model	127
5.2.1 Element Selection	127
5.2.2 Symmetry of the Model	128
5.2.3 End Caps	129
5.2.4 Support Conditions	130
5.2.5 Indenter	132
5.2.6 Material Model	132
5.2.7 Loading Procedure	133
5.2.8 Mesh Study	135
5.2.9 Contact Algorithm	138
5.2.10 Solution Methods and Convergence	142
6. VALIDATION OF FINITE ELEMENT MODEL AND PARAMETRIC STUDY	
6.1 General	165
6.2 Comparison of the FEA and Experimental results	165
6.2.1 Specimen LRP20D4 and LRP40D4	166
6.2.2 Specimen SSP20D8	167
6.2.3 Specimen SRP20D8, SRP20D10, and SRP20D12	168
6.3 Parametric Study	169
6.3.1 Effect of Dent Depth	170
6.3.1.1 Spherical Dent	170
6.3.1.2 Rectangular Dent	171
6.3.2 Effect of Internal Pressure	172
6.3.3 Effect of Indenter Shape	173
6.4 Conclusions	173
7. ASME DENT STRAIN EQUATIONS	
7.1 General	218
7.2 Dent Strain	219
7.3 ASME B31.8 Equations	219

7.4 Finite Element Analysis	221
7.5. Review of ASME B31.8 Equations and Assumptions	222
7.5.1 Membrane Strain in Circumferential Direction.....	222
7.5.2 Membrane Strain in Longitudinal Direction	226
7.5.3 Review of the ASME Equations for Calculating Effective Strain	227
7.5.4 Incorporation of Circumferential Membrane Strain.....	229
7.5.5 Comparison between the Effective Strains Calculated Using Different Equations.....	229
7.6 Conclusions	230
8. SUMMARY, CONCLUSIONS AND RECOMMENDATIONS	
8.1 General	249
8.2 Summary.....	249
8.3 Conclusions	250
8.4 Recommendations	252
REFERENCES	253
APPENDIX.....	258
VITA AUCTORIS.....	278

LIST OF TABLES

Table 2.1: Details of the indenter used by Keating and Hoffman (1997).....	30
Table 3.1: Test Matrix.....	48
Table 3.2: Material Properties.....	49
Table 4.1: Effect of internal pressure on the maximum strain values.....	86
Table 4.2: Effect of indenter shape on the maximum strain values.....	87
Table 4.3: Effect of dent depth for rectangular indenter.....	88
Table 4.4: Effect of dent depth for spherical indenter.....	89
Table 4.5: Effect of dent depth for dome indenter.....	90
Table 5.1: Mesh Study.....	145
Table 6.1: Maximum circumferential strain values.....	176
Table 6.2: Maximum longitudinal strain values.....	178
Table 7.1: Parameters Used for FEA Analysis.....	232
Table 7.2: Maximum circumferential tensile membrane strain obtained from the FEA Model.....	233
Table 7.3: Effect of dent depth and internal pressure on circumferential membrane strain.....	234

Table 7.4: Effect of pressure on the circumferential membrane strain.....	235
Table 7.5: Effect of pressure on the longitudinal membrane strain.....	236
Table 7.6: Maximum strain components in dent.....	237
Table 7.7: Effect of circumferential membrane strain on the effective strain.....	238

LIST OF FIGURES

Figure 2.1: Photograph of a dent in the pipe wall (Source: http://www.google.ca/images)	31
Figure 2.2: Dimensions of a dent (Macdonald et al. 2006)	31
Figure 2.3: Photograph of kinked dent in field pipeline (Macdonald et.al. 2006).....	32
Figure 2.4: Photograph of a dent-crack defect (Source: http://www.easervices.com)	32
Figure 2.5: Geometric parameter of a dent (ASME B31.8-2007)	33
Figure 2.6: Flank of a dent.....	33
Figure 2.7: Definition of dent length (Noronha et al. 2010).....	34
Figure 3.1: Photograph of a large pipe specimen	50
Figure 3.2: Photograp of small pipe specimen.....	51
Figure 3.3 Photographs of the indenters	52
Figure 3.4: Schematic of the indenters	53
Figure 3.5: Tensiel stress-strain behavior of coupon from large diameter pipe	54
Figure 3.6: Tensile stress-strain behavior of coupon from small diameter pipe.....	55
Figure 3.7: Schematic of the experimental setup.....	56
Figure 3.8: Photograph of the experimental setup	57
Figure 3.9: Strain gauge layout pattern for specimen LRP20D4 and LRP40D4.....	58
Figure 3.10: Strain gauge layout pattern for specimen SRP20D8, SRP20D10 and SRP20D12.....	59
Figure 3.11: Strain gauge layout pattern for specimen SSP20D8	60
Figure 3.12: Strain gauge layout pattern for specimens SDP0D8, SDP20D8 and SDP40D8	61

Figure 3.13: Load-deformation behavior of specimen LRP20D4	62
Figure 3.14: Load-deformation behavior of specimen LRP40D4	62
Figure 3.15: Load-deformation behavior of specimen SSP20D8	63
Figure 3.16: Load-deformation behavior of specimen SRP20D10	63
Figure 3.17: Load-deformation behavior of specimen SRP20D8	64
Figure 3.18: Load-deformation behavior of specimen SRP20D12	64
Figure 3.19: Load-deformation behavior of specimen SDP0D8	65
Figure 3.20: Load-deformation behavior of specimen SDP20D8	65
Figure 3.21: Load-deformation behavior of specimen SDP40D8	66
Figure 4.1: Effect of internal pressure on the load deformation behavior for a rectangular indenter.	91
Figure 4.2: Effect of internal pressure on the load deformation behavior for a dome indenter	91
Figure 4.3: Effect of indenter shape on the lod deformation behavior	92
Figure 4.4: Photograph of the dent in specimen LRP20D4	92
Figure 4.5(a): Circumferential strain distribution along Line 1 for specimen LRP20D4.	93
Figure 4.5(b): Circumferential strain distribution along Line 2 for specimen LRP20D4	93
Figure 4.6(a): Longitudinal strain distribution along Line 3 for specimen LRP20D4	94
Figure 4.6(b): Longitudinal strain distribution along Line 4 for specimen LRP20D4	94
Figure 4.7: Strain distributiona along the Line 5 for specimen LRP20D4	95
Figure 4.8: Photograph of the dent in specimen LRP40D4	95
Figure 4.9(a): Circumferential strain distribution along Line 1 for specimen LRP40D4.	96
Figure 4.9(b): Circumferential strain distribution along Line 2 for specimen LRP40D4	96

Figure 4.10(a): Longitudinal strain distribution along Line 3 for specimen LRP40D4 ...	97
Figure 4.10(b): Longitudinal strain distribution along Line 4 for specimen LRP40D4 ...	97
Figure 4.11: Strain distributiona along the Line 5 for specimen LRP40D4	98
Figure 4.12: Photograph of the dent in specimen SSP20D8.....	98
Figure 4.13: Circumferential strain distribution for specimen SSP20D8.....	99
Figure 4.14: Longitudinal strain distribution for specimen SSP20D8.....	99
Figure 4.15: Oblique strain distribution for specimen SSP20D8	100
Figure 4.16: Photograph of the dent in specimen SRP20D10	100
Figure 4.17(a): Circumferential strain distribution along Line 1 for specimen SRP20D10	101
Figure 4.17(b): Circumferential strain distribution along Line 2 for specimen SRP20D10	101
Figure 4.18(a): Longitudinal strain distribution along Line 3 for specimen SRP20D10	102
Figure 4.18(b): Longitudinal strain distribution along Line 4 for specimen SRP20D10	102
Figure 4.19: Strain distributiona along the Line 5 for specimen SRP20D10	103
Figure 4.20: Photograph of the dent in specimen SRP20D8	103
Figure 4.21(a): Circumferential strain distribution along Line 1 for specimen SRP20D8	104
Figure 4.21(b): Circumferential strain distribution along Line 2 for specimen SRP20D8	104
Figure 4.22(a): Longitudinal strain distribution along Line 3 for specimen SRP20D8..	105
Figure 4.22(b): Longitudinal strain distribution along Line 4 for specimen SRP20D8 .	105
Figure 4.23: Photograph of the dent in specimen SRP20D12	106

Figure 4.24(a): Circumferential strain distribution along Line 1 for specimen SRP20D12	106
Figure 4.24(b): Circumferential strain distribution along Line 2 for specimen SRP20D12	107
Figure 4.25(a): Longitudinal strain distribution along Line 3 for specimen SRP20D12	107
Figure 4.25(b): Longitudinal strain distribution along Line 4 for specimen SRP20D12	108
Figure 4.26: Photograph of the dent in specimen SDP0D8	108
Figure 4.27: Circumferential strain distribution for specimen SDP0D8	109
Figure 4.28: Longitudinal strain distribution for specimen SDP0D8	109
Figure 4.29: Oblique strain distribution for specimen SDP0D8	110
Figure 4.30: Photograph of the dent in specimen SDP20D8	110
Figure 4.31: Circumferential strain distribution for specimen SDP20D8	111
Figure 4.32: Longitudinal strain distribution for specimen SDP20D8	111
Figure 4.33: Oblique strain distribution for specimen SDP20D8	112
Figure 4.34: Photograph of the dent in specimen SDP40D8	112
Figure 4.35: Circumferential strain distribution for specimen SDP40D8	113
Figure 4.36: Longitudinal strain distribution for specimen SDP40D8	113
Figure 4.37: Oblique strain distribution for specimen SDP40D8	114
Figure 4.38(a): Effect of internal pressure on the circumferential strain distribution for rectangular indenter along Line 1	114
Figure 4.38(b): Effect of internal pressure on the circumferential strain distribution for rectangular indenter along Line 2	115

Figure 4.38(c): Effect of internal pressure on the longitudinal strain distribution for rectangular indenter along Line 3	115
Figure 4.38(d): Effect of internal pressure on the longitudinal strain distribution for rectangular indenter along Line 4	116
Figure 4.38(e): Effect of internal pressure on the oblique strain distribution for rectangular indenter along Line 5	116
Figure 4.39(a): Effect of internal pressure on the circumferential strain distribution for dome indenter along Line 1	117
Figure 4.39(b): Effect of internal pressure on the longitudinal strain distribution for dome indenter along Line 2	117
Figure 4.39(c): Effect of internal pressure on the oblique strain distribution for dome indenter along Line 3	118
Figure 4.40(a): Effect of dent shape on circumferential strain distribution.....	118
Figure 4.40(b): Effect of dent shape on longitudinal strain distribution.....	119
Figure 4.41(a): Effect of dent depth on circumferential strain distribution along Line 1	119
Figure 4.41(b): Effect of dent depth on circumferential strain distribution along Line 2	120
Figure 4.41(c): Effect of dent depth on longitudinal strain distribution along Line 3	120
Figure 4.41(d): Effect of dent depth on longitudinal strain distribution along Line 4....	121
Figure 4.42(a): Effect of dent depth on the maximum circumferential strain for rectangular indenter	121
Figure 4.42(b): Effect of dent depth on the maximum longitudinal strain for rectangular indenter	122

Figure 4.42(c): Effect of dent depth on the maximum circumferential strain for spherical indenter	122
Figure 4.42(d): Effect of dent depth on the maximum longitudinal strain for spherical indenter	123
Figure 4.42(e): Effect of dent depth on the maximum oblique strain for spherical indenter	123
Figure 4.42(f): Effect of dent depth on the maximum circumferential strain for dome indenter	124
Figure 4.42(g): Effect of dent depth on the maximum longitudinal strain for dome indenter	124
Figure 4.42(h): Effect of dent depth on the maximum oblique strain for dome indenter	125
Figure 5.1 Half symmetry in the FEA model	146
Figure 5.2: Comparison between Load-deformation behaviour of full-pipe model and half symmetric model.....	147
Figure 5.3: Comparison between circumferential strain distribution of full-pipe model and half-symmetric model	148
Figure 5.4: Types of end caps used in FE model.....	149
Figure 5.5: Effect of shapes of end caps on load-deformation behavior	150
Figure 5.6: Cross section of pipe end showing 18° roller or pin support.....	151
Figure 5.7: Effect of various boundary conditions at mid-span support.....	152
Figure 5.8: Effect of end-span support condition	153
Figure 5.9: True stress-strain behavior of 762 mm pipe material.....	154
Figure 5.10: Top view of the pipe.....	155

Figure 5.11: Effect of mesh refinement in longitudinal direction on the load-deformation behavior.....	156
Figure 5.12: Effect of mesh refinement in longitudinal direction on the longitudinal strain distribution along the longitudinal center line	157
Figure 5.13: Effect of local mesh refinement on load –deformation behavior.....	158
Figure 5.14: Effect of local mesh refinement on strain distribution along longitudinal centerline.....	159
Figure 5.15: Effect of circumferential mesh refinement on the load-deformation behavior	160
Figure 5.16: Effect of circumferential mesh refinement on the strain distribution along circumferential centerline	161
Figure 5.17: Mesh configuration for large pipe model.....	162
Figure 5.18: Mesh configuration for half small pipe model	163
Figure 5.19: Mesh configuration for small pipe model	164
Figure 6.1: Experimental and numerical load-deformation behaviors of Specimen LRP20D4	180
Figure 6.2(a): Experimental and numerical circumferential strain distributions for Specimen LRP20D4 for Line 1.....	181
Figure 6.2(b): Experimental and numerical circumferential strain distributions for Specimen LRP20D4 for Line 2.....	181
Figure 6.3(a): Experimental and numerical longitudinal strain distributions for Specimen LRP20D4 for Line 3	182

Figure 6.3(b): Experimental and numerical longitudinal strain distributions for Specimen LRP20D4 for Line	182
Figure 6.4: Experimental and numerical load-deformation behaviors of Specimen LRP40D4	183
Figure 6.5(a): Experimental and numerical circumferential strain distributions for Specimen LRP40D4 for Line 1.....	184
Figure 6.5(b): Experimental and numerical circumferential strain distributions for Specimen LRP40D4 for Line 2.....	184
Figure 6.6(a): Experimental and numerical longitudinal strain distributions for Specimen LRP40D4 for Line 3	185
Figure 6.6(b): Experimental and numerical longitudinal strain distributions for Specimen LRP40D4 for Line 4	185
Figure 6.7: Experimental and numerical load-deformation behaviors of Specimen SSP20D8.....	186
Figure 6.8: Experimental and numerical circumferential strain distributions for Specimen SSP20D8.....	187
Figure 6.9: Experimental and numerical longitudinal strain distributions for Specimen SSP20D8.....	188
Figure 6.10: Experimental and numerical load-deformation behaviors of Specimen SRP20D8.....	189
Figure 6.11(a): Experimental and numerical circumferential strain distributions for Specimen SRP20D8 for Line 1.....	190

Figure 6.11(b): Experimental and numerical circumferential strain distributions for Specimen SRP20D8 for Line 2.....	190
Figure 6.12(a): Experimental and numerical longitudinal strain distributions for Specimen SRP20D8 for Line 3.....	191
Figure 6.12(b): Experimental and numerical longitudinal strain distributions for Specimen SRP20D8 for Line 4.....	191
Figure 6.13: Experimental and numerical load-deformation behaviors of Specimen SRP20D10.....	192
Figure 6.14(a): Experimental and numerical circumferential strain distributions for Specimen SRP20D10 for Line 1.....	193
Figure 6.14(b): Experimental and numerical circumferential strain distributions for Specimen SRP20D10 along Line 2.....	193
Figure 6.15(a): Experimental and numerical longitudinal strain distributions for Specimen SRP20D10 for Line 3.....	194
Figure 6.15(b): Experimental and numerical longitudinal strain distributions for Specimen SRP20D10 for Line 4.....	194
Figure 6.16: Experimental and numerical load-deformation behaviors of Specimen SRP20D12.....	195
Figure 6.17(a): Experimental and numerical circumferential strain distributions for Specimen SRP20D12 for Line 1.....	196
Figure 6.17(b): Experimental and numerical circumferential strain distributions for Specimen SRP20D12 for Line 2.....	196

Figure 6.18(a): Experimental and numerical longitudinal strain distributions for Specimen SRP20D12 for Line 3.....	197
Figure 6.18(b): Experimental and numerical longitudinal strain distributions for Specimen SRP20D12 for Line 4.....	197
Figure 6.19(a): Effect of dent depth on the maximum circumferential tensile strain for spherical indenter and pipe with D/t of 34.....	198
Figure 6.19(b): Effect of dent depth on the maximum circumferential compressive strain for spherical indenter and pipe with D/t of 34	198
Figure 6.19(c): Effect of dent depth on the maximum longitudinal tensile strain for spherical indenter and pipe with D/t of 34.....	199
Figure 6.19(d): Effect of dent depth on the maximum longitudinal compressive strain for spherical indenter and pipe with D/t of 34.....	199
Figure 6.19(e): Effect of dent depth on the maximum circumferential tensile strain for spherical indenter and pipe with D/t of 70.....	200
Figure 6.19(f): Effect of dent depth on the maximum circumferential compressive strain for spherical indenter and pipe with D/t of 70	200
Figure 6.19(g): Effect of dent depth on the maximum longitudinal tensile strain for spherical indenter and pipe with D/t of 70.....	201
Figure 6.19(h): Effect of dent depth on the maximum longitudinal compressive strain for spherical indenter and pipe with D/t of 70.....	201
Figure 6.19(i): Effect of dent depth on the maximum circumferential tensile strain for rectangular indenter and pipe with D/t of 34	202

Figure 6.19(j): Effect of dent depth on the maximum circumferential compressive strain for rectangular indenter and pipe with D/t of 34.....	202
Figure 6.19(k): Effect of dent depth on the maximum longitudinal tensile strain for rectangular indenter and pipe with D/t of 34	203
Figure 6.19(l): Effect of dent depth on the maximum longitudinal compressive strain for rectangular indenter and pipe with D/t of 34	203
Figure 6.20(a): Effect of internal pressure on the maximum circumferential tensile strain for spherical indenter and pipe with D/t of 34	204
Figure 6.20(b): Effect of internal pressure on the maximum circumferential compressive strain for spherical indenter and pipe with D/t of 34	204
Figure 6.20(c): Effect of internal pressure on the maximum longitudinal tensile strain for spherical indenter and pipe with D/t of 34.....	205
Figure 6.20(d): Effect of internal pressure on the maximum longitudinal compressive strain for spherical indenter and pipe with D/t of 34	205
Figure 6.20(e): Effect of internal pressure on the maximum circumferential tensile strain for spherical indenter and pipe with D/t of 70	206
Figure 6.20(f): Effect of internal pressure on the maximum circumferential compressive strain for spherical indenter and pipe with D/t of 70	206
Figure 6.20(g): Effect of internal pressure on the maximum longitudinal tensile strain for spherical indenter and pipe with D/t of 70.....	207
Figure 6.20(h): Effect of internal pressure on the maximum longitudinal compressive strain for spherical indenter and pipe with D/t of 70	207

Figure 6.20(i): Effect of internal pressure on the maximum circumferential tensile strain for rectangular indenter and pipe with D/t of 34.....	208
Figure 6.20(j): Effect of internal pressure on the maximum circumferential compressive strain for rectangular indenter and pipe with D/t of 34.....	208
Figure 6.20(k): Effect of internal pressure on the maximum longitudinal tensile strain for rectangular indenter and pipe with D/t of 34	209
Figure 6.20(l): Effect of internal pressure on the maximum longitudinal compressive strain for rectangular indenter and pipe with D/t of 34.....	209
Figure 6.21(a): Effect of indenter shape on the maximum circumferential tensile strain at 0 internal pressure and pipe with D/t of 34.....	210
Figure 6.21(b): Effect of indenter shape on the maximum circumferential compressive strain at 0 internal pressure and pipe with D/t of 34	210
Figure 6.21(c): Effect of indenter shape on the maximum longitudinal tensile strain at 0 internal pressure and pipe with D/t of 34.....	211
Figure 6.21(d): Effect of indenter shape on the maximum longitudinal compressive strain at 0 internal pressure and pipe with D/t of 34.....	211
Figure 6.21(e): Effect of indenter shape on the maximum circumferential tensile strain at 0 internal pressure and pipe with D/t of 34.....	212
Figure 6.21(f): Effect of indenter shape on the maximum circumferential compressive strain at $0.25p_y$ internal pressure and pipe with D/t of 34.....	212
Figure 6.21(g): Effect of indenter shape on the maximum longitudinal tensile strain at $0.25 p_y$ internal pressure and pipe with D/t of 34	213

Figure 6.21(h): Effect of indenter shape on the maximum longitudinal compressive strain at 0.25p _y internal pressure and pipe with D/t of 34.....	213
Figure 6.21(i): Effect of indenter shape on the maximum circumferential tensile strain at 0.45p _y internal pressure and pipe with D/t of 34.....	214
Figure 6.21(j): Effect of indenter shape on the maximum circumferential compressive strain at 0.45p _y internal pressure and pipe with D/t of 34.....	214
Figure 6.21(k): Effect of indenter shape on the maximum longitudinal tensile strain at 0.45 p _y internal pressure and pipe with D/t of 34	215
Figure 6.21(l): Effect of indenter shape on the maximum longitudinalcompressive strain at 0.45 p _y internal pressure and pipe with D/t of 34.....	215
Figure 6.21(m): Effect of indenter shape on the maximum circumferential tensile strain at 0.65p _y internal pressure and pipe with D/t of 34.....	216
Figure 6.21(n): Effect of indenter shape on the maximum circumferential compressive strain at 0.65p _y internal pressure and pipe with D/t of 34.....	216
Figure 6.21(o): Effect of indenter shape on the maximum longitudinal tensile strain at 0.65 p _y internal pressure and pipe with D/t of 34	217
Figure 6.21(p): Effect of indenter shape on the maximum longitudinalcompressive strain at 0.65 p _y internal pressure and pipe with D/t of 34.....	217
Figure 7.1: Geometric parameter of a dent (ASME B31.8-2007)	239
Figure 7.2(a): Photograph of a dent created by a spherical indenter	240
Figure 7.2 (b): FEA simulation of a spherical dent.	240
Figure 7.2: Experimental and FEA dent shapes simulated by spherical indenter	240
Figure 7.3(a): Photograph of a dent produced by rectangular indenter	241

Figure 7.3(b). FEA simulation of a rectangular dent	241
Figure 7.3: Experimental and FEA dent shapes simulated by rectangular indenter	241
Figure 7.4 (a): Effect of dent depth on circumferential membrane strain for rectangular indenter	242
Figure 7.4 (b): Effect of internal pressure on circumferential membrane strain for rectangular indenter	242
Figure 7.5 (a): Effect of dent depth on circumferential membrane strain for spherical indenter	243
Figure 7.5 (b): Effect of internal pressure on circumferential membrane strain for spherical indenter	243
Figure 7.6: Effect of internal pressure on longitudinal membrane strain for rectangular indenter	244
Figure 7.7: Effect of internal pressure on longitudinal membrane strain for spherical indenter.	244
Figure 7.8: Effect of circumferential membrane strain on the inner surface effective strain calculation for dent created with rectangular indenter under different internal pressure level	245
Figure 7.9: Effect of circumferential membrane strain on the outer surface effective strain calculation for dent created with rectangular indenter under different internal pressure level	246
Figure 7.10: Effect of circumferential membrane strain on the inner surface effective strain calculation for dent created with spherical indenter under different internal pressure level	247

Figure 7.11: Effect of circumferential membrane strain on the outer surface effective strain calculation for dent created with spherical indenter under different internal pressure level 248

CHAPTER 1

INTRODUCTION

1.1 General

The energy related industries in North America use steel pipelines as the primary mode for transporting natural gas, crude oil, and various petroleum products. In Canada alone, about 700,000 km of energy pipelines are in operation. Many additional pipelines projects especially in West Canada and Alaska of various scales such as Mackenzie Gas Project and Alaska Highway Pipeline are underway. The Alaska Highway Pipeline Project which will run between Prudhoe Bay in Alaska to various parts of USA through Yukon, British Columbia, and Alberta will alone cost about US\$ 20 billion (Yukon Government, 2011). The majority of these pipelines run below ground. A significant threat to the structural integrity of the buried pipeline is damage or defect resulting from third party interference or backfill loads over hard spots underneath the pipeline. Defects in the field pipeline can occur in the form of dent, corrosion, gouge, crack, and wrinkle. A combination of two or more defects is also common in the field pipelines. These defects may pose serious threats to the structural and/or operational integrity of the pipeline. According to the Office of Pipeline Safety of US Department of Transportation, 28% of the pipeline accidents reported from 1985 to 2003 is caused by mechanical damage (Kiefner et al. 2006).

A dent is an inward permanent plastic deformation of the pipe wall which causes a gross distortion of the pipe cross section. A dent can form due to many reasons. Onshore pipelines are often subjected to transverse load, often concentrated on a small area of pipe wall and as a result, a dent can form. Dent can also form due to transverse loading from

the impact by excavation equipment. Often dent in the field pipeline forms because of the fact that the line pipe is resting on a rock or hard surface for a considerable time period. Dents in the pipeline can form alone or may be combined with additional surficial damage such as cracks and gouges. Dents with additional damages are typically caused by third party actions and result in immediate failure approximately 80% of the time (Rosenfeld, 2002). On the other hand, dents without any other damages (plain dents) may not be an immediate threat to the structural integrity of pipeline. However, a plain dent is able to cause damages to the structural integrity in the long run due to fluctuations of the operating pressure in the pipeline. Apart from this, dent alone can create other damages due to the development of ancillary problems, such as coating damage, corrosion, and stress-corrosion cracking (Baker, 2004).

A large number of studies by various research groups and individual researchers were completed to study the effect of dent on the structural behavior of the pipe under monotonically increasing quasi-static and cyclic pressure loadings. Cosham and Hopkins (2003) reviewed the existing literature on burst strength of pipe with *plain-smooth dent* (dent for which the change in curvature is smooth and free of other forms of defects). It was found that from 1958 to 2000 about 75 burst tests were completed and only four pipes failed in the dent. Hence, it was concluded that a plain-smooth dent does not reduce the burst strength of pipe much unless the dent is very deep. There is no research reported in the literature regarding the burst strength of pipe with *plain-kinked dent* (dent for which the change in curvature is sharp and which is free of other forms of defects). Cosham and Hopkins (2003) presumed that the plain-kinked dent would have lower burst strength than the plain-smooth dent of the same depth. Most pioneering work on the

fatigue behavior of dented pipes under cyclic internal pressure was performed by Fowler et al. (1995) and Keating and Hoffman (1997). These studies found that a dent in the pipeline can fail due to fatigue loading. It was also found that fatigue life of a dent is dependent on the depth, length, and width of the dent. Apart from depth and length of the dent its sharpness (change in curvature at the dent) plays a very important role on the fatigue life of the dent. For example, Cosham and Hopkins (2003), reported a significant difference can be expected between the fatigue life of a plain-smooth and the fatigue life of a plain-kinked dent.

1.2 Statement of the Problem

Dent is a common form of defect in field pipelines. It can pose serious threat to the operational and/or structural integrity of these pipelines. Hence, a reliable criterion for the accurate assessment of dent is very important. Dent depth as a percentage of outer diameter of the pipe is the only parameter most commonly used by the different codes, standards, and manuals for determining the severity and acceptability of a dent (for example, ASME 2006; DNV, 2007; CSA, 2007; EPRG; and PDAM). However, dent depth which is merely a geometric parameter, is not always the most useful parameter for identifying whether or not a dent could be a threat to the structural integrity of a field pipeline. Studies showed that other parameters such as length, width, and sharpness of dent also play a significant role in the structural behavior of the dent. Therefore, a dent depth-based criterion alone for the assessment of dent severity is not rational. Dent is a defect in the form of permanent depth in the pipe wall, and hence, the local strains and strain concentrations in the pipe wall material is a more appropriate criterion for judging its severity (Baker, 2004). ASME B31.8 code (Rinehart and Keating (2002), ASME

(2007)) acknowledges this concept and hence, offers an option for using strain-based criterion for determining severity of dents. It also provides non-mandatory formulas for calculating the total (critical) strains in a dent. However, the equations presented in this code are not universally accepted and many researchers raised questions about the assumptions and equations presented in the ASME B 31.8 code (2007). Hence, this study performed a detailed review of the strain-based dent evaluation criterion recommended in the ASME B31.8 code (2007) and provided recommendations for the improvement of this criterion

Majority of the previous works on strain analysis of a dent were completed primarily to determine the strain values and strain distributions in the dent when an already dented pipe is being loaded with monotonically increasing pressure load. However, no experimental and numerical studies to determine the strains in the dent as the dent being formed are found in the literature. A few studies were presented analytical approaches for the calculation of dent strains. However, these studies did not investigate the effect of different parameters such as dent depth, dent shape, and internal pressure during indentation on the strain distributions of the dent. Hence, this research undertook a thorough study of the effect of different parameters on the strain distributions in a dent of pipeline.

1.3 Objectives

Therefore, the current study was undertaken to understand the behavior of the pipeline under concentrated lateral loading and internal pressure, and to study the distributions of

strain in the dent of oil and gas pipes. The following are the objectives of this research project.

1. To study the overall structural behavior of the pipe while subjected to concentrated lateral (denting) loading.
2. To investigate the effect of internal pressure during denting, dent depth, and dent shapes on the strain values in a dent.
3. To review and revisit the ASME strain-based dent evaluation criterion and provide recommendations for improvement of the criterion.

1.4 Organization of the Thesis

The thesis is divided into eight chapters. The first chapter is introduction and the very last chapter, Chapter 8 is Summary, Conclusions and Recommendations. Chapter 2 summarizes the findings of the previous research works and the recommendations made by various codes, standards, and manuals. Chapters 3 and 4 discuss the test program and the results obtained from the full-scale tests. The development of the finite element (FE) model is presented in chapter 5. Chapter 6 presents the validation of the FE model and the results of the parametric study completed using the FE model. Review of the ASME B31.8 dent strain equations based on the result of FE model is presented in Chapter 7.

CHAPTER 2

REVIEW OF LITERATURE

2.1 General

A review of the literature was conducted to study how current guidelines and the previous research works address the significance of dent in pipeline. It was found that the dent depth as a percentage of outer diameter of the pipe, which is a geometric parameter, is most commonly used by different codes, standards, and manuals for determining the severity of a dent. Majority of the research work has been conducted to determine the burst strength and fatigue life of pipe containing dent. Some research works, reported in the literature focused on the concentration of strain in a pressurized dent. Though current codes, standards, and manuals consider depth as the only geometric parameter for assessing the severity of the dent, previous research works indicated that use of depth alone may results an underestimation or overestimation of dent severity. Consequently, it was proposed to use local strain in a dent as a more relevant criterion for judging its severity and acceptability.

2.2 Dent

A dent is a permanent plastic deformation of the pipe wall which causes a gross inward distortion of pipe cross section. A photograph of a dent in pipeline is shown in Figure 2.1. Dent depth (d) is the maximum reduction in the diameter of the pipe compared to the original diameter of the pipe (D) (Figure 2.2).

Dents are often classified into different categories. Based on the curvature of the dent it can be classified as *smooth dent* and *kinked dent*. A smooth dent is one which causes a smooth change in the curvature of the pipe wall. A kinked dent causes an abrupt change

in the curvature of the pipe wall (Cosham and Hopkins 2003). However, there is no universally accepted value of the threshold curvature that differentiates the two dents. European Pipeline Research Group (EPRG) provides an approximate definition of kinked dent. According to EPRG, a dent can be classified as a kinked dent, when the radius of curvature (in any direction) of the sharpest part of the dent is less than five times the wall thickness of the pipe (Roovers et al. 2000). Photograph of kinked dent is presented in Figure 2.3.

Depending on the surrounding conditions and constraints, dents can be classified as constrained dent or as unconstrained dent. A constrained dent is the one which is not free to rebound or reround, with the change in internal pressure; because the indenter is not removable. A rock dent is an example of constrained dent. A dent which is free to rebound when the indenter is removed and is free to reround with the increasing internal pressure is termed as an unconstrained dent (Cosham and Hopkins 2003).

Dent in a field pipeline can form along with other defects such as gouges, corrosion, and cracks. Photograph of a dent with a crack defect is shown in Figure 2.4. Dent might also interact with the weld of a pipe wall. Dent without any other forms of defect is called as *plain dent* which is often found in the field pipelines. The main focus of the current research project is the study the behavior of plain dents. Consequently, the literature review presented in this chapter is mainly concerned with the current guidelines and research work regarding dent without any other forms of defects, which is referred to as plain dent. The plain dent includes plain-smooth dent and plain-kinked dent.

The classification of dents such as smooth dent, kinked dent, and plain dent are not universally accepted. For the discussion in this thesis following terminology will be used for classifying the dents.

(a) Plain-smooth dent: It is the dent for which the change in curvature is very smooth and which is free of other forms of defects (cracks, gouges, welds and corrosion).

(b) Plain-kinked dent: It is the dent for which the change in curvature is sharp and which is free of other forms of defects (cracks, gouges, welds and corrosion).

(c) Dent with defect: It is the dent which is found in combination with other forms of defects (cracks, corrosion, welds and corrosion). It can be a smooth dent or a kinked dent.

2.3 Recommendations in Codes and Manuals

Recommendations provided in different pipeline codes, standards, and manuals for the assessment of the severity and acceptability of a dent are based on following two criteria.

(i) Depth based criteria

(ii) Strain based criteria

2.3.1 Depth Based Criteria

The current codes, standards, and manuals provides recommendations on the assessment of dent severity considering the fact that dent may form in conjunction with other mechanical damage (cracks, gouges, corrosion, seam or girth weld etc.) and it may also form alone. Most of these guidelines consider dent depth as a percentage of pipe's outer diameter as the most critical parameter for its severity when it does not contain any other

mechanical damage. The assessment criteria of dent based on its depth as outlined in different codes, standards, and manuals are summarized in the following sections.

2.3.1.1 ASME B31.4

ASME B 31.4: Pipeline Transportation Systems for Liquid Hydrocarbons and other Liquids (ASME 2006) code defines dent as a gross disturbance in the curvature of the pipe wall. It recommends that if a dent contains a stress concentrator, such as a scratch, gouge, groove, or arc burn, it shall be removed by cutting out the damaged portion of the pipe. A dent which affects the curvature of the pipe at the seam or at any girth weld is also recommended to be removed. This code also recommends removing the dents containing metal loss resulting from corrosion or grinding where less than 87.5% of the nominal wall thickness remains.

Allowable depth is specified for dents which do not interact with the girth or seam weld and also do not contain scratch, gouge, groove, or arc burn. This code recommends that all dents which exceeds a maximum depth of $\frac{1}{4}$ inch (6mm) in pipe NPS 4 (nominal diameter is 4 inch) and smaller, or 6% of the nominal pipe diameter in sizes larger than NPS 4, should not be permitted in pipelines intended to operate at a hoop stress of more than 20% of the specified minimum yield strength (SMYS) of pipe. It also recommends that dent that could restrict the passage of inline inspection (ILI) tools shall be removed, since it causes operational and maintenance problem.

2.3.1.2 ASME B31.8

ASME B31.8: Gas Transmission and Distribution Piping Systems (ASME 2007) code defines dent as a depression that produces a gross disturbance in the curvature of the pipe

wall. This code recommends that the depth of dent should be measured as the gap between the lowest point of the dent and a prolongation of the original contour of the pipe in any direction. The code requires that a dent which contains any stress concentrator such as a scratch, gouge, groove or arch burn, should be removed by cutting out the damaged portion of the pipe as a cylinder.

The code classifies the dents whose curvature vary smoothly and do not contain creases, mechanical damages, corrosion, arc burns, girth, or seam welds as plain dent. Plain dents are considered harmful if they exceed a depth of 6% of the nominal pipe diameter. In evaluating the depth of plain dents, the need for the segment to be able to safely pass an internal inspection or cleaning device shall also be considered. A dent that is not acceptable for this purpose should be removed prior to passing these devices through the segment, even if the dent is not harmful.

This code also specifies that the dent that affect ductile girth or seam weld are harmful if they exceed a depth of 2% of the nominal pipe diameter, except those evaluated and determined to be safe by an engineering analysis considering weld quality, nondestructive examination, and operation of the pipeline are acceptable provided that strain levels associated with the deformation do not exceed 4%. It is also recommends that the dent of any depth that affect nonductile welds, such as acetylene girth welds or seam welds that are prone to brittle fracture are harmful.

2.3.1.3 DNV-OS-F101

According to DNV-OS-F101: Submarine Pipeline Systems (DNV, 2007) for dents without any cold formed notches and sharp bottom gouges, the length in any direction

should be less than or equal to $0.5D$, where D is the nominal diameter of the pipe. The depth, measured as the gap between the extreme of the dent and the prolongation of the normal contour of the pipe, shall not exceed 6.4 mm (DNV 2007).

2.3.1.4 CSA Z662-07

According to CSA Standard Z662-07: Oil and Gas pipeline Systems (CSA 2007) following dents should be considered as defects unless determined by an engineering assessment to be acceptable.

1. Dents containing stress raisers (gouges, grooves, arc burns, or cracks).
2. Dents located on a mill or field weld and exceed a depth of 6 mm in pipe with outer diameter 323.9 mm or smaller or 2% of outside diameter in pipe with outer diameter larger than 323.9 mm.
3. Dents that are located on the pipe body and exceed a depth of 6 mm in pipe of 101.6 mm outer diameter or smaller or 6% of outside diameter in pipe with outer diameter larger than 101.6 mm.
4. Dents that contain corroded areas with a corrosion depth greater than 40% of the nominal wall thickness of the pipe.

2.3.1.5 EPRG Methods

For dents without any other mechanical damages (plain dents) European Pipeline Research Group (EPRG) (Roovers et al. 2000) provides recommendation for assessment of its severity based on its depth and radius of curvature. This guideline provide recommendation by considering the difference between the dent depths measured at

pressurized (H) and unpressurised (H_0) conditions of the pipe. The recommendations made by them are based on experimental studies completed by them.

A plain-smooth dent is defined as damage to a pipeline that causes a smooth change in curvature of the pipe wall without any reduction in wall thickness. EPRG considers that this criterion applies to dents with a radius of curvature of more than five times the wall thickness.

For plain-smooth dents not in combination with the pipeline seam weld, EPRG concludes that dents up to 10% of the pipeline outer diameter (unpressurised) will not fail at stress levels below 72% of SMYS (Equation 2.1).

$$\frac{H_0}{2R} \leq 10\% \quad (2.1)$$

Where H_0 is the depth of the dent measured at unpressurised condition if the pipe and R is the radius of the pipe. Since the internal pressure tends to push out the dent, thus, reducing the dent depth (spring back phenomenon), the measured depth on an operational pipeline has, therefore, to be corrected in order to use the EPRG method in a conservative manner.

The relationship between the dent depth on an unpressurised pipeline (H_0) and a pressurized pipeline (H) proposed by EPRG is as follows.

$$H_0 = 1.43 H \quad (2.2)$$

Therefore EPRG's limit for acceptance plain dents in an operational pipeline (when there is pressure) can be written as follows.

$$\frac{H}{2R} \leq 7\% \quad (2.3)$$

The acceptable limit of dent depth is less in operating pipeline. This is because the dent the dent rebounds as internal pressure is applied.

2.3.1.6 PDAM

Pipeline Defect Assessment Manual (PDAM) (Cosham and Hopkins 2003) is based upon a comprehensive, critical, and authoritative review of available pipeline defect assessment methods. This critical review includes a comparison of all of the published full-scale test data used in the development and validation of existing defect assessment methods. The full-scale test data was used to assess the inherent accuracy of the defect assessment methods and identify the best methods and their range of applicability. However it should be noted that no separate work was concluded by PDAM.

PDAM recommends a depth of 10% of the pipe diameter for the depth of a plain-smooth dent measured at zero pressure as the dent acceptability criterion. A limit of 7% of the pipe diameter is recommended for the depth of an unconstrained plain-smooth dent measured at pressure.

From the comparison of the recommendations provided in EPRG guidelines with the other codes and standards it is found that EPRG considers the radius of curvature as a criteria for the assessment of dent, while other codes and standards do not include curvature or strain in the dent

2.3.2 Strain Based Criteria

ASME B 31.8 (2007) provides dent acceptance criterion, based on strain values as well. According to this code, plain dent of any depth are acceptable provided strain levels associated with the deformation do not exceed 6%. This code also provides guidelines for estimating the strains in the dent (Equations 2.4 to 2.8). However these equations are nonmandatory.

According to the ASME B31.8 (2007) the estimation of the total (critical) strain in a dent requires the following strain components.

1. Bending strain in circumferential direction
2. Bending strain in longitudinal direction, and
3. Membrane strain in longitudinal direction

The strain components are then combined by assuming that each of the components occurs coincidentally at dent apex (Noronha et al 2010). The equations presented in ASME B31.8 for calculation of different strain components are as follows.

1. Bending strain in circumferential direction

$$\varepsilon_1 = \left(\frac{t}{2}\right) \left(\frac{1}{R_0} - \frac{1}{R_1}\right) \quad (2.4)$$

2. Bending strain in longitudinal direction

$$\varepsilon_2 = -\left(\frac{t}{2}\right) \left(\frac{1}{R_2}\right) \quad (2.5)$$

3. Membrane strain in longitudinal direction

$$\varepsilon_3 = \left(\frac{1}{2}\right) \left(\frac{d}{L}\right)^2 \quad (2.6)$$

Where,

R_0 = radius of curvature of undeformed pipe surface = $\frac{1}{2}$ (Nominal pipe outside diameter)

t , d , L correspond to the wall thickness, dent depth, and dent length in longitudinal direction respectively.

R_1 and R_2 are the external surface radii of curvature in the transverse and longitudinal planes through the dent, respectively (Figure 2.5). The value of R_1 is positive when dent partially flattens the pipe, in which case the curvature of the pipe surface in the transverse plane is in the same direction as the original surface radius of curvature. Otherwise, if the dent is reentrant, R_1 is negative, which is usually the case. Value of R_2 is generally negative.

All of the strain components are combined according to the following equations to calculate the total (critical) strain acting on the inside and outside pipe surfaces. These are ε_i and ε_o , respectively.

$$\varepsilon_i = \sqrt{\varepsilon_1^2 - \varepsilon_1(\varepsilon_2 + \varepsilon_3) + (\varepsilon_2 + \varepsilon_3)^2} \quad (2.7)$$

$$\varepsilon_o = \sqrt{\varepsilon_1^2 + \varepsilon_1(-\varepsilon_2 + \varepsilon_3) + (-\varepsilon_2 + \varepsilon_3)^2} \quad (2.8)$$

The dent is considered acceptable when the larger of the values ε_i and ε_o is lower than the allowable strain limits, which is 6%. It should be noted that this code assumes that the

membrane strain in the circumferential direction is negligible. It is presumed that this 6% limit is recommended to ensure safety of a dent under static a cyclic fatigue loads.

Codes and standards, other than ASME B31.8 (ASME 2007) all current pipeline codes and standards consider dent depth as the only criterion for the assessment of dent acceptability.

2.4 Burst Strength of Pipe with Dent

As discussed earlier the main objective of this research project is to study the behavior of the plain dents (dents without any other defects). Hence, in this section the effect of the both plain-smooth and plain-kinked dent on the burst strength of line pipe is discussed.

2.4.1 Burst Strength of Pipe with Plain-Smooth Dent

Numerous research works were completed to study the effect of plain-smooth dents on the static pressure strength of line pipes (Balonos and Ryan (1958); Eiber et al. (1981); Wang and Smith (1982); Hopkins et al. (1989); Hopkins et al. (1992); Kiefner et al. (1996); Alexander and Keifner (1997); and Bjornoy et al. (2000)). Cosham and Hopkins (2003) reviewed the existing literature on burst strength of pipe with plain-smooth dents. It was found that, from 1958 to 2000, about 75 burst tests were completed and only four pipes failed in the dent under monotonically increasing pressure load. Hence, it was concluded that a plain-smooth dent does not reduce the burst strength of pipe much unless the dent is very deep. When a pipe with plain-smooth dent subjected to internal pressure, the dent is pushed out as the pipe attempts to regain circularity, leaving behind a smaller residual dent on removal of pressure (Lancaster and Palmer 1996). High plastic deformation is involved with the outward movement of dent during pressurization. The

deep dents tend to fail either because of their inability to reround or because of wall thinning in the dented area (Cosham and Hopkins 2003).

Literature review found no published analytical method for predicting the burst strength of plain-smooth dents. Various codes, standards, and manuals provide various empirical limits on the depth of the plain-smooth dent and these limits are based on the result of the full scale tests.

2.4.2 Burst Strength of Pipe with Plain-Kinked Dent

A plain-kinked dent is the one which contains a sharp change in the curvature of the pipe wall and also which is free from other forms of defects (cracks, corrosion, gouge etc). EPRG provides an approximate limit on the radius of curvature of kinked dent and this is the radius of curvature in any direction of the sharpest part of the dent is less than five times the wall thickness of the pipe (Roovers et al. 2000). There is no research reported in the literature regarding the burst strength of pipe with kinked dent. Cosham and Hopkins (2003) presumed that the kinked dent would have lower burst strength than the plain dent of the same depth, though there is also no method available for predicting the burst strength of pipe containing a kinked dent (Hopkins 2009). Most pipeline codes, standards, and design manuals of current practice recommend the removal of the portion of the pipe with kinked dent since there are not enough test data available on the behavior of the kinked dent.

2.5 Fatigue Life of Pipe with Dent

The fatigue behavior of pipe with dent was studied by several researchers. Fowler et al. (1995) considered wide ranges of pipe diameter, wall thickness, and dent depth. The

effect of dent weld proximity was also considered. However, dent geometry was not varied in this study. This work clearly demonstrated that a pipe with dent can fail under fatigue loading. This study concluded that the final dent depth after spring back and rerounding is an indicator of dent severity. This study suggested that stress concentrations associated with the dent is a source of fatigue failure. The stress concentration was found to as to pipe diameter to thickness ratio (D/t) vary.

A second experimental study conducted by Keating and Hoffman (1997) considering the effect of dent depth, dent geometry, pipe D/t ratio, and the presence or absence of dent restraint. Pipe diameters ranged from 305 mm to 914 mm and wall thickness were either 6.4 mm or 9.5 mm. Four different types of indenter were used as described in Table 2.1. Type A indenter was 150 mm long and 12.5 mm wide block of steel, where the end of the blocks were rounded to 25 mm radius and the edge of the block were rounded to 12.5 mm radius. The Type BH indenter was actual teeth taken from a backhoe excavator bucket. The BH indenter was 50 mm long and 7.6 mm wide. Type BH indenter was used in both longitudinal and transverse orientation for creating the dent. The type R indenter was relatively round piece of rock. Multiple dent of variable depths were formed in a given pipe specimen. Each pipe specimen was then subjected to cyclically applied, variable amplitude pressurization sequences.

Keating and Hoffman (1997) confirmed the importance of dent depth. This study also demonstrated that at least one other aspect of dent geometry, namely dent length, plays a major role in determining dent fatigue life for unconstrained dents. It was observed that relatively long dent created by Type A indenter developed fatigue cracks in the dent center. In case of relatively short dents, created by Type BH-L and BH-T indenters,

cracks developed at the periphery of the dent. It was also observed that the dent length influences the fatigue life significantly. Long dents produced much shorter fatigue lives compared to short dents of similar initial depth.

Cosham and Hopkins (2003) completed a review of the existing literature regarding fatigue behavior of plain-smooth dent. It was found that the fatigue life of a plain-smooth dent is less than the fatigue life of a pipe without any dent. They also mentioned that the fatigue life of a constrained plain dent is at least equal to the fatigue life of an unconstrained plain dent of similar depth. There is no test data reported in the literature regarding the fatigue life of the plain-kinked dent. However, it was presumed that the fatigue life of a plain-kinked dent would be less than the fatigue life of a plain-smooth dent (Cosham and Hopkins 2003).

From the above discussion, it can be summarized that the fatigue life of a dent is not only dependent on the depth of the dent, but also on the other parameters of the dent such as strain and dent geometry. For example, the difference in fatigue life for a short and a long dent of similar depth was observed in the study of Keating and Hoffman (1997). Apart from depth and length of the dent its sharpness also plays a very important role regarding the fatigue life of the dent. For example, Cosham and Hopkins (2003), guessed a significant difference can be expected between the fatigue life of a plain-smooth and plain-kinked dent. Consequently, it can be understood that a purely depth based assessment of dent severity is not rational.

2.6 Strain Analysis of a Dent

Analysis of strains in a dent of a pipeline can be undertaken in two different situations.

Analysis of strains in a dent when dented pipe is subjected to monotonically increasing internal pressure, and

Analysis of the strain introduced in a pipe wall due to formation of a dent

2.6.1 Strain During Pressure Application

Researchers studied the variations of strains in a dent under increasing internal pressure. Ong et al. (1992) conducted experimental and finite element analyses of a plain dent to investigate the elastic strain distribution. The specimen had a length of 900 mm, a mean diameter of 160 mm and wall thickness of 2 mm. The dent was created using a 63.5 mm diameter spherical indenter. The dent depth was 13.5 mm. Strain gauges were installed in the dented region to obtain the elastic strain distribution. The primary objective of their test was to study the elastic strain distributions, to ensure there is not any further yielding of pipe material all strain values were checked during the test. This study found that maximum strain occurred in the hoop direction and it was located at the flank along the dent axial axis (Figure 2.6). This study also found that strain gauge results can only reflect the strain increments under incremental pressure loading and not the actual state of stresses, which consists of residual stresses induced from the denting process and the subsequent elastic recovery.

Lancaster and Palmer (1995) presented the results of a series of tests completed to measure strains and displacements in previously dented aluminum pipes subjected to increasing internal pressure. The study considered short smooth dents of depth up to 13% of pipe diameter. Strain changes on external pipe surface were monitored by strain gauges and photo elastic coating. Small scale pipes were chosen to model the elastic-plastic behavior of full-size transmission lines, made from high-strength pipeline steel,

free from cracks. The model pipe material and geometry were chosen to ensure that strains in the models would be identical to strains in the full size pipes. The specimens used in the study were of 100 mm diameter and 338 mm length and the dents were created using steel sphere of diameter 50.8 mm. This study showed that the highest hoop strains developed near the axial extremity (Figure 2.6) of initial dent. The results for different internal pressures showed that the location of maximum strain does not change significantly despite substantial change in internal pressure. This important finding signifies the existence of two stationary regions of high external hoop strain near the axial extremity of the initial dent.

2.6.2 Strain in a Dented Pipe Wall

The strain introduced in the pipe wall due to the formation of a dent was investigated by many researchers. Literature review found most of the works are mainly concerned about the methods for calculation of the strain associated with a dent. Most pioneering work regarding the methods for calculation of strain in the dent was performed by Rosenfeld et al. (1998). They developed a technique for processing the signal from Tuboscope-Vecto deformation inline inspection (ILI) tools in order to derive the local cold (residual) strain associated with the indentation of the pipe. This study mentioned that three components of strain are of interest for the assessment of dent and these are: the circumferential bending strain, the longitudinal bending strain and the longitudinal membrane strain. It was suggested that the circumferential membrane strain may occur during the complex redistribution of loads that takes place as the material in the dent yields and is displaced. This quantity cannot easily be extracted from the analysis of the dent profile. It was considered insignificant owing to the flexibility of pipe wall in the circumferential

direction, except perhaps locally in very deep dents. Current ASME B31.8 (ASME 2007) recommendations on dent strains discussed in section 2.3.2 are based on this study.

Dent contour and curvature was first determined from the ILI tool data to be able to determine the strains in a dent. Piece-wise cubic Bessel interpolation technique was used to obtain dent contour by interpolating deformation between the sensor positions of ILI tools. Osculating circle technique was used to estimate radii of curvature. It was stated that bending strain is proportional to the change in pipe wall curvature. The pipe wall curvature was denoted by κ and it was considered positive when the pipe wall curves outward and negative where the pipe wall curvature is reversed. After calculating the curvature of the pipe wall in the dented region the change in curvature ($\Delta\kappa$) was calculated as follows.

$$\Delta\kappa = \kappa - \frac{1}{R_o} \quad (2.9)$$

Where R_o is the outer surface radius of the pipe. Bending strain in circumferential direction (ε_b) can be calculated as a function of thickness and curvature change as follows.

$$\varepsilon_b = \Delta\kappa \left(\frac{t}{2} \right) \quad (2.10)$$

Where t is the thickness of the pipe wall. The method of calculation of longitudinal bending strain proposed in this study is similar to the circumferential bending strain. The contour of the dent in the longitudinal direction required to be determined from the ILI data. Once the contour is known the curvature can be determined either using the

analytical technique or using osculating circle method. Based on the change in curvature the strain is then calculated.

The membrane strain in longitudinal direction was defined as follows.

$$\varepsilon_{xm} = (L_s - L_o)/L_o \quad (2.11)$$

Where L_s the arc length of is deformed longitudinal cross section and L_o is the initial straight length.

After calculating the all the three components it was assumed that all of the strain components occur simultaneously at the dent apex and following equations were proposed for calculating the total/effective strain on the outer and inner surfaces.

$$\varepsilon_o = \sqrt{\varepsilon_{co}^2 - \varepsilon_{co}\varepsilon_{xo} + \varepsilon_{xo}^2} \quad (2.12)$$

$$\varepsilon_i = \sqrt{\varepsilon_{ci}^2 - \varepsilon_{ci}\varepsilon_{xi} + \varepsilon_{xi}^2} \quad (2.13)$$

Where ε_o and ε_i are the total/effective strain on outer and inner surface, respectively. ε_{co} and ε_{ci} are net circumferential strain on the outside and inside surfaces, respectively. ε_{xo} and ε_{xi} are the net longitudinal strain in the outside and inside surface ,respectively (Rosenfeld et al. 1998).

Lukasiewicz et al. (2006) presented a method for calculating strain in the dent. This method combines analytical technique with numerical technique using finite element method (FEM). The bending strain was calculated from the pipe wall curvature using analytical method, and the membrane strain was obtained using finite element analysis. It was considered that the geometry of a dent is provided by an inline caliper tool, which

measures the pipe wall deflection w in the radial direction along the normal axis Z . It was suggested that the longitudinal bending strain (ε_x^b) can be calculated directly from the curvature of the radial displacement w in the axial (x) direction. The circumferential bending strain (ε_y^b) is calculated directly from the curvature of the radial displacement w in the circumferential (y) direction. The equations presented for calculating the longitudinal and circumferential bending strain are as follows:

$$\varepsilon_x^b = z \frac{\partial^2 w}{\partial x^2} \quad (2.14)$$

$$\varepsilon_y^b = z \frac{\partial^2 w}{\partial y^2} \quad (2.15)$$

In both of the above equations z is the distance measured from the mid-surface (neutral plane) of pipe wall.

This study showed that the remaining two components of the displacement vector beside the normal displacement w , i.e. the tangential displacements u and v in the axial (x) and circumferential (y) direction respectively is necessary to calculate the membrane strains. The membrane strain-displacements relationships for large deformation of a cylindrical shell are

$$\varepsilon_x^m = \frac{\partial u}{\partial x} + \frac{1}{2} \left(\frac{\partial w}{\partial x} \right)^2 + \varepsilon_x^o \quad (2.16)$$

$$\varepsilon_y^m = \frac{\partial v}{\partial y} + \frac{w}{R} + \frac{1}{2} \left(\frac{\partial w}{\partial y} \right)^2 + \varepsilon_y^o \quad (2.17)$$

$$\gamma_{xy} = \frac{\partial u}{\partial y} + \frac{\partial v}{\partial x} + \left(\frac{\partial w}{\partial x} \right) \left(\frac{\partial w}{\partial y} \right) \quad (2.18)$$

Here ε_x^m and ε_y^m are the membrane strains in axial (x), and circumferential (y) directions respectively, γ_{xy} is the shear strain in the plane x, y, and R is the mean radius of the pipe. The ε_x^o and ε_y^o are the initial strains due to the pressure in the pipe, thermal expansion etc. Study in order to calculate the membrane strains it is necessary to determine first the displacements u and v . For calculating these displacements a two dimensional FEM model was presented. The fundamental equation of FEM is as follows.

$$[k] \begin{Bmatrix} u \\ v \\ w \end{Bmatrix} = \{F\} \quad (2.19)$$

Where $[k]$ is the stiffness matrix of the system and $\{F\}$ is the vector of nodal forces. If the displacement w is known the equation can be transformed in to

$$[k_M] \begin{Bmatrix} u \\ v \end{Bmatrix} = \{F_M\} \quad (2.20)$$

Where $[k_M]$ is the stiffness matrix for a membrane shell problem and $\{F_M\}$ is the modified vector of equivalent nodal forces. Having solved Equation 2.20 for u and v the membrane strains can be calculated using Equation 2.13. These membrane strains can be superimposed with the bending components ε_x^b , ε_y^b , producing following maximum values in axial and circumferential directions

$$\varepsilon_x = \varepsilon_x^m \pm \varepsilon_x^b \quad (2.21)$$

$$\varepsilon_y = \varepsilon_y^m \pm \varepsilon_y^b \quad (2.22)$$

The membrane and bending strains can be combined together into effective/total strain defined as

$$\varepsilon_{Ef} = \frac{2}{\sqrt{3}} \sqrt{\varepsilon_x^2 + \varepsilon_x \varepsilon_y + \varepsilon_y^2} \quad (2.23)$$

Noronha et al. (2010) Presented a piece-wise interpolation technique based on fourth order B-spline curves, to approximate the dent profile in both longitudinal and circumferential directions. Since such curves have second order continuity, radius of curvature can be calculated at any location directly from the classical two-dimensional equation of curvature. The bending strain can then be calculated from the radii of curvature. This B-spline methodology, considering data gathered by ILI tools with different resolution, is validated with results from non linear finite element analysis of dented pipelines. The result of this methodology is also compared to those achieved by a procedure proposed by Rosenfeld et al (1998). From the result obtained, the B-spline methodology is proven to be effective for calculating circumferential and longitudinal bending strains where the co-ordinates of the deepest point of the dent are known.

ASME B 31.8 (2007) provides equation for calculating the longitudinal membrane strain as a function of dent depth and dent length. However the code does not provide any guidelines on how the length of the dent can be measured. Noronha et al. (2010) employed the results of finite element analysis to assess the estimation of longitudinal membrane strains using the formula proposed in ASME B 31.8, considering two different definition of dent length (Figure 2.7), which are as follows.

1. The distance (L) between two transverse cross sections of the pipe, one before and another after the dent, whose original circular shapes have not been affected by the dents.
2. The distance (l) measured at dent half depth

Noronha et al. (2010) compared the calculated membrane strain using both of the definition of the dent length and compared with the result obtained from finite element analysis. From there comparison it was concluded that values of strain obtained using length L is significantly smaller than the finite element result. On the other hand result obtained using length l compared relatively well with the FE results. They also concluded that a proper estimation of longitudinal membrane strain is highly dependent on the definition of dent length. This suggested that a future revision of ASME B31.8 might define how the length shall be measured.

From the comparison of the methods proposed by different researcher it can be concluded that calculation of bending strain in the circumferential and longitudinal direction is fairly straight forward. The method proposed by Rosenfeld et al. (1998) has been accepted by Lukasiewicz et al. (2006) and Noronha et al. (2010). The only difference is the method of obtaining the curvature of dent. Rosenfeld et al. (1998) did not provide any method for calculating the membrane strain in circumferential direction and Noronha et al (2010) ignored this strain components. Lukasiewicz et al. (2006) considered the membrane strain in circumferential direction is not negligible and provided a method for calculating membrane strain based on FEM.

The major difference between the works of different researcher can be observed in the equations for calculating total (critical) strain. It can be noted that the equations (Equation 2.9 and 2.10) proposed by Rosenfeld et al. (1998) is missing the factor $\frac{2}{\sqrt{3}}$ of Equation 2.23 proposed by Lukasiewicz et al. (2006) and also there is a sign difference between the equations. Noronha et al. (2010) mentioned that the differences in sign between the

two equations arise from the assumption used for developing the equations. The equation of Rosenfeld et al. (1998) was based on the assumption of plane strain state in the dent region. On the other hand the equation proposed by Lukasiewicz et al. (2006) was obtained by considering that the strains in the dent region are mostly in the plastic state.

The experimental on numerical work reported on the literature regarding the distribution of strain in the dent region is very limited. Only the result of few experimental and finite element analyses regarding the distribution of strain in the circumferential and longitudinal direction of dent was reported by Bolton et al. (2008).

2.7 Conclusions

Summary of findings from literature review are as follows.

Very limited information on the dent depth and dent shape commonly observed in the field pipeline is reported in the open literature. However dent shape can form with any shape depending in the shape of the foreign object.

Plain-smooth dent do not reduce the burst strength of pipe much. It is presumed that the burst strength of pipe with plain-kinked dent is significantly lower. However, no specific values for strength reductions in these two dented pipe are available in public domain. It was also found that fatigue life of the pipe with dent is dependent on both the depth and shape of the dent. Except ASME B31.8 (ASME 2007) all other codes, standards, and manuals recommend the assessment of dent severity and acceptability based on its depth only. Previous studies found that, both burst strength and fatigue life are not only dependent on the dent depth but also other geometric parameters. Hence the assessment of dent based on its depth alone is not realistic and reliable.

Most of the experimental and numerical works reported in the literature on strain analysis of a dent are mainly concerned with the strain values as a dented pipe is being pressurized. Studies on the analysis of cold (residual) strains in pipe wall due to formation of a dent are limited to the development of analytical methods for calculation of the strains in the dented region and no experimental data are available to validate these analytical methods. There is a very few experimental or numerical work reported in the literature about the study of the distribution of strain in the dented region. No research work reported in the literature about the study of the effect of different parameters such as dent depth, dent shape, internal pressure during indentation, pipe diameter to thickness ratio etc on the strain distributions on the dent.

The analytical methods for calculation of strains in a dent of a pipe wall proposed by various researchers are different. For example, some study ignored circumferential membrane strain whereas Lukasiewicz et al. (2006) included the effect of circumferential membrane strain. ASME B31.8 (2007) provides a set of non mandatory equations for calculating the strain in the dent of a pipe wall. Researchers raised questions about the assumptions and equations presented in the ASME B 31.8 (2007) code. A universally accepted method for calculating different strain components in the dented region is not available.

This research project was designed to determine strain distributions in a dent of various dent shapes, dent depths, level of internal pressure during indentation, and diameter to wall thickness. In addition, the assumption and equations presented by ASME B31.8 (ASME 2007) was verified with the result of finite element analysis.

Table 2.1: Details of the indenter used by Keating and Hoffman (1997)

Indenter type	Description	Orientation
A	150 mm (6 inch) long x 25 mm (1 inch) wide	Longitudinal
BH-L	50 mm (2 inch) long x 7.6 mm (0.3 inch) wide	Longitudinal
BH-T	50 mm (2 inch) long x 7.6 mm (0.3 inch) wide	Transverse
R	Rock	N/A



Figure 2.1: Photograph of a dent in the pipe wall (Source:<http://www.google.ca/images>)

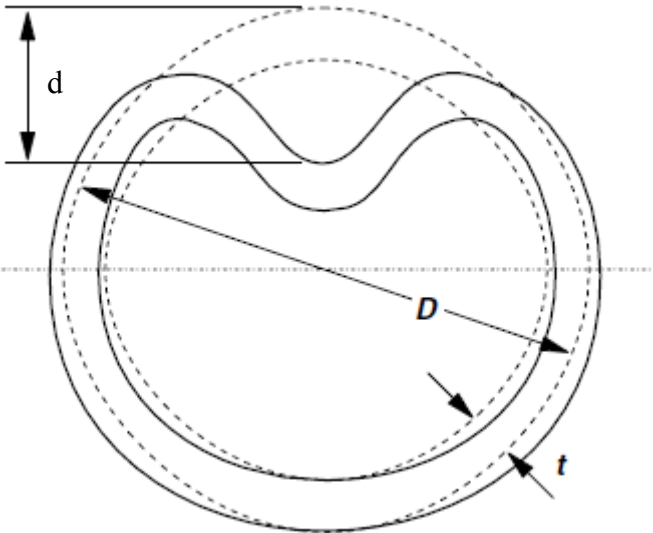


Figure 2.2: Dimensions of a dent (Macdonald et al. 2006)



Figure 2.3: Photograph of kinked dent in field pipeline (Macdonald et.al. 2006)



Figure 2.4: Photograph of a dent-crack defect (Source:<http://www.easervices.com>)

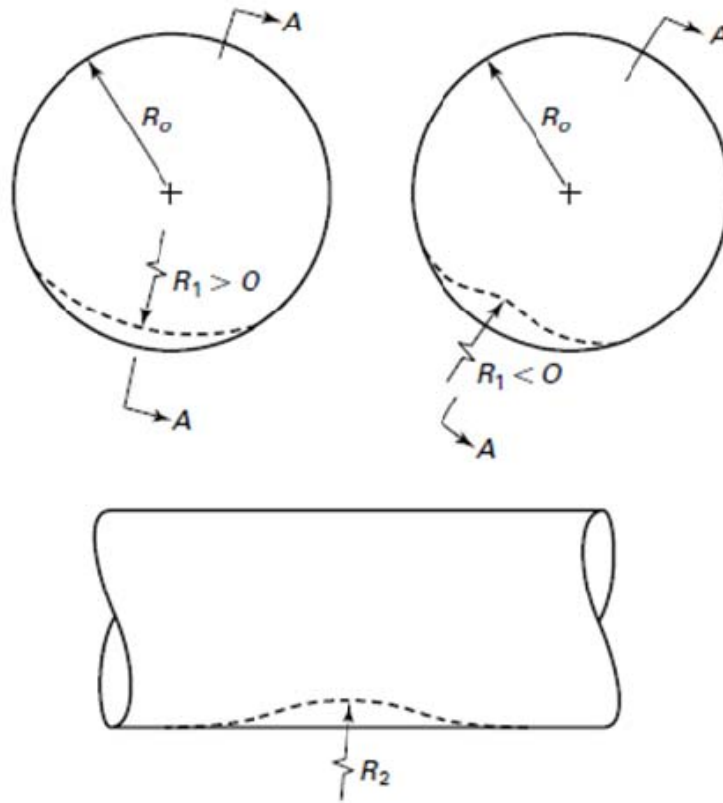


Figure 2.5: Geometric parameter of a dent (ASME B31.8-2007)

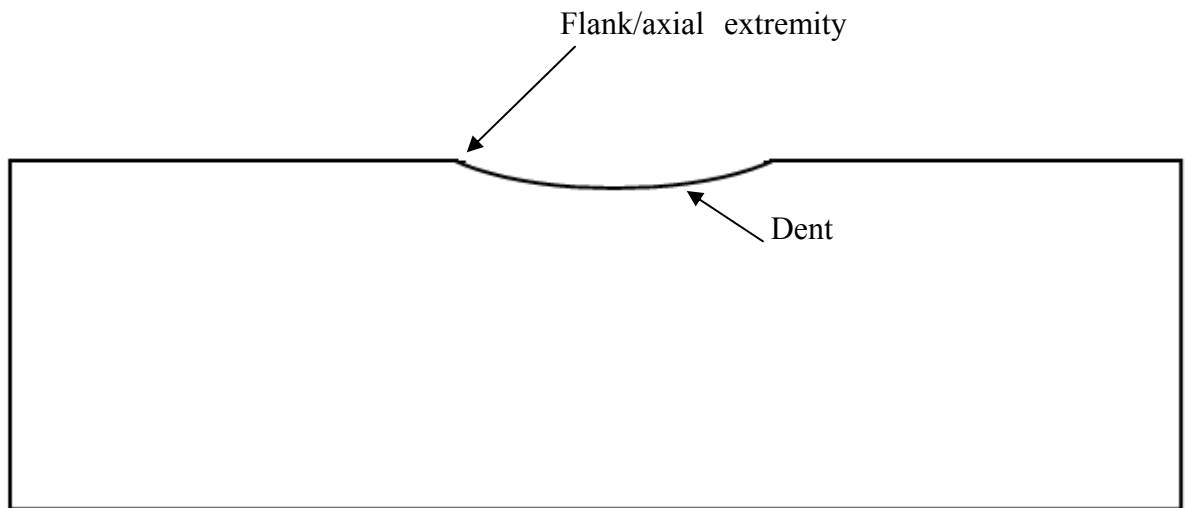


Figure 2.6: Flank of a dent

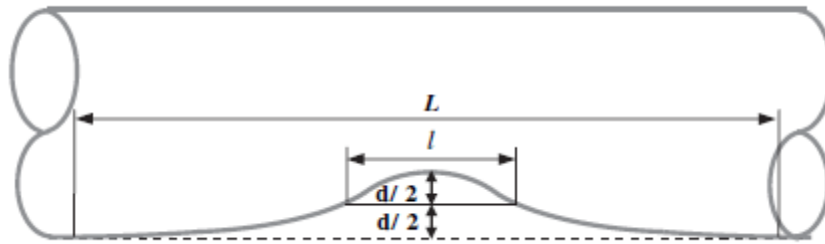


Figure 2.7: Definition of dent length (Noronha et al. 2010)

CHAPTER 3

EXPERIMENTAL PROGRAM

3.1 General

From the literature review it was found that a significant research work was performed by various researchers to study the effect of dent on the burst strength and fatigue life of pipe. Research works on strains in a dent while subjected to monotonically increasing internal pressure was also reported in the literature. These studies found that the dent depth is one of the major factors which influence the burst strength and fatigue life of pipe. However, it is not the only factor. Other geometric parameters such as dent shape, radius of curvature also have strong influences on the burst strength and fatigue life of pipe containing dent. These studies also found that strain concentrations in a pressurized dent is dependent on both the depth and shape of the dent. However, except ASME B31.8 (2007), all other codes, standards, and manuals recommend the assessment of dent severity and acceptability based on its depth alone. ASME B31.8 (2007) first included the strain based criteria for the assessment of a dent. Majority of the research works on strain concentrations in a pipe wall due to formation of a dent reported in the literature, are mainly concerned about developing analytical techniques for calculating dent strains. The experimental study on the strain distribution in a pipe wall due to formation of a dent is limited. No study was undertaken to investigate the effect of different parameters such as dent depth, dent shape, level of internal pressure during indentation on the strain distributions of a dent. Therefore, the current project focuses on the study of the effect of various parameters on the strain distributions in the dent of a pipeline.

It is not feasible to try to cover the entire range of pipeline geometries, dent geometries, internal pressure that may exist in the field in an experimental program. Therefore, the goal of the project was to develop an experimental database of the strain distributions in a dent of oil and gas steel pipes typically used in the field for different dent shapes, dent depths and internal pressures. The test results of the experiments were then used to validate numerical models.

3.2 Selection of Specimen Parameters

The purpose of full-scale testing was to determine experimentally the structural behaviors and strain distributions in field pipe under circumferential denting load. Therefore, the size and material properties of pipe specimens were selected in such a way that it represents the properties of pipes typically used in the oil and gas pipeline industry. Two different pipes with different diameters, thicknesses and material properties were used in the study. First set of pipe specimens was made of pipes with 762 mm outer diameter, 8.5 mm wall thickness and material grade API 5L X65 (API 2008). Other set was made of pipe with 274 mm outer diameter, 8.2 mm wall thickness, and grade API 5L X52 (API 2008). Most of the pipelines used in current practice have a D/t ratio ranging from 20 to 90. The diameter to thickness ratios (D/t) of the two sets of specimens were about 90 and 34 which falls in this range. The length of these pipe specimens were 2000 mm for larger pipes ($D/t = 90$) and 1100 mm for smaller pipes ($D/t = 34$).

3.3 Preparation of the specimen

A total of nine specimens were prepared. Out of the nine specimens, two specimens were fabricated from 762 mm outer diameter, 8.5 mm thick ($D/t \sim 90$) X65 grade steel pipes. Each specimen was 2000 mm long. For these specimens the length to diameter ratio was

~ 2.6. As the length to diameter ratio was small hemispherical dome shaped end caps were used for these specimens. The end caps were welded to the pipe specimen. Hence the entire length to diameter ratio of these pipes was 3.3. A photograph of a pipe specimen with dome shaped end cap is shown in Figure 3.1. The rest seven specimens were made of 274 mm outer diameter, 8.2 mm thick ($D/t \sim 34$) X52 grade steel pipes. Each of the specimens was 1100 mm long. The length to diameter ratio of the specimens was ~4. Flat plates were used as end caps for these specimens. A photograph of a pipe specimen with flat end cap is shown in Figure 3.2. The specimens made out of 762 mm diameter pipe will be called large specimen and the specimens made out of 274 mm diameter pipe will be denoted as small specimen.

3.4 Selection of Boundary Conditions

Since the research work was planned to investigate the load-deformation behavior and strain distributions of field pipe under circumferential denting load, the boundary conditions were chosen to try best simulating the conditions of a line pipe in the field while subjected to denting load. A buried field line pipe rests on the ground and hence, in the experiment the pipes were resting on a rigid steel platform. The boundary condition between the pipe and the support plane can be defined as a contact interaction. The denting load was applied on the top surface of the pipe resting on the steel platform.

3.5 Selection of Indenter Shape

The shape of the indenter was one of the primary parameters chosen in the test program. In the field different shapes of dent are observed in the body of pipe. The shape of the dent is dependent on the shape of the object which has caused the indentation. The indenter can be a tooth of the excavator and dent can form accidentally during

excavations. On the other hand, a rock of regular or irregular shape can be an indenter and dent can form if a line pipe sits on it. Hence, in the experimental program, three different shapes of indenter were used to introduce dent of three different shapes and curvatures in the pipe wall. The indenters are designated as follows.

1. Dome or smooth indenter
2. Rectangular or moderate indenter
3. Spherical or sharp indenter

The photographs of the three indenters are shown in Figure 3.3 and schematics are shown in Figure 3.4. Rectangular shaped indenter was used for both the large diameter ($D/t \sim 90$) and the small diameter ($D/t \sim 34$) pipe. For large diameter pipe the width of the rectangular indenter was higher than that of the rectangular indenter used for small pipe specimen. The width of rectangular indenter for small pipes was reduced by the ratio of diameter of small pipe to the diameter of the large pipe. The ratio between the diameters of the pipe small pipe and large pipe was 0.36. The same ratio was maintained between the widths of the two indenters. The length for both of the indenter was same. The dome and spherical indenter were used only in the small pipe specimen.

3.6 Internal pressure

The internal pressure in a pipeline is caused by the action of the fluid that is being transported. The internal pressure in the test specimens were applied as a function of p_y , which is the pressure that causes the stress in the hoop direction to reach material's yield stress level, σ_y . The relationship between p_y and σ_y is given by the following equation.

$$p_y = \frac{\sigma_y t}{r} \quad (3.1)$$

Where t is the thickness of the pipe wall and r is the inner radius of the pipe. The maximum allowable operating pressure for a field pipeline is usually limited to 80% of p_y or $0.80 p_y$. In the experimental program, the internal pressure was applied during the indentation to simulate the field condition as closely as possible. Also the level of internal pressure was varied in some pipe specimen to study the effect of internal pressure on the load-deformation behavior and also on the strain distributions in the dented region of the pipe. For large pipe specimen two different internal pressures (20% and 40% of p_y) were applied. The value of p_y for large pipe specimen was 12.67 MPa (1837 psi). For small diameter specimen the value of p_y was 23.5 MPa (3408 psi). Five of the small diameter pipe specimen was tested under an internal pressure level of 20% of p_y . High internal pressure (40% of p_y) was used for one of the small pipe specimen.

3.7 Test Variables

The objective of the study was to create an experimental database on the effect of different parameters on the load-deformation behavior and the strain distributions around the dented region while subjected to denting load. The parameters chosen are as follows (Table 3.1).

1. Internal pressure
2. Dent depth, and
3. Indenter shape

It is not feasible to conduct a large number of experiments for wide range of various parameters and investigate their effects on the strain distributions and on the load deformation behavior of the pipe while subjected to denting load. Therefore, in the

experimental program, the variables were limited to above mentioned values (see Table 3.1). A parametric study using finite element method was conducted to investigate the effect of a wide range of parameters.

3.8 Designation of Specimen

Each specimen was given a name as shown in Table 3.1. These names were chosen to recognize most of the attributes of the tests. For example, for specimen LRP20D4 the first character (L) indicates that this is a large diameter pipe specimen, second character R indicates that it was indented using a rectangular shaped indenter, next three characters (P25) indicate that the internal pressure during indentation was 20% of p_y or $0.2p_y$ and last of the characters (D4) indicate that the specimen was indented up to a depth of 4% of outer pipe diameter. Similarly, first character of small diameter pipe specimen is S. As specified earlier three different shapes of indenters was used in the experimental program. The characters used for different shapes of indenter are: R for rectangular indenter, S for spherical indenter, and D for dome shaped indenter.

3.9 Material Property

All pipe specimens with same diameter-to-thickness ratio were made from same material. For example, the material properties for two specimens with $D/t \sim 90$ were identical and the material properties for seven specimens with $D/t \sim 34$ were identical. Tensile coupon specimens from both sets of the pipe specimens were obtained. The specimens were obtained from the longitudinal direction of the pipe segment and far away from the weld. The tension coupon specimens were prepared and tested in accordance with ASTM E 8/E 8M-08 specifications (ASTM, 2008). A total of three coupon specimens were obtained from each sets of pipe specimen. An extensometer of 50.8 mm (2 in) gauge length was

mounted on the tension coupon to measure the longitudinal strain in the reduced area of the coupon and load versus deformation response was recorded until rupture.

The objective of these coupon tests was to obtain mechanical properties of the pipe steel. This information was used in the finite element modeling. Typical engineering stress-strain behavior obtained for the material of large pipe specimen is shown in Figure 3.5. A typical stress-strain behavior obtained for small pipe specimen is shown in Figure 3.6 and Table 3.2 outlines the mechanical properties for the pipe material.

3.10 Experimental Setup

The experimental program was carried out in the Structural Engineering Laboratory of the University of Windsor. Figure 3.7 shows a schematic of the test setup used for the experimental program. A photograph of the experimental setup is shown in Figure 3.8. The pipes were resting on the raised thick steel platforms. Hence, the boundary condition between the pipe and the support plane can be defined as a contact interaction. The denting load was applied on the top surface of the pipe wall using a universal loading actuator of 900 kN (200 kips). Majority of pipe specimens were dented under the internal pressure. Specimen SRP0D8 was indented at zero internal pressure. However, the specimen was filled with water. The internal pressure was applied to the pipe specimen using an air-driven hydraulic pump. The following sections describe the various instruments used in the experimental program.

3.10.1 Loading Jack and Loadcell

Denting load was applied to the pipe specimen using a 900 kN (200 kips) compression-tension type hydraulic loading jack with a 900 kN (200 kips) capacity loadcell. The

loadcell was used to acquire the denting load applied to the pipe specimen. Same loadcell was used in all pipe specimens.

3.10.2 Fluid Pump and Pressure Transducer

An air-pressure driven hydraulic pump was used to pressurize the water inside the pipe specimen. The capacity of the pump was 10000 psi (69MPa). A pressure transducer which was connected to the data acquisition system was used to control and acquire the internal pressure data.

3.10.3 Linear Voltage Displacement Transducers

The deformation of the pipe due to application of denting load was measured using linear voltage displacement transducers (LVDTs). A total of 4 LVDTs were used. . Two LVDTs (LVDTs 1 and 2 in Figure 3.7) were mounted on the actuator and at right angle apart from each other to capture stroke of the actuator and hence, to determine the dent depth data. One LVDT (LVDT 3 in Figure 3.7) was used to measure the ovalization of the pipe due to the denting load and placed at the mid height of the pipe specimen. The fourth LVDT was used at the end of the specimen to measure the vertical upward displacements of the end of the specimen as the pipe specimen was being indented.

3.10.4 Electronic Resistance Strain Gauges.

Strain gauge is used to measure the local strain of an object. The gauge is attached to the object by a suitable adhesive. As the object is deformed, the foil is deformed, causing its electrical resistance to change. This resistance change, usually measured using a Wheatstone bridge, is related to the strain by the quantity known as the gauge factor.

Strain gauges of 5 mm gauge length and electrical resistance (120Ω) were used to measure localized material strains in the pipe outer surface as the load was being applied. The total length including foil of the strain gauge was 9 mm. Strain gauges were installed in both circumferential and longitudinal directions on the outer surface of each pipe specimen. Also a line of strain gauges were installed at an angle 45° with the longitudinal axis of the pipe. The number of strain gauges used and the strain gauge layout was dependent on the pipe diameter and indenter shape. Strain gauge layout pattern for different pipe specimens are shown in Figures 3.9, 3.10, 3.11, and 3.12. It should be noted that no strain gauges were installed under the indenter since first trial of doing so failed.

3.10.5 Data Acquisition System

Data scan 7021, manufactured by Adept Scientific located in England was used to record all the test data. Each of the modules had eight channels. Total number of channels required was different for different specimens. The number of channels required was dependent on the strain gauge pattern used for a particular test. The data acquisition speed was set to be one reading per second. Data collection was facilitated using Dalite software and all data were stored in a computer file.

3.11 Test Procedure

Same test procedure was used in all of the specimens. First, the pipe specimen was filled with water and pressurized using the pump up to the desired pressure level. Next, a monotonically increasing denting load was applied using the displacement control method while keeping the level of internal pressure unchanged. The denting load was applied using the indenter through the universal loading actuator and in a several loading

and unloading steps. After completion of each load step, that is, after complete removal of denting load, the internal pressure in the pipe specimen was reduced to zero. The objective was to obtain strain data when the pipe is completely unloaded. Discussions on test procedure for all of the specimens are presented below.

3.11.1 Test 1: Specimen LRP20D4

The load-deformation behavior of specimen LRP20D4 is shown in Figure 3.13. The diameter-to-thickness ratio of the specimen was 90. Rectangular shaped indenter was used for the denting. Strain gauge layout of this specimen is shown in Figure 3.9. For this specimen internal pressure of 20% of p_y was applied in the first step. After application of internal pressure it was kept constant and the denting load was applied. Denting load was applied in a single load step. The maximum deformation of 63.5 mm was applied to the specimen and a final dent depth of about 30 mm was obtained. Hence the dent depth is 4%.

3.11.2 Test 2: Specimen LRP40D4

The load-deformation behavior of specimen LRP40D4 is shown in Figure 3.14. The diameter-to-thickness ratio of the specimen was same as specimen LRP20D4. The same rectangular indenter was used to create the dent. The strain gauge layout pattern for this specimen was same as specimen LRP20D4 (Figure 3.9). The major difference between the specimen LRP20D4 and LRP40D4 was the level of internal pressure during indentation. The internal pressure for this specimen was 5.70 MPa (40% of the p_y). A dent of permanent depth of 4% of the outer diameter of the pipe was obtained at unloaded condition. The internal pressure was applied at the first step. The denting load was applied in two loading-unloading steps. The maximum deformation applied was 68.5 mm

and a permanent depth of 30 mm was obtained after the removal of the denting load. Hence the dent depth is 4% of the outer diameter of the pipe.

3.11.3 Test 3: Specimen SSP20D8

Specimen SSP20D8 was a small diameter (274 mm) pipe specimen. A spherical indenter as shown in Figure 3.3 (b) was used for denting of this specimen. The strain gauge layout used for this specimen is shown in Figure 3.11. The load-deformation diagram of specimen SSP20D8 is shown in Figure 3.15. Internal pressure of magnitude 4.83 MPa (20% of p_y) was applied to the specimen at the first step. In the second step pressure was kept constant and the denting load was applied. The denting load was applied to the pipe specimen in four loading-unloading steps. After completion of each load step, that is, after complete removal of denting load, the internal pressure in the pipe specimen was reduced to zero. The objective was to obtain strain data when the pipe is completely unloaded. The permanent dent depth obtained after the first load step was 3.3% of the outer diameter of the pipe. Permanent deformations of 4.7% and 6.2% of the outer diameter of the pipe were obtained after the second and third load step. Maximum deformation applied to the specimen was 28 mm and a final dent depth of ~22 mm (8% of pipe's outer diameter) was obtained.

3.11.4 Tests 4 to 6: Specimen SRP20D10, SRP20D8 and SRP20D12

Specimen SRP20D10, SRP20D8, and SRP20D12 were small diameter pipe specimens. A rectangular indenter as shown in Figure 3.3 (c) was used for the indentation of these specimens. The strain gauge layout used for these three specimens is shown in Figure 3.10. For all of the three specimens same internal pressure of 4.83 MPa (20% of p_y) was

used. The only difference among these specimens was the final dent depth and the loading history in case of the denting load application.

For specimen SRP20D10, internal pressure of 4.83 MPa (20% of p_y) was applied in the first step. In the second step, the denting load was applied and increased monotonically in quasi static manner to the specimen. The load-deformation behavior of the specimen is shown in Figure 3.16. From this figure it can be observed that during the application of the denting load an accidental partial unloading occurred. The maximum amount of deformation applied to the specimen was 39.3 mm and a final permanent dent depth of 28.5 mm was obtained. This corresponds to 10% dent depth.

The load-deformation behavior of specimen SRP20D8 is shown in Figure 3.17. At the first step, the internal pressure was applied to the specimen. After the application of the internal pressure, the denting load was applied to the specimen. Denting load was applied to the specimen in three loading-unloading steps. After completion of each step, that is, after complete removal of denting load, the internal pressure in the pipe specimen was reduced to zero. The objective was to obtain strain data when the pipe is completely unloaded. The maximum deformation applied to the specimen was 33.4 mm and a final permanent depth of 22.5 mm was obtained. This corresponds to a 8% dent depth. The dent depth obtained after the first and second load steps were 7.8 mm (2.8% of the outer diameter of pipe) and 14.3 mm (5.2% of the outer diameter of the pipe) respectively.

The load-deformation behavior of specimen SRP20D12 is shown in Figure 3.18. Internal pressure was applied first. The denting load was then applied to the specimen. For this specimen the denting load was applied in a single step. Maximum deformation applied to

the specimen was 42.5 mm and the final depth obtained was 33.6 mm (12.3% of the outer diameter of the pipe).

3.11.5 Tests 7 to 9: Specimen SDP0D8, SDP20D8 and SDP40D8

Specimens SDP0D8, SDP20D8, and SDP40D8 were small diameter pipe specimens. A dome indenter as shown in Figure 3.3 (d) was used for the indentation of these specimens. The strain gauge layout used for these three specimens is shown in Figure 3.12. The specimens were indented to obtain a permanent dent depth of 8% of the outer diameter of the pipe. The major difference among these specimens was the level of internal pressure during indentation. The level of internal pressure for specimens SDP0D8, SDP20D8 and SDP40D8 were 0%, 20%, and 40% of the yield pressure of the pipe p_y . All of these specimens were indented in several loading and unloading steps. The load-deformation behavior for Specimens SDP0D8, SDP20D8 and SDP40D8 are shown in Figures 3.19, 3.20, and 3.21, respectively.

Table 3.1: Test Matrix

Test No.	Specimen	D/t	Internal Pressure (% of p_y)	Indenter Shape	Depth of Dent (% of Diameter)
1	LRP20D4	90	20	Rectangular	4
2	LRP40D4		40	Rectangular	4
3	SSP20D8	34	20	Sphere	8
4	SRP20D10		20	Rectangular	10
5	SRP20D8		20	Rectangular	8
6	SRP20D12		20	Rectangular	12
7	SDP0D8		0	Dome	8
8	SDP20D8		20	Dome	8
9	SDP40D8		40	Dome	8

Table 3.2: Material Properties

Specimen	Modulus of Elasticity (MPa)	Yield Strength (MPa)	Tensile Strength (MPa)
Large Specimen	200	540	620
Small Specimen	200	410	498



Figure 3.1: Photograph of a large pipe specimen

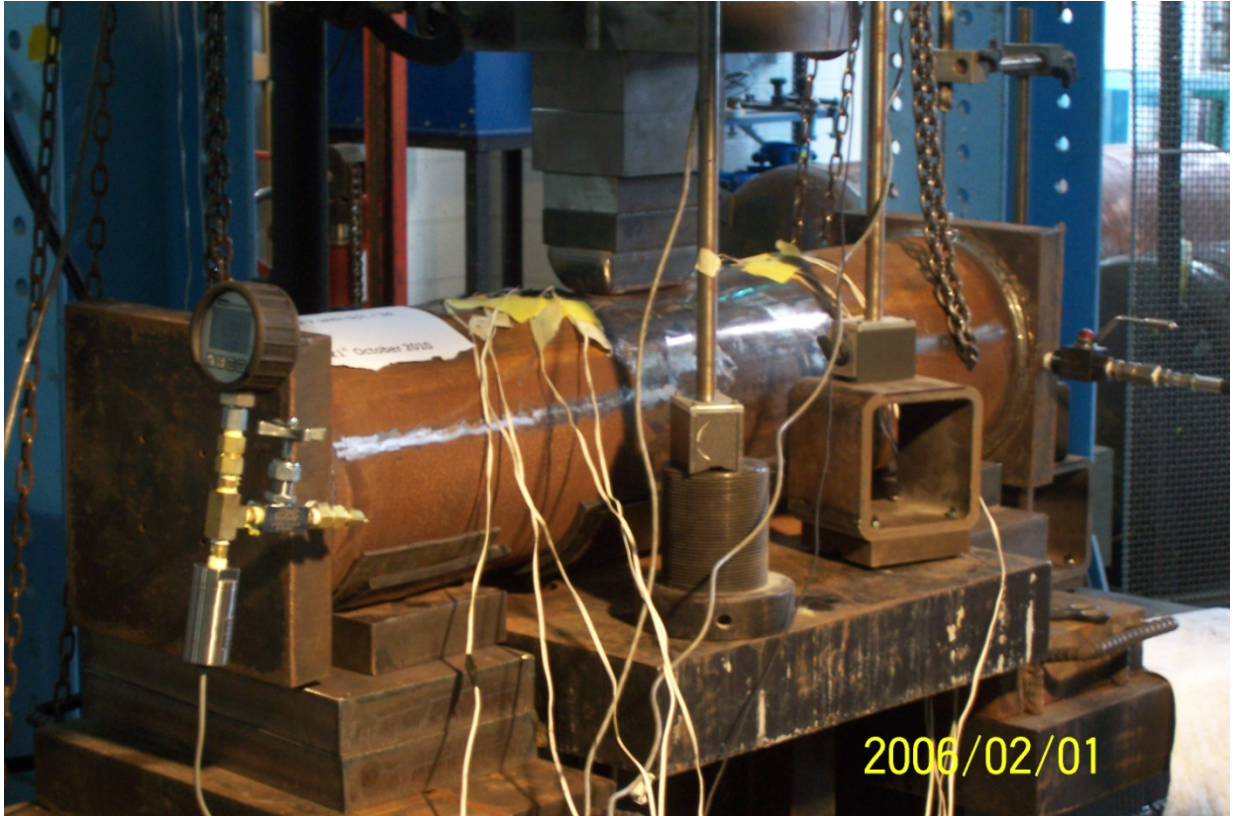
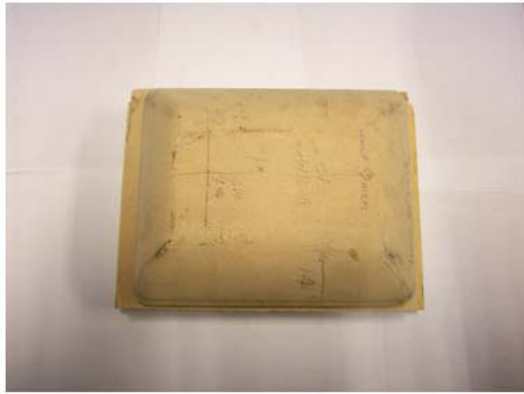


Figure 3.2: Photograph of small pipe specimen



(a) Rectangular indenter for large pipe



(b) Spherical indenter

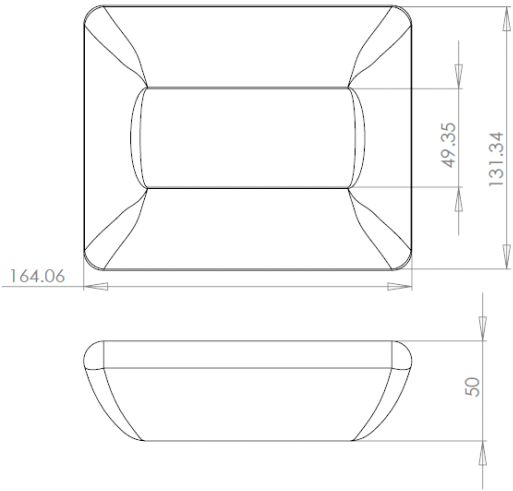


(c) Rectangular indenter for small pipe

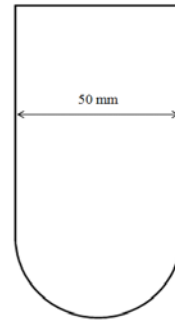


(d) Dome indenter

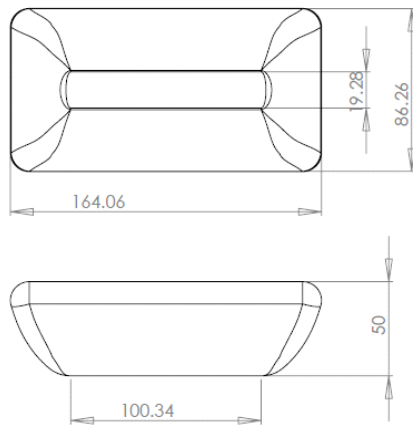
Figure 3.3 Photographs of the indenters



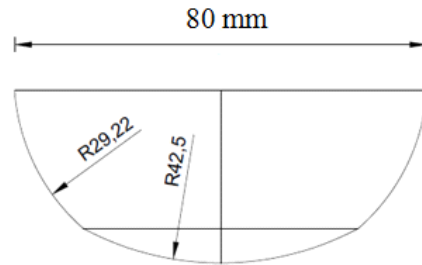
(a) Rectangular indenter for large pipe



(b) Spherical indenter



(c) Rectangular indenter for small pipe



(d) Dome indenter

Figure 3.4: Schematic of the indenters

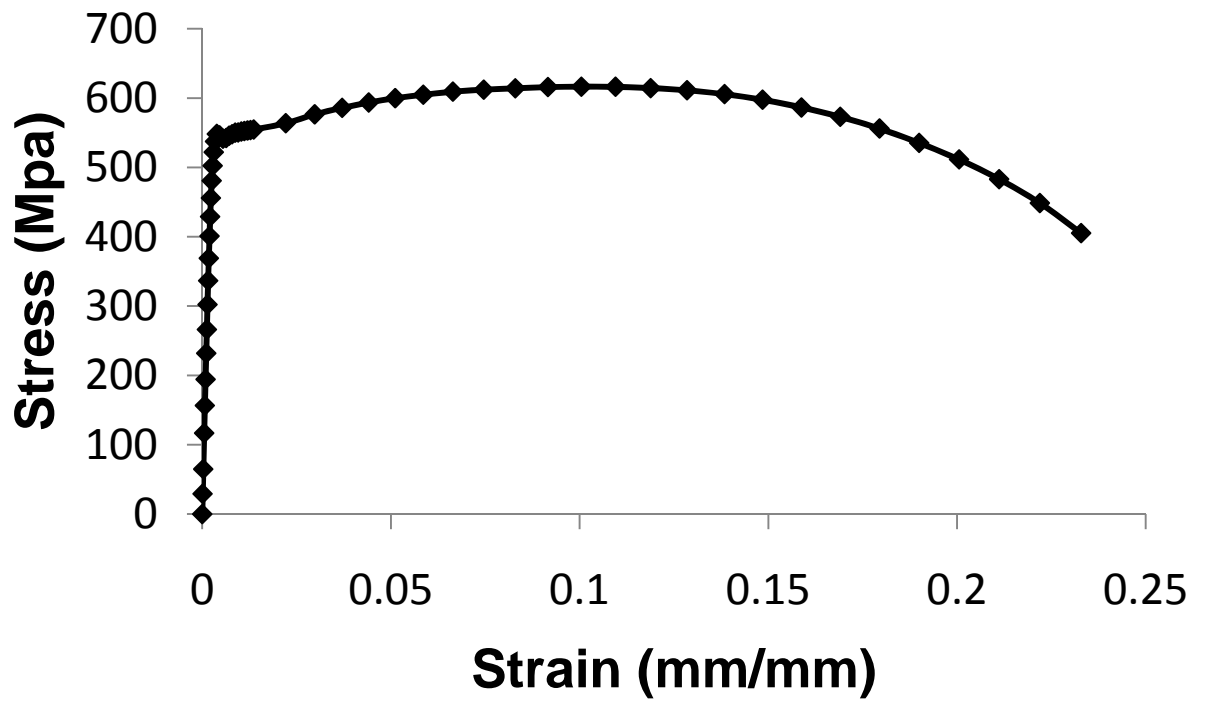


Figure 3.5: Tensile stress-strain behavior of coupon from large diameter pipe

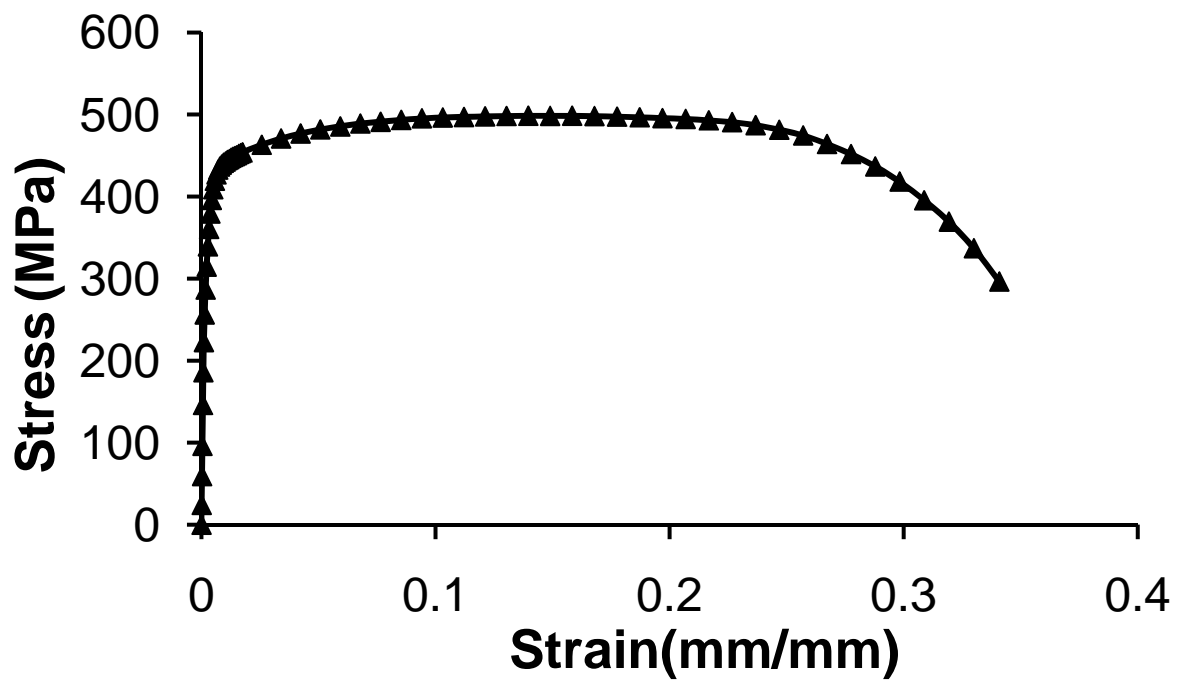


Figure 3.6: Tensile stress-strain behavior of coupon from small diameter pipe.

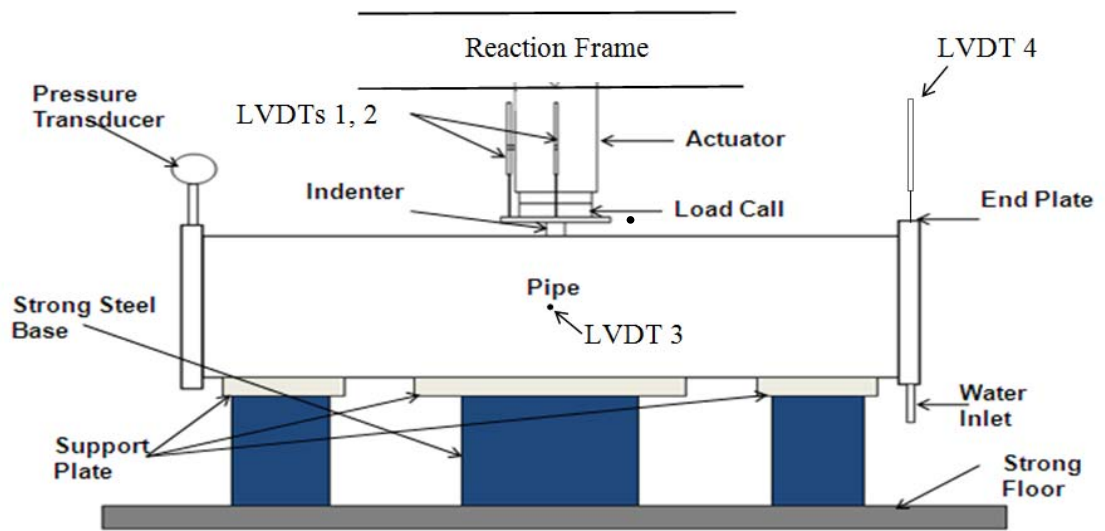


Figure 3.7: Schematic of the experimental setup

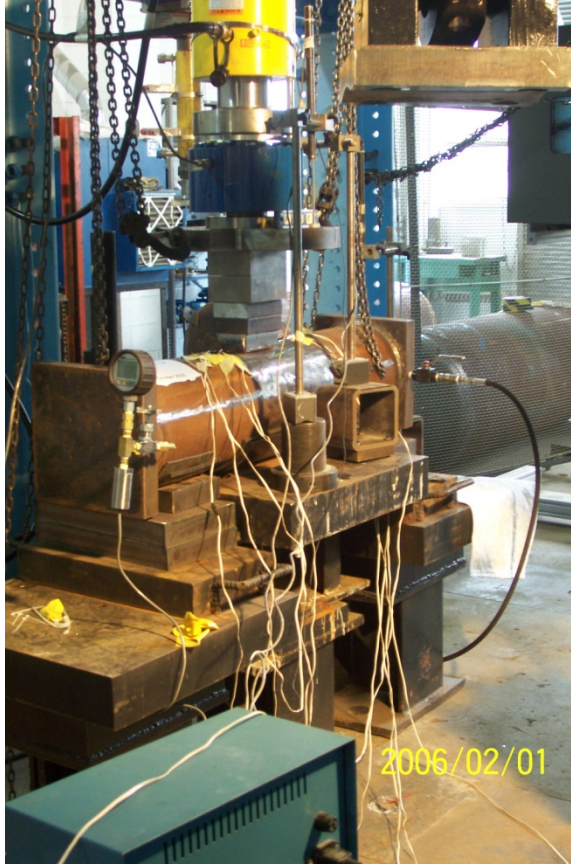
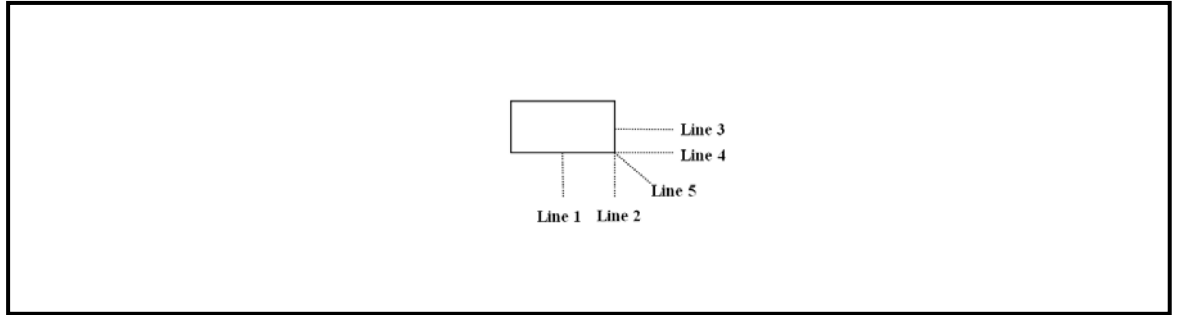
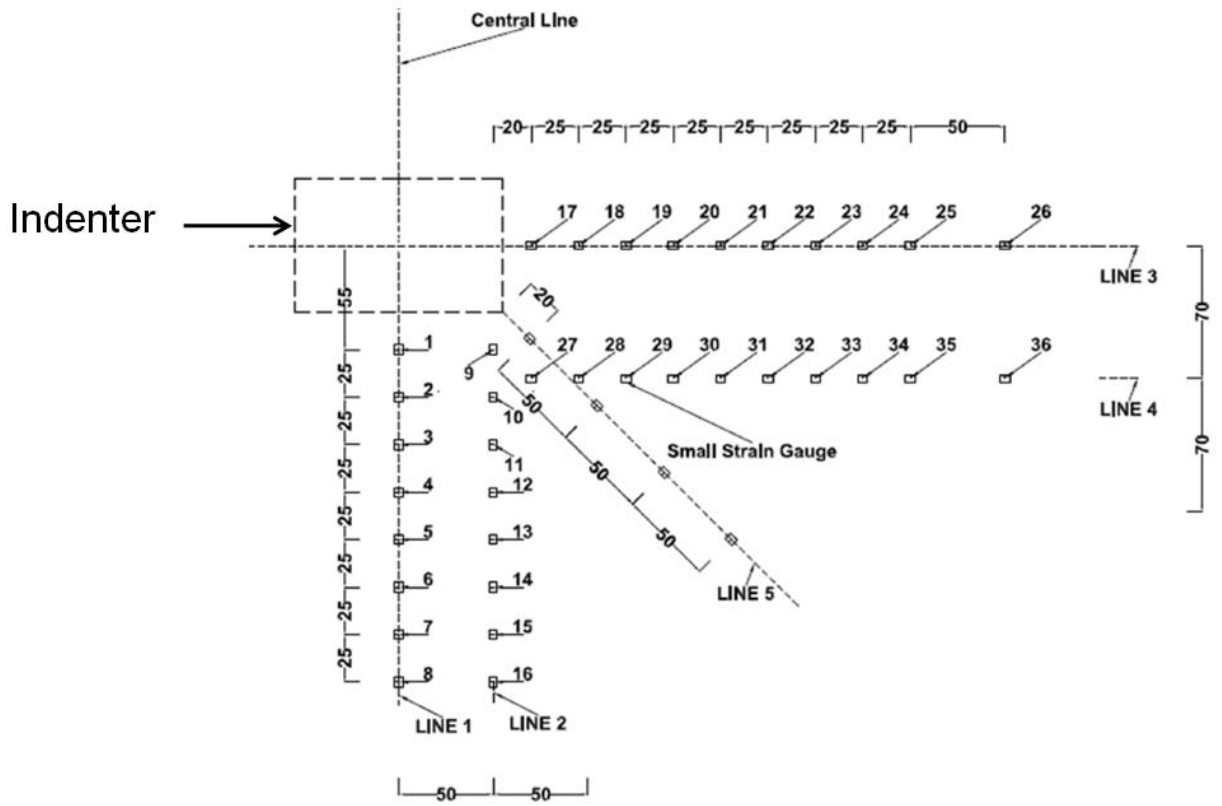


Figure 3.8: Photograph of the experimental setup

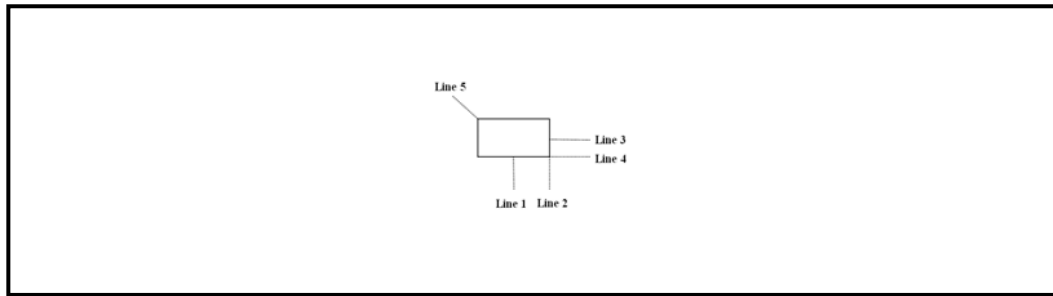


(a)

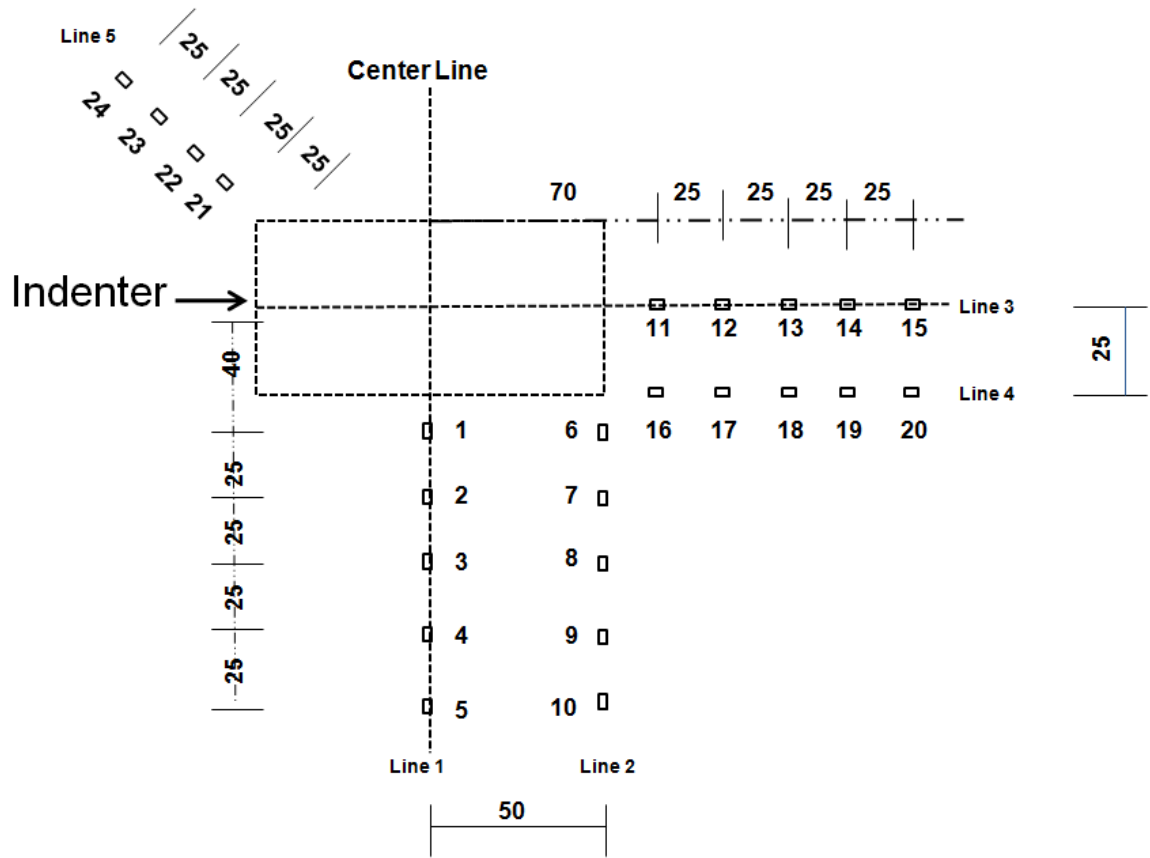


(b)

Figure 3.9: Strain gauge layout pattern for specimen LRP20D4 and LRP40D4

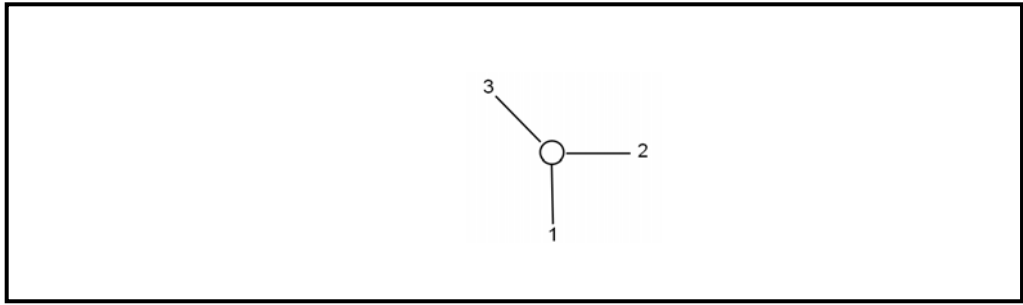


(a)

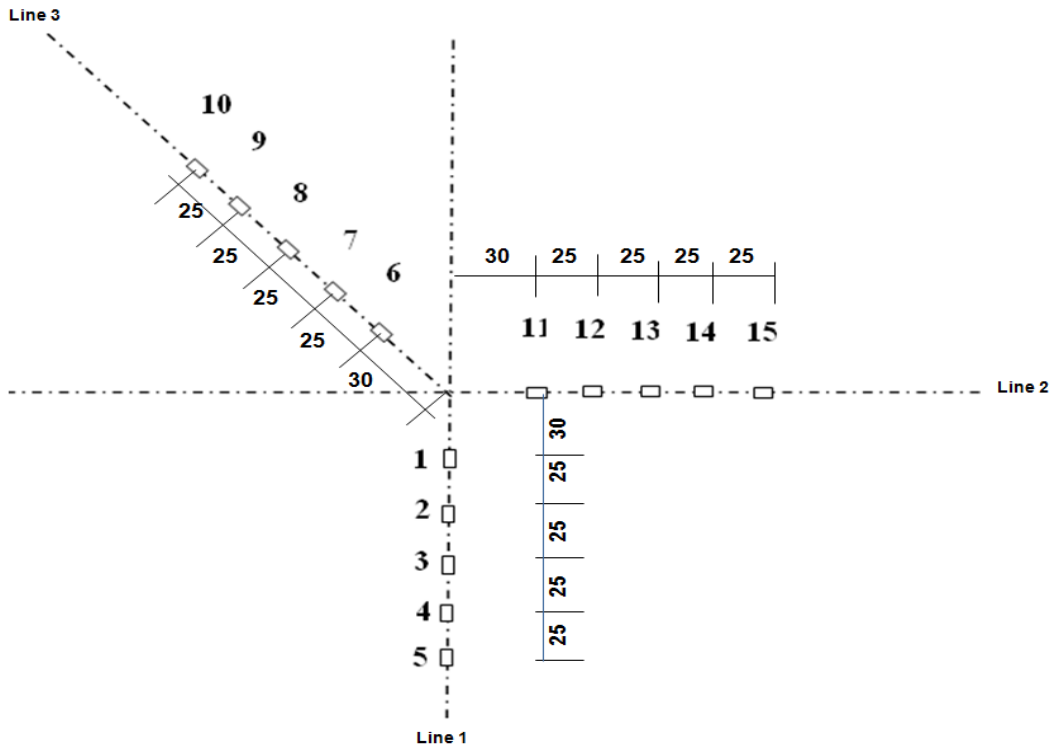


(b)

Figure 3.10: Strain gauge layout pattern for specimen SRP20D8, SRP20D10 and SRP20D12

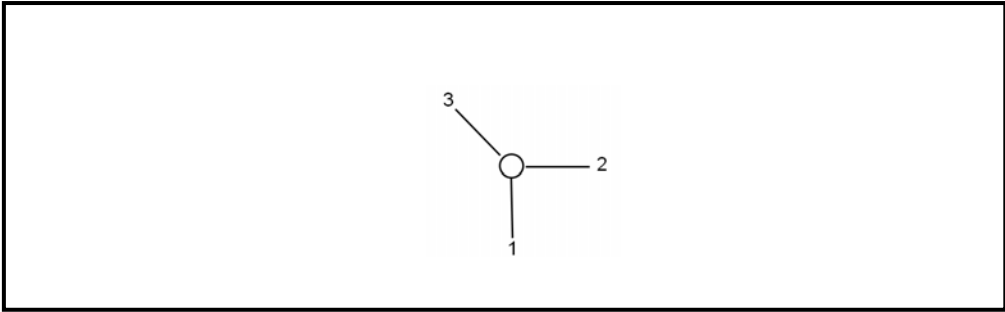


(a)

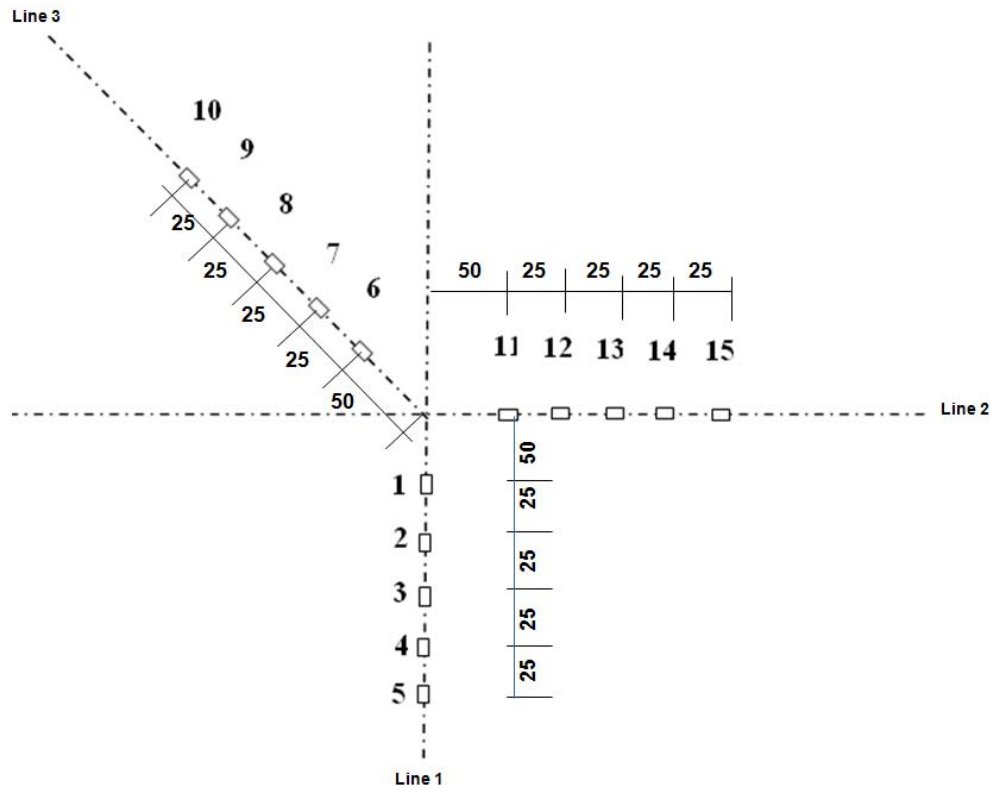


(b)

Figure 3.11: Strain gauge layout pattern for specimen SSP20D8



(a)



(b)

Figure 3.12: Strain gauge layout pattern for specimens SDP0D8, SDP20D8 and SDP40D8

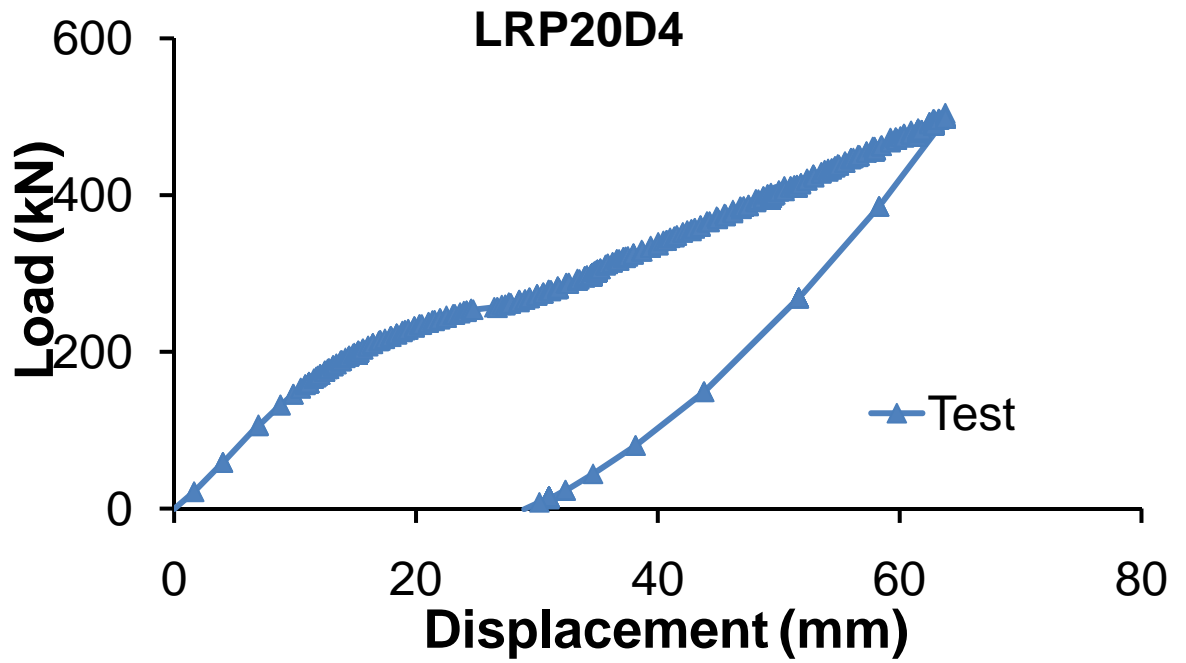


Figure 3.13: Load-deformation behavior of specimen LRP20D4

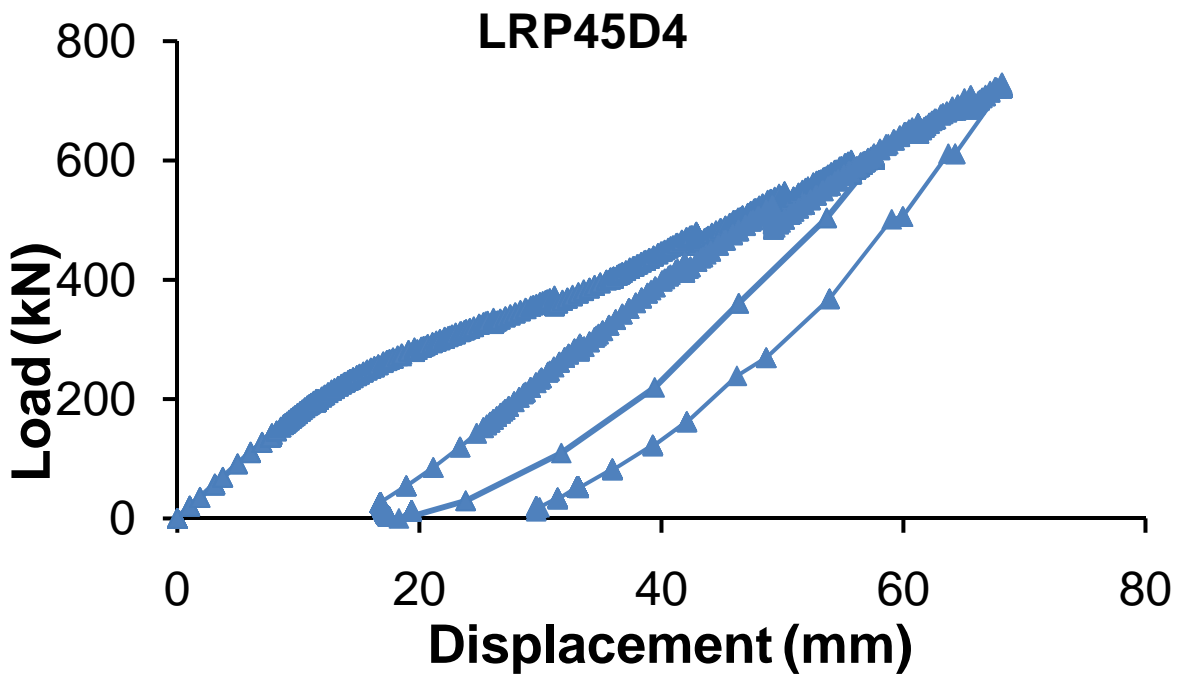


Figure 3.14: Load-deformation behavior of specimen LRP40D4

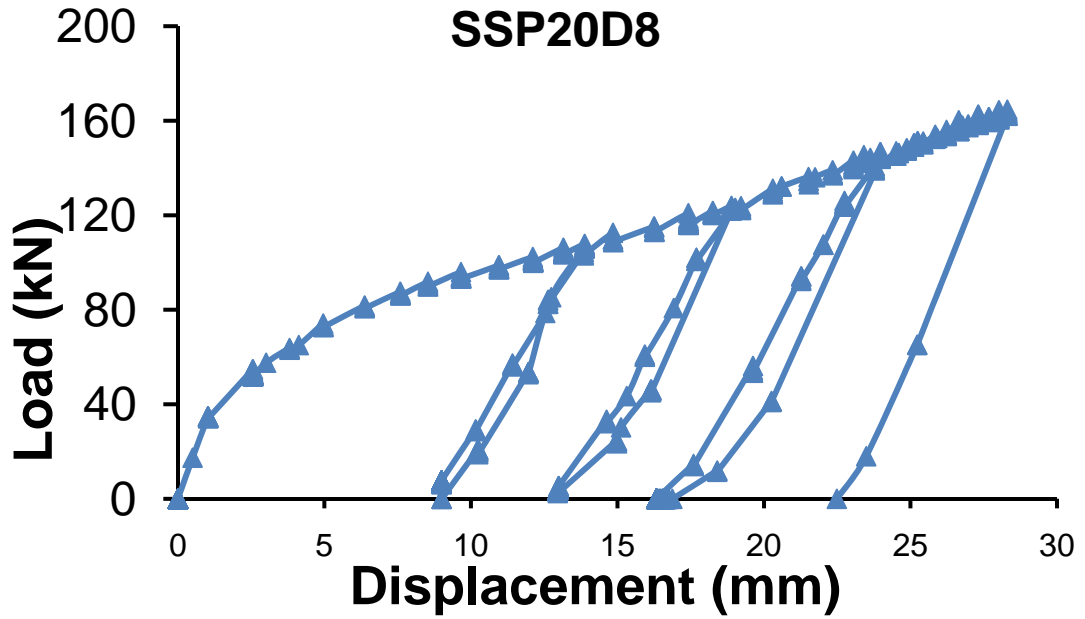


Figure 3.15: Load-deformation behavior of specimen SSP20D8

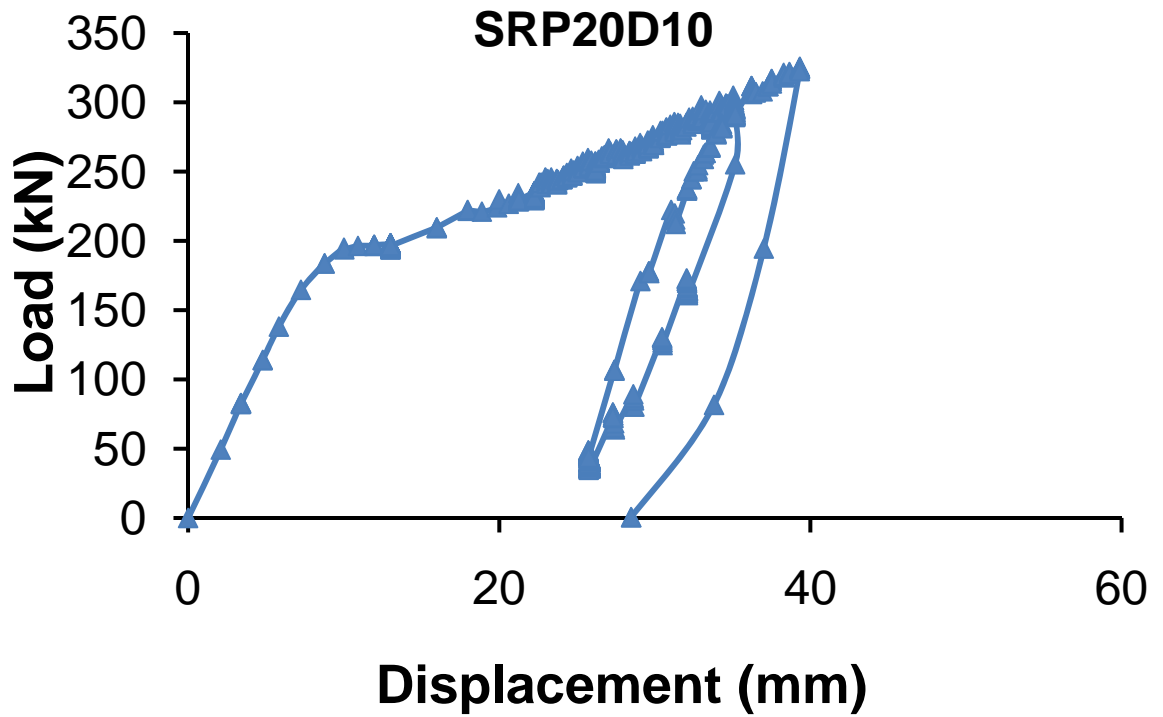


Figure 3.16: Load-deformation behavior of specimen SRP20D10

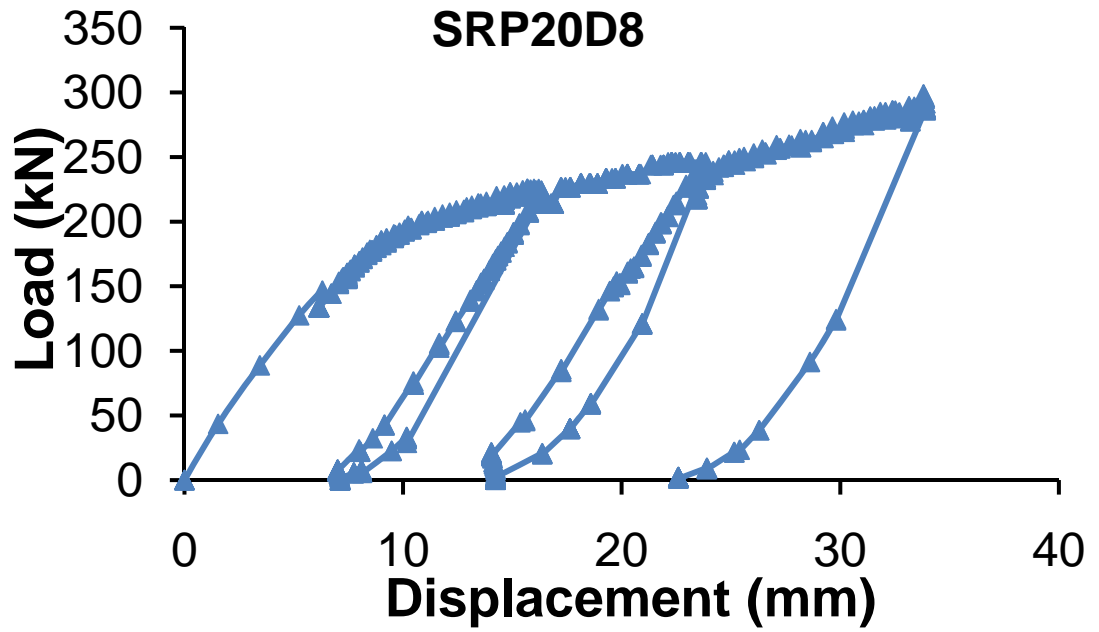


Figure 3.17: Load-deformation behavior of specimen SRP20D8

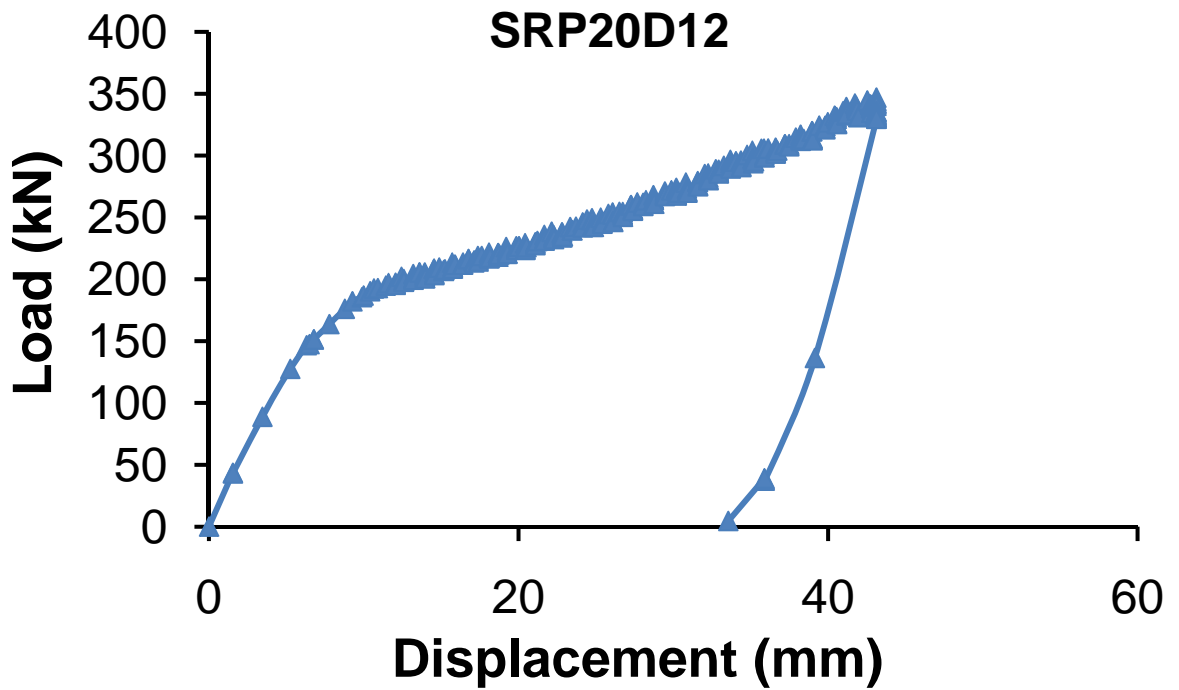


Figure 3.18: Load-deformation behavior of specimen SRP20D12

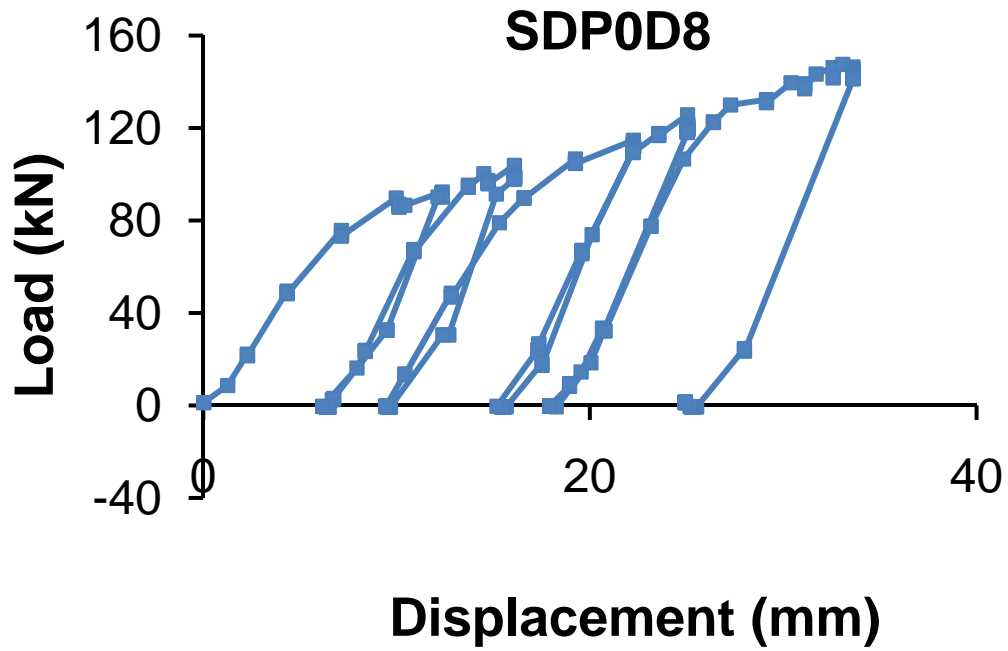


Figure 3.19: Load-deformation behavior of specimen SDP0D8

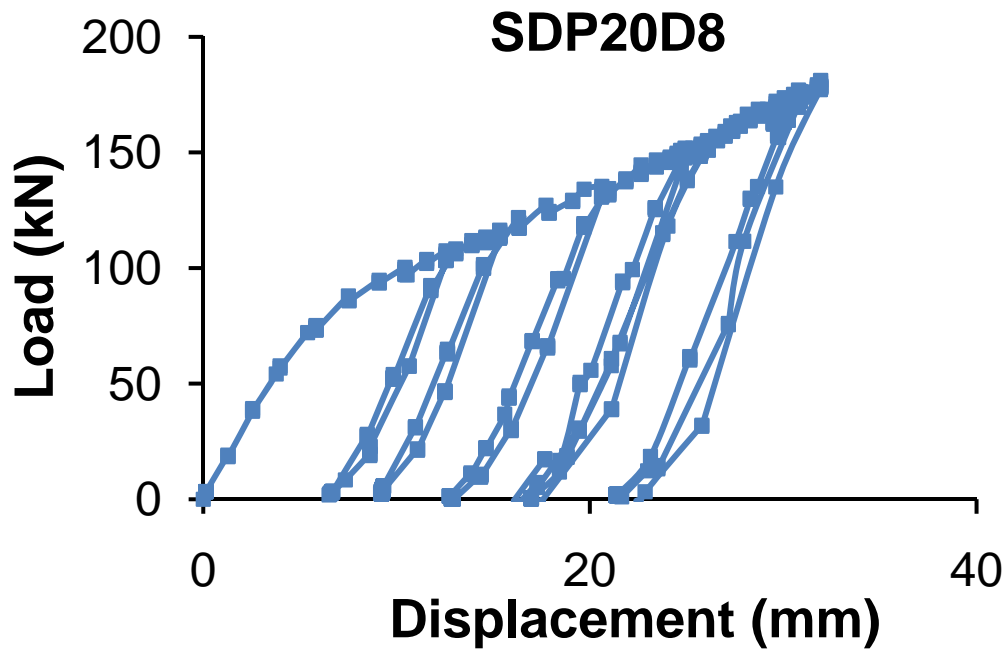


Figure 3.20: Load-deformation behavior of specimen SDP20D8

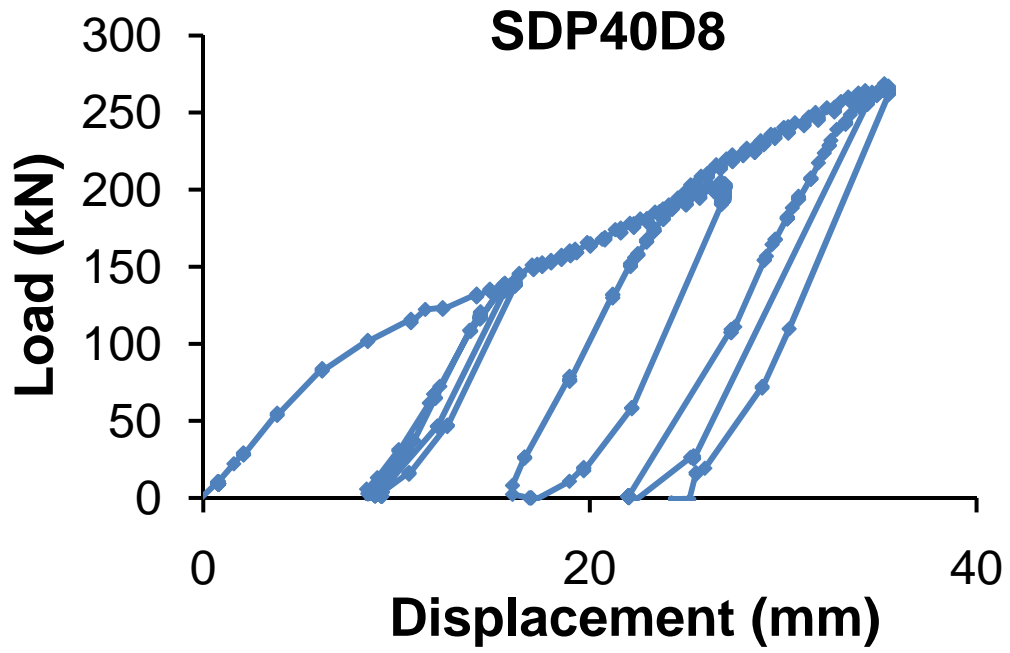


Figure 3.21: Load-deformation behavior of specimen SDP40D8

CHAPTER 4

TEST RESULTS

4.1 General

The objective of this chapter is to present the results obtained from the experimental program described in Chapter 3 for the specimens tested under lateral denting load. The details of the test specimens and test procedure are laid out in that chapter. Two types of plots obtained from the experimental program are presented in this chapter and these are as follows.

Load-deformation behavior, and
Strain distributions in the dent

The load-deformation behavior for the test specimens was presented in the previous chapter. In this chapter, the effect of different parameters which are internal pressure and indenter shape on the load-deformation behavior is presented. Strain gauges were installed on the outer surface of the test specimens to obtain strain distributions around the dent. However, no strain gauges were installed under the indenter. In this chapter, the strain gauge data for the test specimens are first presented. Then, the effect of various parameters such as the internal pressure, dent shape, and dent depth on the strain distributions on a dent is discussed.

4.2 Load-deformation Behaviour

The load-deformation behaviors of test specimens were presented in the previous chapter. In this section the effect of different parameters on the load-deformation behavior of pipe specimen are presented. The parameters used in this study are as follows.

1. Internal pressure during indentation and
2. The shape of the indenter

4.2.1 Effect of Internal Pressure

The effect of internal pressure was studied for two different shapes of indenter. The shapes were: rectangular and dome (Figures 3.3(a) and 3.3 (d)). It is important to note that the shape of the indenter and dent shape were similar. For large pipe specimens, only rectangular shaped indenter was used. For small pipe specimens all of the dome, spherical, and rectangular shape indenter were used. The dome shaped indenter was used when internal pressure was varied. Specimen LRP20D4 and LRP40D4 were large diameter pipe specimens and dented with a rectangular indenter to create a permanent dent depth of 4% of the outer diameter of the pipe. The only difference between the specimens was the internal pressure during indentation. For specimen LRP20D4 internal pressure during indentation was $0.2p_y$ and for specimen LRP40D4 internal pressure during indentation was $0.4p_y$ where, p_y is the pressure required to cause yielding of the pipe material. The comparison between the load-deformation behaviors of these two specimens is shown in Figure 4.1. From the comparison between the behaviors it is observed that the internal pressure has a significant effect on the load-deformation behavior of the pipe. Due to increase in internal pressure there is a significant increase in the load required for producing same amount of deformation. For example, to produce 40 mm deformation, 330 kN load is required for indentation under internal pressure of $0.2p_y$, while 450 kN load is required for indentation under internal pressure of $0.4p_y$.

The load-deformation behaviors of specimen SDP0D8, SDP20D8, and SDP40D8 are shown in Figure 4.2. All these specimens were made of small diameter pipe (274 mm

diameter) and dented with the dome shape indenter. The only difference between the specimens was the internal pressure during indentation. The internal pressures during indentation for Specimens SDP0D8, SDP20D8, and SDP40D8 were 0, $0.2p_y$, and $0.4p_y$ respectively. From Figure 4.2 it is again observed that internal pressure plays a significant role in the load-deformation behavior. With the increase in internal pressure denting load required to produce a certain amount of deformation increased significantly. For example to produce a deformation of 20 mm at internal pressure of 0, $0.2p_y$, and $0.4p_y$, the denting load required are 114 kN, 134 kN, and 175 kN respectively.

4.2.2 Effect of Indenter Shape

Three different shapes of indenter (rectangular or R, spherical or S, and dome or D) were used in the experimental program (see Figure 3.3 for photos and Figure 3.4 for sketches). Three test specimens were chosen in such a way that the only difference between the specimens was the shape of the indenter. These specimens are SSP20D8, SRP20D8, and SDP20D8. The internal pressure during the test for these specimens was same ($0.2p_y$). The effect of indenter shape on the load-deformation behavior of the pipe specimen is shown in Figure 4.3. From this figure it can be observed that the difference between the load-deformation behavior for a dome indenter (D) and a spherical indenter (S) is negligible. However, the load deformation behavior for a rectangular (R) shaped indenter is significantly different than other two indenters (D and S). A significantly high level of load is required for rectangular shaped indenter as compared to dome and spherical indenters, to produce same amount of deformation. For example, for a displacement of 10 mm, a load of 100 kN is required in the case of spherical and dome indenters, while in the case of a rectangular shaped indenter, the required load was 193 kN. This is due to the

fact that for the rectangular shaped indenter a larger area of the pipe comes into contact with the indenter compared to dome shaped and spherical indenter. Though diameters of dome indenter larger as compare to the diameter of spherical indenter, the initial contact area with the pipe wall was not much different. This may be the reason why load-deformation behaviors for these two shapes were similar.

4.3 Deformed Shapes and Strain Distributions

The main purpose of the experimental program was to study the effect of different parameters in the strain distributions around a dent. The parameters were: dent depth, dent shape, and the internal pressure during indentation. In this section the final deformed shape and strain data obtained from the strain gauges for different test specimens is discussed. Strain gauges in the first specimen underneath the indenter were installed. However, these gauges failed as soon as load was applied and hence, no strain-gauges were installed in the remaining test specimens where the indenter made contact with the pipe wall.

4.3.1 Specimen LRP20D4

Specimen LRP20D4 was a large (L) diameter pipe specimen and dented using a rectangular (R) indenter at an internal pressure of $0.2p_y$ (P20). The load-deformation behavior of the specimen was presented in the previous chapter (Figure 3.13). In this specimen, a dent with permanent depth of 4% (D4) of the outer diameter of the pipe was introduced in the pipe wall. A photograph of the dent introduced in specimen is presented in Figure 4.4. The stain gauge layout pattern for this specimen was presented in in Figure 3.9. The circumferential strain distributions along Lines 1 and 2 are presented in Figures 4.5 (a) and 4.5 (b), respectively. From the comparison between the Line 1 and Line 2, it is

observed that the circumferential strain distribution is different for these two lines. In Line 1, maximum strain value was obtained at a distance of 130 mm from the axial center line and the strain value was 1.4%. In Line 2, maximum strain value was obtained at a distance 80 mm from the axial centerline and the strain value was 1.1%. Line 1 shows a small compressive strain. However Line 2 does not show any compression

Figures 4.6 (a) and 4.6 (b) show the longitudinal strain distributions for Lines 3 and 4, respectively. From the comparison of the strain distributions along Lines 3 and 4 it is found that the pattern of strain distribution for both of the lines is similar. However, more strain concentrations was observed along the Line 3, which was along the axial centerline of the dent. The maximum strain obtained for both of the lines was at the same distance of 95 mm from the circumferential centerline of the dent. The value of maximum strain for Line 3 was 1.9%, while the value of maximum strain for Line 4 was 0.9%. The strain along the oblique line (Line 5) is shown in Figure 4.7.

4.3.2 Specimen LRP40D4

Specimen LRP40D4 was a large (L) diameter pipe specimen and indented using a rectangular (R) indenter at an internal pressure of $0.40p_y$ (P40). In this specimen a dent with permanent depth of 4% (D4) of the outer diameter of the pipe was introduced in the pipe wall. A photograph of the dent in specimen LRP40D4 is shown in Figure 4.8. This pipe specimen was dented in two load steps. The load-deformation diagram was presented in Chapter 3 (Figure 3.14). The strain gauge layout used for this specimen was same as the Specimen LRP20D4 and presented in Figure 3.9. Figures 4.9 (a) and 4.9 (b) show the strain distribution along Lines 1 and 2, respectively. In Line 1 maximum strain value was recorded at a distance 80 mm from the axial center line and the value strain

was 2.1%. In Line 2 maximum strain value was recorded at a distance 80 mm from the axial centerline and the strain value was 2.5%. Hence, the trend is opposite in this specimen compared to Specimen LRP20D4.

The longitudinal strain distributions for Lines 3 and 4 are presented in Figures 4.10(a) and 4.10(b), respectively. The maximum strain obtained for both lines was at the same distance of 95 mm from the circumferential centerline of the dent, the value of maximum strain for Line 3 was 3.4%, while the value of maximum strain for Line 4 was 2.6%. Figure 4.11 shows the strain along the oblique line (Line 5).

4.3.3 Specimen SSP20D8

Specimen SSP20D8 was a small (S) diameter pipe and indented using a spherical indenter (S) which produces a sharp dent (see Figure 3.3(b) for photo and Figure 4.4 (b) for sketch). The internal pressure during indentation was $0.2p_y$ (P20). A dent with permanent depth of 8% (D8) of the outer diameter of the pipe was introduced in the pipe wall. Figure 4.12 shows a photograph of the dent in the specimen SSP20D8. The specimen was dented in four load steps and after each load step the internal pressure was also reduced to zero to obtain strain data of the unloaded pipe. The load-deformation behavior of this specimen was presented in previous chapter (Figure 3.15). Also the strain gauge layout of this specimen was presented in previous chapter in Figure 3.11. During the loading process the pipe was unloaded several times and strain data was recorded for four different dent depths of 3%, 4.7%, 6% and 8%. The circumferential strain distributions for Line 1, for different dent depths are presented in Figure 4.13. From this figure it can be observed that with the increase in dent depth, strain along circumferential direction increases. For example maximum strain value was obtained at a distance 30 mm

from the dent center, and the values of maximum strains were 2.2%, 3.1%, 3.8%, and 4.0% for dent depth 3%, 4.7%, 6%, and 8%, respectively. It should be noted that the strain gauge nearest to the dent was placed at 30mm away from the dent center. Hence, the maximum strain values obtained from the test may not be the absolute maximum value.

Figure 4.14 presents the longitudinal strain distributions along Line 2. From this figure, it can be observed that maximum strain occurs at a distance 30 mm from dent center. After the maximum strain value a gradual decrease in strain value was observed as the distance from the dent center increases. It was also observed that with the increase in dent depth there is an increase in strain along the longitudinal direction. For example in the strain gauge located at a distance 30 mm from the dent center the strain values recorded at dent depth of 3%, 4.7%, 6%, and 8% were 2.9%, 4.2%, 5.2%, and 5.7% respectively.

Figure 4.15 presents the strain distributions along the Line 3. From this figure it is also observed that strain on this line increases with the dent depth. Maximum value of strain was obtained in the strain gauge nearest to the dent. Strain value decreases as the distance from the dent center increases.

From the comparison among the longitudinal, circumferential, and oblique strain distributions it can be concluded that for a particular dent depth, strain concentration in the longitudinal direction is higher than that of oblique and circumferential direction. For example, for a dent depth of 6% maximum strain in longitudinal direction is 5.2% while in the circumferential direction maximum strain is 3.8% and in the oblique direction maximum strain is 4.8%.

It should be noted that no compressive strains were recorded in these specimens. This is because the nearest strain gauge was not in the compressive zone.

4.3.4 Specimen SRP20D10

It was a small pipe (S) specimen and indented using a rectangular indenter (R) to produce a permanent dent depth of 10% (D10) of the outside diameter of the pipe. During the indentation the internal pressure level was kept at $0.2p_y$ (P20). The denting was carried out in a single load step. Figure 3.16 shows the load-deformation behavior of specimen SRP20D10. A photograph of the dent introduced in specimen SRP20D10 is presented in Figure 4.16. A dime (coin of 10 cents) can be seen in this photo. An overall gross disturbance of the pipe circular cross section was observed in this test specimen.

Figure 3.10 shows the strain gauge layout for this specimen. Circumferential strain distribution along Lines 1 and 2 are presented in Figures 4.17 (a) and 4.17 (b), respectively. From the observation of strain distributions for Lines 1 and 2 it is found that maximum strain on both lines occurs at a distance 90 mm from the axial centerline of the dent. The value of maximum strain for Line 1 was 3.8% and for Line 2 was 3%. The longitudinal strain distributions along Line 3 and 4 are presented in Figure 4.18(a) and 4.18(b), respectively. For both of the lines maximum value of strain was recorded at a distance 70 mm from the circumferential center line of the dent. The value of maximum strain recorded in Line 3 was higher than the value of maximum strain line 4. For example the value of maximum strain was 4.5% for Line 3 while for Line 4 maximum strain value was recorded 3.2%.

From the comparison between the strains distributions along circumferential and longitudinal directions, it can be concluded that largest strain value was obtained in the longitudinal direction and the value of maximum strain was 4.5%. It was recorded at a distance 70 mm from the circumferential centerline of the dent. It should be noted that closest strain gauge was located at a distance 40 mm in circumferential direction and 70 mm in longitudinal direction.

4.3.5 Specimen SRP20D8

Specimen SRP20D8 was a small (S) pipe specimen and indented by a rectangular (R) shape indenter to introduce a dent of depth 8% (D8) on the pipe wall. The specimen was dented in several loading and unloading steps. After each loading step the internal pressure was reduced to zero pressure to obtain the strain data at completely unloaded condition. The load deformation behavior of the pipe specimen was presented in Figure 3.17 of the previous chapter. The internal pressure level during indentation was $0.2p_y$ (P20). A photograph of the dent introduced in specimen SRP20D10 is presented in Figure 4.20.

The strain gauge layout for this specimen was similar to specimen SRP20D10 and shown in Figure 3.11. Strain data at three different depth 2.5%, 5.2%, and 8% of the outer diameter of the pipe was recorded throughout entire loading and unloading procedure. Circumferential strain distributions for different dent depths along Lines 1 and 2 are presented in Figures 4.21(a) and 4.21(b), respectively. From Figure 4.21(a) it is observed that with the increase in dent depth there is an increase in the strain. Similar trend is also observed for Line 2 in Figure 4.21(b). For both lines, maximum strain was recorded at a distance 90 mm from the axial centerline of the dent. At a dent depth of 8% maximum

strains were recorded 4% and 2.9% in Lines 1 and 2, respectively. It should be noted that closest strain gauge was located at a distance 40 mm in circumferential direction and 70 mm in longitudinal direction.

Figures 4.22(a) and 4.22(b) show the strain distribution in the longitudinal direction along Lines 3 and 4, respectively. From observation of strain distributions along the longitudinal direction it is found that with the increase in dent depth there is a increase in the strain value, and the value of strains in Line 3 was higher than the value of strain in Line 4. For both lines maximum strain value was recorded at a distance 70 mm from the circumferential centerline of the dent. At a dent depth of 8% of the outer diameter of the pipe maximum strain value recorded for Line 3 was 3.5%, while the maximum strain value for Line 4 was 2.5%. The closest strain gauges were at a 40 mm and 70 mm in circumferential and longitudinal direction respectively.

4.3.6 Specimen SRP20D12

Specimen SRP20D12 was a small (S) pipe specimen and dented using a rectangular (R) indenter up to a permanent dent depth of 12% (D12) of the outer diameter of the pipe. The test was completed in a single load step. The load-deformation behavior of the specimen was presented in previous chapter in Figure 3.18. Figure 4.23 presents a photograph of the dent introduce in specimen SRP20D12. The internal pressure during the indentation was $0.2p_y$ (P20). Same strain gauge layout as specimen SRP20D10 and SRP20D8 was used for this specimen.

Circumferential strain distributions along Lines 1 and 2 are presented in Figures 4.24(a) and 4.24(b), respectively. From the observation of the circumferential strain distribution

it was found the strain concentration in Line 1 is higher as compared to strain concentration in Line 2. For example, maximum strain value recorded on Line 1 was 4.1%, while the value of maximum strain in Line 2 was 2.8%.

Figures 4.25(a) and 4.25(b) present longitudinal strain along Line 3 and Line 4, respectively. From the strain distributions of Lines 3 and 4, it is observed that for both lines maximum strain occurs at a distance 70 mm from the circumferential center line of the dent. However, the value of maximum strain for Line 3 was higher than the value of maximum strain for Line 4. For example, maximum strain value recorded for Line 3 is 4.8%, while the value of maximum strain for Line 4 is 2.3%. The closest strain gauges were at a 40 mm and 70 mm in circumferential and longitudinal direction respectively.

4.3.7 Specimen SDP0D8

Specimen SDP0D8 was a small (S) pipe specimen. A dome (D) shaped indenter was used for indentation of this specimen. The internal pressure during indentation was zero (P0). However, the pipe was filled with the water during indentation. The indentation of the pipe specimen was carried out in three load steps. The load deformation diagram of this specimen was presented in the previous chapter in Figure 3.19. A photograph of the specimen with a dent of depth 8% (D8) is shown in Figure 4.26. In this figure photos of a Dime (10 cents) and Nickel (5 cents) are shown.

Strain gauge layout for the specimen was shown in Figure 3.12. The circumferential strain distribution along Line 1 is presented in Figure 4.27. From the observation of circumferential strain it is found that with the increase of dent depth the condition of strain at a particular point changes. For example, at a distance of 50 mm from the dent

center tensile strain value of 1% was recorded at a dent depth of 3%. However, at a dent depth of 8% of compressive strain value of 1% was recorded. Hence this plot shows that at a particular point both strain value and its sign can change if dent depth changes.

Figure 4.28 shows the longitudinal strain distribution along Line 2. From Figure 4.28 it can be observed that the location of maximum strain was changed with the increase in dent depth. For example, for a dent depth of 3% the maximum strain was recorded at a distance of 50 mm from the dent center, while for a dent depth of 8% the location of maximum strain was 75 mm away from the dent center. At 3% dent depth maximum strain was 1% and at a dent depth of 8% maximum strain was 1.5%. Figure 4.29 presents the strain distribution along the Line 3. Therefore strain distribution for a line can change if dent depth changes

4.3.8 Specimen SDP20D8

Specimen SDP20D8 was a small (S) pipe specimen. The dent was introduced in this specimen using a dome (D) shaped indenter (Figure 3.3(d)). During the indentation an internal pressure of $0.2p_y$ (P20) was maintained. The denting load was applied in three load step and after the end of each step the pressure was also reduced to zero to record the strain data when the pipe is completely unloaded. The load-deformation diagram of this specimen was presented in the previous chapter in Figure 3.20. A photograph of the specimen with a dent of depth 8% (D8) is shown in Figure 4.30. The strain gauge layout pattern for this specimen was similar to Specimen SDP0D8 (Figure 3.12).

Figure 4.31 shows the circumferential strain distribution along Line 1. From this figure it can be observed that with the increase in dent depth there is an increase in the magnitude

of strain. From the strain distribution along Line 1 it is found that at distances of 50 mm and 125 mm from the dent center, high strain concentration took place. However, in the region between the high strain locations strains were relatively smaller. Longitudinal strain distribution along Line 2 is presented in Figure 4.32. From this figure it is observed that strain value in longitudinal direction increases with the increase in dent depth. Figure 4.33 presents the oblique strain distribution along Line 3. For Line 3, the location of maximum strain changed as the dent depth increased.

4.3.9 Specimen SDP40D8

Specimen SDP40D8 was a small (S) pipe specimen and dented using the dome (D) shaped indenter (Figure 3.3(d)). The indentation of the specimen was carried out at an internal pressure level of $0.4p_y$ (P40). The denting was performed in three load steps. After each load step the pressure was reduced to zero to obtain the strain data of completely unloaded pipe specimen. The load-deformation plot of the specimen was presented in the previous chapter in Figure 3.21. A photograph of the specimen SDP40D8 with a dent depth of 8% is presented in Figure 4.34. The strain gauge layout of the specimen was similar to that of specimens SDP0D8 and SDP20D8 (Figure 3.12).

The circumferential strain distributions are presented in Figure 4.35. From this figure it is observed that with an increase in dent depth an increase in the strain value occurs at a distance of 100 mm. Figure 4.36 shows the longitudinal strain distributions. An increase in strain value with the increase in dent depth was observed in the longitudinal direction. Strain distribution along Line 3 is presented in Figure 4.37.

4.4 Effect of Different Parameters on Strain Distributions

The objective of this study was to determine the effect of different parameters on the strain distributions in a dent of pipelines and the parameters used in this study are as follows.

1. Internal pressure level during indentation
2. Dent shape
3. Dent depth

In this section, the effect of these parameters on the strain distributions around dent is discussed.

4.4.1 Effect of Internal Pressure

The effect of internal pressure on the strain distribution was studied for two dent shapes rectangular and dome. Specimens LRP20D4 and LRP40D4 were large diameter pipe specimen and indented using a rectangular shape indenter to produce a permanent dent depth of 4% of the outer diameter of the pipe. The main difference between the specimens was the level of internal pressure during indentation. Specimen LRP20D4 was indented at an internal pressure of $0.2p_y$, while the internal pressure for specimen LRP40D4 was $0.4p_y$. As discussed earlier same strain gauge layout pattern was used for both of the specimens (Figure 3.9). The effect of internal pressure on the circumferential strain distribution along Lines 1 and 2 is presented in Figures 4.38(a) and 4.38(b). From these figures it is observed that with the increase in internal pressure there is an increase in circumferential strain. For example, for Line 1 the maximum strain for Specimen LRP20D4 was 1.4% at a distance 130 mm from the dent center, while for Specimen

LRP40D4 recorded maximum strain was 2.1% and was recorded at a distance 80 mm from the dent center. Similar trend was observed for Line 2. For Line 2 maximum strain for Specimen LRP20D4 was 1.1% and for Specimen LRP40D4 was 2.5%. Figures 4.38(c) and 4.38(d) show the effect of internal pressure on the circumferential strain distribution along Lines 3 and 4. From the figures it is observed that with the increase in internal pressure there is an increase in longitudinal strain. For example for Specimen LRP20D4 the maximum strain recorded along Lines 3 and 4 were 1.9% and 0.9%, respectively. On the other hand for Specimen LRP40D4 the maximum strain recorded along Line 3 and 4 were 3.4% and 2.6% respectively. The effect of internal pressure along Line 5 is presented in Figure 4.38(e). From Figure 4.38(e) it is clear that oblique strain along Line 5 increase with the internal pressure.

Specimens SDP0D8, SDP20D8, and SDP40D8, were small diameter pipe specimen and indented using a dome shaped indenter to produce a final dent depth of 8%. The only difference between the specimens was the level of internal pressure during indentation. The internal pressure for the Specimens SDP0D8, SDP20D8, and SDP40D8 were 0, $0.2p_y$, and $0.4p_y$, respectively. The effect of internal pressure on the circumferential, longitudinal and oblique strain distribution is presented in Figures 4.39 (a), 4.39(b), and 4.39(c) respectively. From these figures it is found that the internal pressure level during indentation influences the strain distribution significantly. Effect of internal pressure on the maximum strain values around a dent for dome shaped indenter is presented in Table 4.1.

4.4.2 Effect of Dent Shape

The effect of dent shape on the strain distributions was studied in Specimens SRP20D8, SSP20D8, and SDP20D8. All these specimens were made of small (S) pipe and indented up to a permanent dent depth of 8% (D8) of the outside diameter of the pipe. For these specimens internal pressure during indentation was same ($0.2p_y$). The only difference between the specimens was the shape of the indenter. The shapes of the indenters used were rectangular, spherical, and dome (Figure 3.3) and they were used in specimens SRP20D8, SSP20D8, and SDP20D8, respectively. The influence of indenter shape on the circumferential strain distribution is presented in Figure 4.40(a). From this figure it can be observed that the strain distribution pattern and the location of maximum strain in the circumferential direction are strongly influenced by the shaped of the dent. Figure 4.40(b) shows the effect of indenter shape on the longitudinal strain distribution. Form the longitudinal strain distributions it can be observed that the longitudinal strain distribution and the value and location of maximum longitudinal strain are influenced by the shape of the dent. The maximum strain values for different dent shape along the circumferential and longitudinal directions are presented in Table 4.2

4.4.3 Effect of Dent Depth

Specimens SRP20D8, SRP20D10, and SRP20D12 were small (S) pipe specimen and indented using a rectangular indenter. The internal pressure level during indentation was 20% of the yield pressure p_y of the pipe. The only difference between the specimens was the final dent depth. The permanent dent depth for Specimen SRP20D8, SRP20D10, and SRP20D12 were 8%, 10%, and 12% of the outer diameter of the pipe, respectively. Figures 4.41(a) and 4.41(b) represent the effect of dent depth on the circumferential strain

distribution in Lines 1 and 2(Figure 3.10), respectively. Figures 4.41(c) and 4.41(d) represent the effect of dent depth on longitudinal strain distribution in Lines 3 and 4, respectively.

As described earlier, in the experimental program some specimens were indented in several load steps. After each load step the specimens were completely unloaded to record strain data of the unloaded pipe specimen.

Specimen SRP20D8 was indented in three loading steps. Following the loading and unloading procedure strain data for three dent depths 2.5%, 5.2% and 8% were acquired. The maximum strain values recorded along circumferential and longitudinal direction for these three dent depth, along with the recorded maximum strain value for 10% and 12% dent depth from Specimens SRP20D10 and SRP20D12 is presented in Table 4.3. The variation of maximum circumferential strain with dent depth along Lines 1 and 2 is presented graphically in Figure 4.42(a). Figure 4.42(b) shows graphically the effect of dent depth on maximum longitudinal strain along Lines 3 and 4.

The strain distributions along the circumferential, longitudinal, and oblique directions for specimen SSP20D8 are presented in Figure 4.13, 4.14, and 4.15 respectively. From these figures it can be concluded that the strain concentration along all directions of the pipe increases with the increase in dent depth. Maximum strain values along the circumferential, longitudinal, and oblique directions at different dent depth are presented in Table 4.4. The graphical representation of effect of dent depth on the maximum strain values along circumferential, longitudinal and oblique direction is presented in Figures 4.42(c), 4.42(d) and 4.42(e).

Specimen SDP20D8 was indented using three loading and unloading step to obtain data for various dent depth. The maximum strain values for these dent depth along the circumferential, longitudinal, and oblique direction are presented in Table 4.5. The graphical representation of effect of dent depth on the maximum strain values along circumferential, longitudinal, and oblique direction is presented in Figures 4.42(f), 4.42(g) and 4.42(h). From these figures it is found that with the increase in dent depth there is an increase in maximum strain values in all directions.

4.5 Conclusions

1. Based on the experimental study a number of conclusions are obtained. It should be noted that in the experimental program no strain gauges were installed underneath the indenter and hence, the conclusions regarding the strain distributions are limited to the region around the dent. The conclusions are as follows.
2. The load-deformation behavior of pipe subjected to denting load is significantly influenced by the internal pressure. The increase in internal pressure results in a significant increase in the denting load required to produce a certain amount of deformation.
3. The load-deformation behavior of pipe under lateral denting load is dependent on the size of the contact area between the pipe surface and the indenter. Higher load is required in case of indenter with higher contact area.
4. For rectangular shaped dents, strain concentration in the circumferential and longitudinal centerline is higher than the lines at the ends of the dent.

5. Strain distributions around a dent are significantly influenced by the level of internal pressure during indentation. For rectangular indenter, an increase in strain values in all direction was observed with the increase in internal pressure. For dome shaped indenter, this was same for longitudinal strains. However, no definite pattern was observed in circumferential and oblique strains for dome indenter.
6. Dent depth influences the strain concentrations and the strain values increase as the dent depth increase.
7. Strain distributions in the dented region are dependent on the shape of the dent. Maximum strain concentration was found in spherical indenter and the minimum strain concentration was found in case of dome indenter.

Table 4.1: Effect of internal pressure on the maximum strain values

Dent Depth (d/D) (%)	Internal Pressure p/p _y (%)	Max. Circumferential Strain	Max. Longitudinal Strain	Max. Oblique Strain
3	0	1.1%	1.0%	0.4%
	20	1.1%	1.2%	0.7%
	40	1.6%	1.3%	0.2%
6	0	1.2%	0.8%	1.1%
	20	2.1%	2.4%	0.8%
	40	1.6%	3.7%	0.9%
8	0	-1.0%	1.5%	0.9%
	20	2.6%	3.3%	1.5%
	40	1.6%	6.5%	0.5%

Table 4.2: Effect of indenter shape on the maximum strain values

Indenter Shape	Dent Depth (d/D) (%)	Max. Circumferential Strain	Max. Longitudinal Strain
Rectangle	8	4%	3.5%
Sphere		4%	5.7%
Dome		2.6%	3.3%

Table 4.3: Effect of dent depth for rectangular indenter

Dent Depth (d/D) (%)	Max. Circumferential Strain (Line 1)	Max. Circumferential Strain (Line 2)	Max. Longitudinal Strain (Line 3)	Max. Longitudinal Strain (Line 4)
2.5	1.5%	1.0%	1.1%	0.4%
5.2	1.7%	2.0%	2.2%	1.3%
8	4.0%	2.9%	3.5%	2.5%
10	3.8%	3.0%	4.5%	3.5%
12	4.1%	2.8%	4.8%	2.3%

Table 4.4: Effect of dent depth for spherical indenter

Dent Dept (d/D) (%)	Max. Circumferential Strain	Max. Longitudinal Strain	Max. Oblique Strain
3	2.2%	2.9%	2.3%
4.7	3.1%	4.2%	3.6%
6	3.8%	5.2%	4.8%
8	4.0%	5.7%	5.5%

Table 4.5: Effect of dent depth for dome indenter

Dent Dept (d/D) (%)	Max. Circumferential Strain	Max. Longitudinal Strain	Max. Oblique Strain
3	1.1%	1.2%	0.7%
6	2.0%	2.4%	0.8%
9	2.6%	3.3%	1.5%

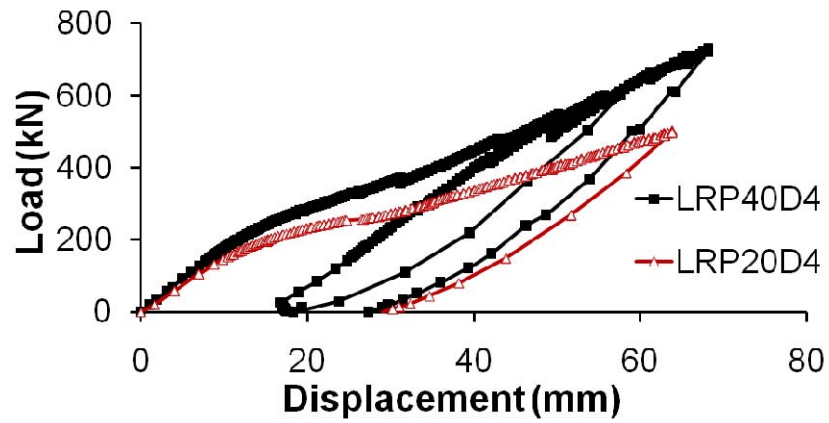


Figure 4.1: Effect of internal pressure on the load deformation behavior for a rectangular indenter.

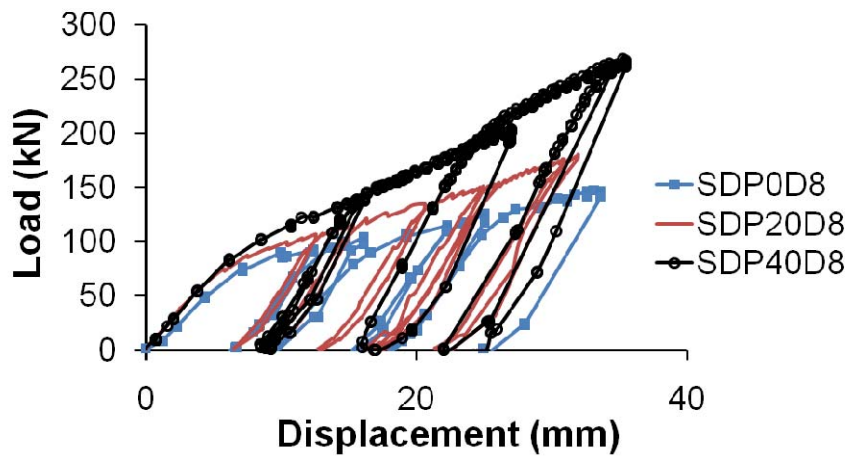


Figure 4.2: Effect of internal pressure on the load deformation behavior for a dome indenter.

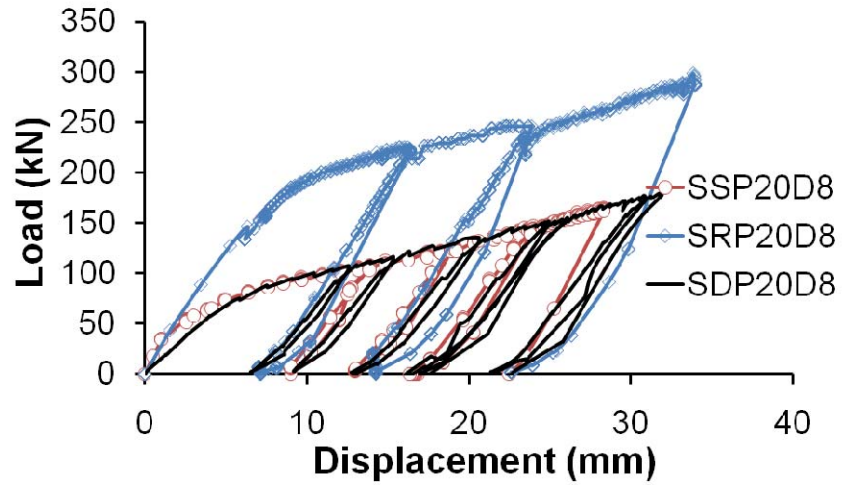


Figure 4.3: Effect of indenter shape on the load deformation behavior



Figure 4.4: Photograph of the dent in specimen LRP20D4

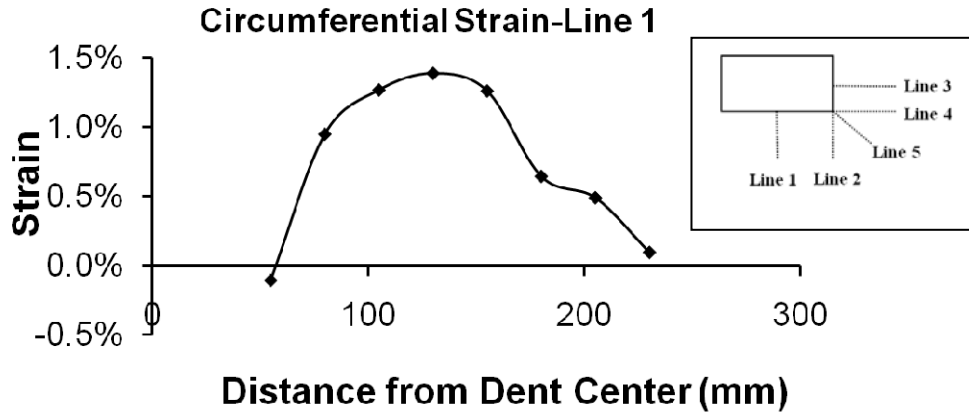


Figure 4.5(a): Circumferential strain distribution along Line 1 for specimen LRP20D4

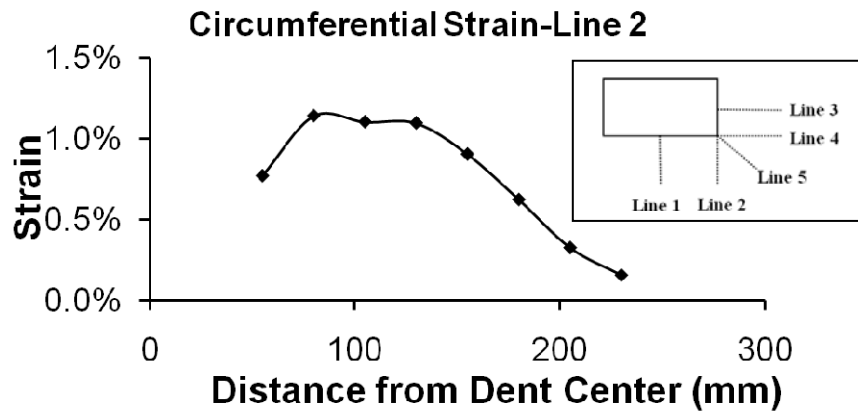


Figure 4.5(b): Circumferential strain distribution along Line 2 for specimen LRP20D4

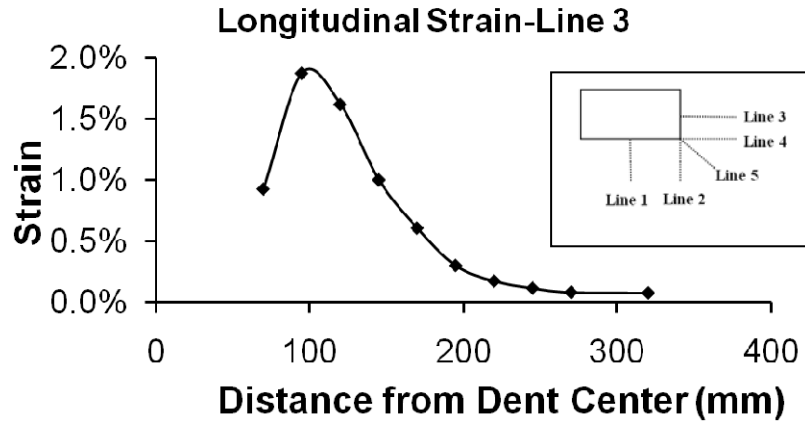


Figure 4.6(a): Longitudinal strain distribution along Line 3 for specimen LRP20D4

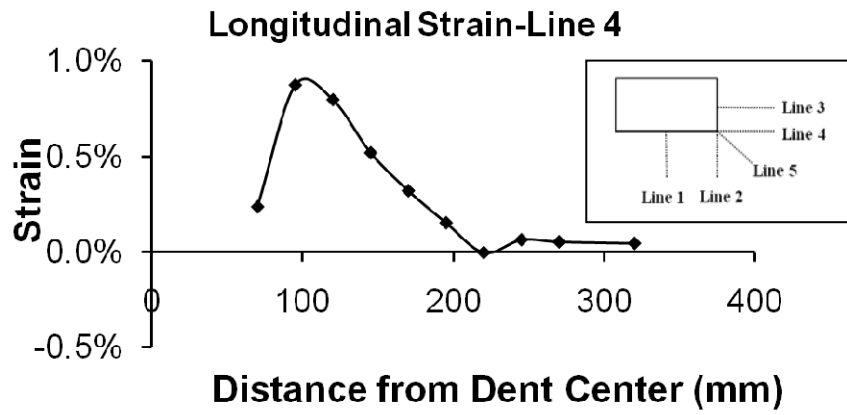


Figure 4.6(b): Longitudinal strain distribution along Line 4 for specimen LRP20D4

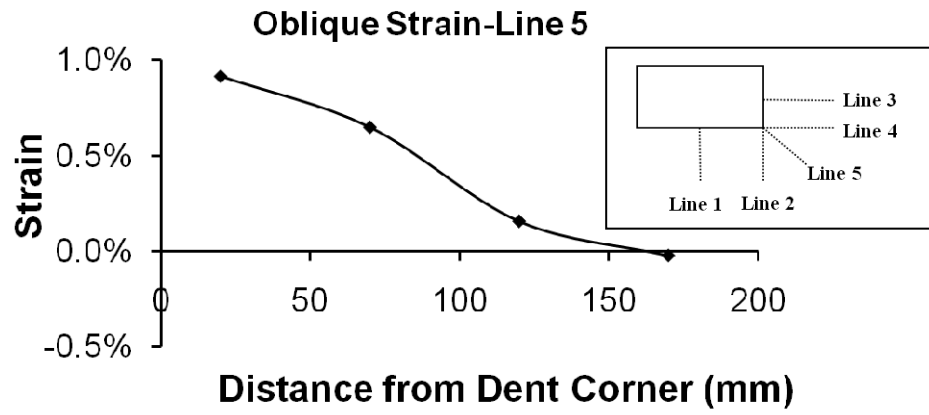


Figure 4.7: Strain distributiona along the Line 5 for specimen LRP20D4



Figure 4.8: Photograph of the dent in specimen LRP40D4

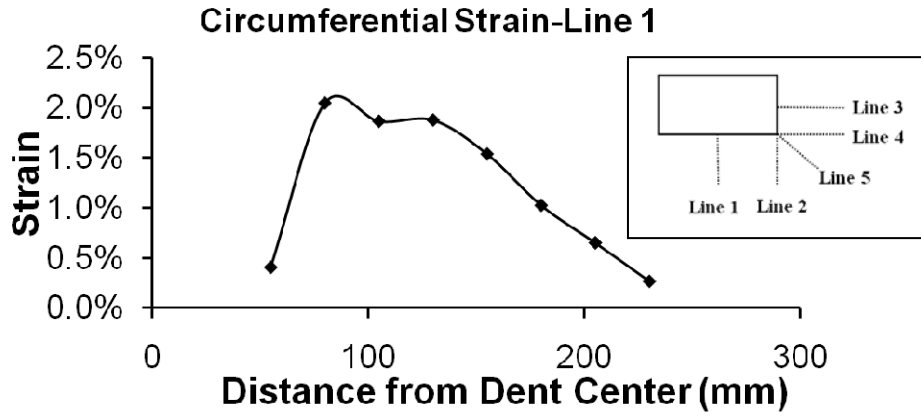


Figure 4.9(a): Circumferential strain distribution along Line 1 for specimen LRP40D4

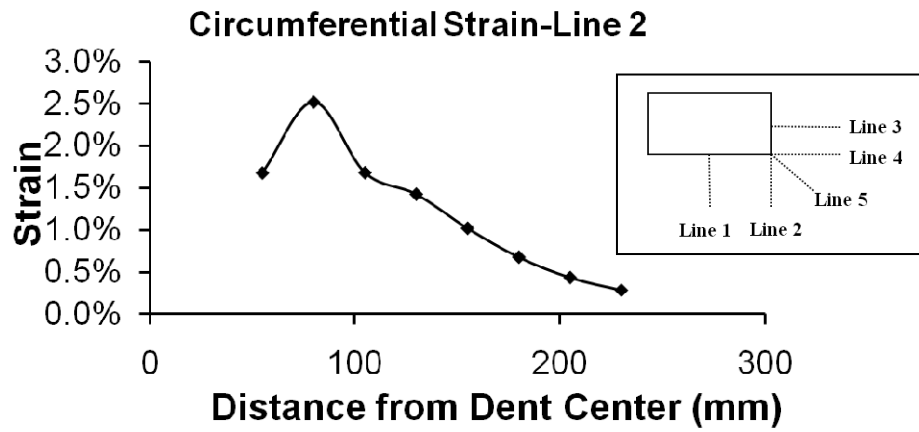


Figure 4.9(b): Circumferential strain distribution along Line 2 for specimen LRP40D4

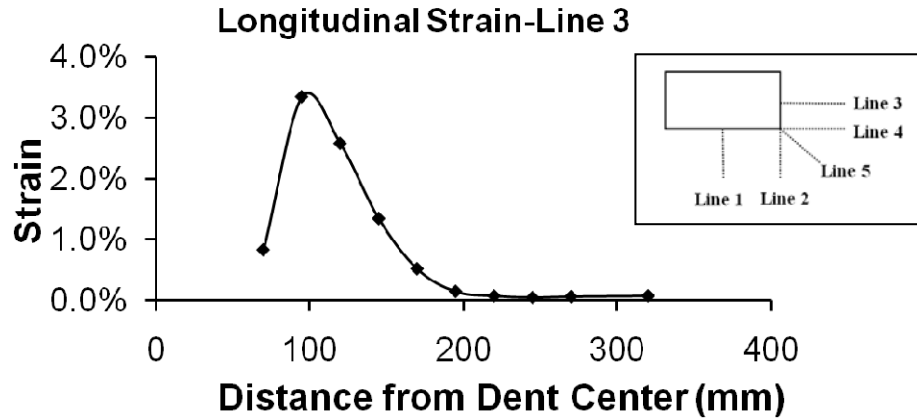


Figure 4.10(a): Longitudinal strain distribution along Line 3 for specimen LRP40D4

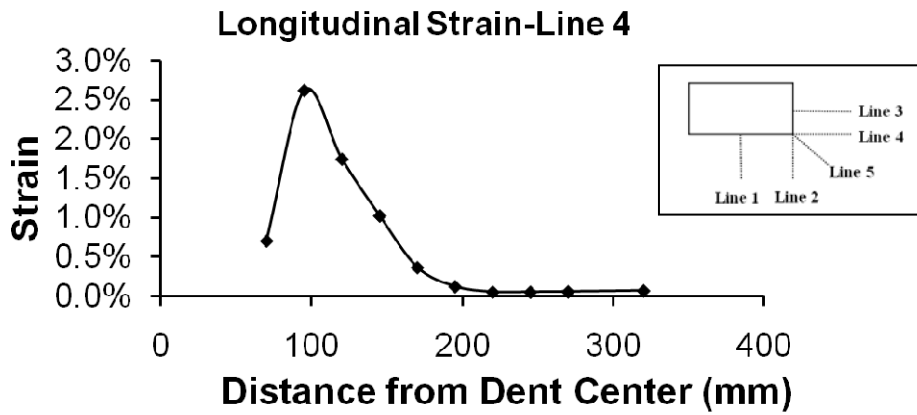


Figure 4.10(b): Longitudinal strain distribution along Line 4 for specimen LRP40D4

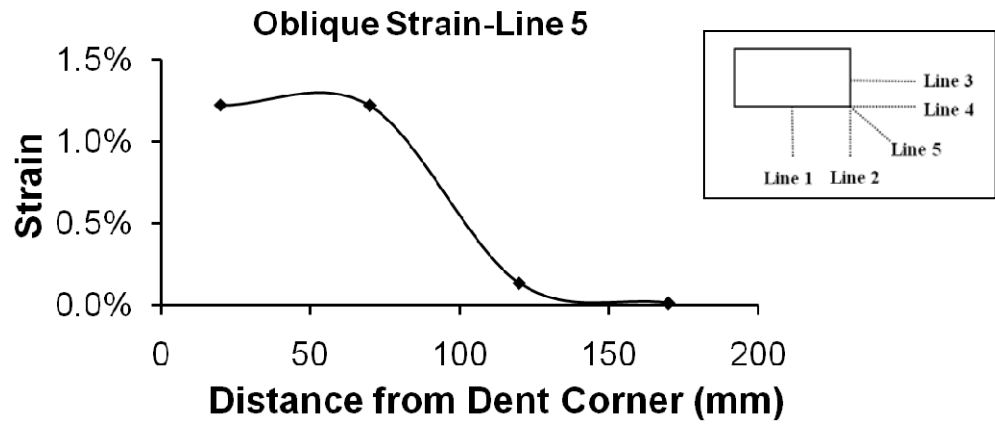


Figure 4.11: Strain distributiona along the Line 5 for specimen LRP40D4



Figure 4.12: Photograph of the dent in specimen SSP20D8

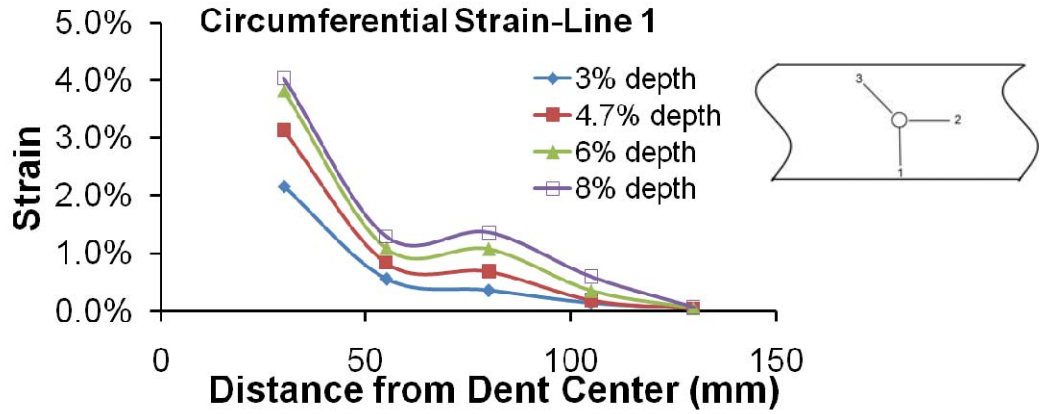


Figure 4.13: Circumferential strain distribution for specimen SSP20D8

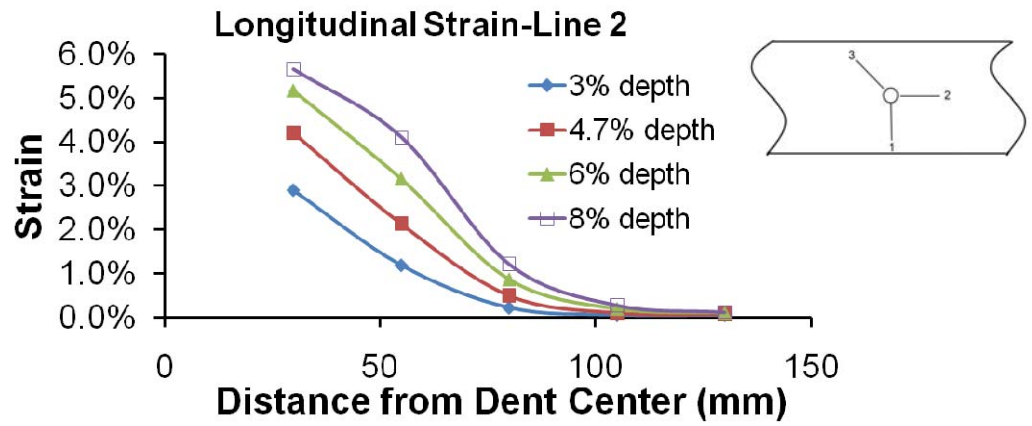


Figure 4.14: Longitudinal strain distribution for specimen SSP20D8

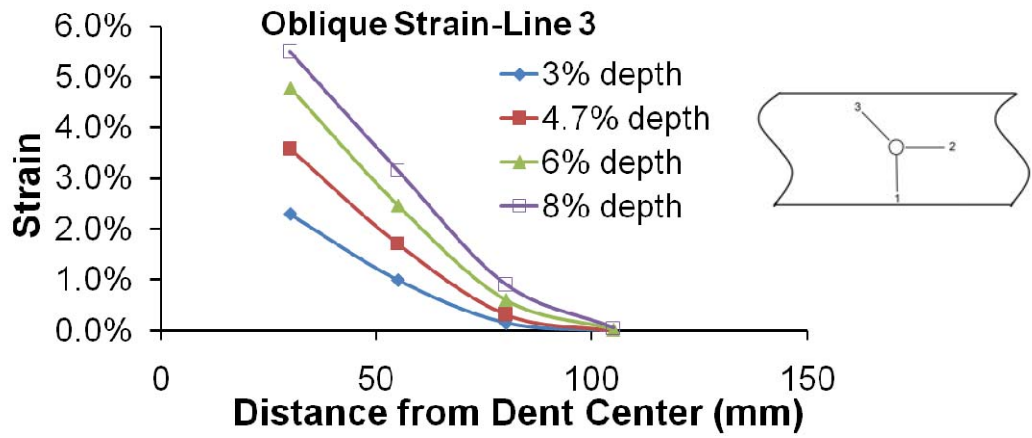


Figure 4.15: Oblique strain distribution for specimen SSP20D8



Figure 4.16: Photograph of the dent in specimen SRP20D10

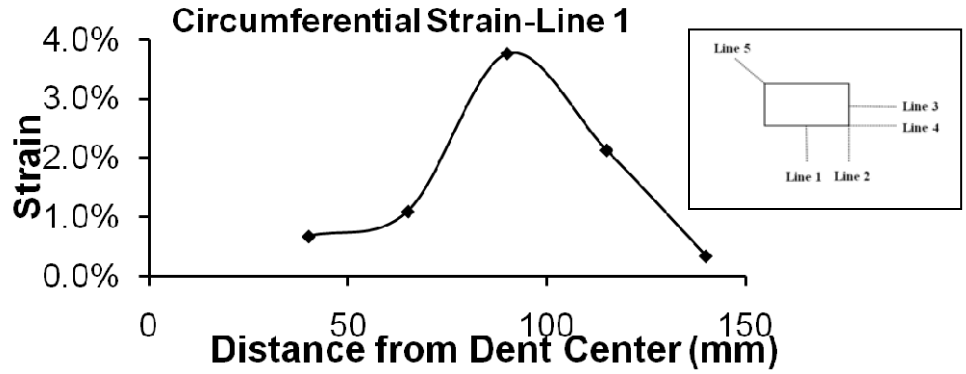


Figure 4.17(a): Circumferential strain distribution along Line 1 for specimen SRP20D10

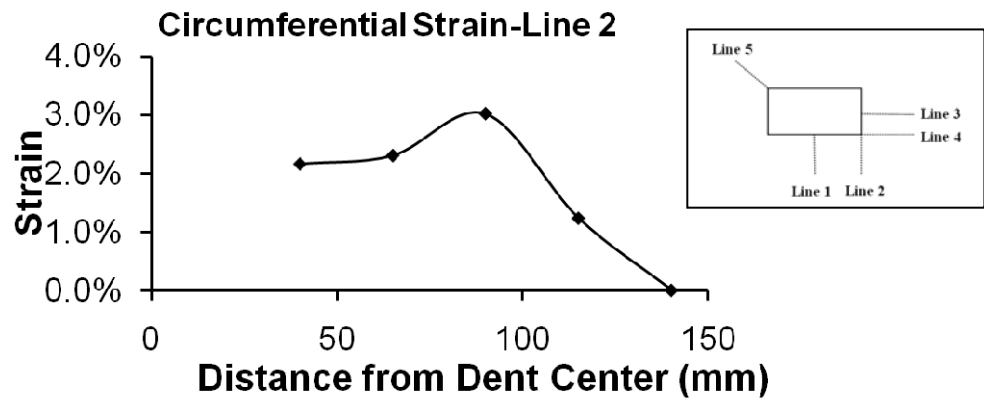


Figure 4.17(b): Circumferential strain distribution along Line 2 for specimen SRP20D10

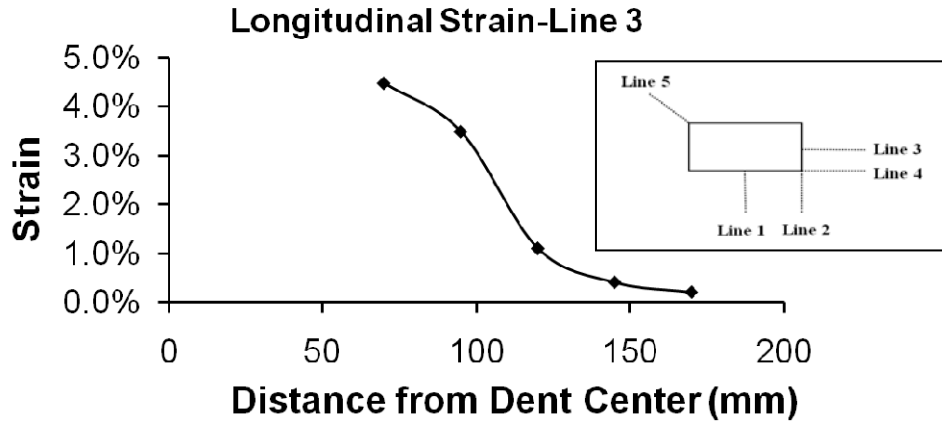


Figure 4.18(a): Longitudinal strain distribution along Line 3 for specimen SRP20D10

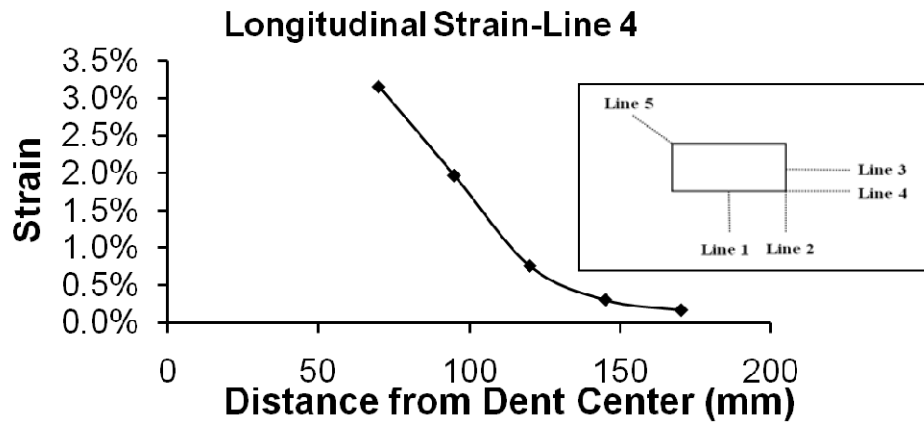


Figure 4.18(b): Longitudinal strain distribution along Line 4 for specimen SRP20D10

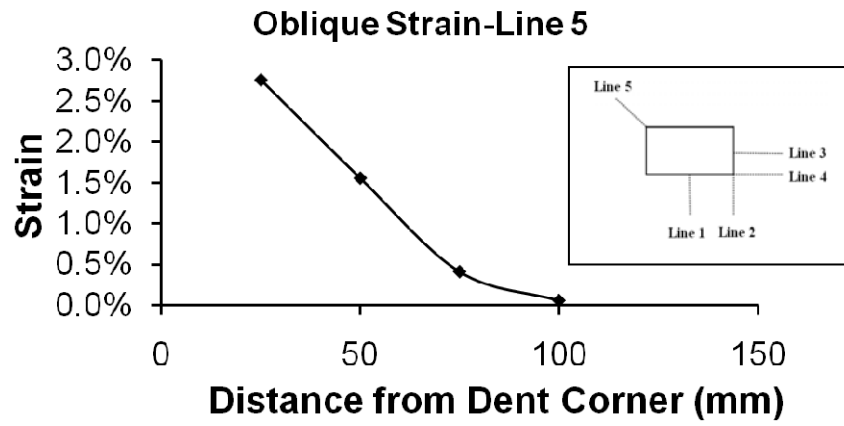


Figure 4.19: Strain distributiona along the Line 5 for specimen SRP20D10

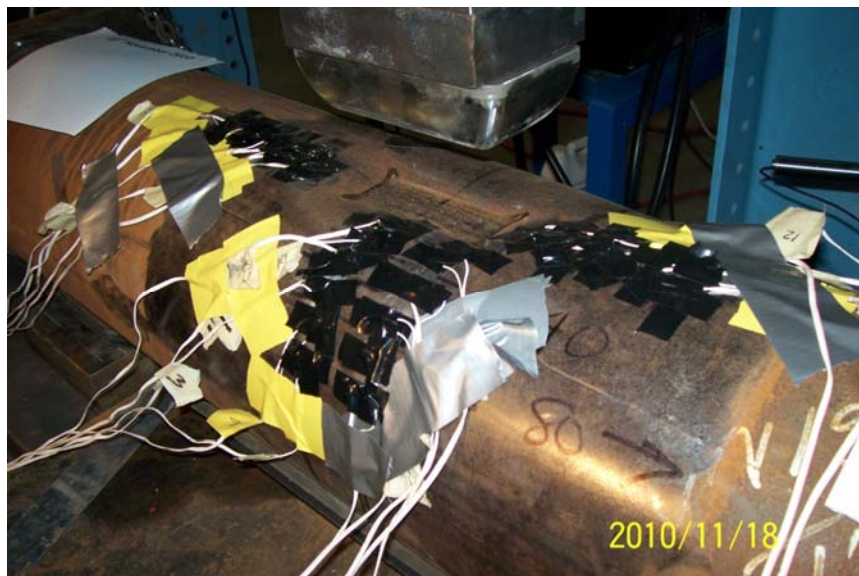


Figure 4.20: Photograph of the dent in specimen SRP20D8

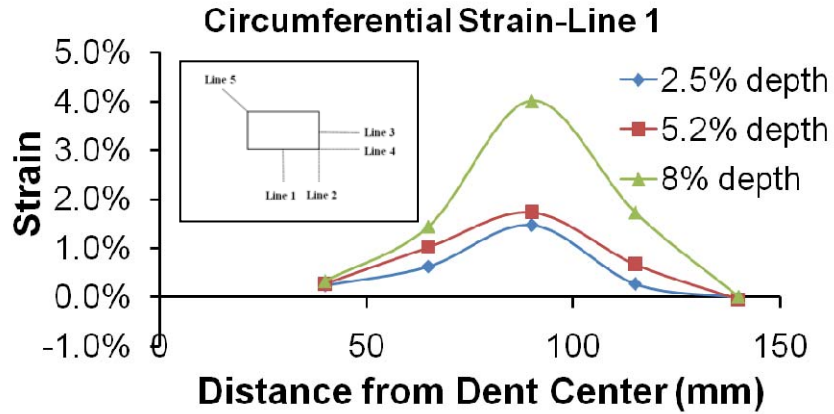


Figure 4.21(a): Circumferential strain distribution along Line 1 for specimen SRP20D8

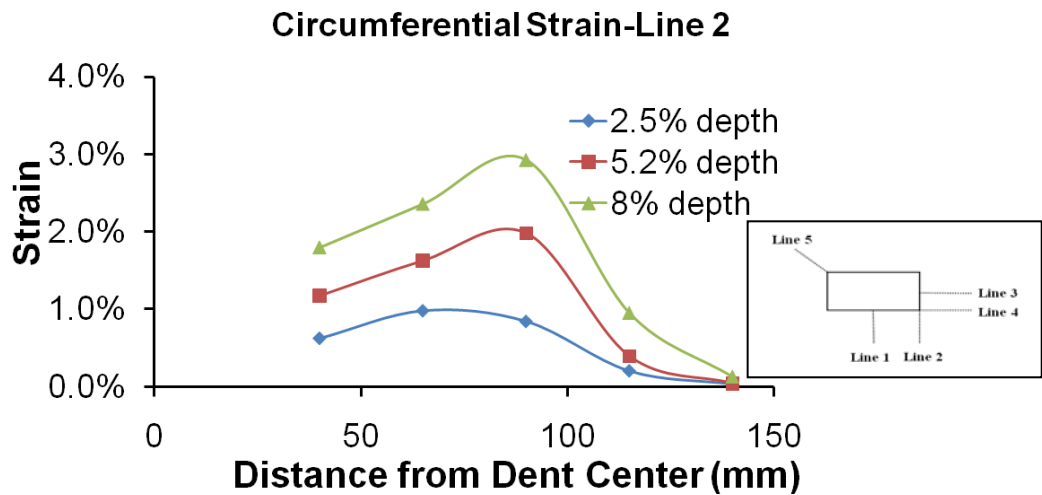


Figure 4.21(b): Circumferential strain distribution along Line 2 for specimen SRP20D8

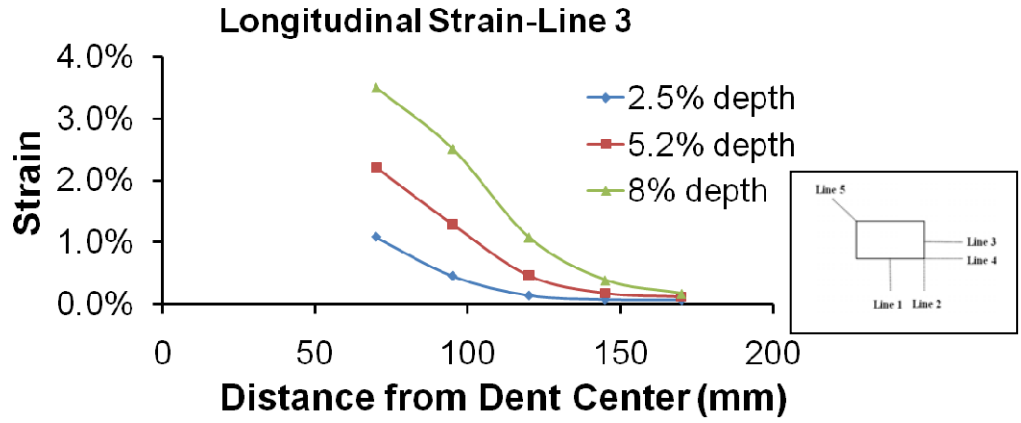


Figure 4.22(a): Longitudinal strain distribution along Line 3 for specimen SRP20D8

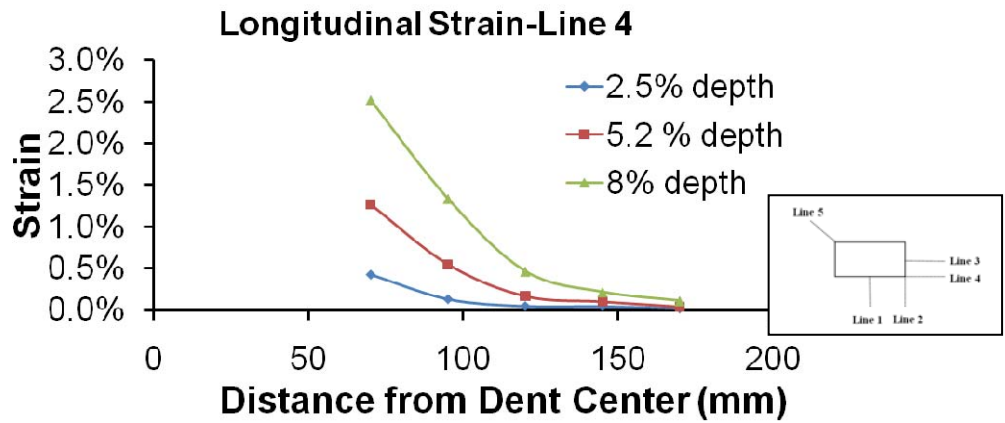


Figure 4.22(b): Longitudinal strain distribution along Line 4 for specimen SRP20D8



Figure 4.23: Photograph of the dent in specimen SRP20D12

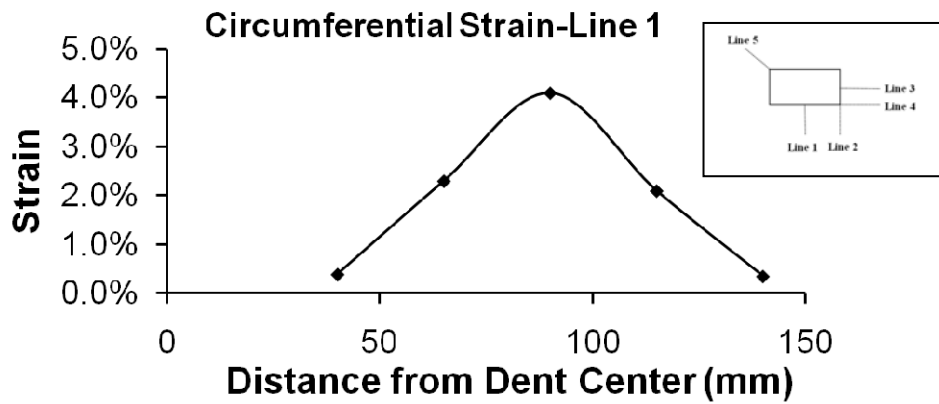


Figure 4.24(a): Circumferential strain distribution along Line 1 for specimen SRP20D12

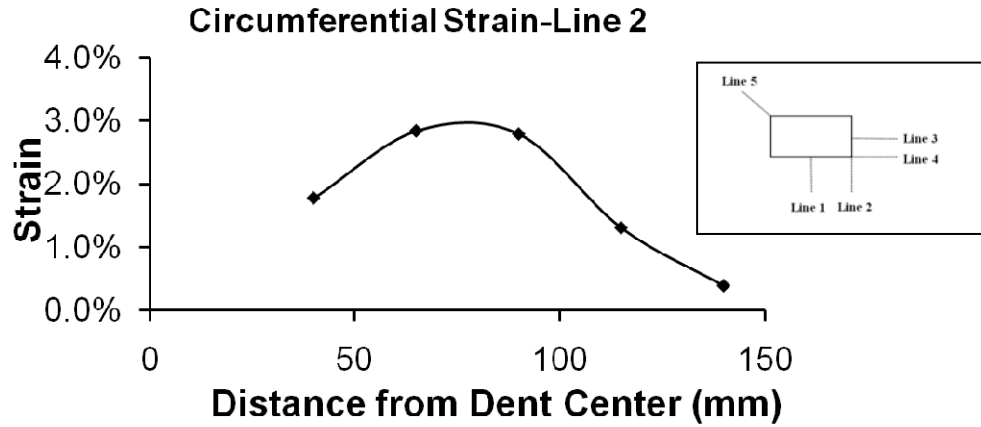


Figure 4.24(b): Circumferential strain distribution along Line 2 for specimen SRP20D12

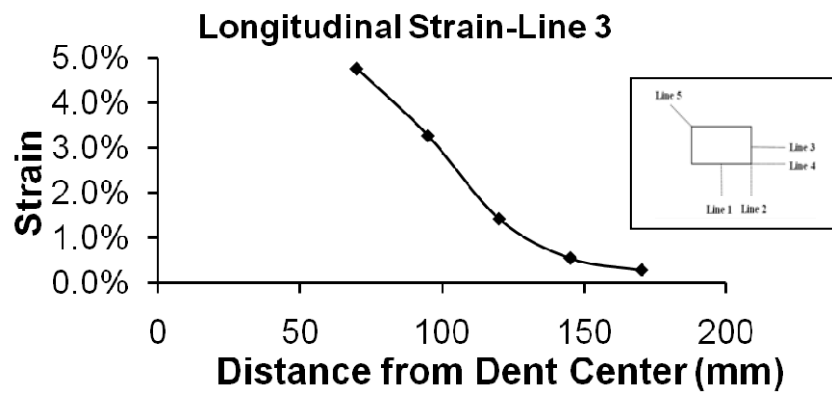


Figure 4.25(a): Longitudinal strain distribution along Line 3 for specimen SRP20D12

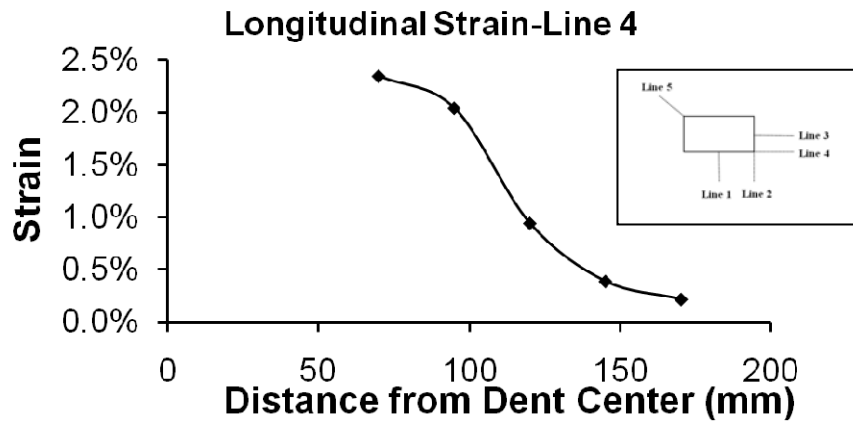


Figure 4.25(b): Longitudinal strain distribution along Line 4 for specimen SRP20D12



Figure 4.26: Photograph of the dent in specimen SDP0D8

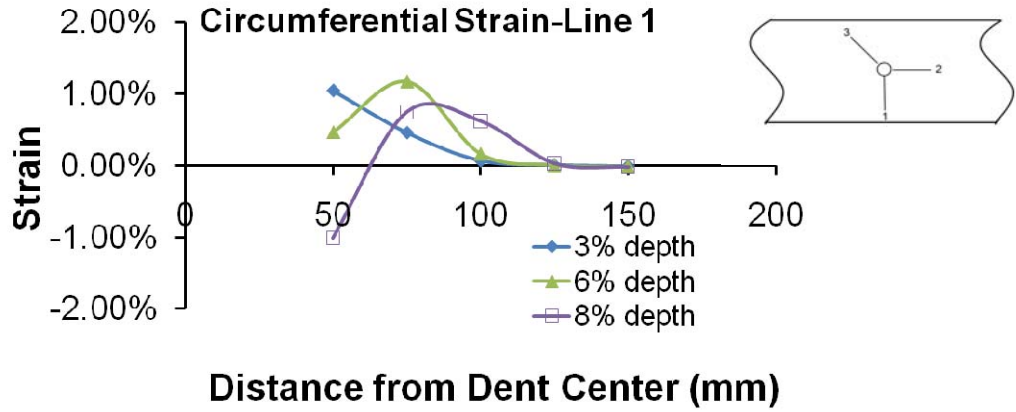


Figure 4.27: Circumferential strain distribution for specimen SDP0D8

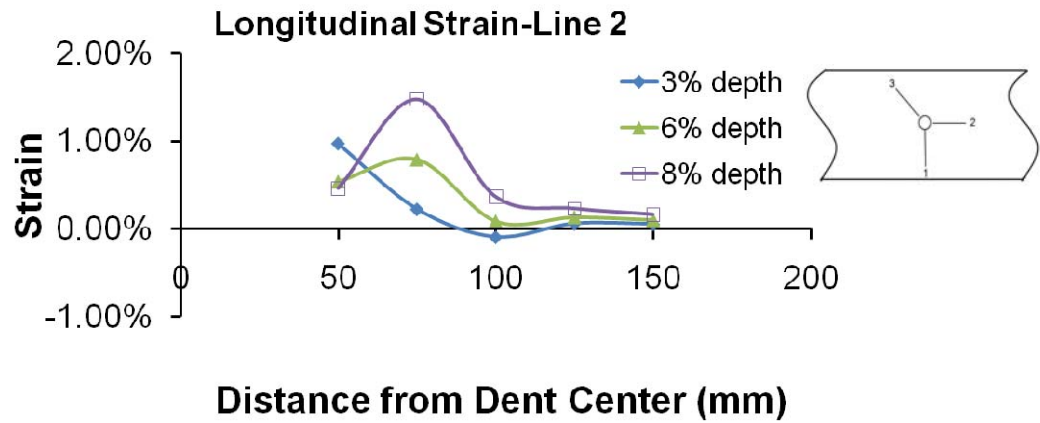


Figure 4.28: Longitudinal strain distribution for specimen SDP0D8

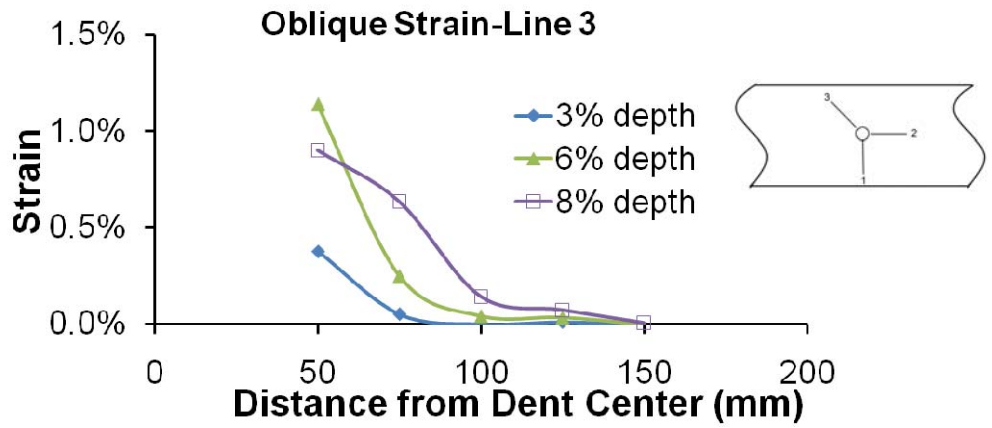


Figure 4.29: Oblique strain distribution for specimen SDP0D8



Figure 4.30: Photograph of the dent in specimen SDP20D8

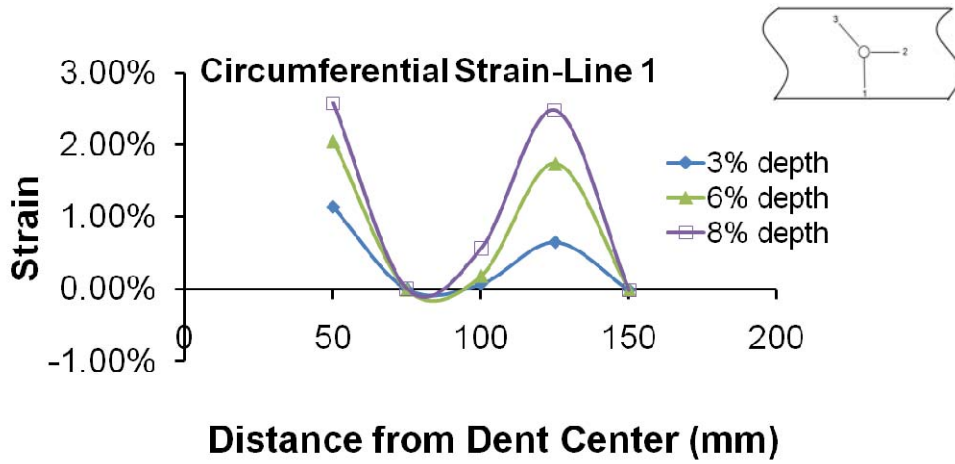


Figure 4.31: Circumferential strain distribution for specimen SDP20D8

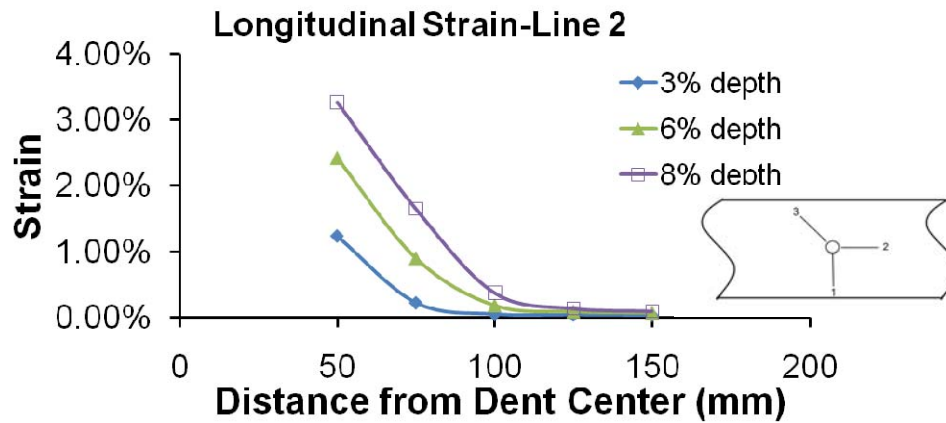


Figure 4.32: Longitudinal strain distribution for specimen SDP20D8

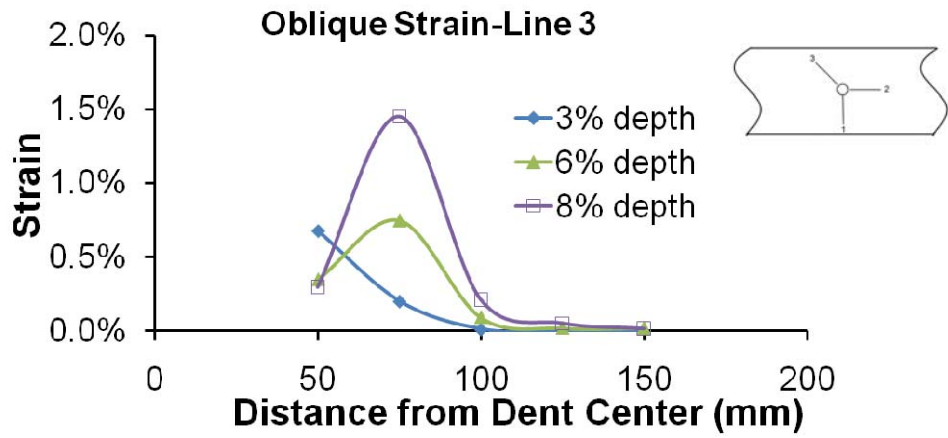


Figure 4.33: Oblique strain distribution for specimen SDP20D8



Figure 4.34: Photograph of the dent in specimen SDP40D8

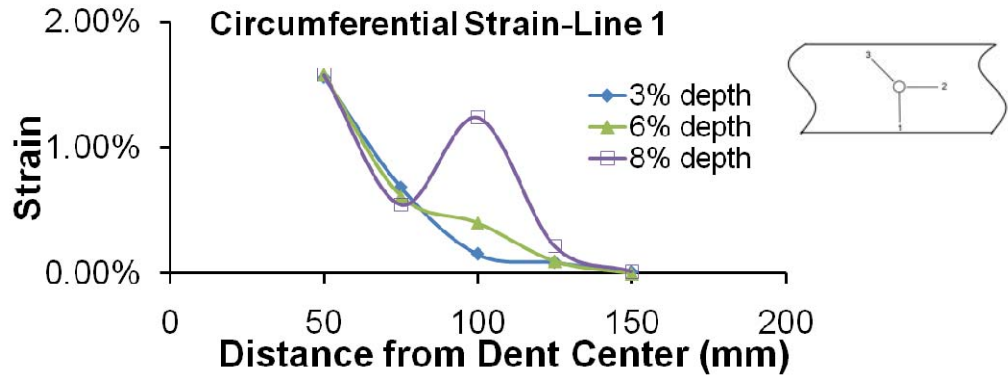


Figure 4.35: Circumferential strain distribution for specimen SDP40D8

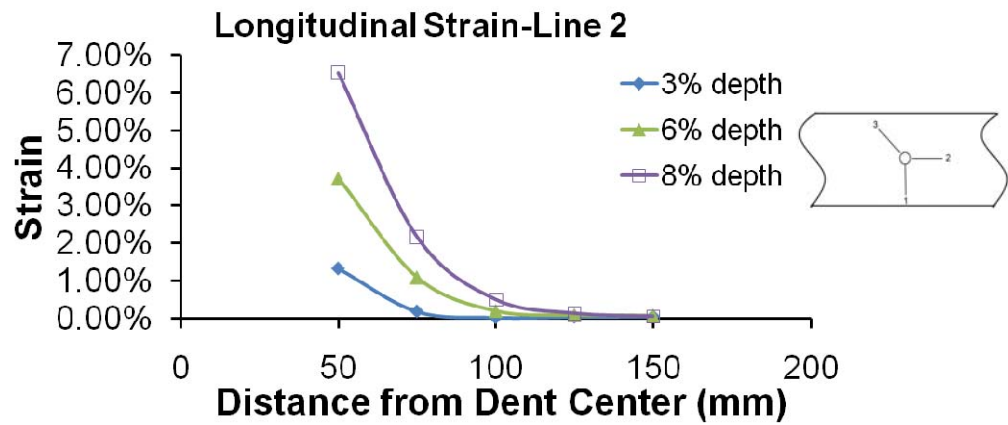


Figure 4.36: Longitudinal strain distribution for specimen SDP40D8

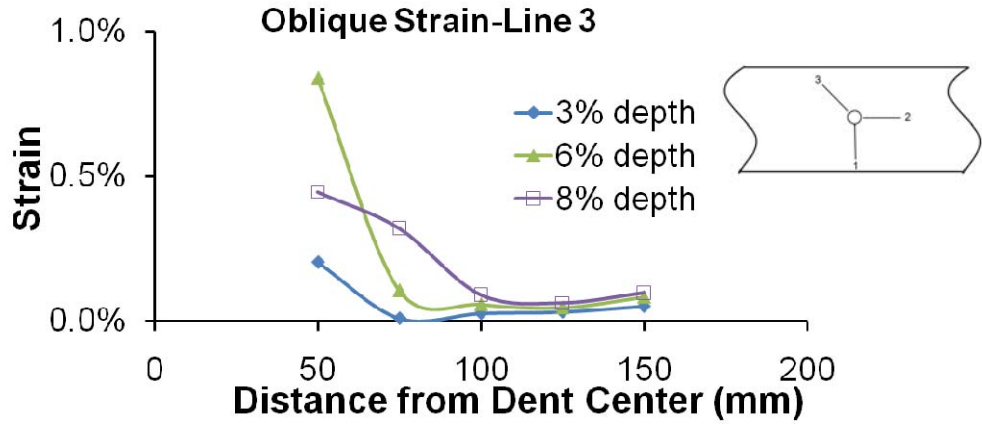


Figure 4.37: Oblique strain distribution for specimen SDP40D8

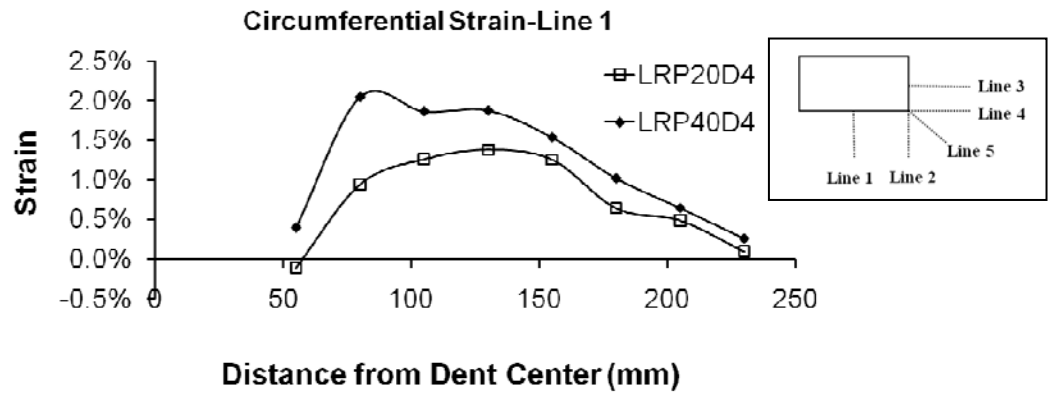


Figure 4.38(a): Effect of internal pressure on the circumferential strain distribution for rectangular indenter along Line 1

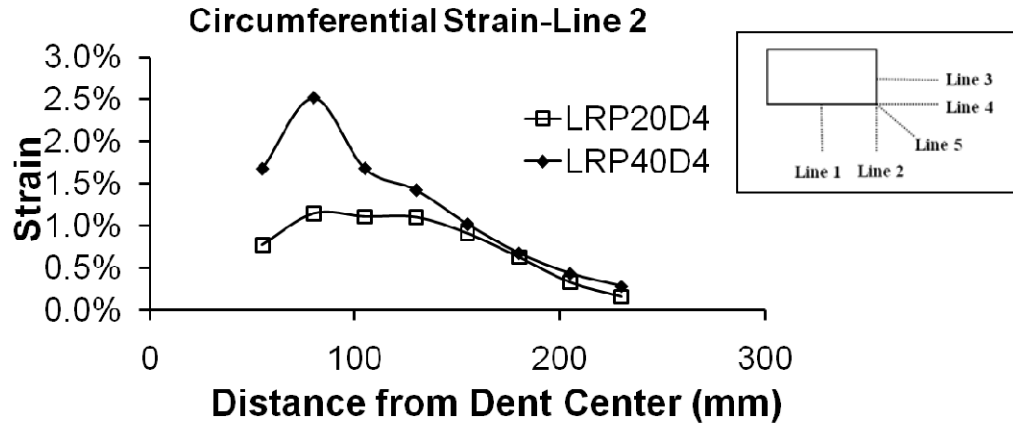


Figure 4.38(b): Effect of internal pressure on the circumferential strain distribution for rectangular indenter along Line 2

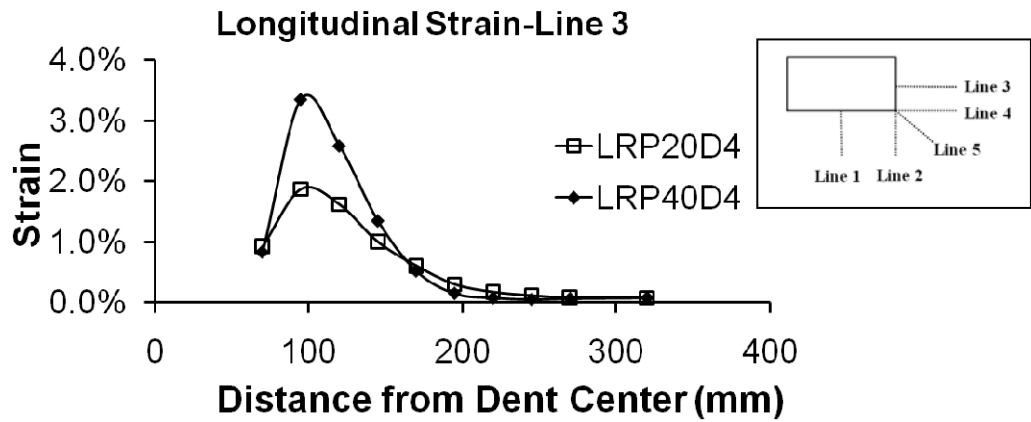


Figure 4.38(c): Effect of internal pressure on the longitudinal strain distribution for rectangular indenter along Line 3

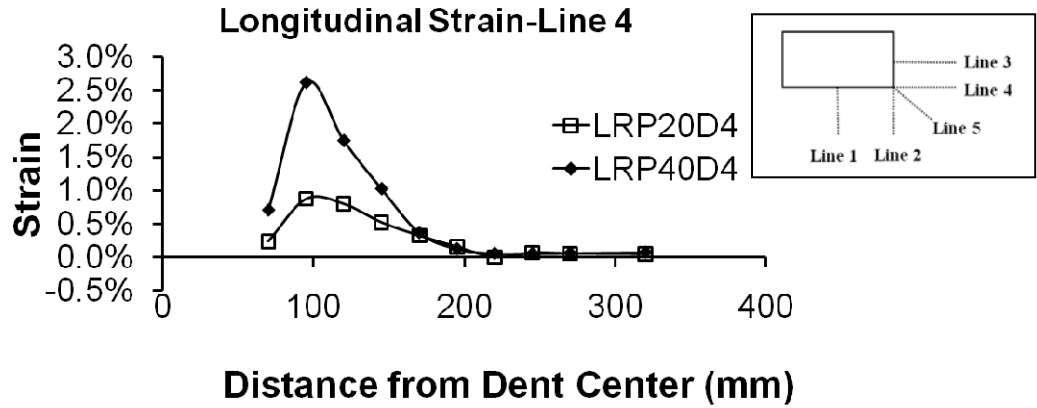


Figure 4.38(d): Effect of internal pressure on the longitudinal strain distribution for rectangular indenter along Line 4

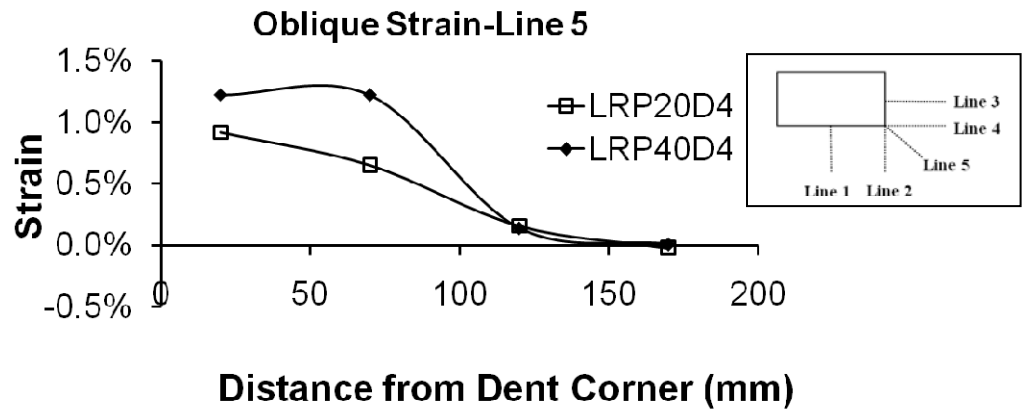


Figure 4.38(e): Effect of internal pressure on the oblique strain distribution for rectangular indenter along Line 5

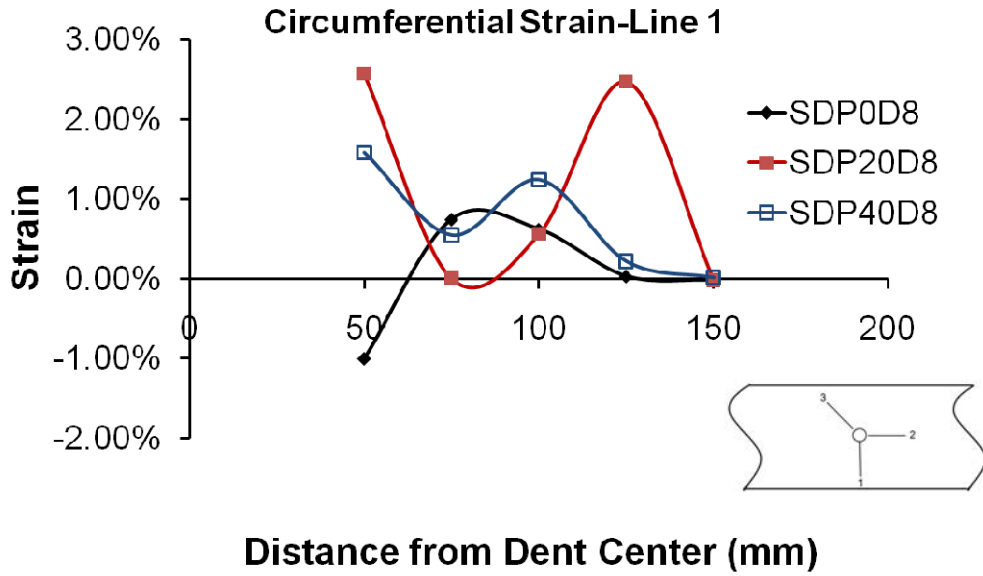


Figure 4.39(a): Effect of internal pressure on the circumferential strain distribution for dome indenter along Line 1

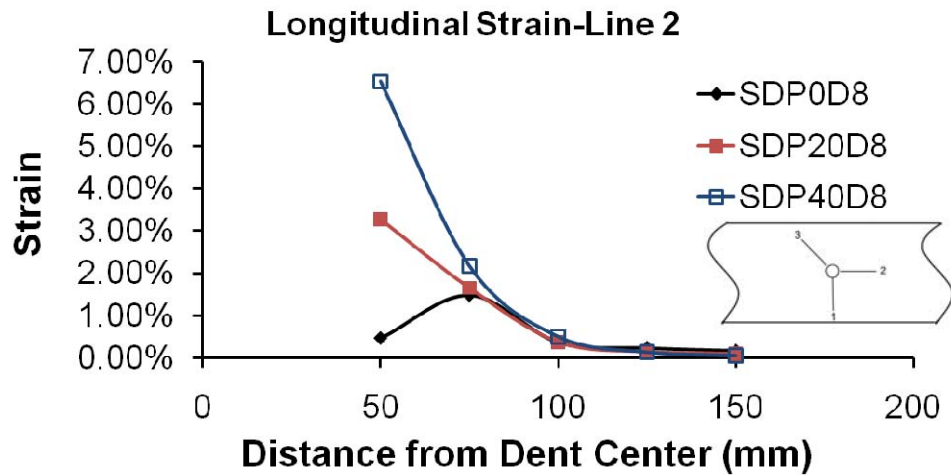


Figure 4.39(b): Effect of internal pressure on the longitudinal strain distribution for dome indenter along Line 2

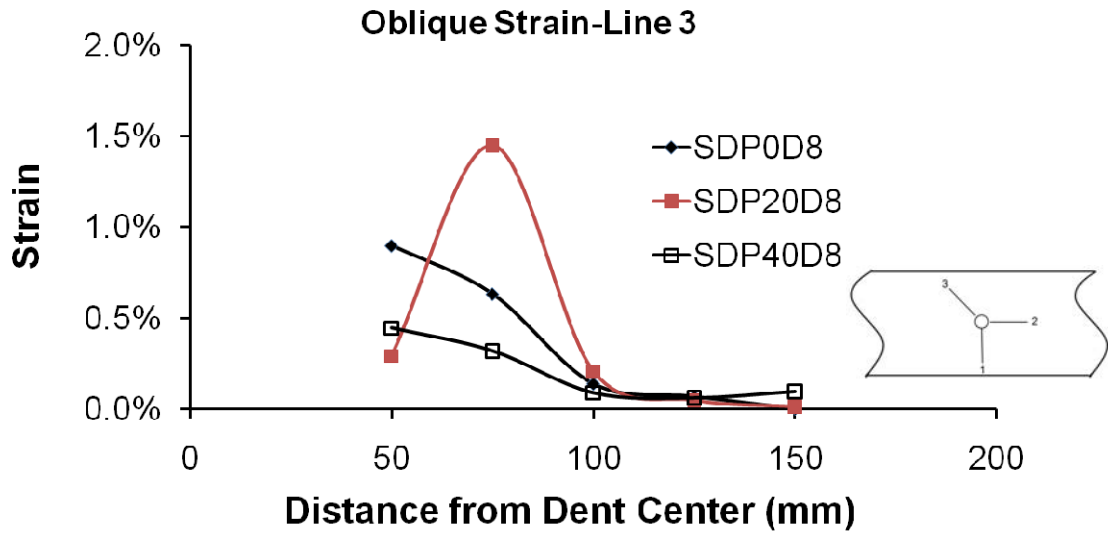


Figure 4.39(c): Effect of internal pressure on the oblique strain distribution for dome indenter along Line 3

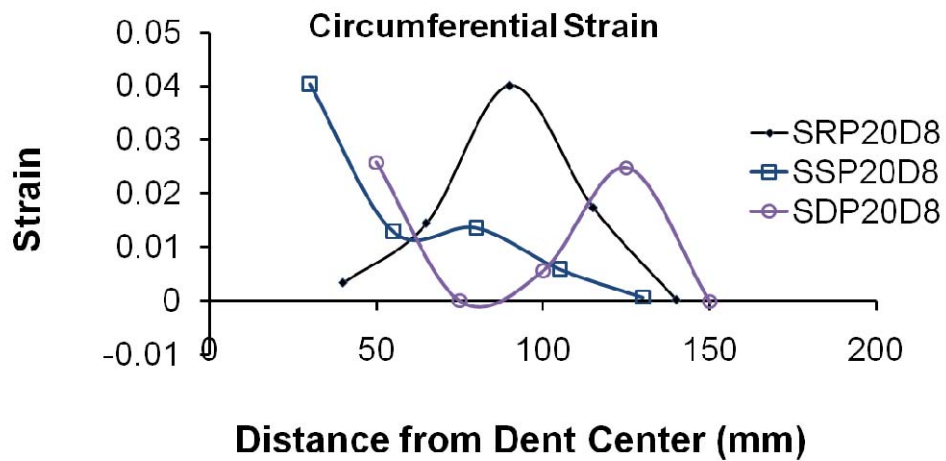


Figure 4.40(a): Effect of dent shape on circumferential strain distribution

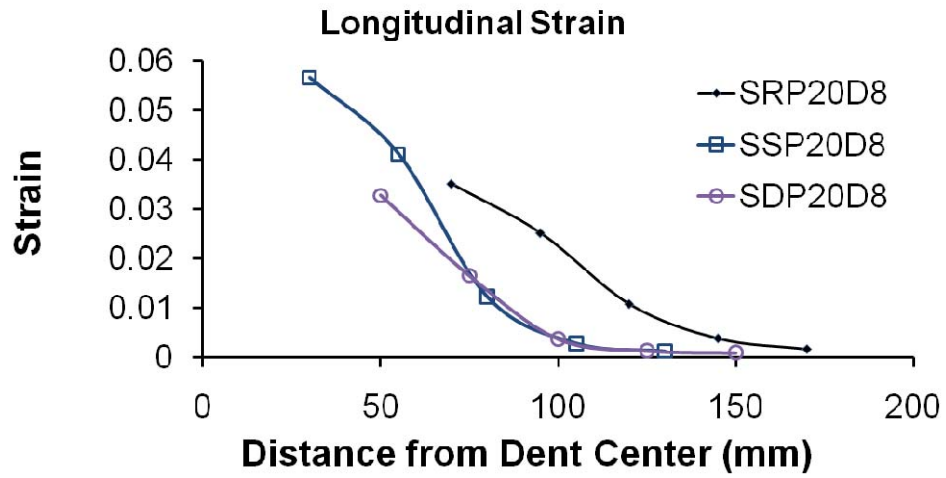


Figure 4.40(b): Effect of dent shape on longitudinal strain distribution

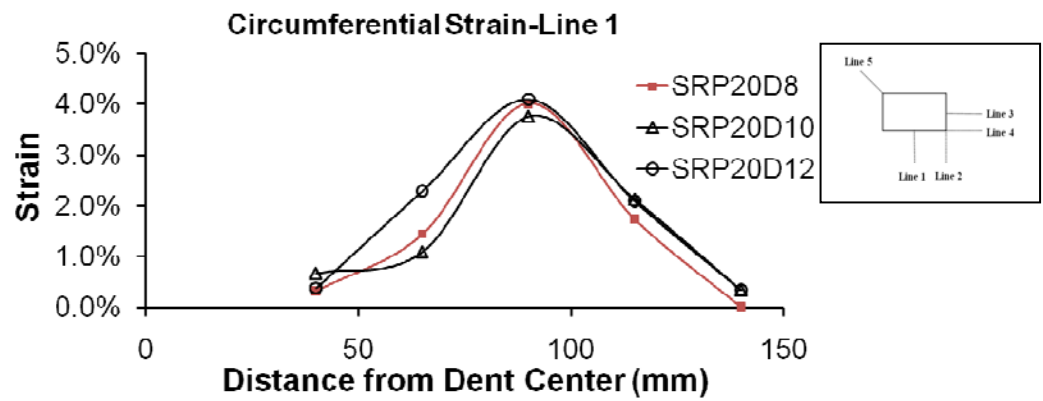


Figure 4.41(a): Effect of dent depth on circumferential strain distribution along Line 1

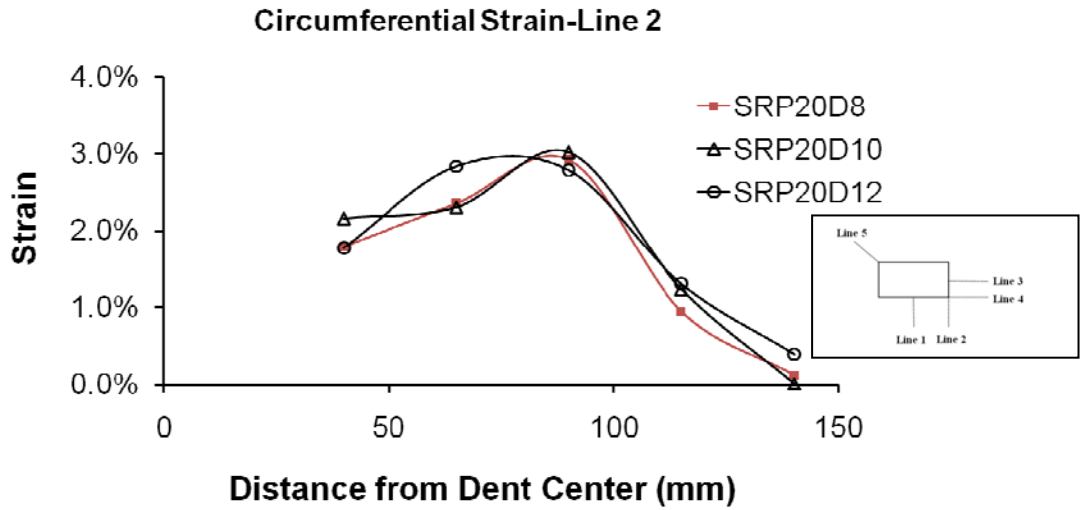


Figure 4.41(b): Effect of dent depth on circumferential strain distribution along Line 2

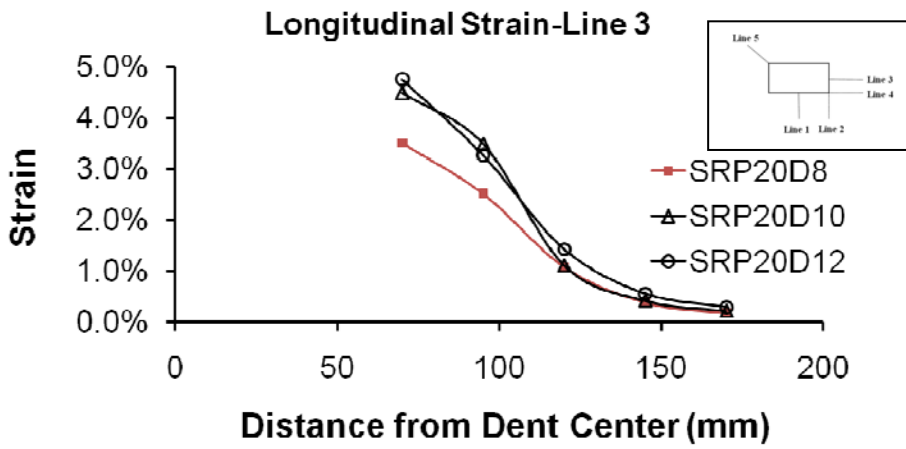


Figure 4.41(c): Effect of dent depth on longitudinal strain distribution along Line 3

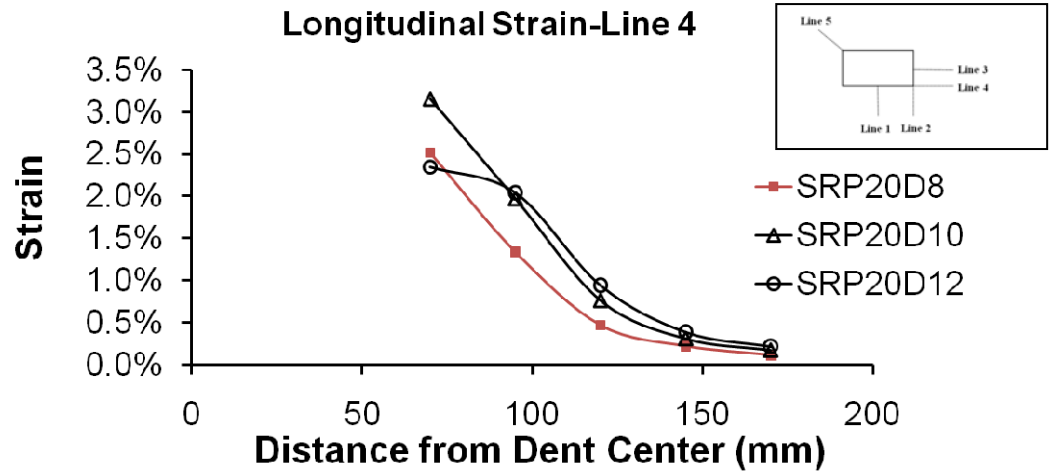


Figure 4.41(d): Effect of dent depth on longitudinal strain distribution along Line 4

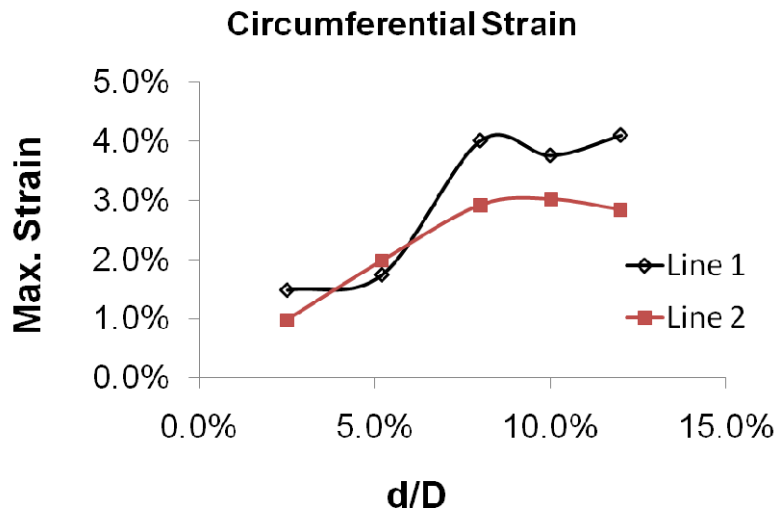


Figure 4.42(a): Effect of dent depth on the maximum circumferential strain for rectangular indenter

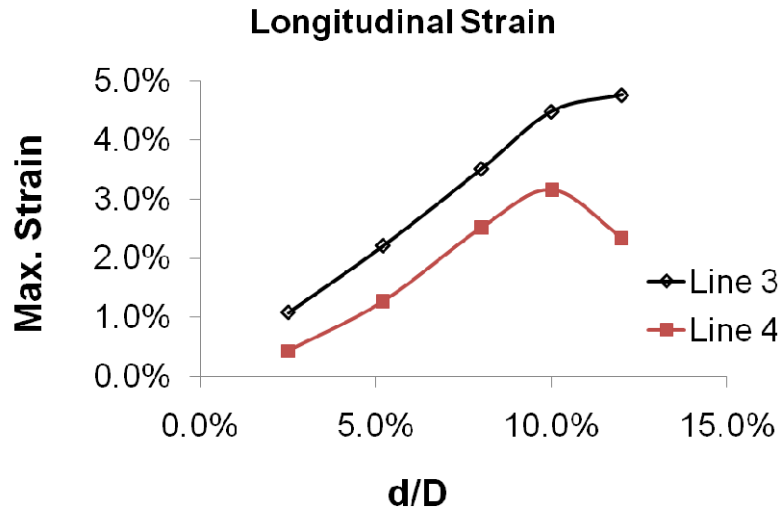


Figure 4.42(b): Effect of dent depth on the maximum longitudinal strain for rectangular indenter

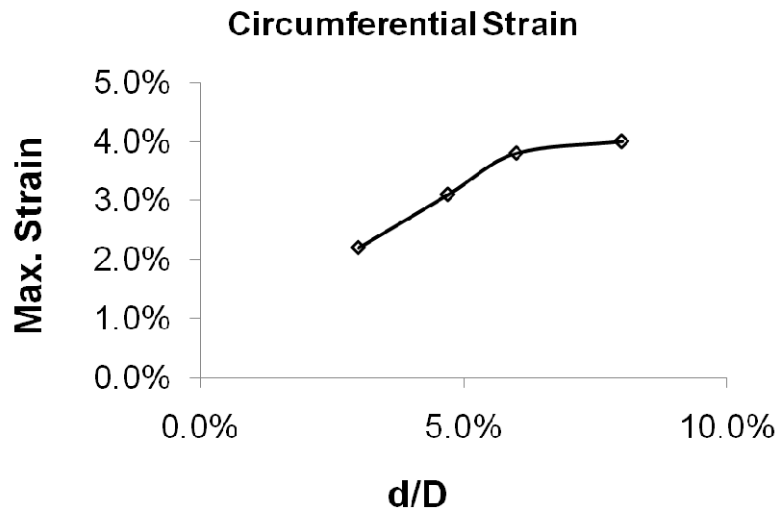


Figure 4.42(c): Effect of dent depth on the maximum circumferential strain for spherical indenter

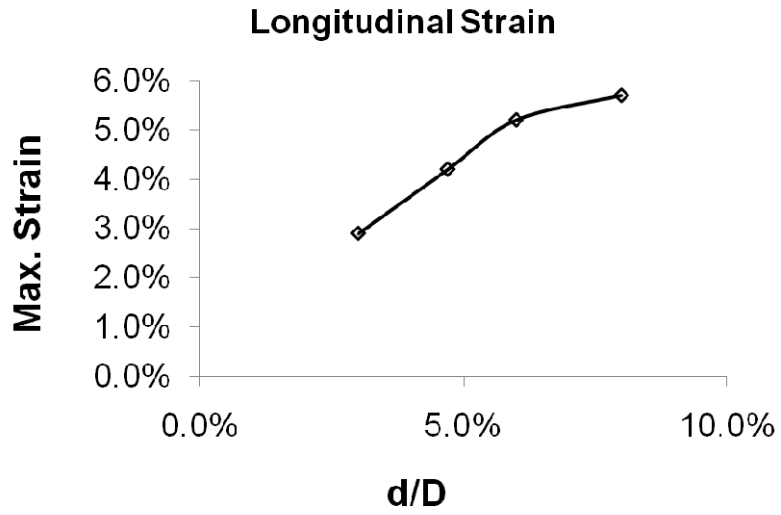


Figure 4.42(d): Effect of dent depth on the maximum longitudinal strain for spherical indenter

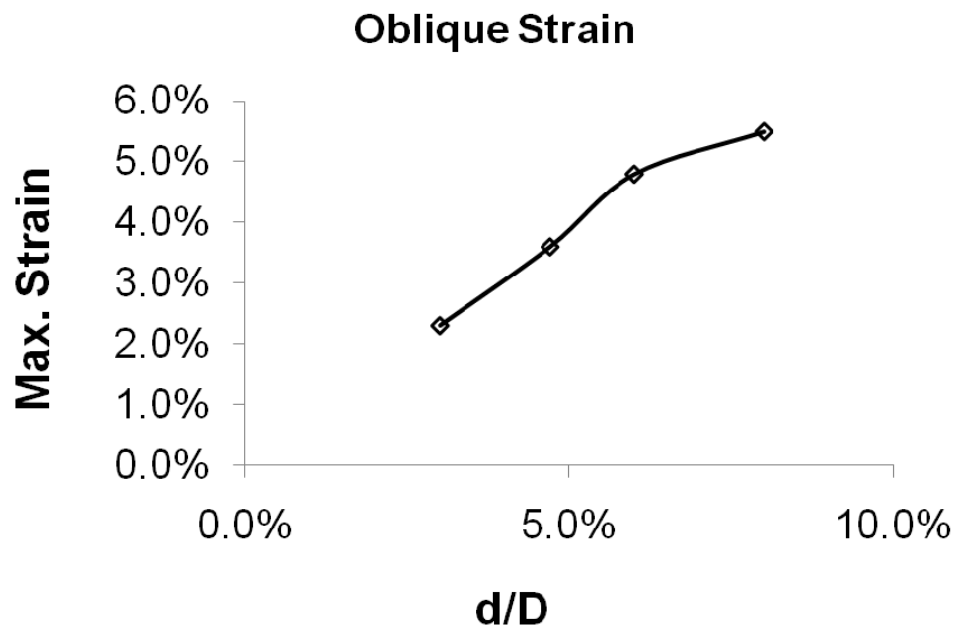


Figure 4.42(e): Effect of dent depth on the maximum oblique strain for spherical indenter

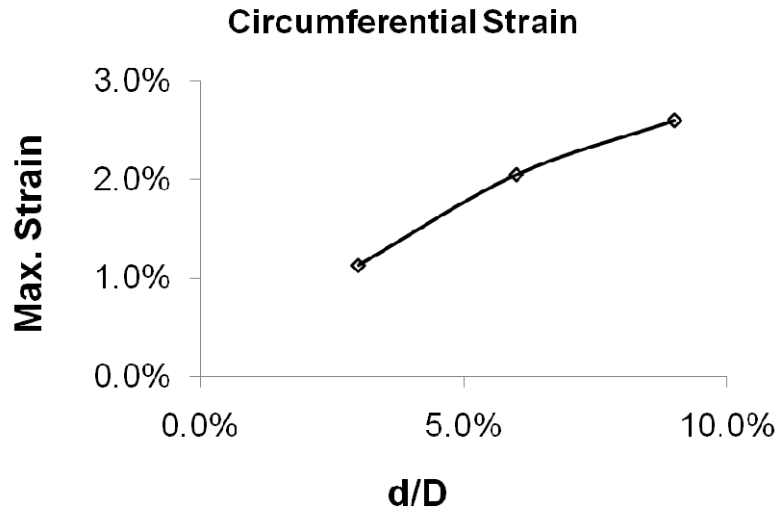


Figure 4.42(f): Effect of dent depth on the maximum circumferential strain for dome indenter

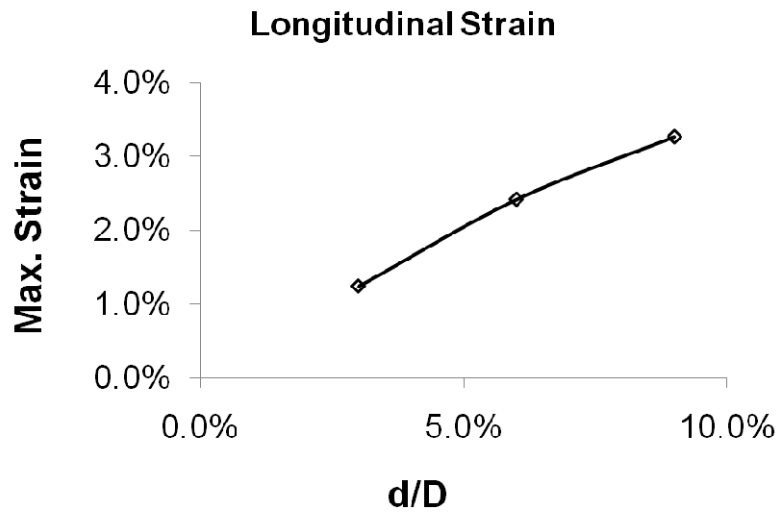


Figure 4.42(g): Effect of dent depth on the maximum longitudinal strain for dome indenter

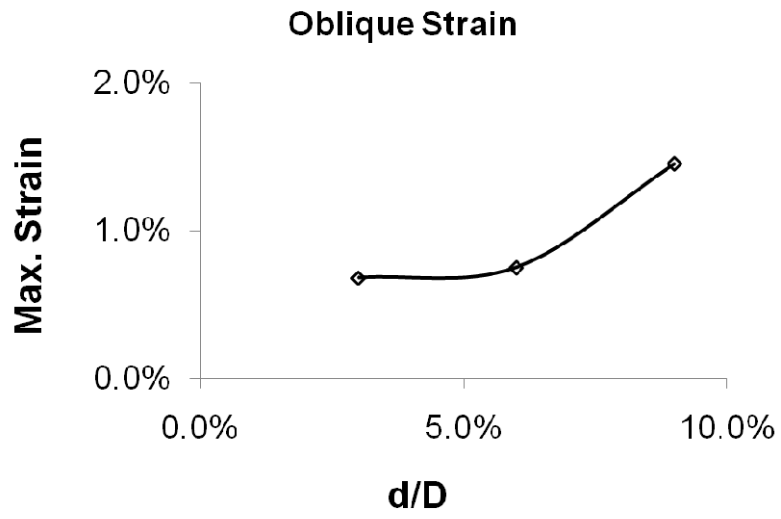


Figure 4.42(h): Effect of dent depth on the maximum oblique strain for dome indenter

CHAPTER 5

DEVELOPMENT OF FINITE ELEMENT MODEL

5.1 General

Experimental testing is the most conventional and reliable way to study the behavior of pipe while subjected to lateral denting load and other loads. However, it is impossible to obtain all the information required for a thorough understanding from the experimental data. For example, the information about the strain in the region underneath an indenter cannot be obtained directly from the tests as the strain gauges under the indenter fails as soon as the load is applied. Experimental testing is expensive and time consuming. It is also not viable to consider full-scale tests for a wide range of test parameters. An alternative method to study and predict the behavior of any structural element is to use numerical tools such as finite element analysis (FEA) method. With the advancement of computing technology finite element method has become more popular. Therefore, the purpose of the chapter is to illustrate the development of a numerical model and validate it with the available test results.

In this study, numerical modeling technique considering both material and geometric nonlinearity was employed to simulate the behavior of the test specimens. Commercially available general purpose finite element analysis code, ABAQUS/Standard version 6.6.9 distributed by SIMULIA (SIMULIA, 2008) was used to model the pipe behavior. The selection of this code to model the behavior of pipe under lateral denting load was based on several reasons. First of all, this code has been used successfully in the past to model the behavior of pipe under denting load by other researchers (Karamanos and Andreadakis (2006), Hertz-Clemens (2006) and Gresnigt et al. (2007)). It has a built-in

elasto-plastic isotropic hardening material model which is suitable for modeling pipe used in the experimental study. It offers both the load control and the displacement control capabilities to simulate the test loads used in this study. It also offers finite sliding formation with strict master-and-slave algorithm for modeling the contact interaction.

The objectives of developing the finite element model are to (i) predict the behavior of the pipe under lateral denting load, (ii) obtain the strain in the region underneath the indenter (load application location), and (iii) conduct a detailed parametric study for various indenter shapes, internal pressures, and dent depths for developing a detail guideline on the strain introduced in the dented region of the pipeline.

5.2 Finite Element Model

5.2.1 Element Selection

Selection of an appropriate element is a critical one for any finite element analysis. For development of the finite element model, four-node quadrilateral doubly symmetric general purpose shell element (S4R) with reduced integration was chosen. Each node of this shell element has three translational and three rotational degrees of freedom. It considers finite membrane strain formulation and is able to account for the effect of plate thinning as a function of in-plane deformation. For this shell element, membrane strain follow finite strain formulation, whereas, bending strain are assumed based on small strain assumptions. However strain normal to the shell thickness is assumed to be constant throughout the shell thickness. Seven section points was chosen through the thickness of the element.

Three different types of end caps were used to study the effect of the shape of the end cap on the behavior of the pipe under denting load. The end caps chosen were hemispherical, flat and cone. For modeling of the hemispherical end cap, S4R element was used. Another shell element STRI3 was used to model the flat and cone shaped end caps of the test specimens. The STRI3 is a three node triangular facet thin shell element. The thin shell element means that the transverse shear flexibility is negligible. The element is a flat element, so the initial curvature is ignored. This element has six degrees of freedom at all nodes. This element can provide arbitrary large rotations but allows only small strains. The change in thickness with deformation is ignored in this element. Since the end plates in test specimens did not experienced inelastic deformation, choice of this element for modeling the end plates is reasonable. Eight node linear brick element C3D8 was used to model the indenter and the support plates.

5.2.2 Symmetry of the Model

Only one half of the pipe was modeled to avail the opportunity of symmetry in the pipe geometry, loading and boundary conditions, which saved computational effort. A full-scale model of the pipe was also developed to ensure that the results obtained using half symmetric model is not different. Figure 5.1(a) shows a full pipe model. The pipe geometry and boundary conditions at the plane of symmetry are shown in half pipe model (Figure 5.1(b)). From the comparison of the result of the two models it was found that the half symmetric model produces exactly same results as the full-scale model. Comparison of load-deformation behavior of the full scale model and half symmetric model is shown in Figure 5.2. Figure 5.3 shows the comparison of the circumferential strain distribution

between full scale and half scale models. These strains were obtained from outer surface of the pipe.

5.2.3 End Caps

In the tests, end caps of two different shapes were used to hold the internal pressure. These shapes were: flat and hemispherical. For 762 mm (30 in) diameter pipe specimens hemispherical dome shaped end cap was used. Flat plates were used as end caps for 274 mm (10 in) diameter pipe specimens. In the FE model, three types of end cap were used to analyze the difference in behavior of the model with different types of end caps and to determine appropriate shape of the end cap which is most reasonable for simulating the test condition. The shapes of the end caps used in the study were as follows

1. Flat end cap- the easiest way to mode the end cap
2. Cone shaped end cap
3. Hemispherical end cap-the most difficult one for modeling

The shapes of end cap used in this study are shown in Figure 5.4. FE model of 762 mm diameter pipe was used to study the effect of different shapes of end caps. For all the cases, the end caps were modeled as 15 mm thick perfectly elastic part having Young's modulus (E) of 200 GPa since the end caps in test specimens did not experience plastic deformation. From the analysis, it was observed that there is not any mentionable difference in the load-displacement behavior of the pipe for various shapes of end cap chosen (Figure 5.5). Hence it was decided to use a hemispherical end cap for 762 mm diameter pipe model and a flat plate end cap for 274 mm diameter pipe model for further

analysis to simulate the test conditions exactly. Nonetheless, the finally end cap types chosen for parametric study are same as those used in test specimens.

5.2.4 Support Conditions

The behavior of the model with different types of support conditions were studied to simulate the support condition as closely as possible to the experimental setup and also to determine the support conditions which is more efficient in terms of processing time. In the full scale tests the pipe was resting on a flat support plane, made of steel plate in such a way that there was contact between the pipe and the flat plane in three locations, one at mid-span and other two at two ends of the specimen. The effect of support conditions were studied using a 762 mm diameter pipe model. For 762 mm diameter test specimens length of the mid-span contact portion was 500 mm and the length on ends were 280 mm each.

In the analysis, first the end support was modeled as contact interaction between the pipe and the support plane and three different types of supports were used for the mid-span, and these were as follows.

1. Pin
2. Roller
3. Contact interaction between pipe and support plane.

The pin and roller boundary conditions were applied in a portion of the pipe which makes an internal angle of 18 degree (Figure 5.6). The length of the portion was chosen similar to the length of contact in the experimental setup. Geometric dimensions used for the

simulation of contact interaction between the support planes were same as used in the tests.

The analysis with pinned or roller boundary condition took 19 min while the analysis with contact interaction takes 24 min to complete the analysis. The analysis result with different types of mid span boundary condition is shown in Figure 5.7. From the result it is observed that there is not any mentionable difference between the load-deformation behavior of the pipe with contact interaction and the 18 degree pinned/roller boundary condition.

In the next step of analysis the mid span support was kept constant as contact interaction while the support at the ends span was changed. Three different types of support used for the end span of the specimen and these were as follows.

1. Pin
2. Roller
3. Contact interaction between pipe and support plane.

Like the mid span, here the pin and roller boundary conditions were applied to the end span portion of the pipe which makes an internal angle of 18 degree (Figure 5.6). The length of the portion where roller/pin was applied was similar to the length of contact in the experimental setup.

The analysis result obtained for these three different types of end span boundary condition is shown in Figure 5.8. From the result it is observed that the use of pin or roller to replace the contact boundary condition make the model stiffer. The use of pin

/roller reduced the analysis time to 19 min while in case of contact the analysis time was 24 min.

From the analysis of result of the study of effect of support condition on the behavior of FEA model it can be concluded that, an 18 degree pin/roller support can be used to replace the contact at the mid span of the pipe. However it is not reasonable to do the same for the end span portion of the pipe as it makes the model stiffer than the experimental results (Figure 5.8). It was decided to model the support conditions both at mid-span and end-span as contact interaction between pipe and the support plates for the analysis.

5.2.5 Indenter

Indenters of two different shapes were used to create dents with two different shapes. These were: (i) rectangular shape and (ii) spherical shape. The rectangular indenter was modeled using eight node C3D8 elements. The spherical indenter was modeled using analytical rigid surface for the ease of modeling. Modeling spherical shaped indenter with a solid element was found to be extremely difficult. The size and shape of both of the indenter was modeled in such a way to simulate exactly the size and shape of the indenter used in the experimental study.

5.2.6 Material Model

In the experimental program pipes with two different types of material were used. Three coupon specimens from the both pipes were tested in accordance with ASTM E E 8/E 8M-08 specification (ASTM, 2008) to obtain the uniaxial engineering stress-strain behavior of the pipe material. Identical behavior was observed for all of the three

specimens. Typical stress strain behaviors of both pipe materials are presented in Figure 3.5 and 3.6 in Chapter 3.

The pipe material underneath and adjacent to the indenter has experienced large plastic deformation. Therefore, an elastic-plastic material model with von Mises yield criterion, isotropic hardening, and associated plastic flow rule was used for numerical modeling. From the coupon tests material property was determined in terms of engineering stresses and strains. However, in the ABAQUS it is required to input true stresses (Cauchy stress) and plastic components of true strain (logarithmic strain). The formulas which were used to convert nominal stress and strain to true stress and strain are shown in Equation 5.1 and 5.2.

$$\sigma_{true} = \sigma_{nom}(1 + \varepsilon_{nom}) \quad (5.1)$$

$$\varepsilon_{ln}^{pl} = \ln(1 + \varepsilon_{nom}) - \frac{\sigma_{true}}{E} \quad (5.2)$$

Where σ_{true} is the true stress, ε_{ln}^{pl} is the true or logarithmic plastic strain, σ_{nom} is the nominal stress or engineering stress, ε_{nom} is the nominal strain or engineering strain and E is the Young's modulus. True stress-true strain behavior of the 762 mm diameter pipe material is shown in Figure 5.9. As mentioned earlier, the indenter, end caps and the support plates were modeled as elastic material, because they did not experience large deformation in the test.

5.2.7 Loading Procedure

In the finite element model load was applied in different steps, and followed the steps used in the experimental program. First internal pressure was applied in small increments.

Pressure was applied as a distributed load on the elements. The internal pressure was varied from 0 to 0.80 p_y , where p_y is the internal pressure causing yielding in the circumferential direction of the pipe. The p_y was calculated according to the formula shown in Equation 5.3.

$$p_y = \frac{\sigma_y t}{r} \quad (5.3)$$

σ_y is the yield stress of the pipe material, t is the thickness of the pipe wall, and r is the outer radius of the pipe.

In the second step, the indenter was brought into contact with the pipe wall. Then the denting load was applied in several increments using a displacement control method. Only the maximum numbers of increments, minimum increment size, and maximum increment size need to be specified in the ABAQUS input file. The ABAQUS solution scheme then determines the optimum increment size and consequently, the total number of increments required for obtaining the equilibrium path and solution. Total deformation applied in a FEA model was same as the deformation applied in the corresponding test specimen.

In the experimental program the indenter was removed gradually to unload the specimen in the third step. In the fourth step, the internal pressure was reduced to zero. The tests were performed in such a way that the internal pressure remained unchanged during the application of denting load. During the removal of the indenter it was observed that there is a significant reduction in the internal pressure as the elastic spring back of the dent occurred. In the FE analysis, the removal of denting load was performed in small steps

and each step was accompanied by a small pressure removal step to simulate the test conditions during the removal of denting force.

5.2.8 Mesh Study

The main purpose for a mesh sensitivity analysis for any numerical work is to determine the optimum mesh size which is able to yield the acceptable results with the least possible computation time. The half symmetric pipe model with D/t of 90, where D is 762 mm and t is 8.5 mm was chosen for mesh convergence study. The length of the half symmetric model was 1125 mm. Influence of mesh refinement on both global load-deformation behavior and local strain distribution of the model was studied.

In the first step of mesh sensitivity analysis, the effect of mesh size along the length of the pipe was studied, while mesh size along the circumferential direction was kept unchanged to 8.2 mm. Four different sizes of mesh used in this study and these are 8.2 mm x 62.5 mm, 8.2 mm x 31.3 mm, 8.2 mm x 11.8 mm, and 8.2 mm x 8.1 mm. These models were designated as 8.2x62.5 global mesh, 8.2x31.3 global mesh, 8.2x11.8 global mesh, and 8.2x8.1 global mesh. The first number refers to the mesh dimension in the circumferential direction of the pipe model, and the second number refers to the mesh size along the length of the pipe model. The effect of longitudinal mesh refinement on the load-deformation behavior and strain distribution along the longitudinal center line (line Y in Figure 5.10) is shown in Figures 5.11 and 5.12, respectively. From Figure 5.11 it can be observed that the effect of longitudinal mesh refinement on the load-deformation behavior is negligible. However, from Figure 5.12, it is obvious that the longitudinal strain distribution is significantly affected by the longitudinal mesh refinement. It was also found that the variation between the results obtained using 8.2 mm x 11.8 mm mesh

and 8.2 mm x 8.1 mm mesh is very small. Therefore 8.2x11.8 mesh was found to be the most efficient one considering both computations time and results.

In the second step of mesh sensitivity analysis the effect of local mesh refinement was studied. In this step the mid length of 500 mm of the pipe was considered for fine mesh (8.2 mm x 11.8 mm), while for the rest of the pipe length relatively coarse mesh (8.2 mm x 31.3 mm) was used. This model was designated as 8.2 mm x 11.8 mm local mesh model. The results obtained using this model was compared with the results obtained using the model where entire pipe length was considered for fine mesh (8.2x11.8 global mesh). The comparison between the load deformation behavior and longitudinal strain distribution along longitudinal center line (line Y in Figure 5.10) is shown in Figures 5.13 and 5.14. From the comparison it can be concluded that there is no difference between the results obtained from these two models. The analysis time for the model with local fine mesh (50 minutes) is significantly lower than that of the model with global fine mesh (130 minutes). Hence it was decided to use the local mesh refinement (8.2 mm x 11.8 mm) for analysis of all the models.

In the third step of analysis, the effect of mesh refinement in the circumferential direction was studied. For this study the local fine mesh in longitudinal direction was considered for mid 500 mm length of the pipe. Effect of three different mesh sizes on the load-deformation behavior and circumferential strain distribution along circumferential centerline (Line X in Figure 5.10) was studied. Three mesh sizes were used and they are: 16.6 mm x 11.8 mm, 8.2 mm x 11.8 mm and 6.6 mm x 11.8 mm. The models were designated as 16.6x11.8 local mesh, 8.2x11.8 local mesh and 6.6x11.8 local mesh. For the remaining length of the pipe 31.3 mm x 11.8 mm mesh size was used in all three

models. The effect of circumferential mesh refinement on the load-deformation behavior and circumferential strain distribution along circumferential center line (Line X in Figure 5.10) is shown in Figures 5.15 and 5.16 respectively. From the observation of Figures 5.15 and 5.16 it can be observed that there is no difference between the results obtained from 8.2 mmx11.81 mm local mesh and 6.6 mmx11.8 mm local mesh size. However, processing time was 50 min and 64 min, respectively. Consequently, it was decided to use a mesh size of 8.2 mm along the circumference of the pipe.

Time required for completion of analysis for the models with different mesh configurations is shown in Table 5.1. From the analysis results presented in this section and the computation time presented in Table 5.1, it can be concluded that model with fine mesh of size 8.2 mm x 11.8 mm at the mid span of 500 mm produces the best results with the most efficient computation time. Consequently it was decided that for all the further analyses 8.2x11.8 local mesh model would be used. The mesh configuration for large (762 mm diameter) pipe model is presented in Figure 5.17.

The number of element for small (274 mm diameter) pipe model was same as the number of element for large pipe (762 mm) model. From mesh sensitivity analysis it was found that for large pipe model 8.2 mm mesh size along the pipe circumferential direction is most efficient. For producing a mesh size of 8.2 mm along the pipe circumference a total of 288 elements was required for large pipe (762 mm diameter). For small pipe model the number of element along pipe circumference was kept same as 288 elements. Consequently, the mesh size along the pipe circumference was 3 mm. The length of the half scale small pipe model was 550 mm which is approximately half of the length of the half scale large pipe model (562.5 mm). The number of element required to produce a

mesh size of 11.8 mm for the middle 500 mm portion of the large pipe model was kept same for the middle 250 mm length of the small pipe model. Consequently the mesh size for the local fine mesh area for small pipe was 5.8 mm. Similarly, the mesh size used for the remaining 300 mm length was 15 mm. The mesh configuration for a half scale small pipe model is presented in Figure 5.18. The mesh configuration for a full scale small pipe model is presented in Figure 5.19. In summary, final mesh sizes for small pipe were 3mm x 5.8 mm in the middle 250 mm length and 3 mm x 15 mm for remaining 300 mm length.

5.2.9 Contact Algorithm

As mentioned earlier in the experimental program the pipe specimen rested on the support plane made of thick steel plates. Hence there was a contact interaction between the pipe wall and the support plane while load was being applied. Further the indenter came in contact before load could be applied and hence, a similar contact interaction existed between the indenter and the pipe surface. Therefore, a finite-sliding contact formulation was used to simulate the contact interaction between the pipe wall and the indenter and also between the pipe wall and the support planes.

Two formulations are available in ABAQUS/Standard for modeling the contact interaction between two deformable bodies (ref), and these are as follows.

1. Small-sliding contact formulation
2. Finite-sliding contact formulation

In small-sliding formulation the contacting surfaces can experience only relatively small sliding relative to each other, however, an arbitrary rotation of the surfaces is permitted.

On the other hand, in finite-sliding formulation, separation and sliding of finite amplitude and arbitrary rotation of the surfaces may arise.

For simulation of the finite-sliding, two approaches are available and either one of these two approaches can be used depending on the type of the contact problem. The approaches are as follows.

(1) Defining possible contact conditions by identifying and pairing potential contact surfaces, and

(2) Using contact elements.

When the first approach is used the contact elements are automatically generated by ABAQUS. Contact element approach is usually used when contact between two bodies cannot be simulated using the first approach. For development of the finite element model in this study the first approach was used.

For simulating the contact of pipe wall with the indenter and support plane master-slave contact algorithm was used. The following guidelines are provided in ABAQUS manual for selection of master and slave surfaces.

1. The larger of the two surfaces should act as the master surface.
2. The surface on the stiffer body should act as the master surface, if the surfaces are of comparable size.
3. The surface with the coarser mesh should act as the master surface, if the surfaces are of comparable size and stiffness

For the contact interaction between the indenter and the pipe the surfaces were of comparable sizes (surface area). Among the two surfaces the stiffness of the indenter was higher than the pipe wall and hence the indenter surface was selected as the master surface. In the case of contact interaction between the pipe wall and the support plane, the size (surface area) of the support plane was relatively higher than the size (surface) of the portion of the pipe wall in contact with the support plane. In addition the stiffness of the support plane was higher than the pipe wall. Therefore, the surface of the support plane was defined as master surface.

A node-to-surface contact discretization was used for the discretization of the contact pair surfaces. In this method the contact conditions are established such that each “slave” node on one side of a contact interface effectively interacts with a point of projection on the “master” surface on the opposite side of the contact interface. Thus, each contact condition involves a single slave node and a group of nearby master nodes from which values are interpolated to the projection point.

For any contact interaction analysis it is required to define contact properties. Contact properties define the mechanical and thermal surface interaction models that control the behavior of the surfaces when they are in contact. Mechanical contact property models may include (i) a constitutive model for the contact pressure-overclosure relationship that governs the motion of the surfaces, (ii) a damping model that defines forces resisting the relative motions of the contacting surfaces, (iii) a friction model that defines the force resisting the relative tangential motion of the surfaces.

In the present analysis, the default contact pressure-overclosure relationship of ABAQUS which is referred to as the “hard” contact model was used. In hard contact; (i) the surfaces transmit no contact pressure unless the nodes of the slave surface contact the master surface, (ii) no penetration is allowed at each constraint location, and (iii) there is no limit to the magnitude of contact pressure that can be transmitted when the surfaces are in contact.

A damping model is primarily used to damp relative motions of the surfaces during approach or separation. It is also recommended that in ABAQUS/Standard contact damping should generally be used only when it is otherwise impossible to obtain a solution. Damping was not considered in developing the models in this study.

Shear and normal forces are usually transmitted by the surfaces those are in contact across their interface. There is generally a relationship between these two force components. The relationship, known as the friction between the contacting bodies, is usually expressed in terms of the stresses at the interface of the bodies. By default, ABAQUS assumes that the contact between surfaces is frictionless. The assumption of frictionless contact could not be used in the models because it is understood that metal (steel) is not smooth enough to be called frictionless. The classical isotropic Coulomb friction model was adapted as the friction model. This model defines friction coefficient in terms of slip rate, contact pressure, average surface temperature at the contact point, and field variables.

The basic concept of the Coulomb friction model is to relate the maximum allowable frictional stress across an interface to the contact pressure between the contacting bodies.

The isotropic friction model assumes that friction coefficient μ is the same in all directions. For a three dimensional contact there are two orthogonal components of shear stress, τ_1 and τ_2 , along the interface between the two bodies. These components act in the slip directions for the contact surfaces. These two shear stress components are combined into one equivalent frictional stress τ_{eq} as follows:

$$\tau_{eq} = \sqrt{\tau_1^2 + \tau_2^2} \quad (5.4)$$

The standard Coulomb frictional model assumes that no relative motion of the contact surfaces occurs if the equivalent frictional stress τ_{eq} is less than the critical stress, τ_{crit} , which is proportional to the contact pressure, p_c , in the form

$$\tau_{crit} = \mu p_c \quad (5.5)$$

Where μ is the friction coefficient at the contact point. Beyond this stress, the contact surfaces start to slide relative to each other. The value of μ used in the present study was 0.8. However effect of μ was studied by varying its value from 0.1 to 0.8 and no change in the load-deformation behavior was found.

5.2.10 Solution Methods and Convergence

Newton's method is used by ABAQUS as a default option for solving nonlinear equilibrium equations. Newton's method was chosen primarily, because of the reason that the convergence rate attained using Newton's method is higher compared to convergence rates exhibited by other alternative methods (usually modified Newton or quasi-Newton methods) for the types of nonlinear problems most often studied using ABAQUS (SIMULIA 2008).

The total time history for a simulation can consist of one or more steps. In ABAQUS each analysis step is broken into a number of increments to follow the non linear solution path. The structure is in equilibrium (approximate) at the end of each increment. For each time increments, the equilibrium solutions are attained by iteration using Newton method. The details of Newton's method are described in ABAQUS manual (SIMULIA, 2008).

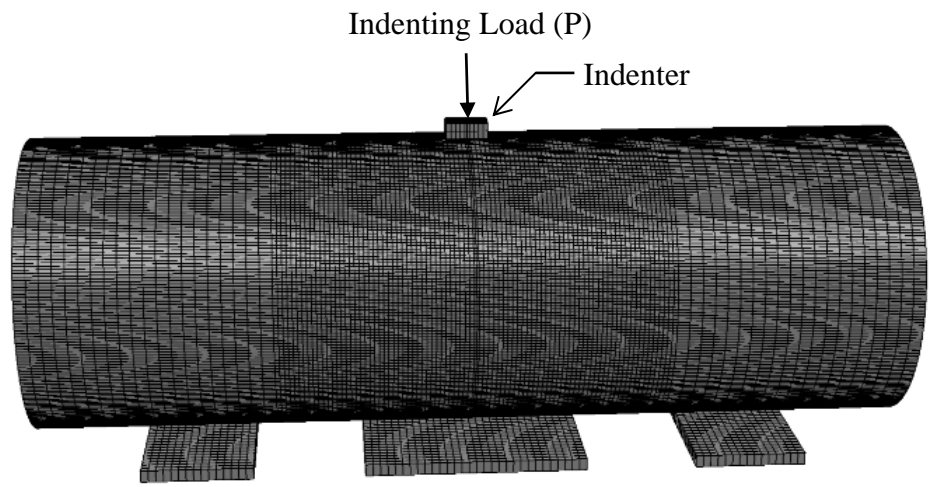
ABAQUS incorporates an empirical algorithm designed to provide an accurate, and at the same time economical solution for the nonlinear systems. In ABAQUS/Standard for structural stress analysis, four parameters are checked for convergence and these are force, moment, displacement, and rotation. For example, convergence is obtained when size of the residual (disequilibrium) force is less than a tolerance times a reference value and/or when the size of the increment in displacement is less than a tolerance times a reference value. In this model, the default tolerance values were used. For some difficult cases, it is often necessary to increase the number of increments and/or use some solution controls. Sometime nonmonotonic convergence may occur because of various nonlinearities interaction. For example, the combination of friction, nonlinear material behavior, and geometric nonlinearity may lead to nonmonotonically decreasing residuals. In this case, some controls in the time increment such as increase the number of equilibrium iterations for residual check and the number of equilibrium for a logarithmic rate of convergence check may be used to obtain convergence.

Automatic increment scheme was chosen in this study because ABAQUS/Standard automatically adjusts the size of the time increments to obtain the solution effectively using the initial time step defined. It may increase or decrease the time increment when convergence is easily obtained to achieve better efficiency. On the other hand,

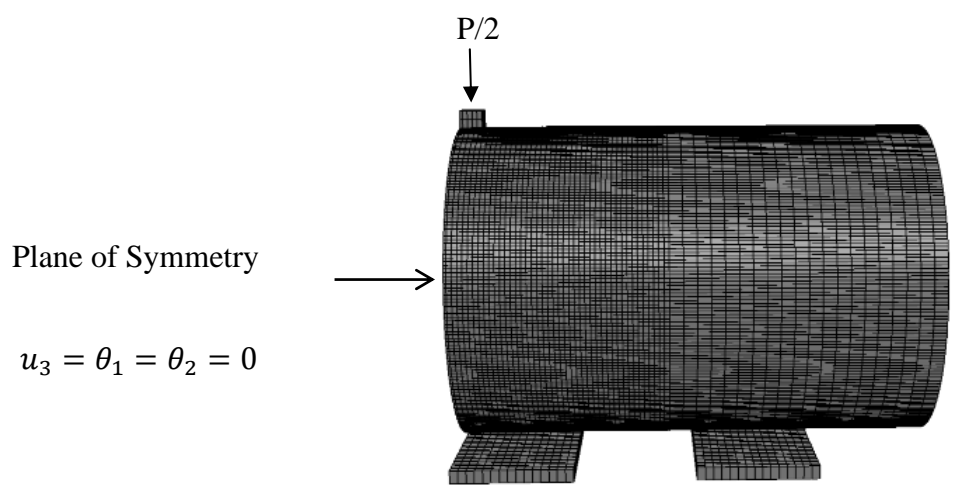
ABAQUS/Standard abandons the increments and starts again with the increments size set to 25% of the previous value if the solution does not converged within certain number of iterations or if the solution appears to diverge.

Table 5.1: Mesh Study

Model	Mesh size	Computation time (minute)
8.2x62.5 global mesh	8.2 mm x 62.5 mm	16
8.2x31.3 global mesh	8.2 mm x 31.25 mm	31
8.2x11.8 global mesh	8.2 mm x 11.81 mm	130
8.2x8.1 global mesh	8.2 mm x 8.14 mm	164
8.2x11.8 local mesh	8.2 mm x 11.81 mm (middle 500 mm) 8.2 mm x 31.3 (remaining of the pipe length)	50
16.6x11.8 local mesh	16.6 mm x 11.81 mm (middle 500 mm) 16.6 mm x 31.3 (rest of the pipe length)	26
6.6x11.8 local mesh	6.6 mm x 11.8 mm (middle 500 mm) 6.6 mm x 31.3 (remaining of the pipe length)	64



(a) Full pipe model



(b) Half pipe model

Figure 5.1 Half symmetry in the FEA model

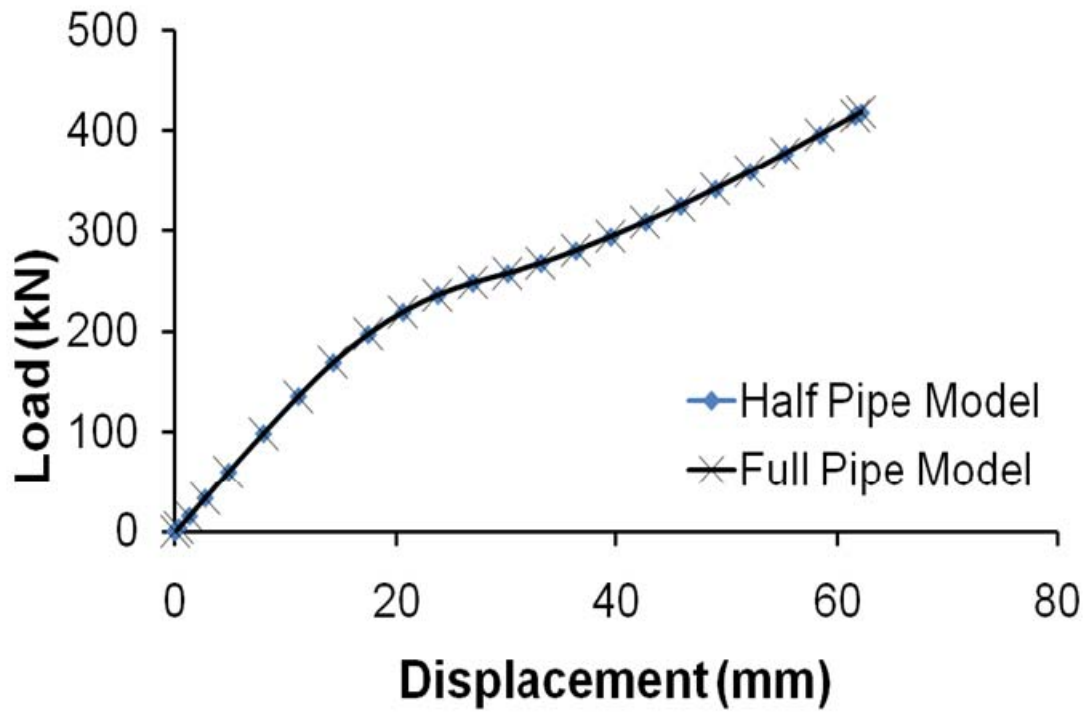


Figure 5.2: Comparison between Load-deformation behaviour of full-pipe model and half symmetric model

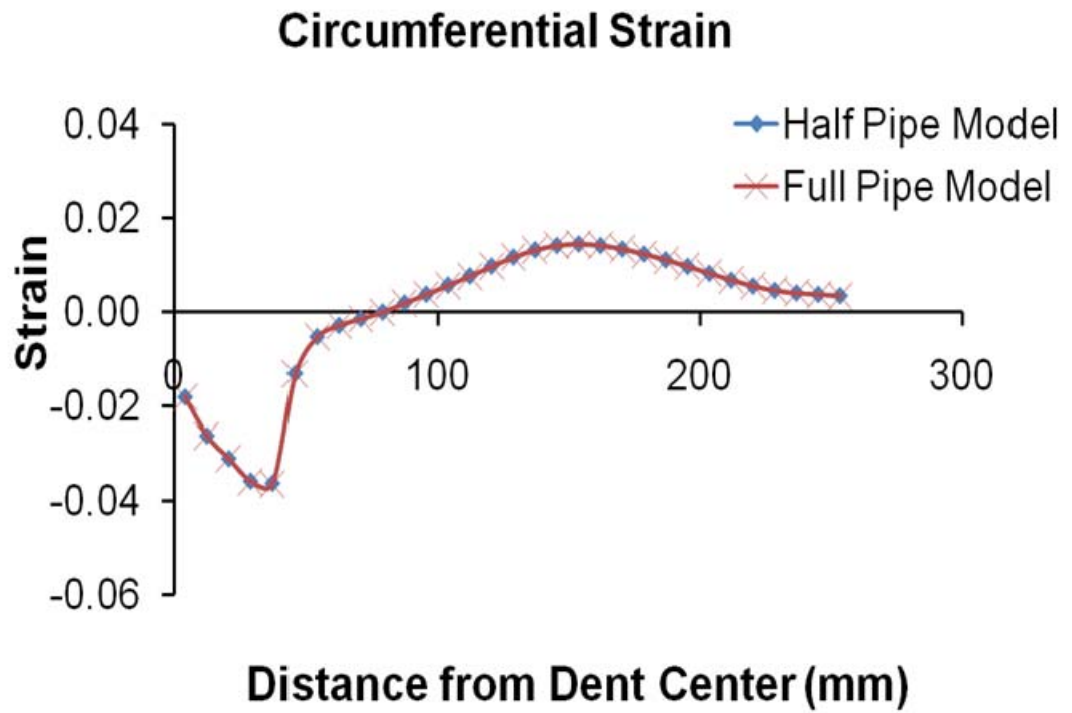
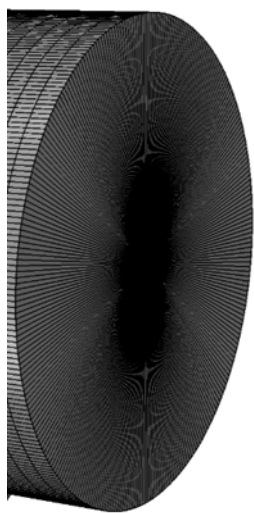
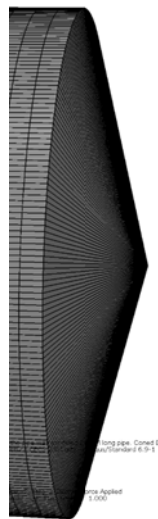


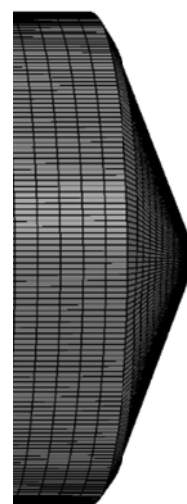
Figure 5.3: Comparison between circumferential strain distribution of full-pipe model and half-symmetric model



Flat



(b) Cone



(c) Hemispherical

Figure 5.4: Types of end caps used in FE model

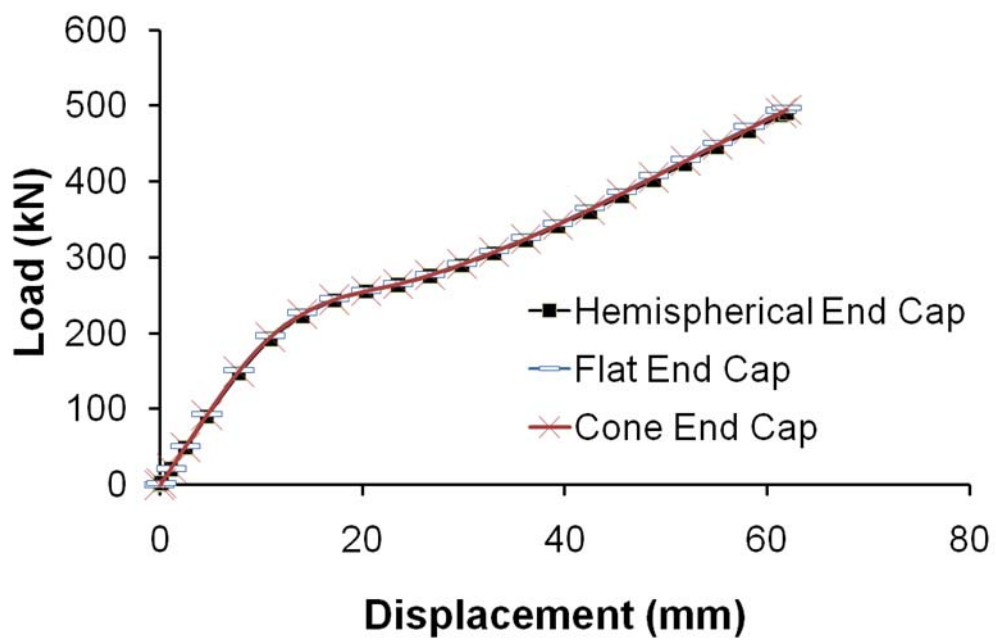


Figure 5.5: Effect of shapes of end caps on load-deformation behavior

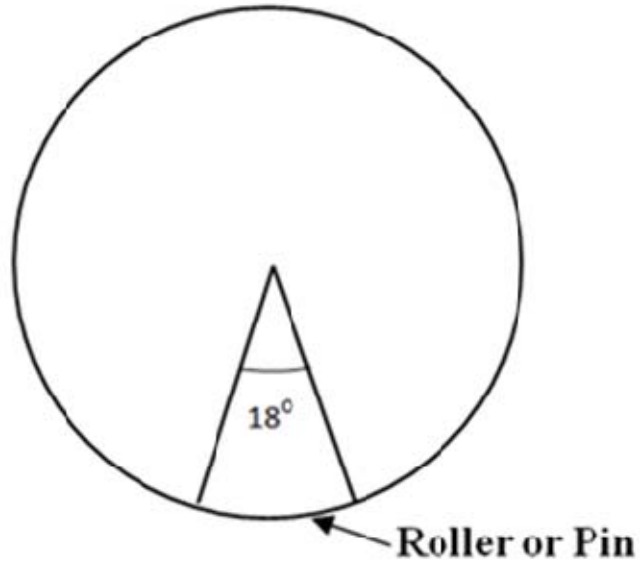


Figure 5.6: Cross section of pipe end showing 18° roller or pin support

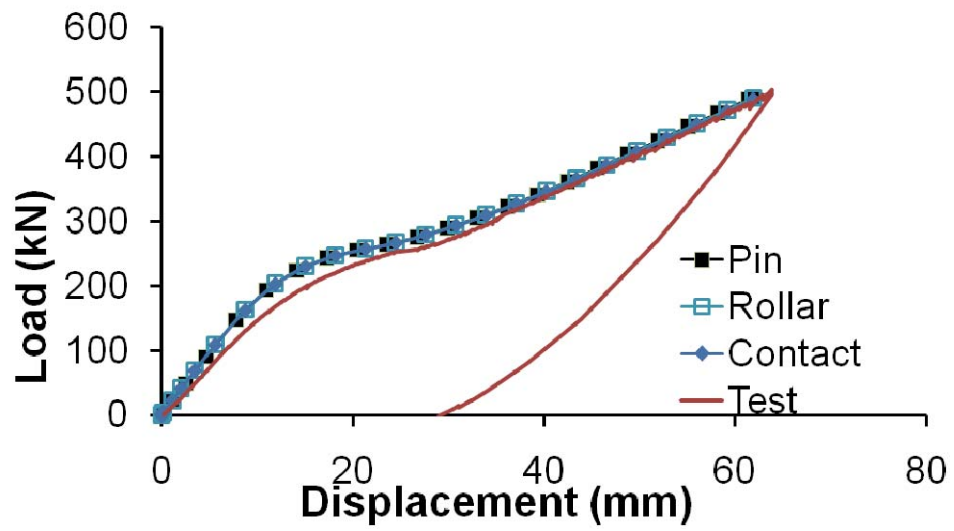


Figure 5.7: Effect of various boundary conditions at mid-span support

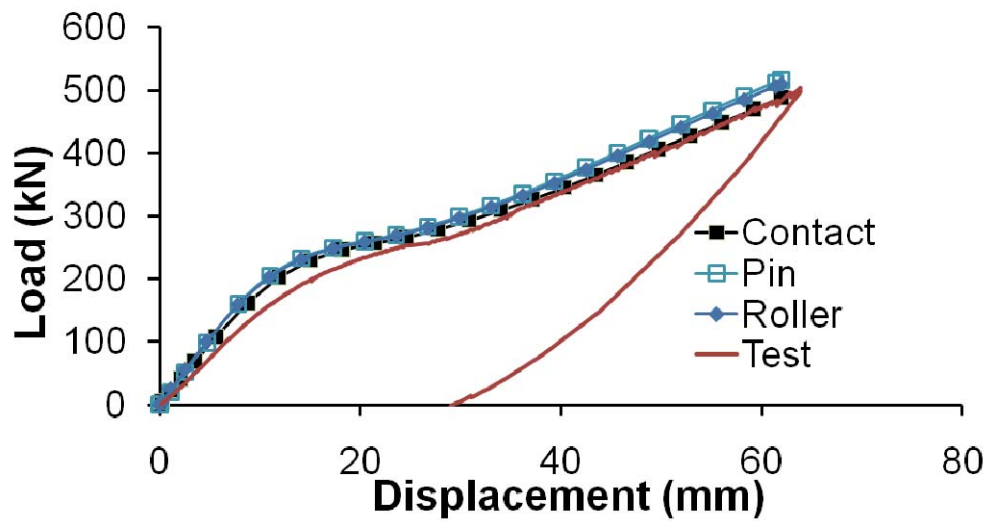


Figure 5.8: Effect of end-span support condition

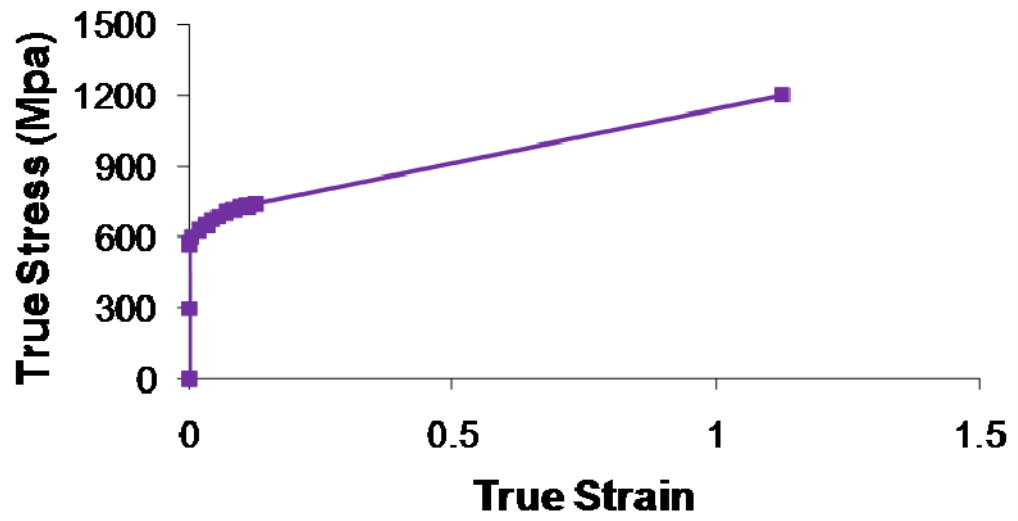


Figure 5.9: True stress-strain behavior of 762 mm pipe material

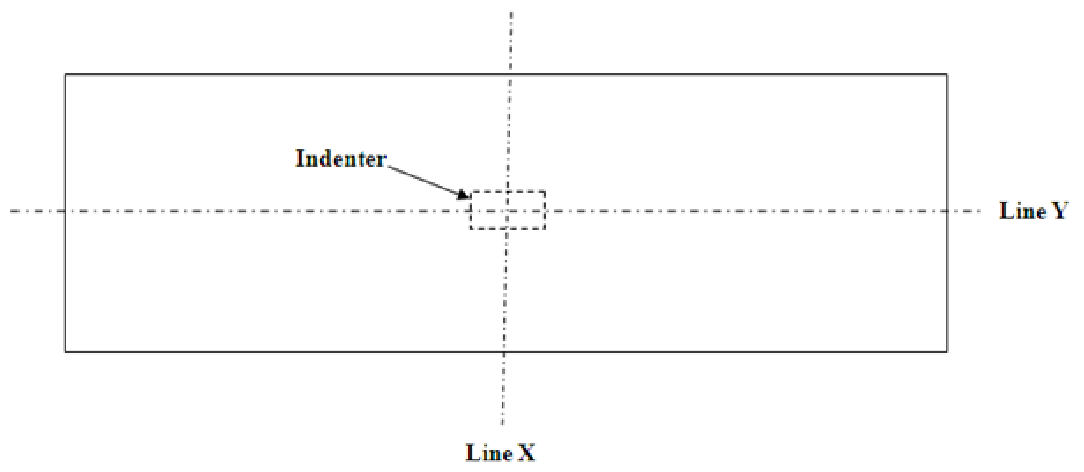


Figure 5.10: Top view of the pipe

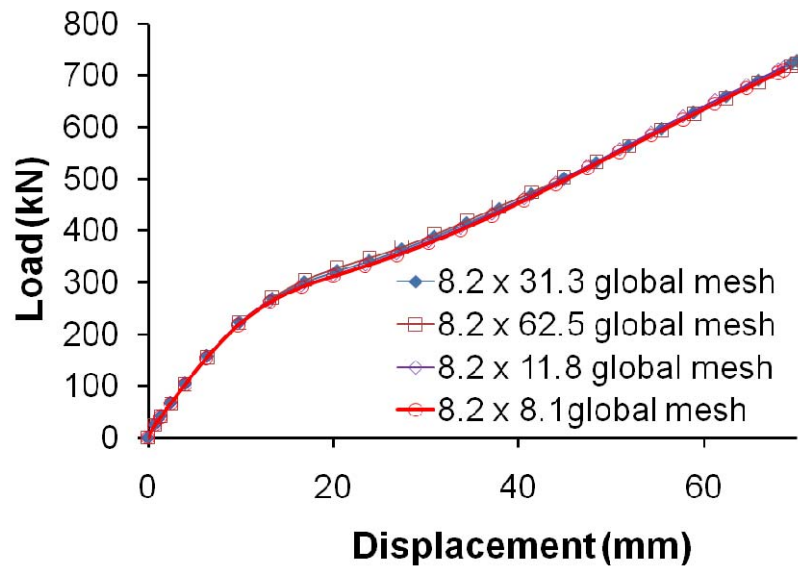


Figure 5.11: Effect of mesh refinement in longitudinal direction on the load-deformation behavior

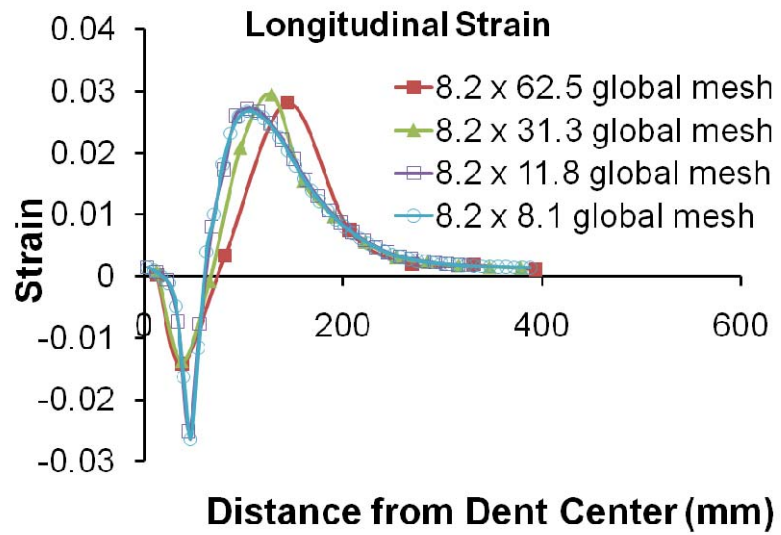


Figure 5.12: Effect of mesh refinement in longitudinal direction on the longitudinal strain distribution along the longitudinal center line

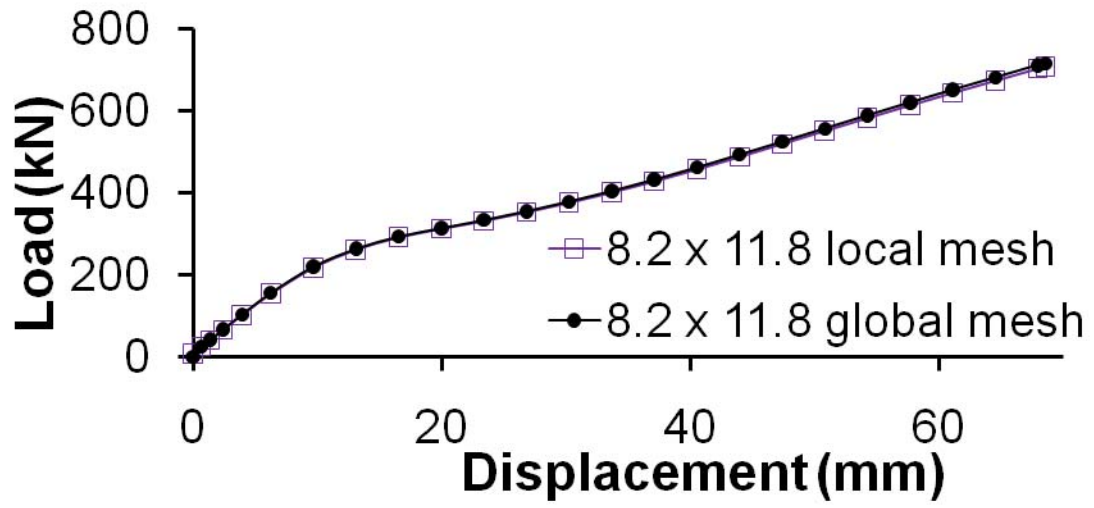


Figure 5.13: Effect of local mesh refinement on load –deformation behavior

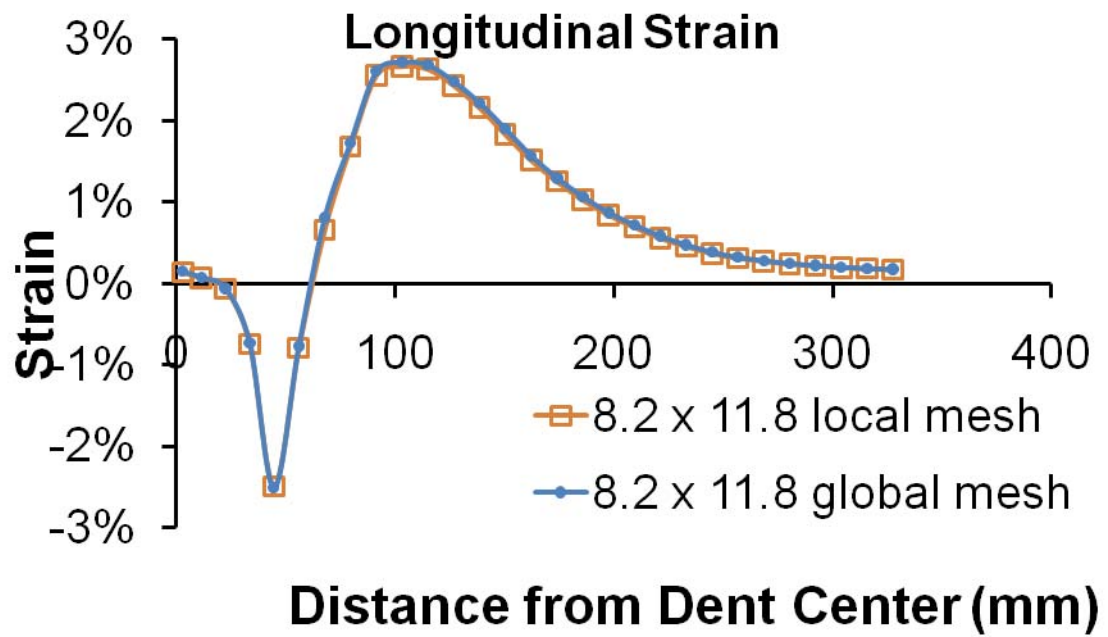


Figure 5.14: Effect of local mesh refinement on strain distribution along longitudinal centerline

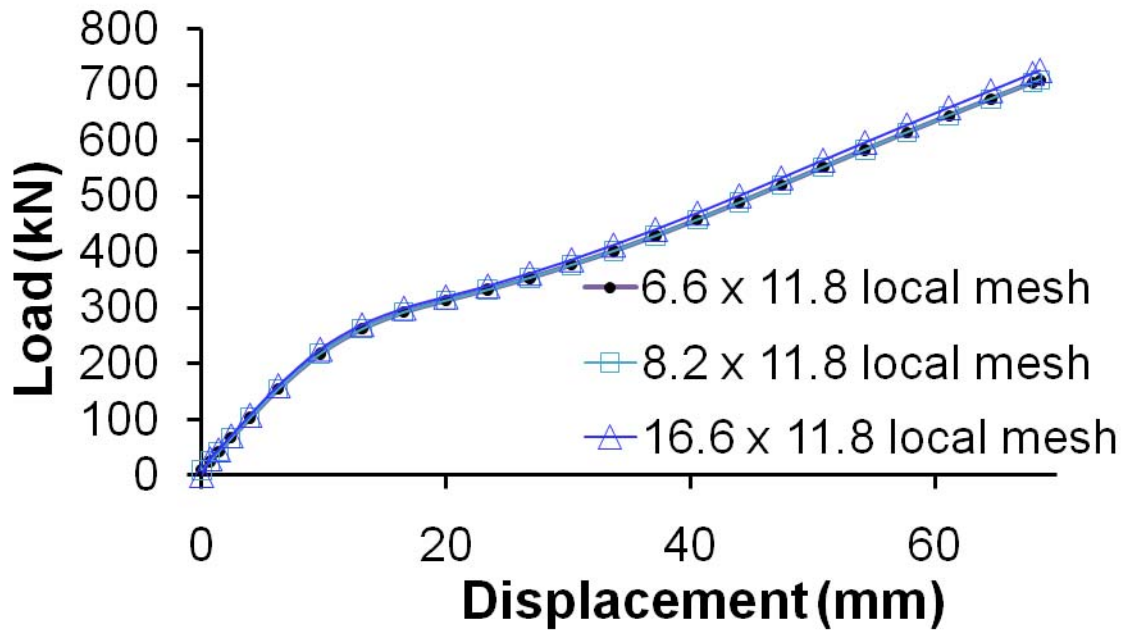


Figure 5.15: Effect of circumferential mesh refinement on the load-deformation behavior

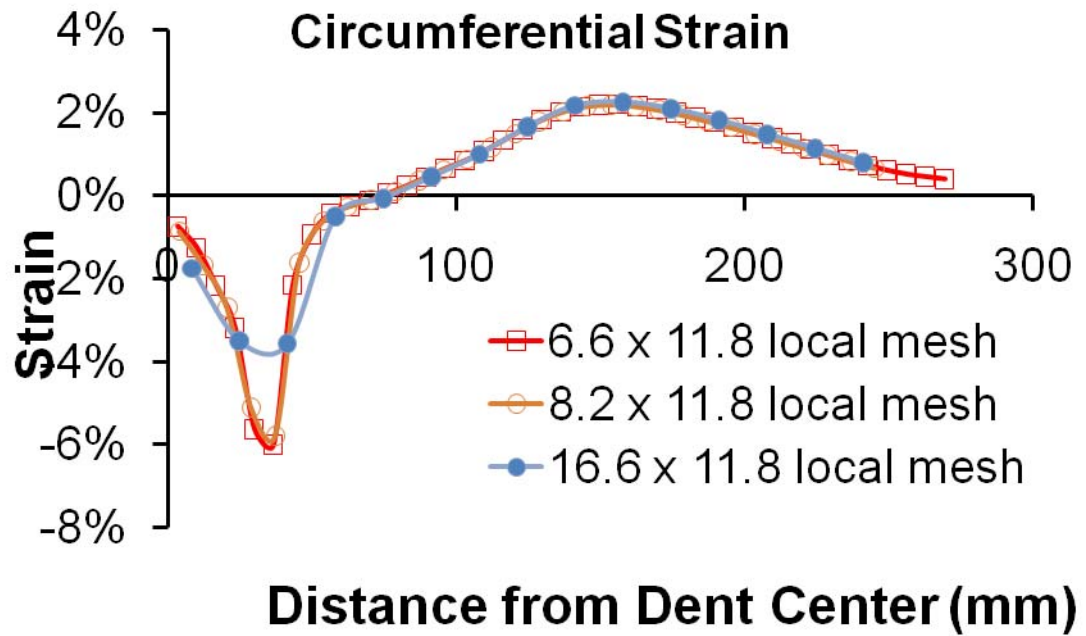


Figure 5.16: Effect of circumferential mesh refinement on the strain distribution along circumferential centerline

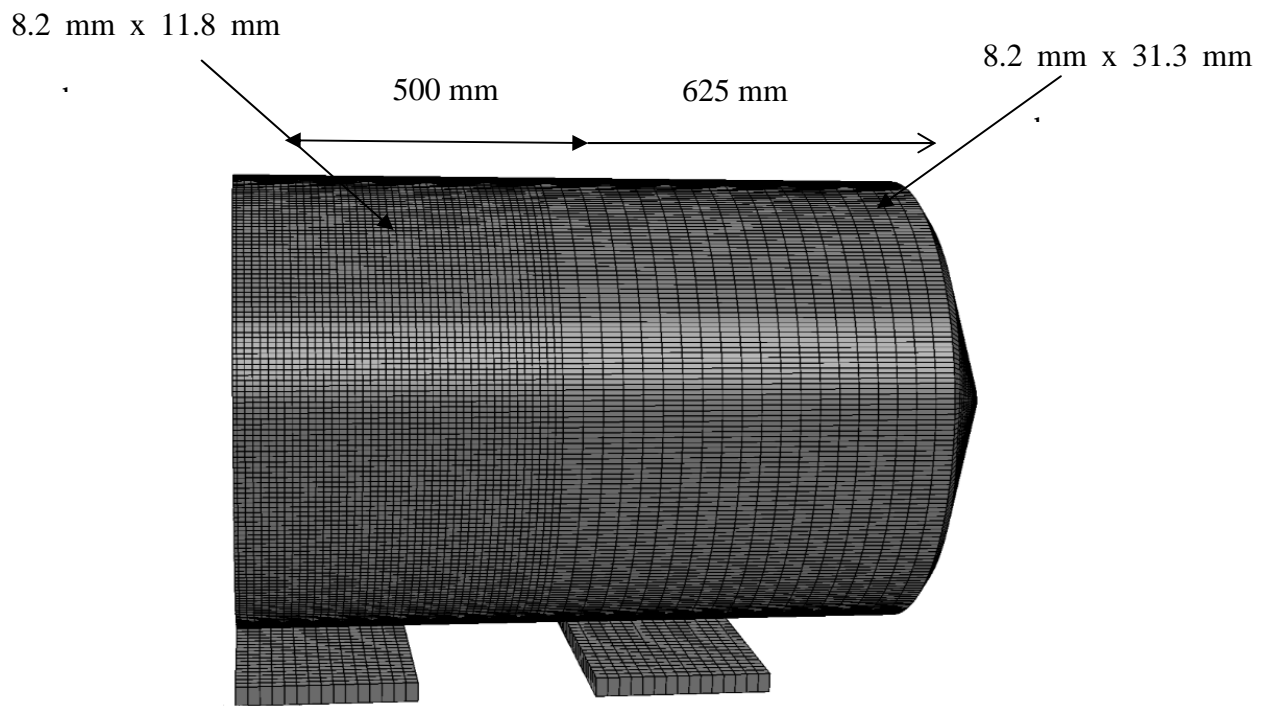


Figure 5.17: Mesh configuration for large pipe model

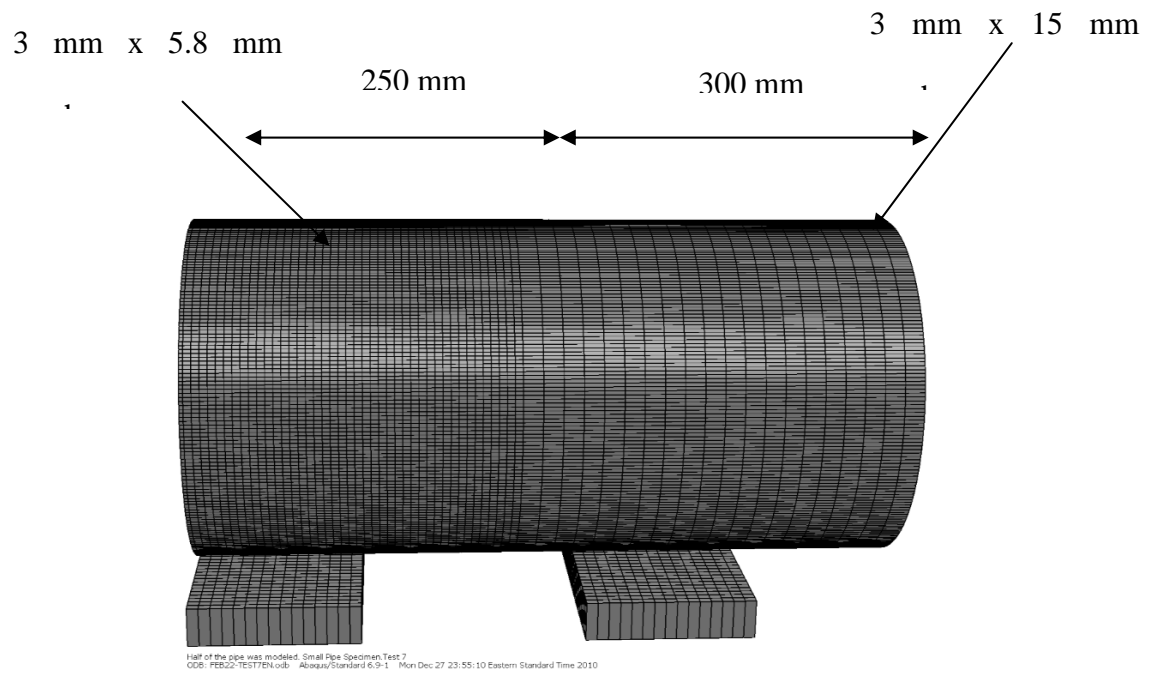


Figure 5.18: Mesh configuration for half small pipe model

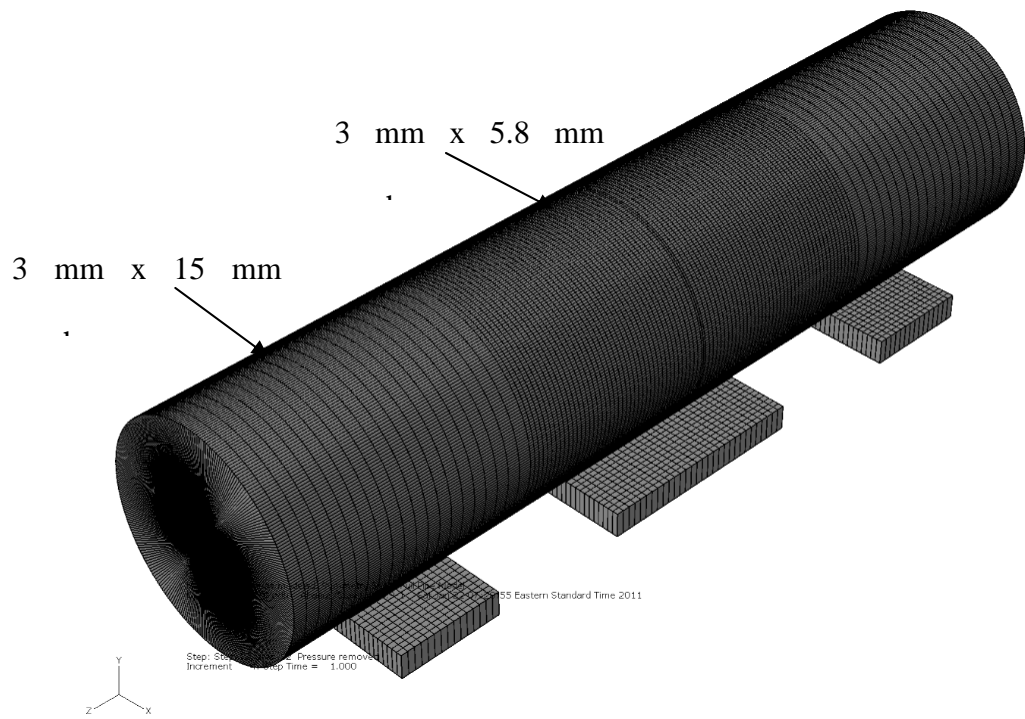


Figure 5.19: Mesh configuration for small pipe model

CHAPTER 6

VALIDATION OF FINITE ELEMENT MODEL AND PARAMETRIC STUDY

6.1 General

In the previous chapter details of the development of the finite element (FE) model using commercially available general purpose finite element analysis code, ABAQUS (SIMULIA 2008) was presented. The results obtained from the finite element analysis (FEA) and their comparisons with the test results are presented in this chapter. A good agreement between the experimental and FEA results was obtained.

One of the primary objectives of the development of the FEA model was to perform a detailed parametric study of the effect of different parameters on the strain distribution on a pipeline dent, using the FE model. Different parameters used in this study were: dent depth, internal pressure, and dent shape. In this chapter the results obtained from the parametric study is presented

6.2 Comparison of the FEA and Experimental results

The main objective of the current research project was to study the effect of various parameters on the strain distributions in a dent of a pipeline. Two types of behavior of the finite element (FE) model are compared with the experimental behavior and these are as follow.

1. Global load-deformation behavior, and
2. Strain distribution in a dent

As described earlier in Chapter 3, in the experimental program the denting load was applied to the pipe specimen using a 900 kN compression-tension hydraulic loading jack

with a 900 kN capacity load cell. The displacement of the loading jack was monitored using LVDTs (Linear Voltage Displacement Transducer). A displacement control method was employed for the application of the denting load. Strain gauges were installed for recording the strain data during the tests. In the finite model the denting load was also applied using a displacement control method. The displacement data was obtained from the nodal displacement of the indenter and the magnitude of applied load was obtained from the support reactions. The strain data for the finite element model were obtained from the integration points of the elements.

In the experimental program parameters such as D/t ratio of the pipe, shape of the indenter, dent depth, and internal pressure were varied. In this section the comparison between the experimental and numerical results for various test specimens is presented.

6.2.1 Specimen LRP20D4 and LRP40D4

Specimen LRP20D4 and LRP40D4 were large diameter (762 mm) pipe specimens and indented using a rectangular indenter (Figure 3.3 (a)) to produce a dent with a permanent depth of 4% of the outer diameter of the pipe. The only difference between the specimens was the internal pressure during indentation. For specimen LRP20D4, internal pressure during indentation was $0.2p_y$. The comparison between the experimental and numerical load-deformation behavior for specimen LRP20D4 is presented in Figure 6.1. From the observation of Figure 6.1 it can be concluded that a very good agreement exists between the experimental and numerical load-deformation behavior. Figures 6.2 (a) and 6.2 (b) show the comparison between the experimental and numerical circumferential strain distributions for Lines 1 and 2 (Figure 3.9) respectively, for this specimen. The comparisons between the experimental and numerical longitudinal strain distributions for

Specimen LRP20D4 for Line 3 and 4 (Figure 3.9) are presented in Figures 6.3(a) and 6.3(b), respectively. From the comparison between the experimental and numerical strain distributions along the circumferential and longitudinal directions a reasonably good agreement between the strain distributions is observed.

Specimen LRP40D4 was indented at an internal pressure of $0.4p_y$. The comparison between the experimental and numerical load-deformation behavior for specimen LRP40D4 is presented in Figure 6.4. A very good agreement between the experimental and numerical load-deformation behavior is observed. Figures 6.5 (a) and 6.5 (b) shows the comparisons between the experimental and numerical circumferential strain distribution along Lines 1 and 2 (Figure 3.9) respectively. From the figures it is observed that the FEA model estimated the circumferential strain reasonably well. The comparisons between the experimental and numerical longitudinal strain distributions for specimen LRP40D4 for Lines 3 and 4 (Figure 3.9) are presented in Figures 6.6(a) and 6.3(b), respectively. A fairly good agreement between the experimental and numerical longitudinal strain distribution is observed.

6.2.2 Specimen SSP20D8

Specimen SSP20D8 was a small diameter (274 mm) pipe specimen and indented using a spherical indenter (Figure 3.3 (b)) at an internal pressure of $0.2p_y$. The specimen was indented to produce a permanent dent depth of 8% of the outer diameter of the pipe. The comparison between the experimental and numerical load-deformation behavior of this specimen is shown in Figure 6.7. Figures 6.8 and 6.9 show respectively the comparison between the experimental and numerical strain distributions along the circumferential and

longitudinal directions for this specimen. From the comparison between the experimental and numerical results a fairly good agreement is observed.

6.2.3 Specimen SRP20D8, SRP20D10, and SRP20D12

Specimens SRP20D8, SRP20D10, and SRP20D12 were small diameter pipe specimen and indented using a rectangular shaped indenter (Figure 3.3 (c)). During indentation an internal pressure of $0.2p_y$ was applied to the specimens. The only difference between the specimens was the final permanent dent depth.

A dent with permanent depth of 8% of the outer diameter of the pipe was introduced in Specimen SRP20D8. The comparison between the experimental and numerical load-deformation behavior for Specimen SRP20D8 is presented in Figure 6.10. Figures 6.11(a) and 6.11(b) show the comparison between the experimental and numerical circumferential strain distribution along Lines 1 and 2 (Figure 3.11), respectively. The comparison between the experimental and numerical longitudinal strain distribution along Line 3 and 4 (Figure 3.11) are presented in Figures 6.12(a) and 6.12(b), respectively. From the comparison between the experimental and numerical results a fairly good agreement is observed.

Specimen SRP20D10 was indented to produce a permanent dent depth of 10% of the outer diameter of the pipe. Figure 6.13 shows the comparison between the experimental and numerical load-deformation behavior for Specimen SRP20D10. The comparisons between the experimental and numerical circumferential strain distributions for Line 1 and 2 (Figure 3.11) are presented in Figures 6.14(a) and 6.14(b) respectively. Figures 6.15(a) and 6.15(b) show the comparison between the experimental and numerical

longitudinal strain distribution for Lines 3 and 4 (Figure 3.11), respectively. A reasonably good agreement between the experimental and numerical results for specimen SRP20D10 is found.

Specimen SRP20D12 was indented to produce a permanent dent depth of 12% of the outer diameter of the pipe. Figure 6.16 shows the comparison between the experimental and numerical load-deformation behavior for Specimen SRP20D12. The comparison between the experimental and numerical circumferential strain distribution along Line 1 and 2 (Figure 3.11) are presented in Figures 6.17(a) and 6.17(b) respectively. Figures 6.18(a) and 6.18(b) shows the comparison between the experimental and numerical longitudinal strain distribution along Lines 3 and 4 (Figure 3.11) respectively. A reasonably good agreement between the experimental and numerical results for specimen SRP20D12 is found from these figures.

6.3 Parametric Study

A detailed parametric study was performed to investigate the effect of different parameters on the strain distribution in a pipeline dent. The parameters used in this study are as follows.

1. Dent depth
2. Internal pressure, and
3. Dent shape

Like the designation of the specimen in experimental program described in section 3.8, each of the specimens in the parametric study was given a unique designation. The designations were chosen to recognize most of the attributes of the numerical specimen.

For example, for specimen 34SP25D3 the first two digits refer to the D/t ratio of the specimen and for this specimen it is 34. The third character (S) indicates that this specimen was indented using a spherical indenter. Next three characters (P25) indicate that the level of internal pressure during indentation was 25% of p_y or $0.25p_y$, and the last characters (D3) indicate that the specimen was indented up to a depth of 3% of the outer diameter of the pipe. Similarly first character used for rectangular indenter is R.

The main focus of the parametric study was to study the effect of different parameters on the maximum strain values in the circumferential and longitudinal strain values. Table 6.1 shows the maximum circumferential tensile and compressive strain values obtained from the FEA models. Table 6.2 shows the maximum longitudinal tensile and compressive strain values obtained from the FEA models. It should be noted that these values are for true or logarithmic strain.

6.3.1 Effect of Dent Depth

Effect of four different dent depths on the maximum circumferential and longitudinal strain values was studied. Dent depths used in this study were 3%, 6%, 9%, and 12% of the outer diameter of the pipe. The effect of dent depth was studied for two different shapes of indenter, spherical and rectangular.

6.3.1.1 Spherical Dent

The effect of dent depth for spherical indenter was studied for pipes with two different D/t ratios and these were 34 and 70. Figures 6.19(a), 6.19(b), 6.19(c), and 6.19(d) show the effect of dent depth on the maximum values of circumferential tensile strain, circumferential compressive strain, longitudinal tensile strain, and longitudinal

compressive strain, respectively for pipe model with D/t ratio of 34 at different internal pressure level. Similar plots for model with D/t ratio of 70 is presented in Figures 6.19(e), 6.19(f), 6.19(g) and 6.19(h). It should be noted that the pipe wall thickness was reduced to obtain higher (70) D/t value, and diameter of pipe was not changed. From these figures it was found that with the increase in dent depth the value of maximum tensile strain, both in circumferential and longitudinal direction for both of the pipe models (D/t ratio of 34 and 70) increases (see Figures 6.19(a), 6.19(c), 6.19(e) and 6.19(g)). The rate of increase of maximum circumferential and longitudinal tensile strain was higher for higher internal pressure. A gradual decrease in the value of maximum circumferential compressive strain was observed with the increase in dent depth for both pipe models (D/t ratio 34 and 70) (see Figures 6.19(b) and 6.19(f)). In case of maximum longitudinal compressive strain no definite pattern was found for pipe model with D/t ratio 34 (Figure 6.19(d)). In case of pipe model with D/t ratio of 70 a decrease in the value of maximum longitudinal compressive strain was observed with the increase in dent depth (Figure 6.19(h)).

6.3.1.2 Rectangular Dent

The effect of dent depth for rectangular indenter was studied for a pipe model with D/t ratio of 34. The effect of dent depth on the maximum values of circumferential tensile strain, circumferential compressive strain, longitudinal tensile strain and longitudinal compressive strain for the rectangular indenter, at different internal pressure is presented in Figures 6.19(i), 6.19(j), 6.19(k) and 6.19(l), respectively. From these figures an increase in all the strain values with the increase in dent depth was observed. It was found that at an internal pressure $0.65p_y$, for an increase in dent depth from 3% to 6% a drastic increase in the strain values occurred.

6.3.2 Effect of Internal Pressure

The maximum allowable operating pressure for a pipeline is $0.80p_y$. In the present study the effect various internal pressure levels ranging from 0 to $0.80p_y$ was studied. The effect of internal pressure was studied for two different shapes of indenter: spherical and rectangular.

The effect of internal pressure on the maximum strain values in a dent created with spherical indenter was studied for pipes with two different D/t ratios (34 and 70). Figures 6.20(a), 6.20(b), 6.20(c) and 6.20(d) show the effect of internal pressure on the maximum values of circumferential tensile strain, circumferential compressive strain, longitudinal tensile strain and longitudinal compressive strain, respectively for pipe model with D/t ratio of 34 at different dent depths. Similar plots for model with D/t ratio of 70 are presented in Figures 6.20(e), 6.20(f), 6.20(g) and 6.20(h). From these figures it was found that with the increase in internal pressure the value of maximum tensile strain, both in circumferential and longitudinal direction for both of the pipe models (D/t ratio 34 and 70) increases (see Figures 6.20(a), 6.20(c), 6.20(e) and 6.20(g)). The rate of increase of maximum circumferential and longitudinal tensile strain was higher for dent with higher depths. However, decrease in the value of maximum circumferential compressive strain was observed with the increase in internal pressure for both pipe models (D/t ratio 34 and 70) (see Figures 6.20(b) and 6.20(f)). For pipe models with D/t ratio of 34 the decrease in maximum circumferential compressive value was more rapid as compared to pipe with D/t ratio of 70 (compare figure 6.20(b) with 6.20(f)). In case of maximum longitudinal compressive strain no definite pattern was found for pipe model with D/t ratio 34 (Figure 6.20(d)). For pipe models with D/t ratio of 70 a very low decrease in the value of

maximum longitudinal compressive strain was observed with the increase in dent depth (Figure 6.20(h)).

The effect of internal pressure for rectangular indenter was studied for a pipe model with D/t ratio of 34. The effect of internal pressure on the maximum values of circumferential tensile strain, circumferential compressive strain, longitudinal tensile strain, and longitudinal compressive strain for rectangular indenter, at different internal pressure is presented in Figures 6.20(i), 6.20(j), 6.20(k) and 6.20(l), respectively. From the figures an increase in all the strain values with the increase in internal pressure was observed.

6.3.3 Effect of Indenter Shape

The effect of two different shapes of indenter on the maximum strain values in the dented region was studied. The shapes of indenter used in these studies were rectangular and spherical.

Figures 6.21(a), 6.21(b), 6.21(c), and 6.21(d) show the effect of indenter shape on the maximum values of circumferential tensile strain, circumferential compressive strain, longitudinal tensile strain, and longitudinal compressive strain at zero internal pressure. Similar plots for different internal pressure levels ($0.25p_y$, $0.45p_y$, and $0.65p_y$) are presented in Figures 6.21(e) through 6.21(p). From these figures it was observed that the strain concentration in both directions for spherical indenter was significantly higher than the rectangular indenter. However, for very high internal pressure an opposite phenomenon was observed (Figure 6.21(m), 6.21(n) and 6.21(o)).

6.4 Conclusions

Based on the parametric study following conclusions can be drawn.

1. Values of maximum tensile strains in the circumferential and longitudinal direction increases with the increase in dent depth, for both shapes of dent. The rate of increase is influenced by the level of internal pressure during indentation. At high internal pressure the rate of increase of maximum tensile strain with the dent depth is higher as compared to that at low internal pressure.
2. Value of maximum compressive strain in the circumferential direction decreases with the increase in dent depth, for dent created with spherical indenter. However the rate of decrease with the increase in dent depth is very low. In case of longitudinal compressive strain no definite pattern was observed.
3. Value of maximum compressive strain in the circumferential and longitudinal direction increases with the increase in dent depth, for dent created with rectangular indenter.
4. Value of maximum tensile strain in the circumferential and longitudinal direction increases with the increase in internal pressure during indentation, for both shapes of dent.
5. In case of spherical dent, values of maximum compressive strain in circumferential directions decreases with the increase in internal pressure during indentation. However, no definite pattern was observed in case of the value of maximum compressive strain in longitudinal direction.
6. In case of rectangular dent, values of maximum compressive strain in circumferential and longitudinal directions increase with the increase in internal pressure during indentation.

7. The shape of the dent has a significant influence on the maximum strain value in a pipeline dent. In case of spherical dent a higher strain concentration was observed as compared to rectangular dent. However at a very high internal pressure level some discrepancies were observed.

Table 6.1: Maximum circumferential strain values

Model	D/t ratio	Internal pressure (p/p _y) (%)	Dent depth (d/D) (%)	Maximum Circumferential Tensile Strain	Maximum Circumferential Compressive Strain	
34SP0D3	34	0	3	2.8%	30.3%	
34SP0D6			6	3.2%	30.2%	
34SP0D9			9	3.2%	30.1%	
34SP0D12			12	3.0%	29.7%	
34SP25D3		25	25	3	3.7%	29.0%
34SP25D6				6	4.4%	29.2%
34SP25D9				9	4.7%	28.9%
34SP25D12				12	4.5%	28.2%
34SP45D3		45	45	3	4.3%	28.7%
34SP45D6				6	5.3%	28.7%
34SP45D9				9	6.1%	28.1%
34SP45D12				12	6.0%	27.8%
34SP65D3		65	65	3	4.6%	27.7%
34SP65D6				6	6.5%	27.8%
34SP65D9				9	7.8%	27.4%
34SP65D12				12	8.9%	27.0%
34SP80D3		80	80	3	5.1%	27.1%
34SP80D6				6	7.5%	27.1%
34SP80D9				9	9.7%	26.4%
34SP80D12				12	12.4%	26.4%
70SP25D3	70	25	3	2.2%	12.9%	
70SP25D6			6	2.3%	12.1%	
70SP25D9			9	3.1%	11.9%	
70SP25D12			12	5.1%	11.4%	
70SP45D3		45	45	3	2.7%	12.6%
70SP45D6				6	3.4%	11.6%
70SP45D9				9	6.1%	11.1%
70SP45D12				12	11.1%	10.8%
70SP65D3		65	65	3	3.5%	12.1%
70SP65D6				6	4.8%	10.7%
70SP65D9				9	10.6%	10.2%
70SP65D12				12	15.0%	9.9%
70SP80D3		80	80	3	4.1%	11.5%
70SP80D6				6	6.8%	10.0%
70SP80D9				9	14.1%	9.4%
70SP80D12				12	23.6%	9.7%

Model	D/t ratio	Internal pressure (p/p _y) (%)	Dent depth (d/D) (%)	Maximum Circumferential Tensile Strain	Maximum Circumferential Compressive Strain
34RP0D3	34	0	3	1.2%	9.6%
34RP0D6			6	2.4%	15.7%
34RP0D9			9	3.1%	20.1%
34RP0D12			12	3.5%	21.7%
34RP25D3		25	3	1.4%	11.4%
34RP25D6			6	2.5%	19.2%
34RP25D9			9	3.2%	23.4%
34RP25D12			12	3.6%	24.8%
34RP45D3		45	3	1.5%	12.6%
34RP45D6			6	2.8%	21.5%
34RP45D9			9	4.4%	25.8%
34RP45D12			12	4.6%	27.1%
34RP65D3		65	3	2.0%	13.7%
34RP65D6			6	7.2%	27.3%
34RP65D9			9	7.2%	28.8%
34RP65D12			12	7.4%	31.1%

Table 6.2: Maximum longitudinal strain values

Model	D/t ratio	Internal pressure (p/p _y) (%)	Dent depth (d/D) (%)	Maximum Longitudinal Tensile Strain	Maximum Longitudinal Compressive Strain
34SP0D3	34	0	3	4.4%	27.3%
34SP0D6			6	6.3%	27.7%
34SP0D9			9	6.9%	27.3%
34SP0D12			12	7.3%	27.1%
34SP25D3		25	3	5.3%	28.5%
34SP25D6			6	7.8%	27.9%
34SP25D9			9	9.0%	27.7%
34SP25D12			12	10.0%	27.4%
34SP45D3		45	3	5.7%	28.4%
34SP45D6			6	8.8%	27.9%
34SP45D9			9	10.4%	27.4%
34SP45D12			12	12.5%	27.5%
34SP65D3		65	3	5.7%	27.8%
34SP65D6			6	9.9%	27.4%
34SP65D9			9	11.7%	26.6%
34SP65D12			12	16.6%	26.4%
34SP80D3		80	3	5.9%	27.5%
34SP80D6			6	10.4%	27.0%
34SP80D9			9	13.8%	26.5%
34SP80D12			12	20.6%	26.8%
70SP25D3	70	25	3	3.3%	11.1%
70SP25D6			6	5.0%	9.6%
70SP25D9			9	6.6%	9.1%
70SP25D12			12	10.1%	8.7%
70SP45D3		45	3	3.7%	11.2%
70SP45D6			6	6.5%	9.2%
70SP45D9			9	11.1%	8.8%
70SP45D12			12	17.8%	8.5%
70SP65D3		65	3	4.9%	10.9%
70SP65D6			6	8.1%	8.8%
70SP65D9			9	16.6%	8.6%
70SP65D12			12	25.5%	8.4%
70SP80D3		80	3	5.4%	10.5%
70SP80D6			6	11.3%	9.0%
70SP80D9			9	22.6%	8.5%
70SP80D12			12	33.7%	8.9%

Model	D/t ratio	Internal pressure (p/p _y) (%)	Dent depth (d/D) (%)	Maximum Longitudinal Tensile Strain	Maximum Longitudinal Compressive Strain
34RP0D3	34	0	3	1.0%	6.7%
34RP0D6			6	2.1%	9.8%
34RP0D9			9	3.2%	10.6%
34RP0D12			12	4.0%	11.2%
34RP25D3		25	3	1.2%	7.1%
34RP25D6			6	2.8%	10.8%
34RP25D9			9	4.6%	12.6%
34RP25D12			12	5.7%	13.4%
34RP45D3		45	3	1.6%	7.2%
34RP45D6			6	3.6%	12.3%
34RP45D9			9	6.9%	14.7%
34RP45D12			12	8.3%	15.4%
34RP65D3		65	3	2.0%	8.0%
34RP65D6			6	14.9%	17.5%
34RP65D9			9	19.4%	18.5%
34RP65D12			12	24.4%	19.2%

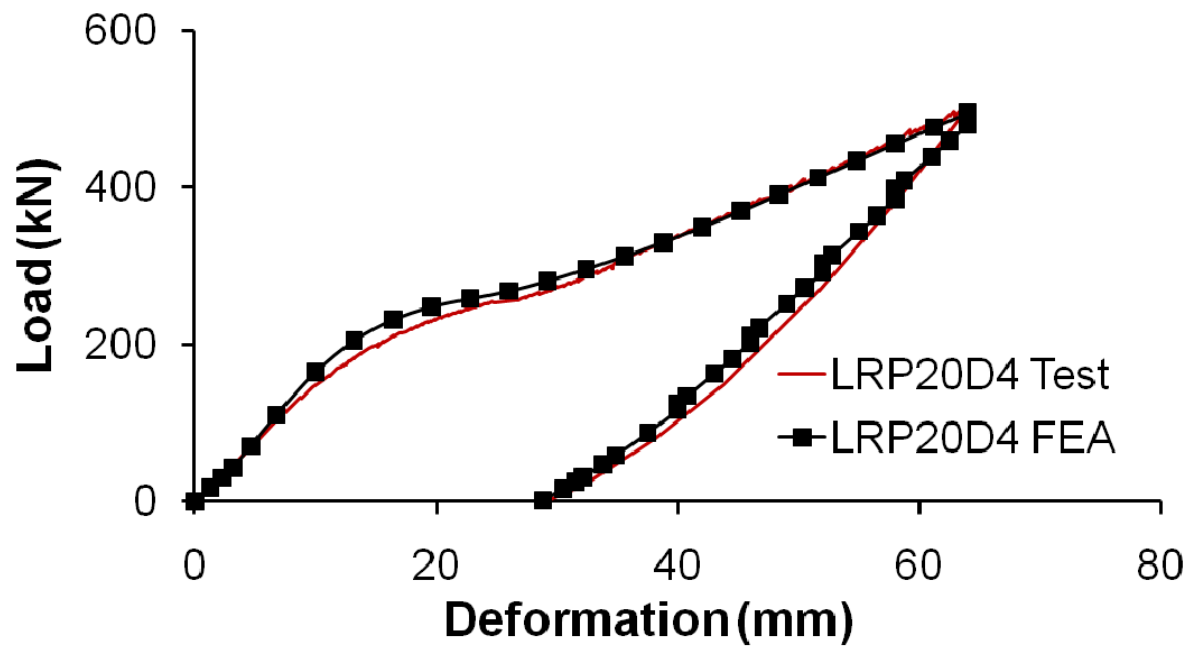


Figure 6.1: Experimental and numerical load-deformation behaviors of Specimen LRP20D4

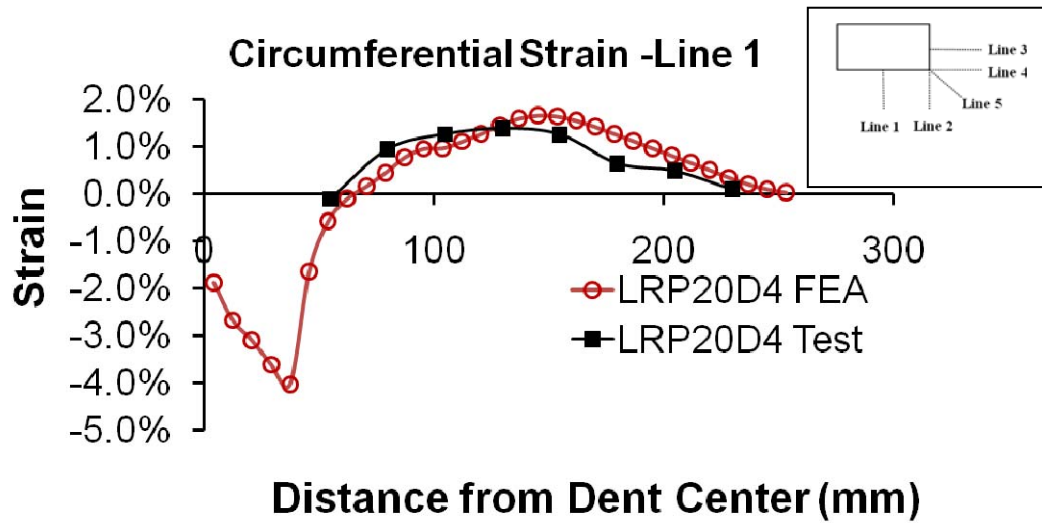


Figure 6.2(a): Experimental and numerical circumferential strain distributions for Specimen LRP20D4 for Line 1

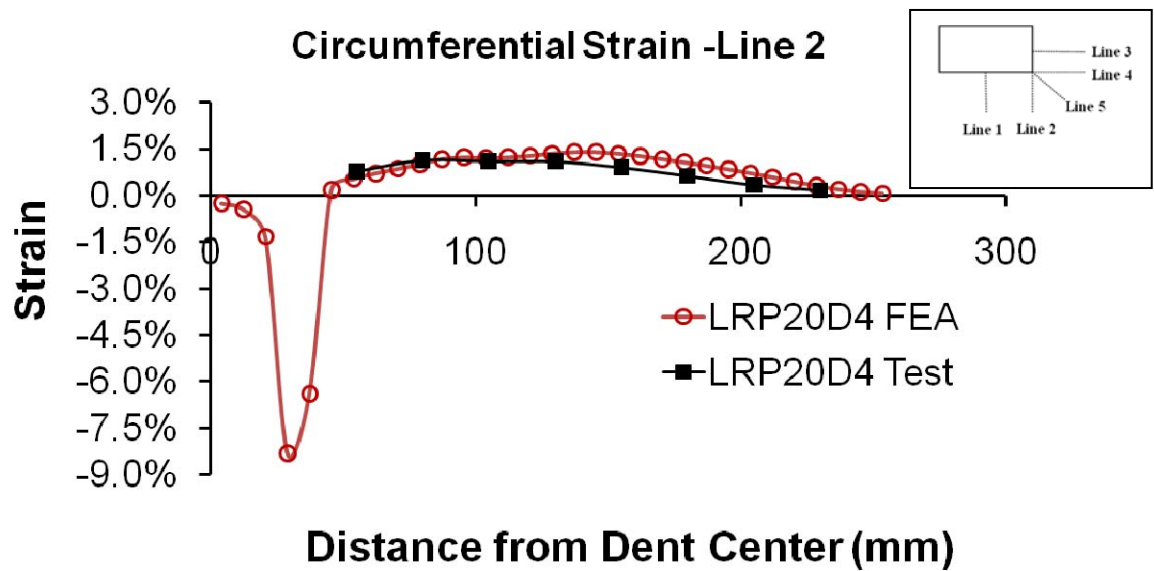


Figure 6.2(b): Experimental and numerical circumferential strain distributions for Specimen LRP20D4 for Line 2

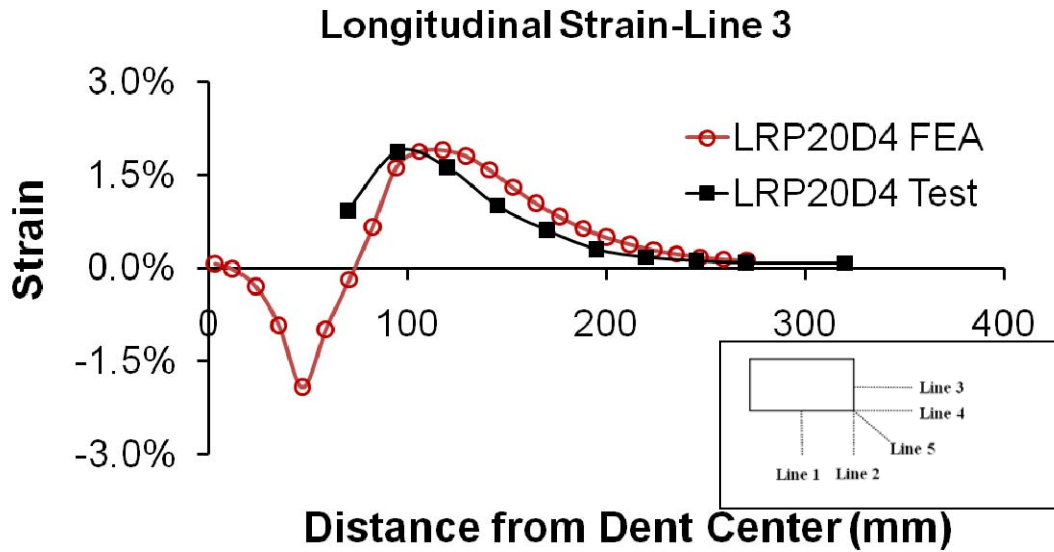


Figure 6.3(a): Experimental and numerical longitudinal strain distributions for Specimen LRP20D4 for Line 3

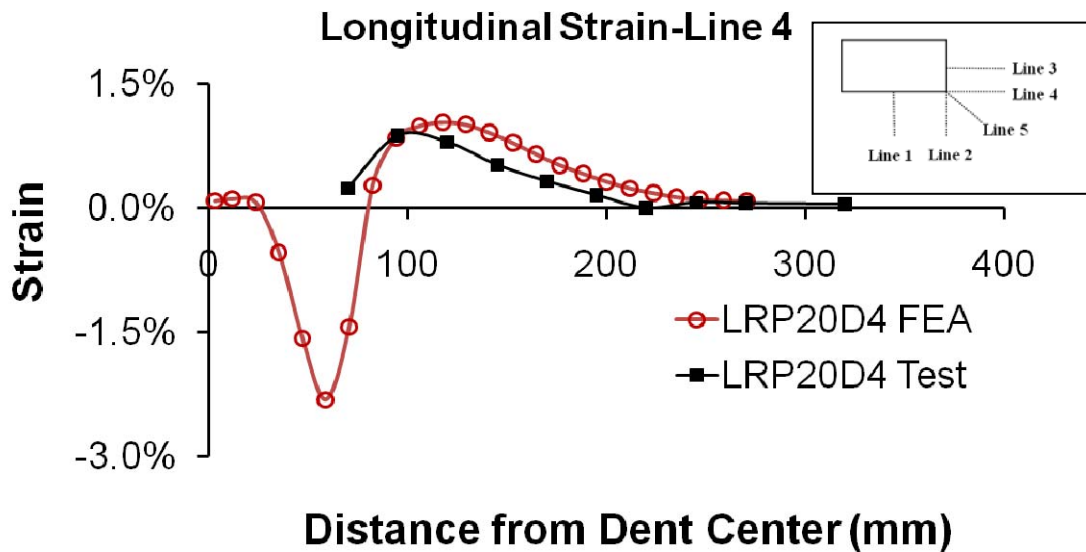


Figure 6.3(b): Experimental and numerical longitudinal strain distributions for Specimen LRP20D4 for Line 4

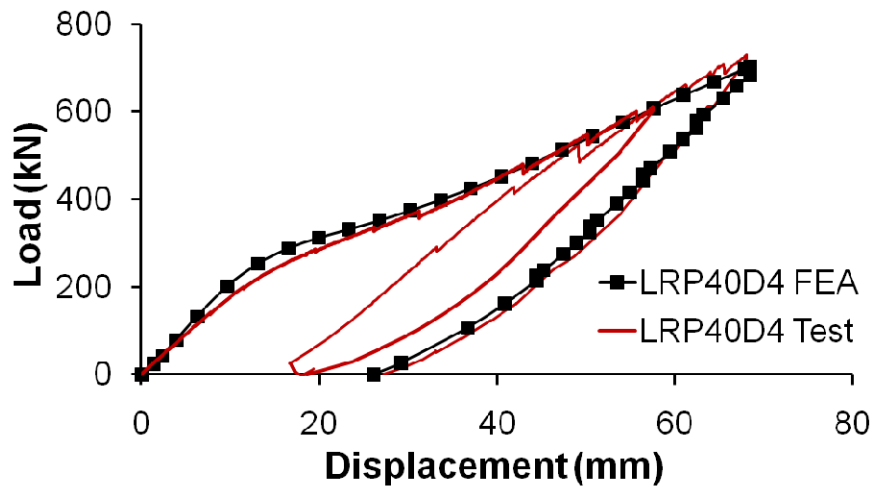


Figure 6.4: Experimental and numerical load-deformation behaviors of Specimen

LRP40D4

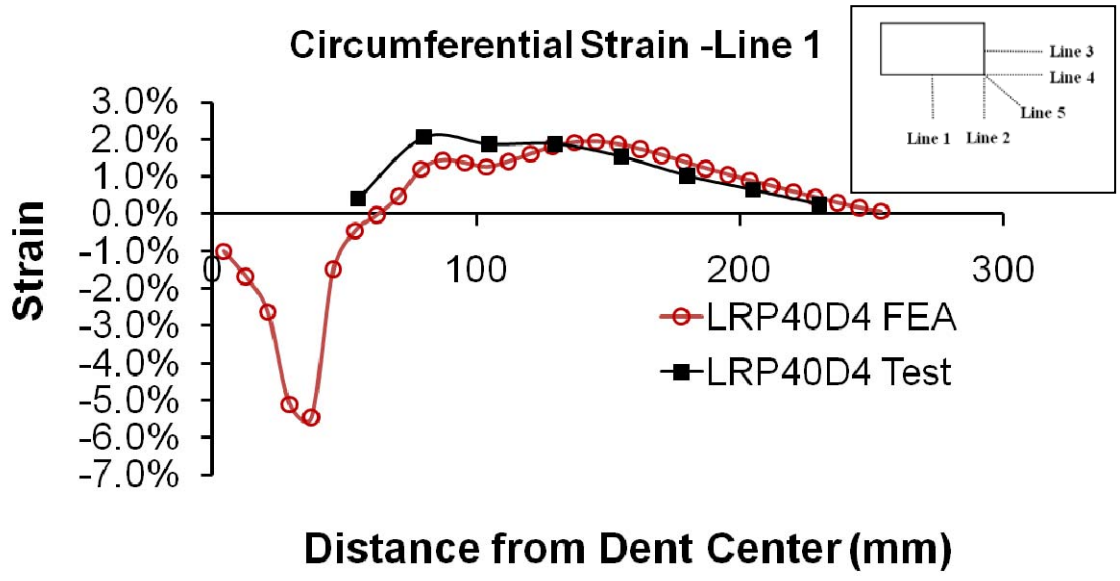


Figure 6.5(a): Experimental and numerical circumferential strain distributions for Specimen LRP40D4 for Line 1

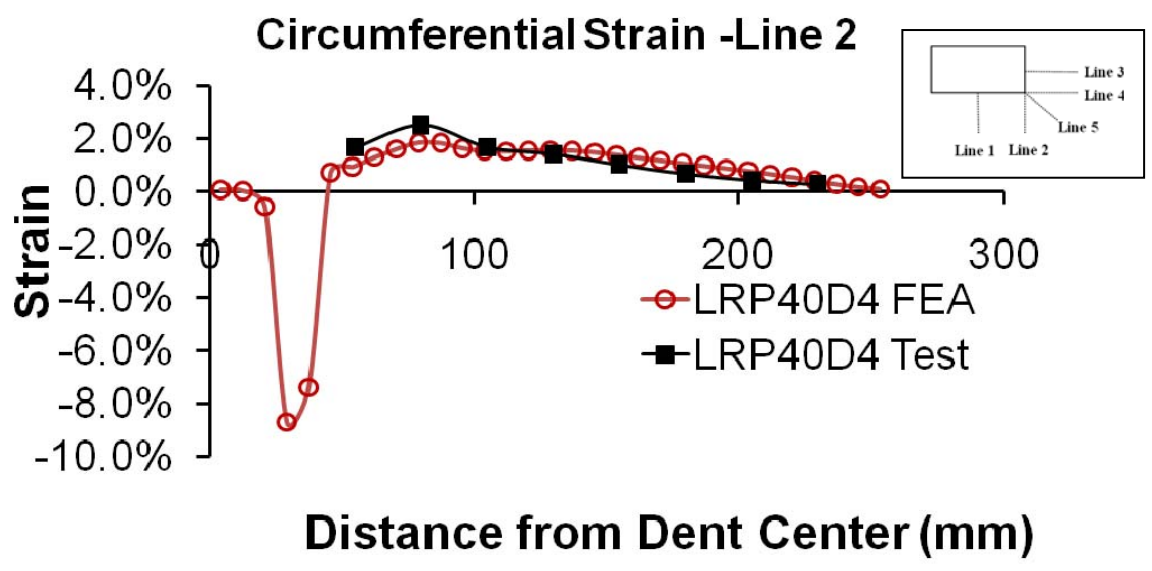


Figure 6.5(b): Experimental and numerical circumferential strain distributions for Specimen LRP40D4 for Line 2

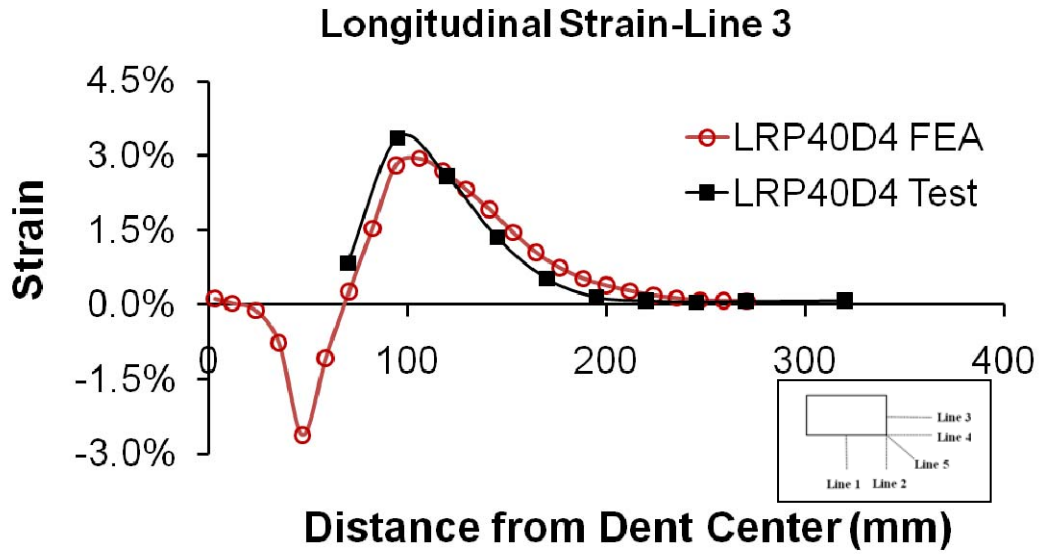


Figure 6.6(a): Experimental and numerical longitudinal strain distributions for Specimen LRP40D4 for Line 3

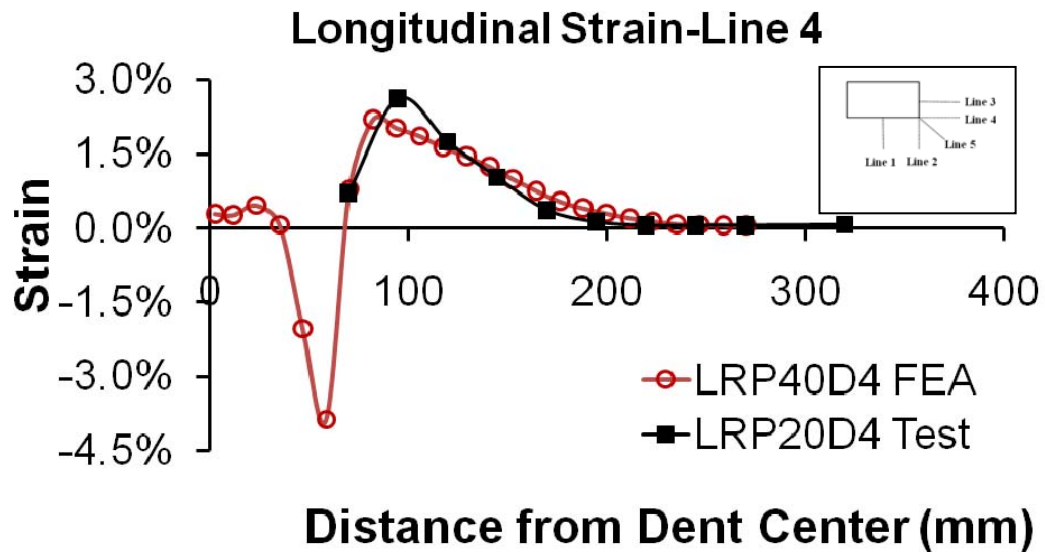


Figure 6.6(b): Experimental and numerical longitudinal strain distributions for Specimen LRP40D4 for Line 4

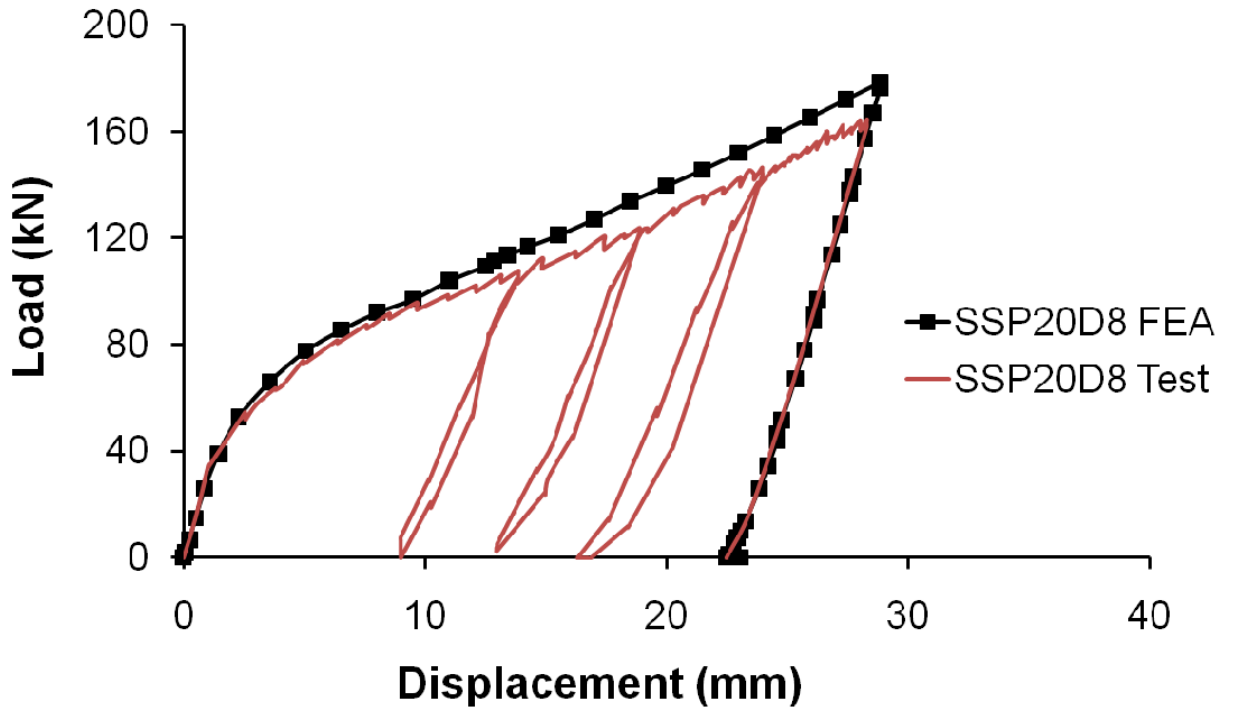


Figure 6.7: Experimental and numerical load-deformation behaviors of Specimen SSP20D8

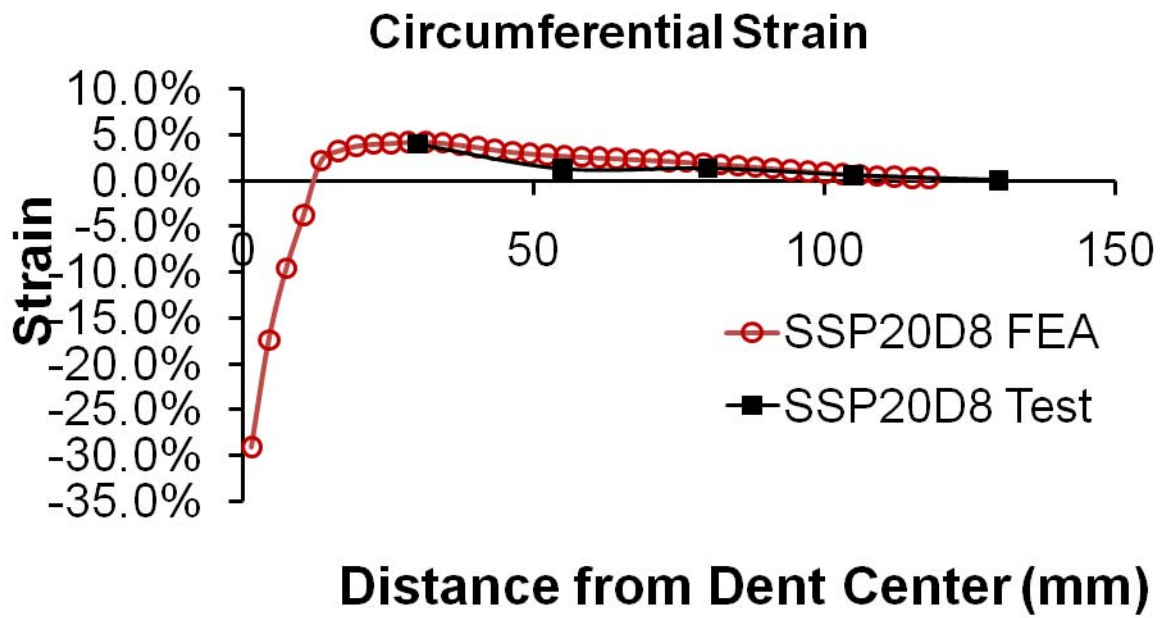


Figure 6.8: Experimental and numerical circumferential strain distributions for Specimen SSP20D8

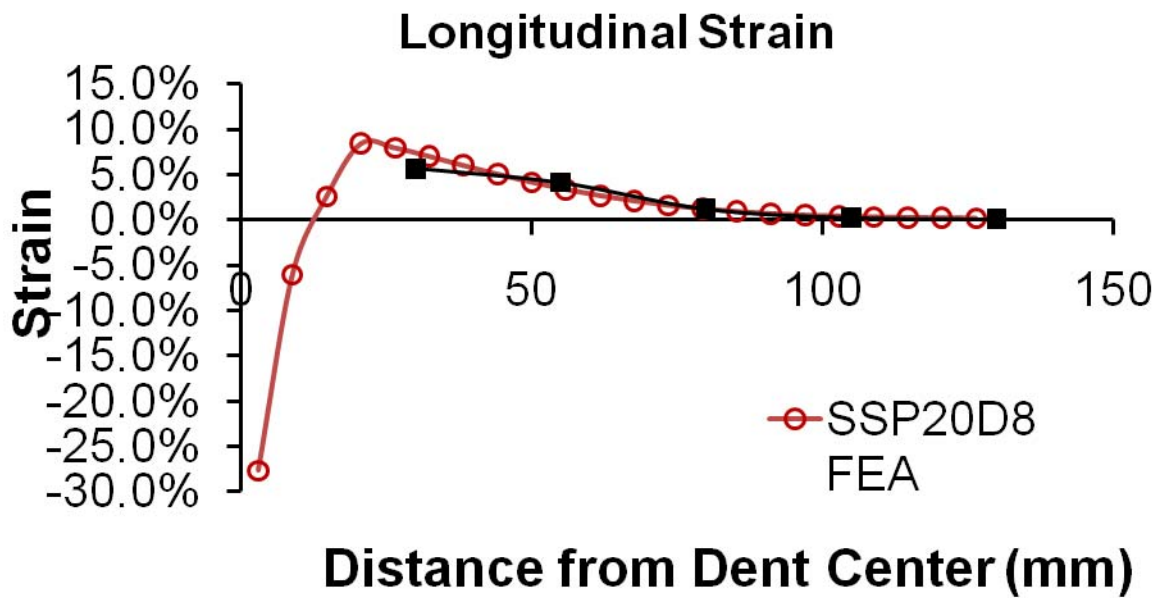


Figure 6.9: Experimental and numerical longitudinal strain distributions for Specimen SSP20D8

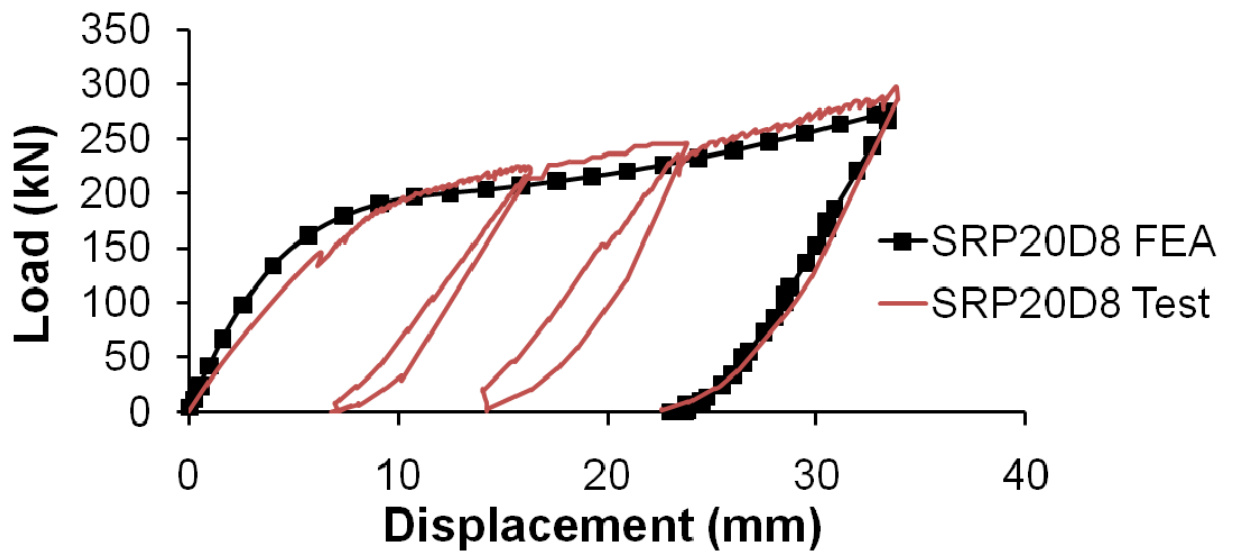


Figure 6.10: Experimental and numerical load-deformation behaviors of Specimen

SRP20D8

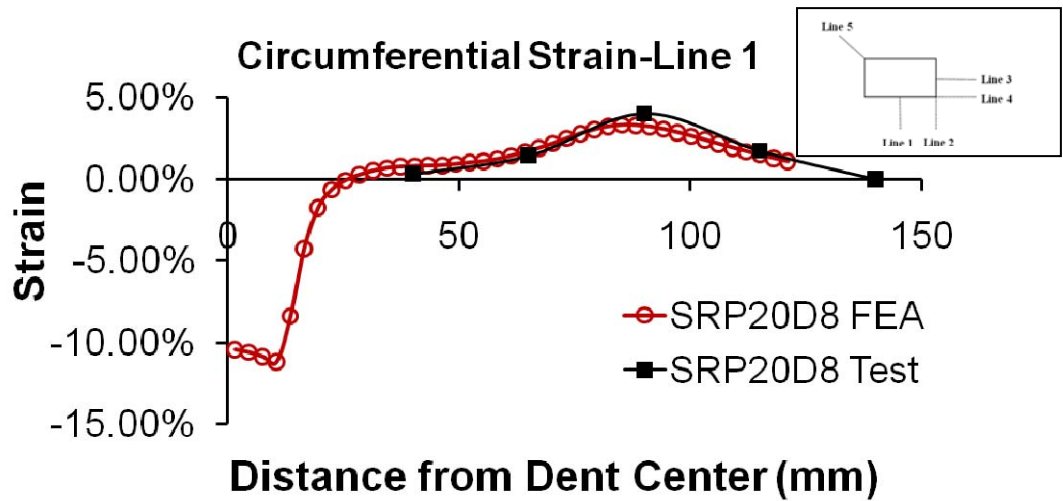


Figure 6.11(a): Experimental and numerical circumferential strain distributions for Specimen SRP20D8 for Line 1

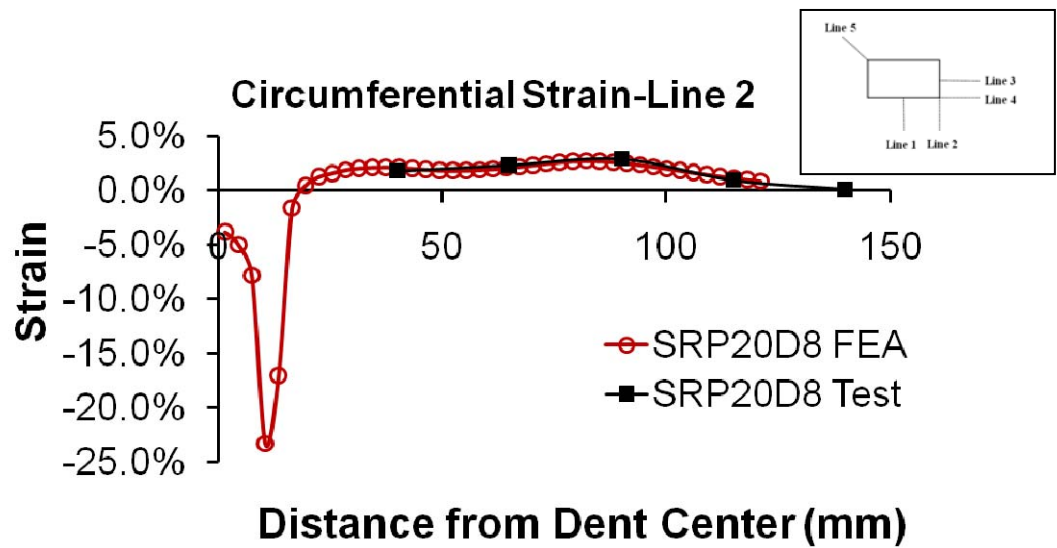


Figure 6.11(b): Experimental and numerical circumferential strain distributions for Specimen SRP20D8 for Line 2

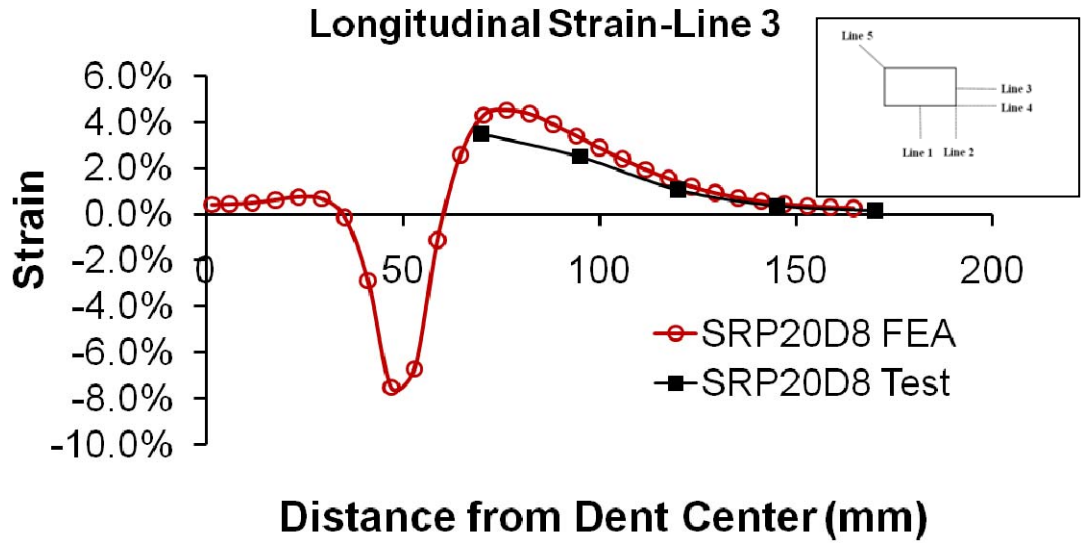


Figure 6.12(a): Experimental and numerical longitudinal strain distributions for Specimen SRP20D8 for Line 3

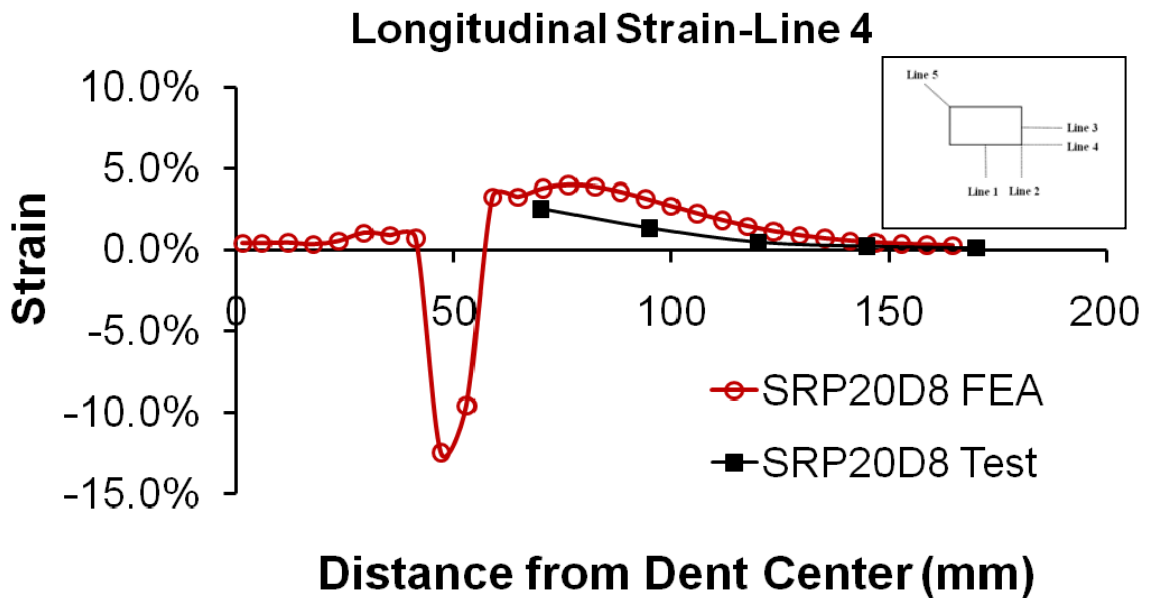


Figure 6.12(b): Experimental and numerical longitudinal strain distributions for Specimen SRP20D8 for Line 4

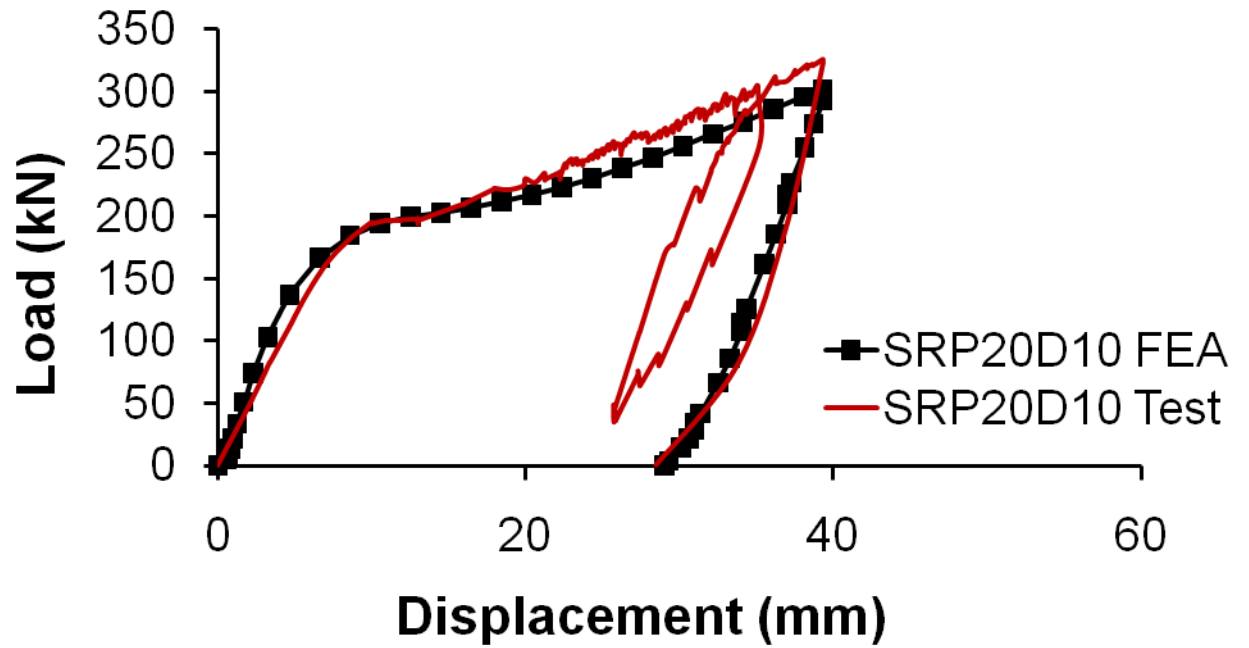


Figure 6.13: Experimental and numerical load-deformation behaviors of Specimen

SRP20D10

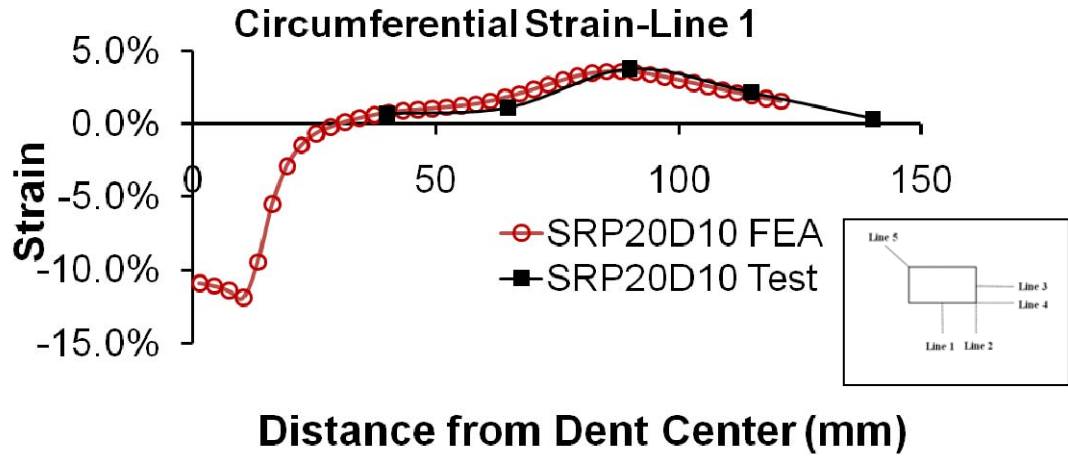


Figure 6.14(a): Experimental and numerical circumferential strain distributions for Specimen SRP20D10 for Line 1

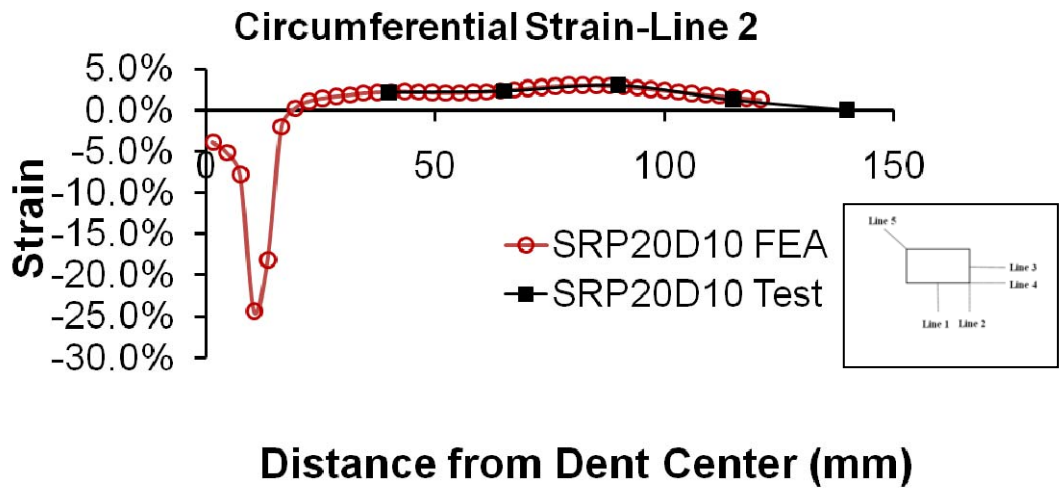


Figure 6.14(b): Experimental and numerical circumferential strain distributions for Specimen SRP20D10 along Line 2

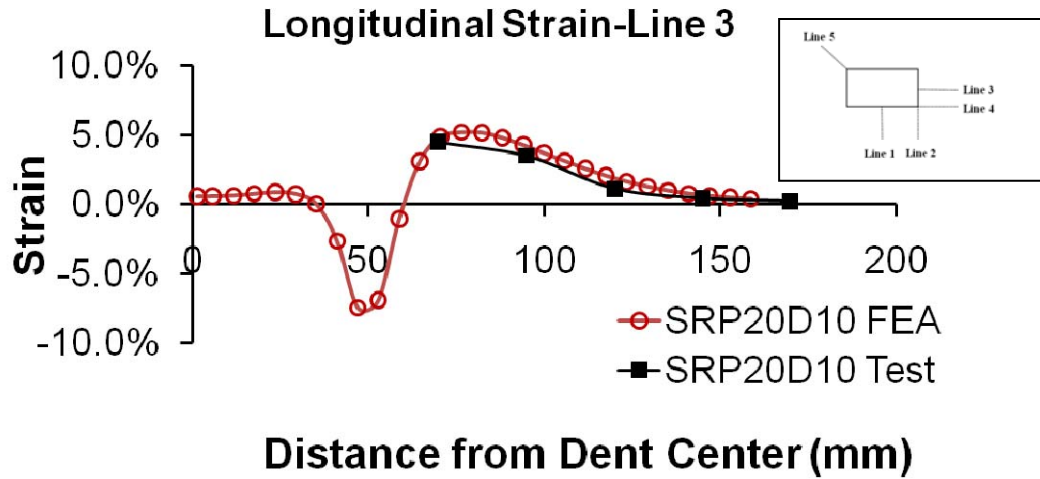


Figure 6.15(a): Experimental and numerical longitudinal strain distributions for Specimen

SRP20D10 for Line 3

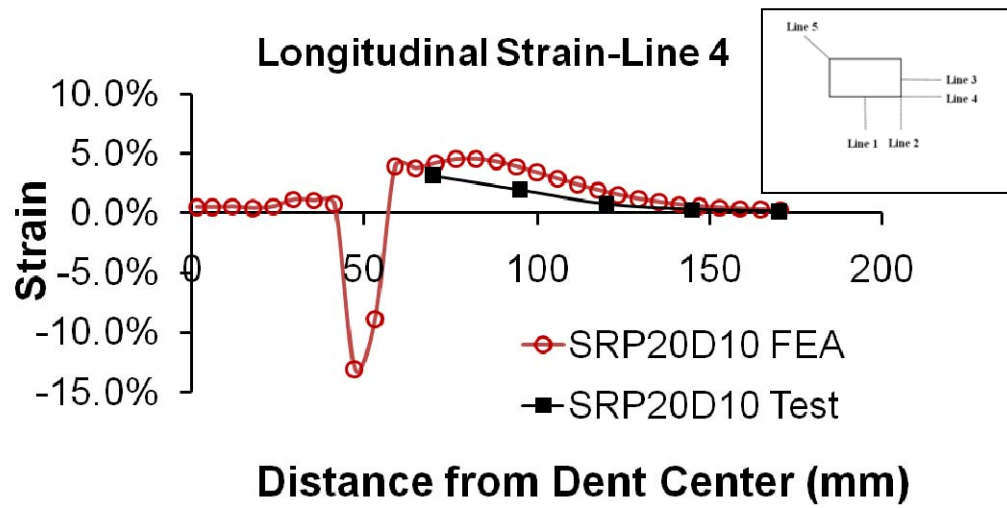


Figure 6.15(b): Experimental and numerical longitudinal strain distributions for

Specimen SRP20D10 for Line 4

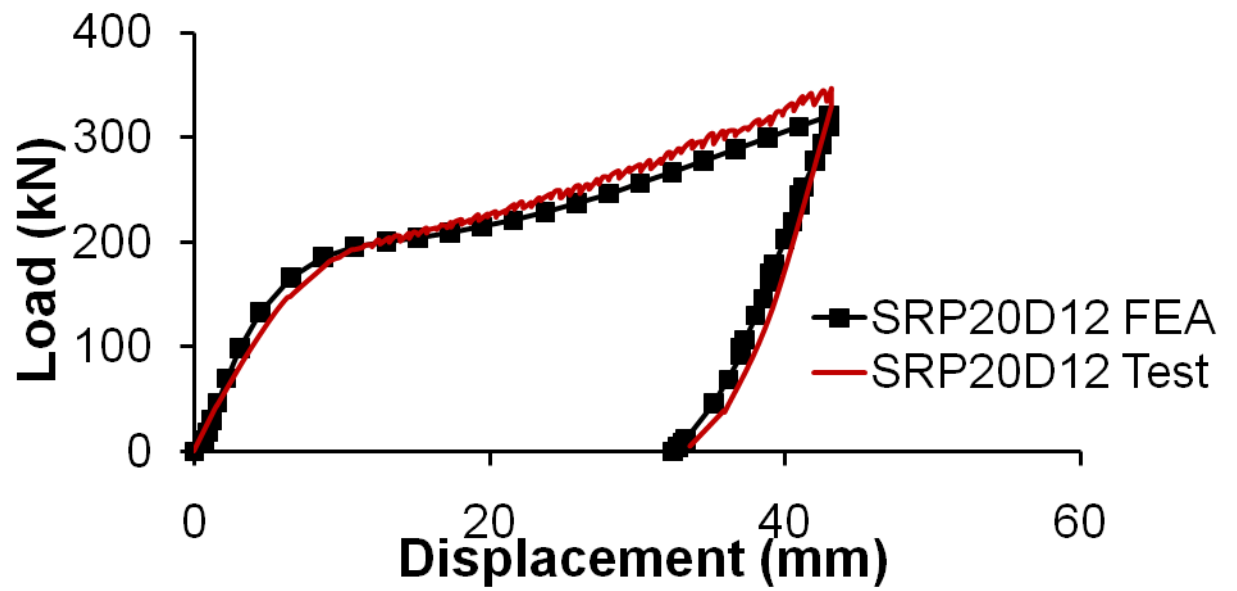


Figure 6.16: Experimental and numerical load-deformation behaviors of Specimen

SRP20D12

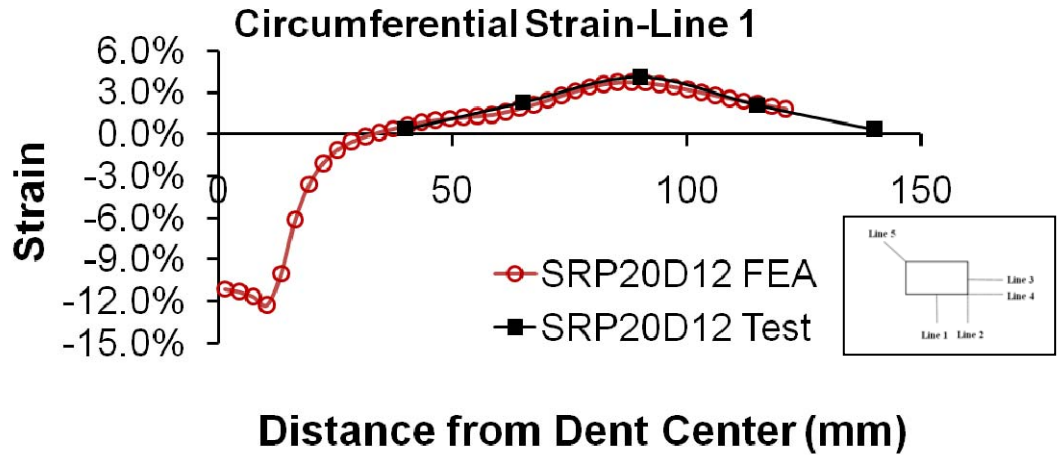


Figure 6.17(a): Experimental and numerical circumferential strain distributions for Specimen SRP20D12 for Line 1

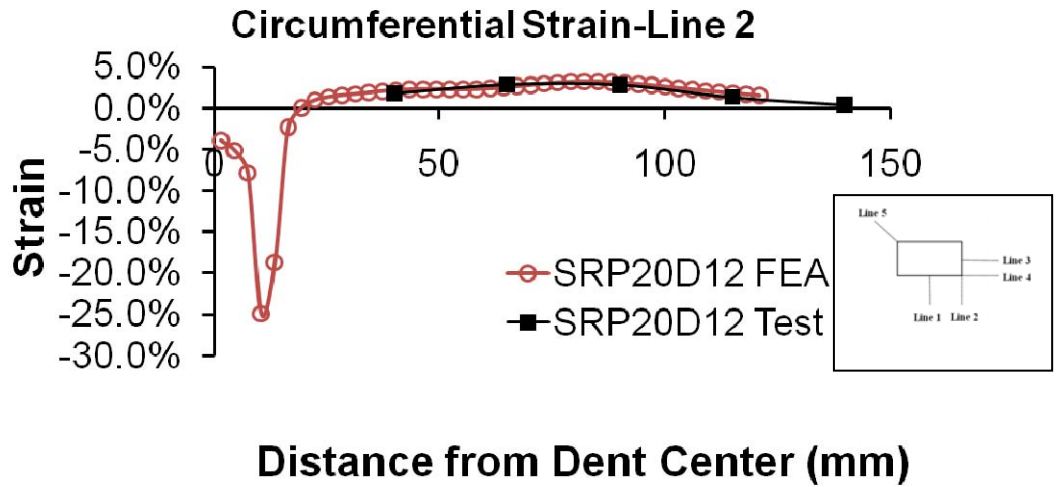


Figure 6.17(b): Experimental and numerical circumferential strain distributions for Specimen SRP20D12 for Line 2

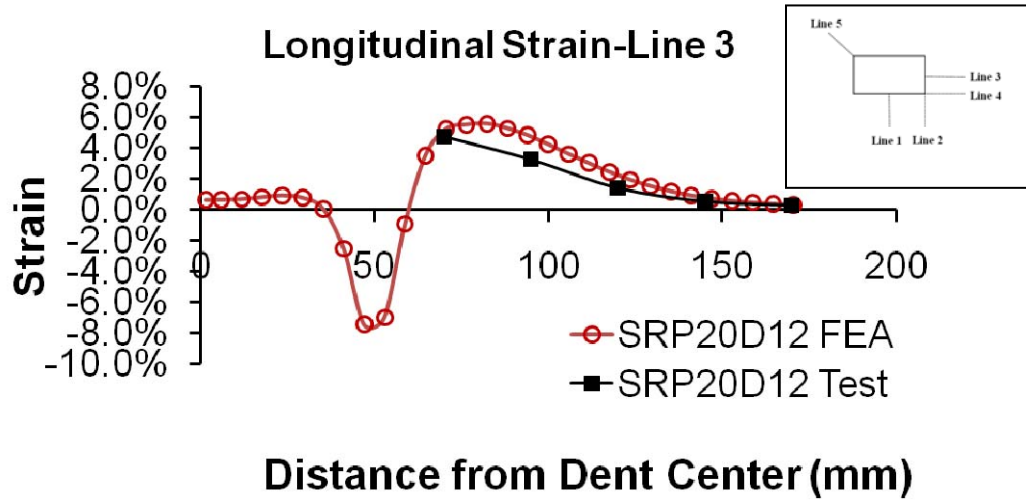


Figure 6.18(a): Experimental and numerical longitudinal strain distributions for Specimen

SRP20D12 for Line 3

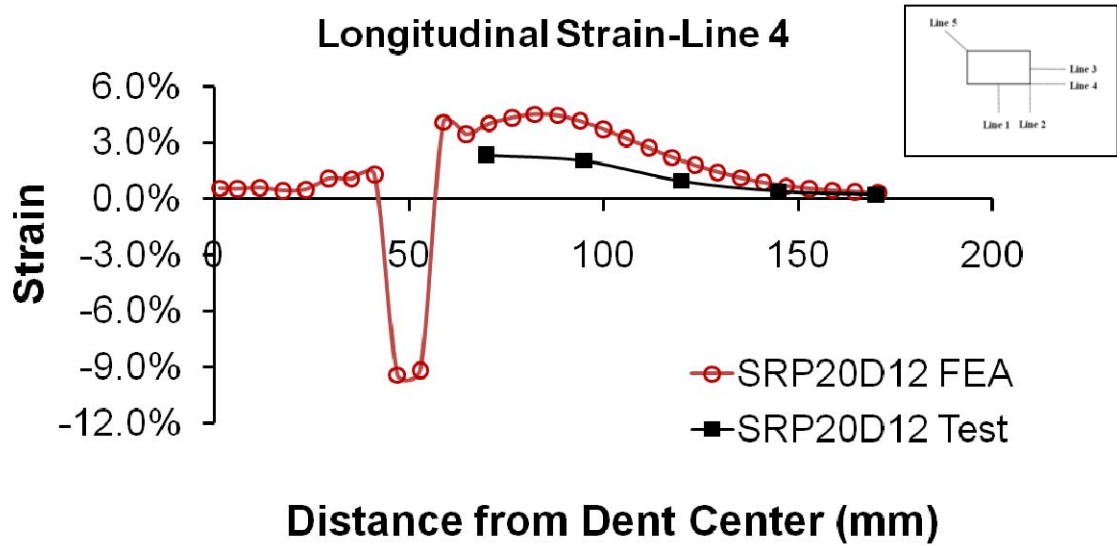


Figure 6.18(b): Experimental and numerical longitudinal strain distributions for

Specimen SRP20D12 for Line 4

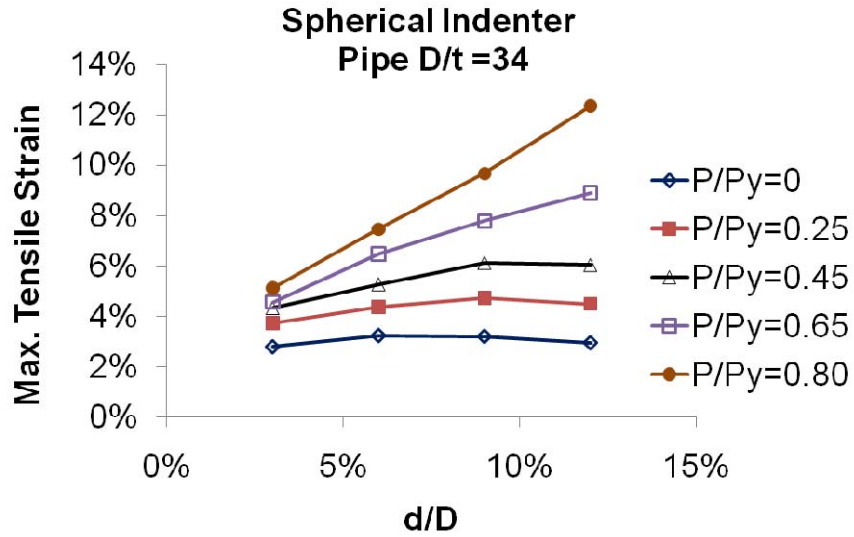


Figure 6.19(a): Effect of dent depth on the maximum circumferential tensile strain for spherical indenter and pipe with D/t of 34

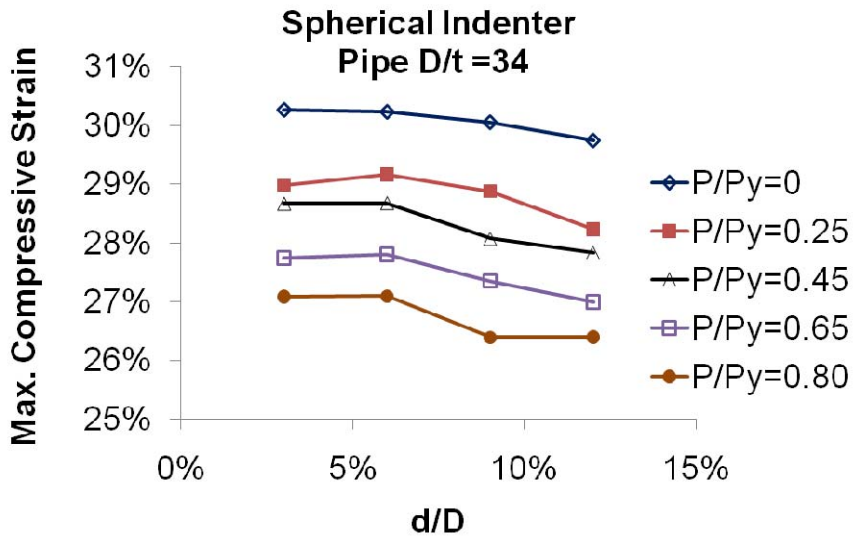


Figure 6.19(b): Effect of dent depth on the maximum circumferential compressive strain for spherical indenter and pipe with D/t of 34

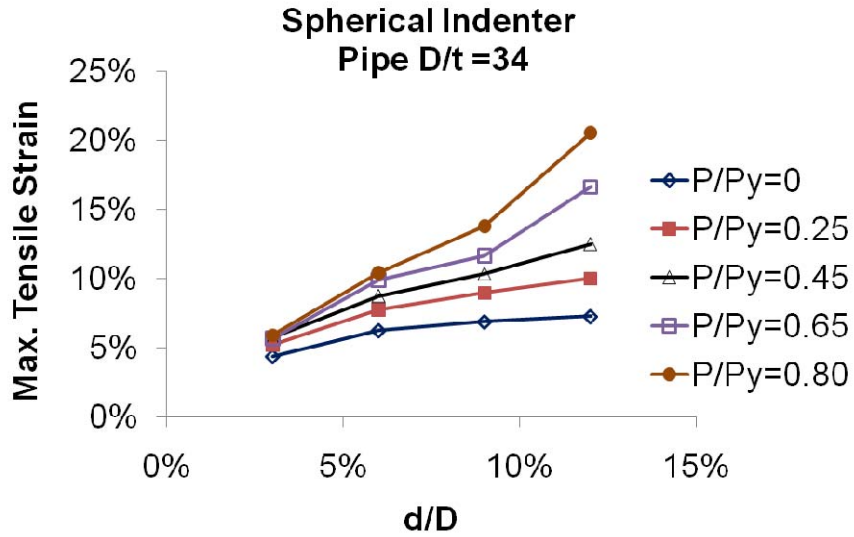


Figure 6.19(c): Effect of dent depth on the maximum longitudinal tensile strain for spherical indenter and pipe with D/t of 34

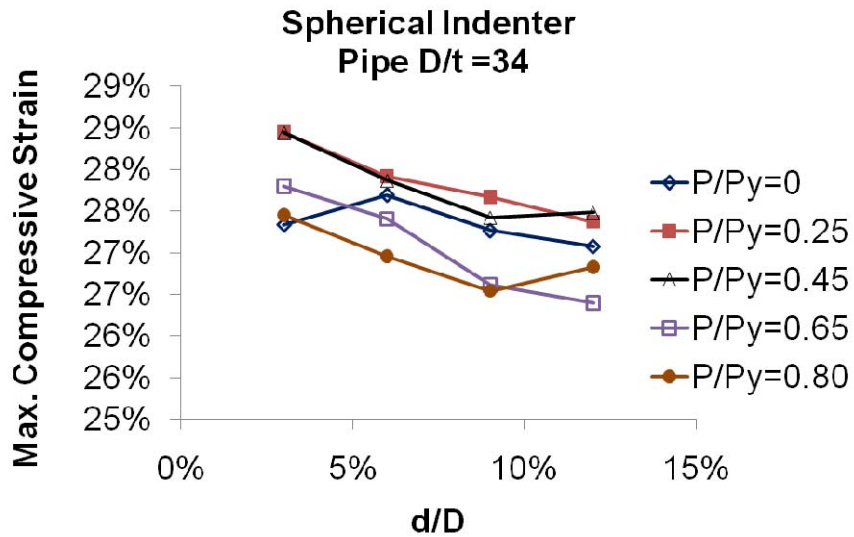


Figure 6.19(d): Effect of dent depth on the maximum longitudinal compressive strain for spherical indenter and pipe with D/t of 34

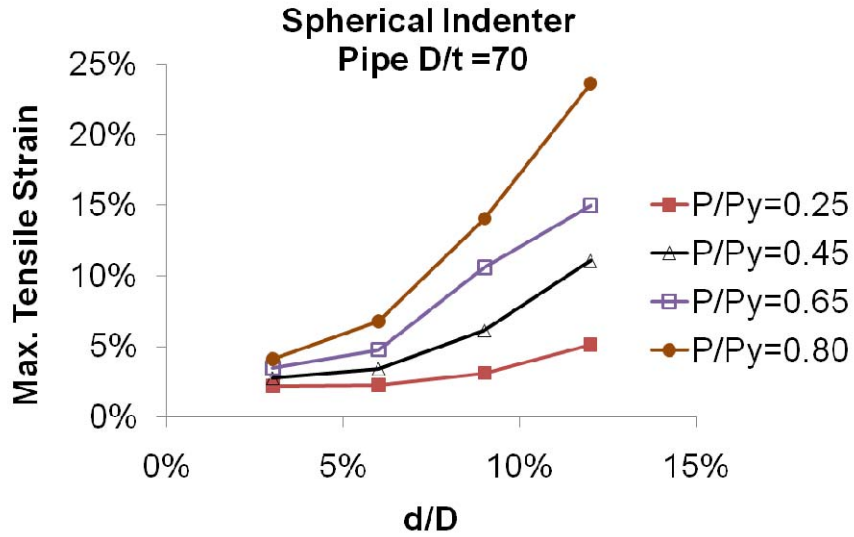


Figure 6.19(e): Effect of dent depth on the maximum circumferential tensile strain for spherical indenter and pipe with D/t of 70

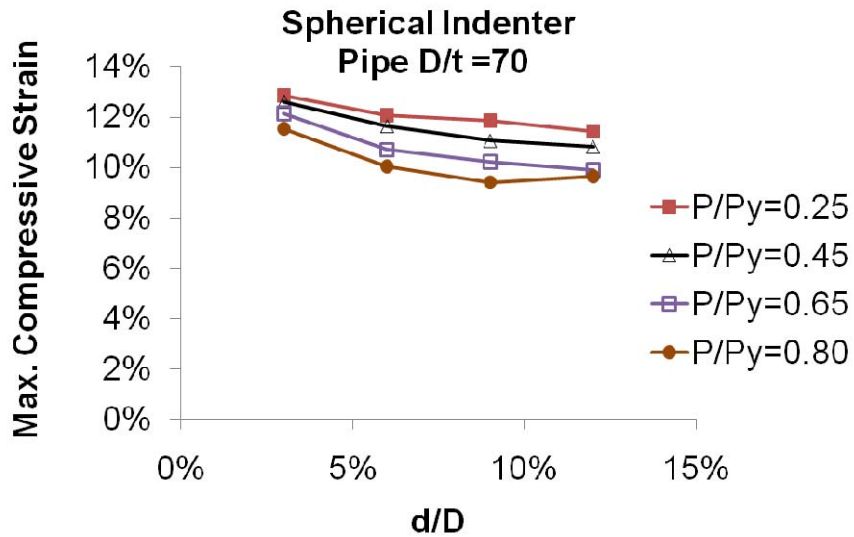


Figure 6.19(f): Effect of dent depth on the maximum circumferential compressive strain for spherical indenter and pipe with D/t of 70

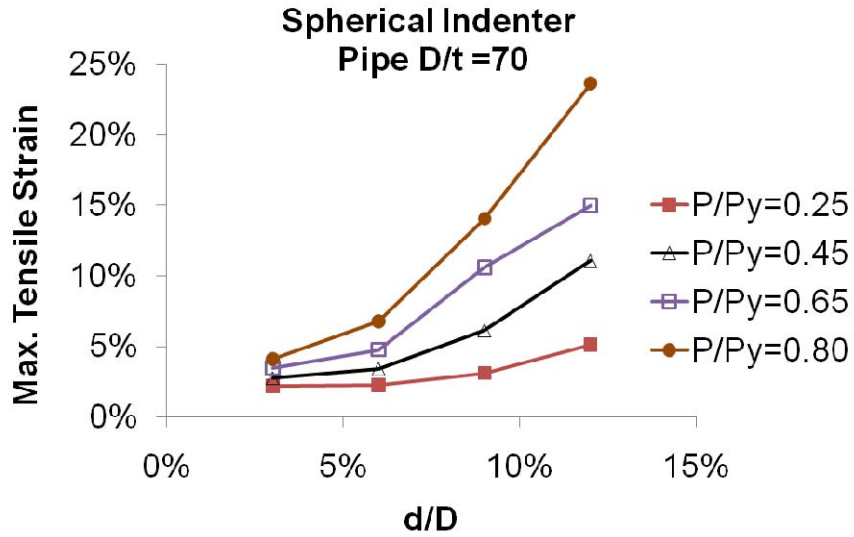


Figure 6.19(e): Effect of dent depth on the maximum circumferential tensile strain for spherical indenter and pipe with D/t of 70

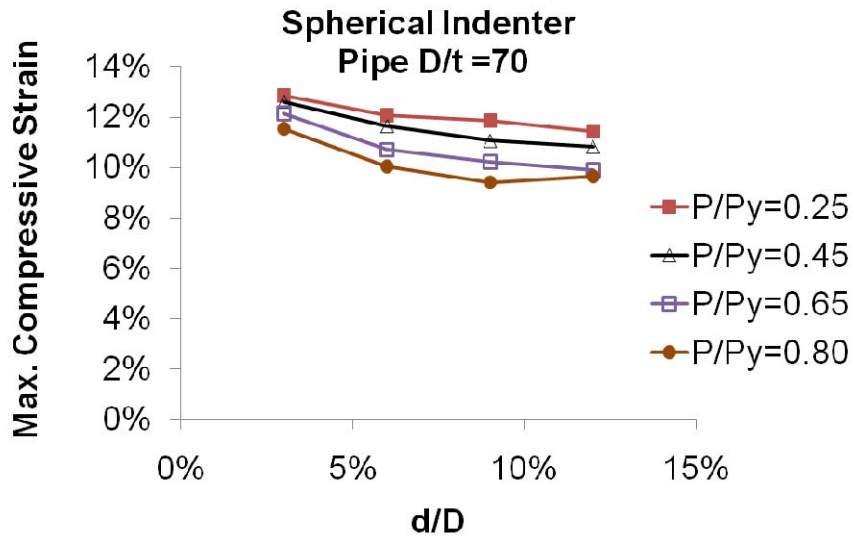


Figure 6.19(f): Effect of dent depth on the maximum circumferential compressive strain for spherical indenter and pipe with D/t of 70

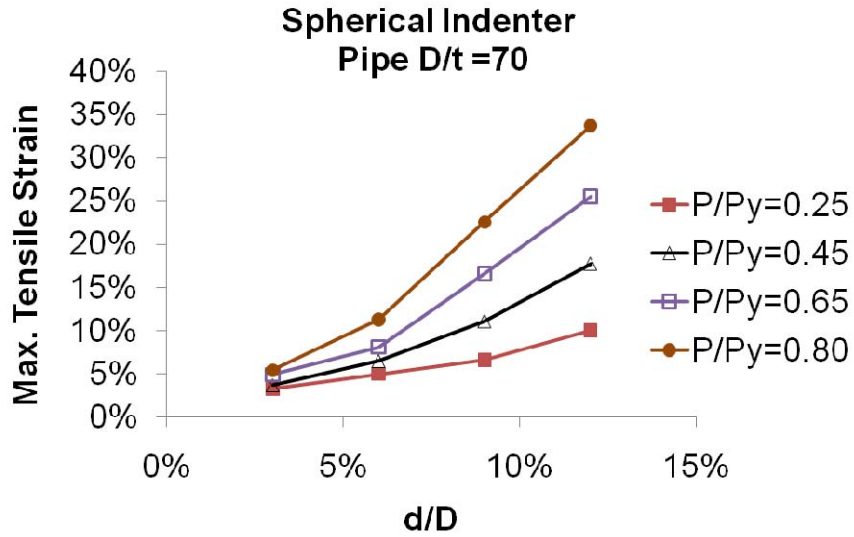


Figure 6.19(g): Effect of dent depth on the maximum longitudinal tensile strain for spherical indenter and pipe with D/t of 70

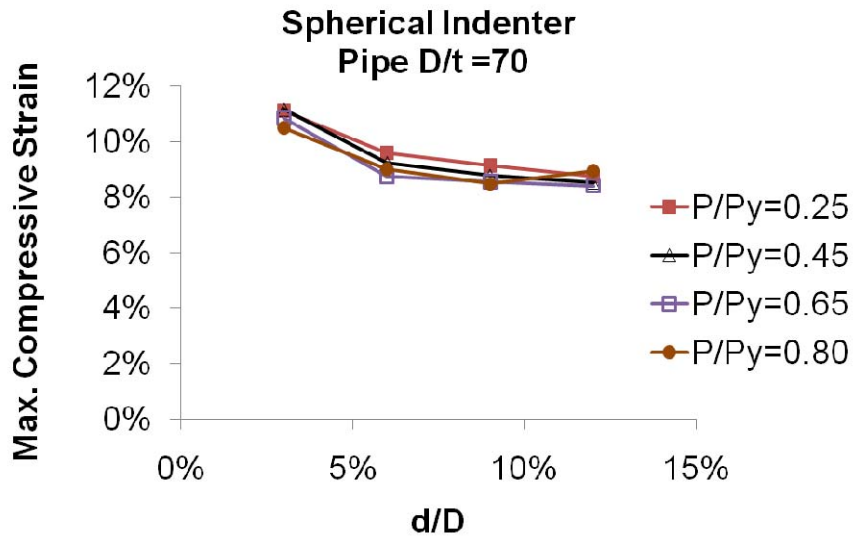


Figure 6.19(h): Effect of dent depth on the maximum longitudinal compressive strain for spherical indenter and pipe with D/t of 70

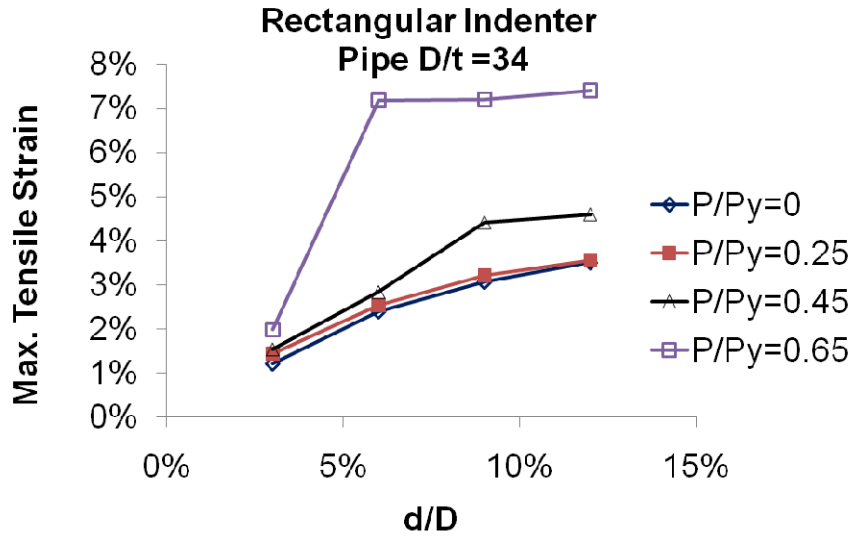


Figure 6.19(i): Effect of dent depth on the maximum circumferential tensile strain for rectangular indenter and pipe with D/t of 34

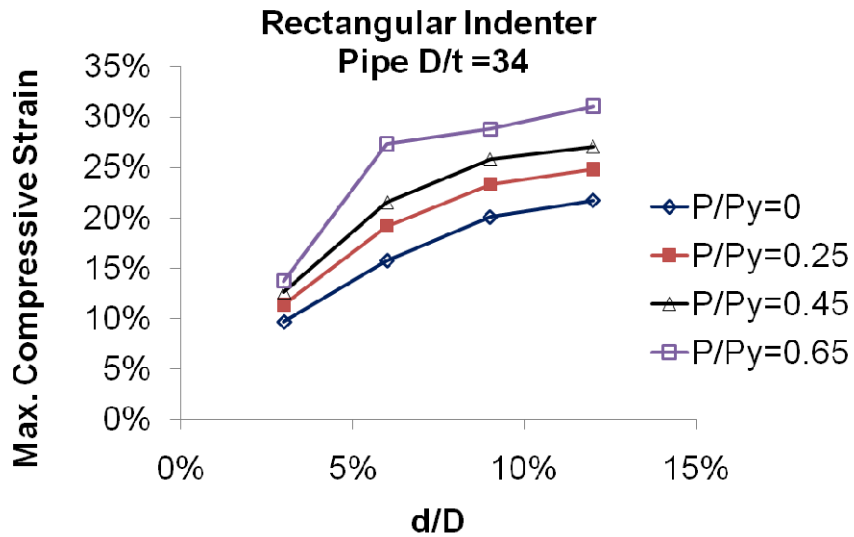


Figure 6.19(j): Effect of dent depth on the maximum circumferential compressive strain for rectangular indenter and pipe with D/t of 34

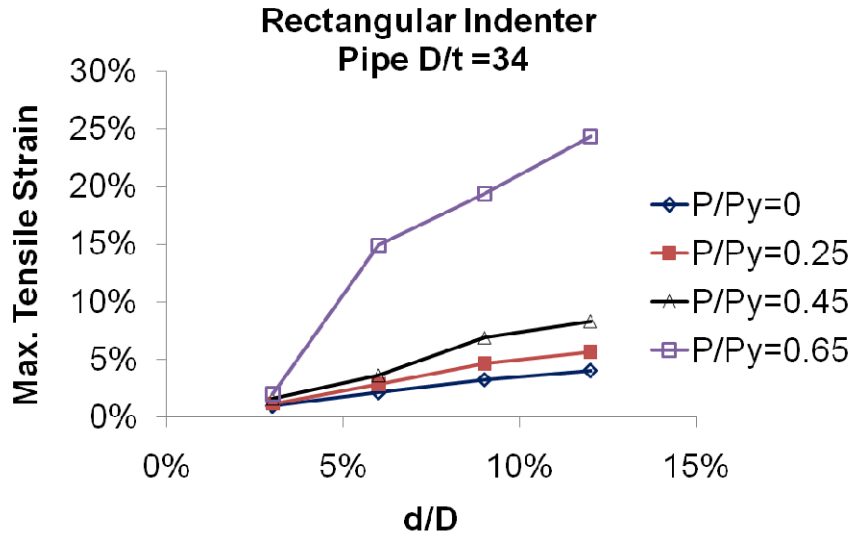


Figure 6.19(k): Effect of dent depth on the maximum longitudinal tensile strain for rectangular indenter and pipe with D/t of 34

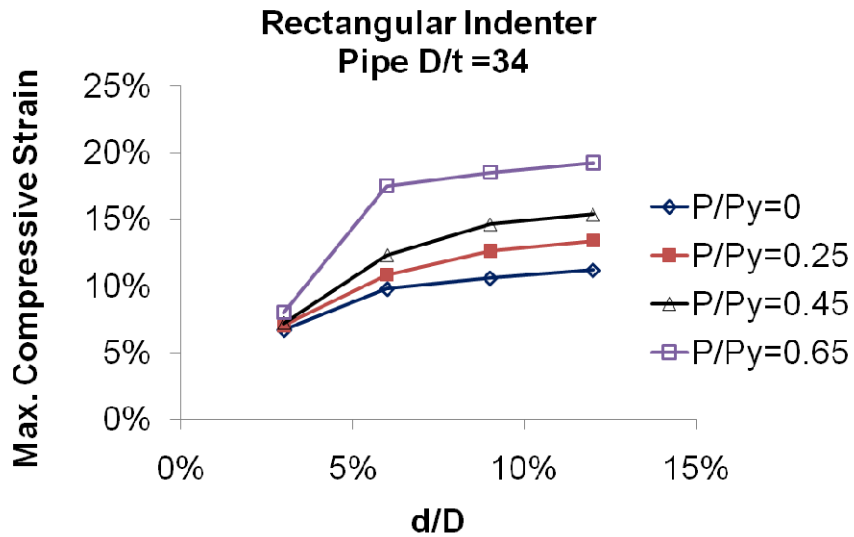


Figure 6.19(l): Effect of dent depth on the maximum longitudinal compressive strain for rectangular indenter and pipe with D/t of 34

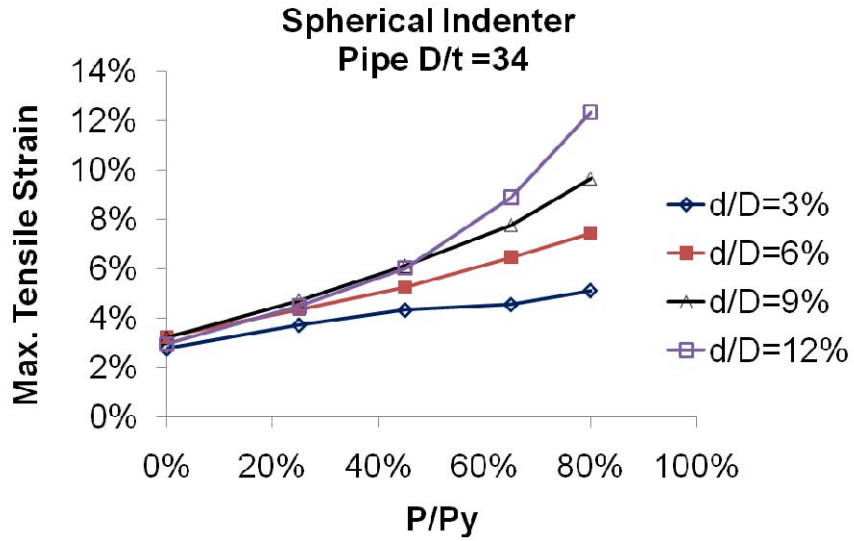


Figure 6.20(a): Effect of internal pressure on the maximum circumferential tensile strain for spherical indenter and pipe with D/t of 34

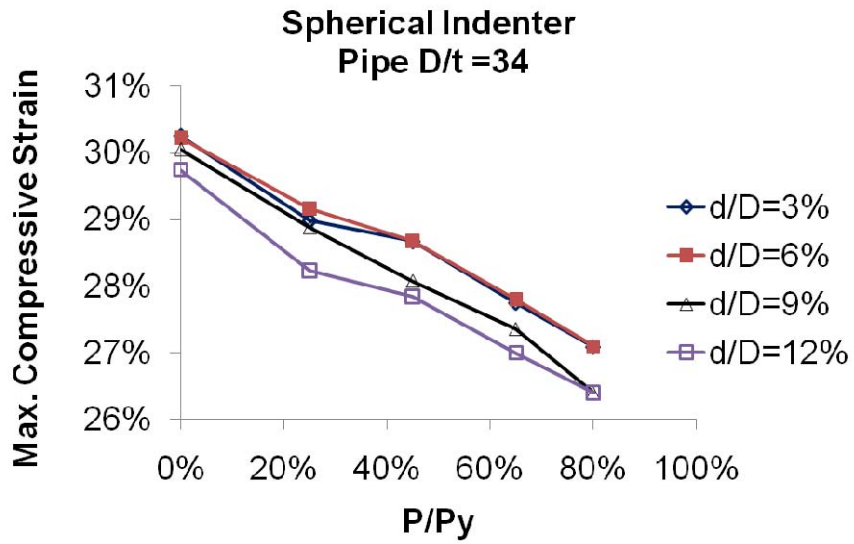


Figure 6.20(b): Effect of internal pressure on the maximum circumferential compressive strain for spherical indenter and pipe with D/t of 34

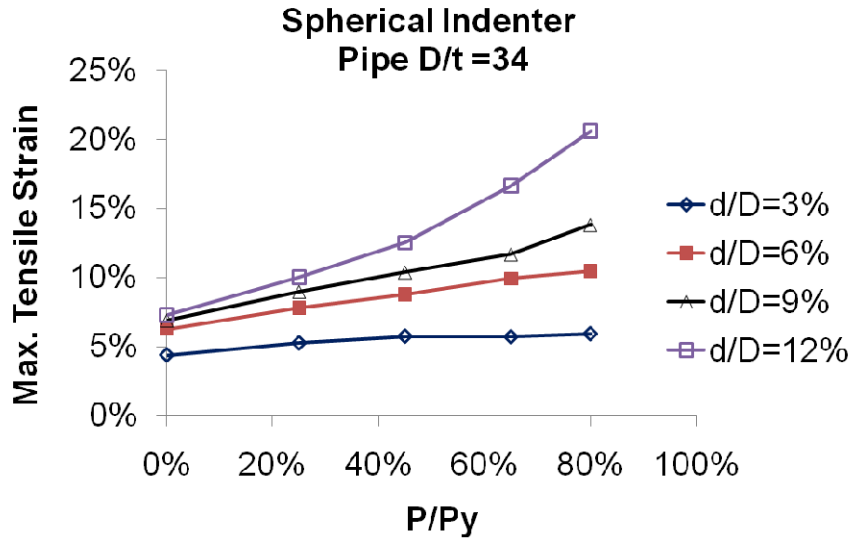


Figure 6.20(c): Effect of internal pressure on the maximum longitudinal tensile strain for spherical indenter and pipe with D/t of 34

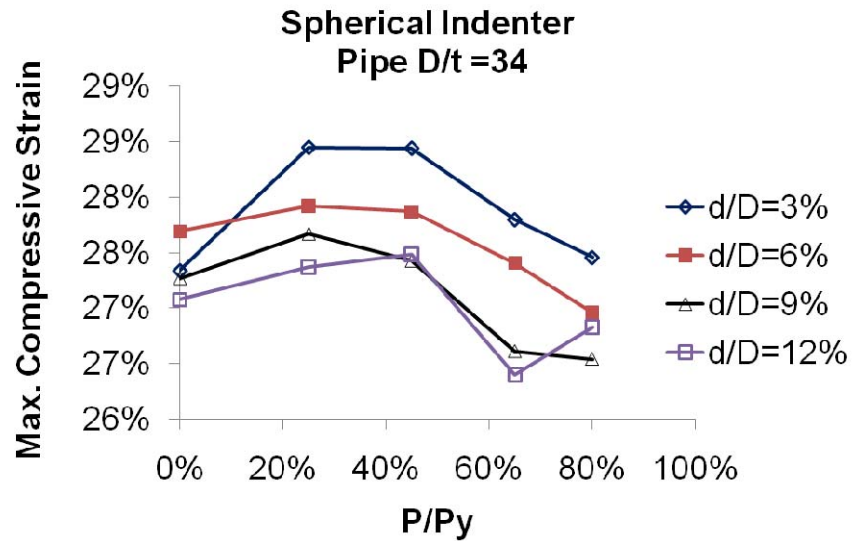


Figure 6.20(d): Effect of internal pressure on the maximum longitudinal compressive strain for spherical indenter and pipe with D/t of 34

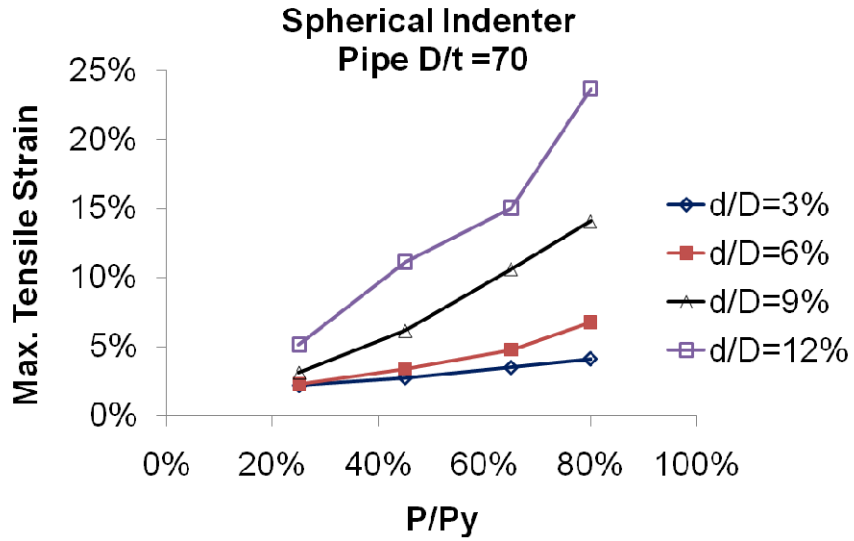


Figure 6.20(e): Effect of internal pressure on the maximum circumferential tensile strain for spherical indenter and pipe with D/t of 70

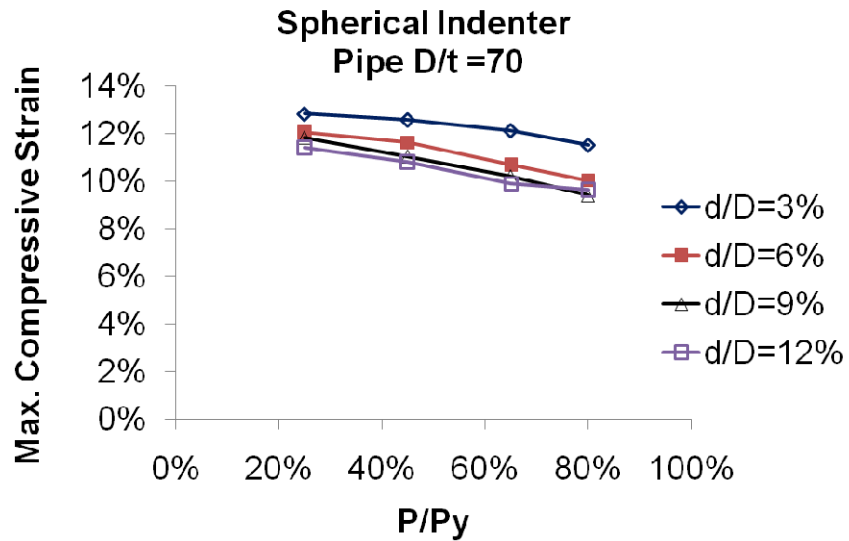


Figure 6.20(f): Effect of internal pressure on the maximum circumferential compressive strain for spherical indenter and pipe with D/t of 70

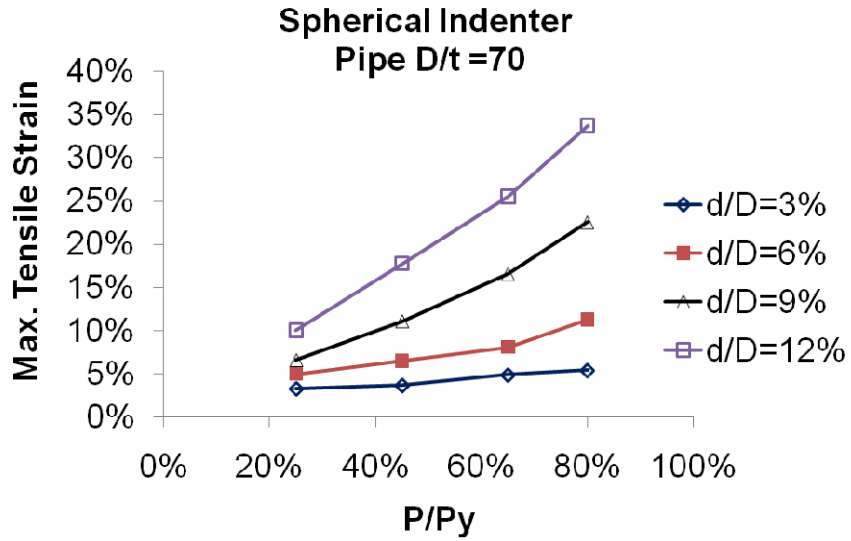


Figure 6.20(g): Effect of internal pressure on the maximum longitudinal tensile strain for spherical indenter and pipe with D/t of 70

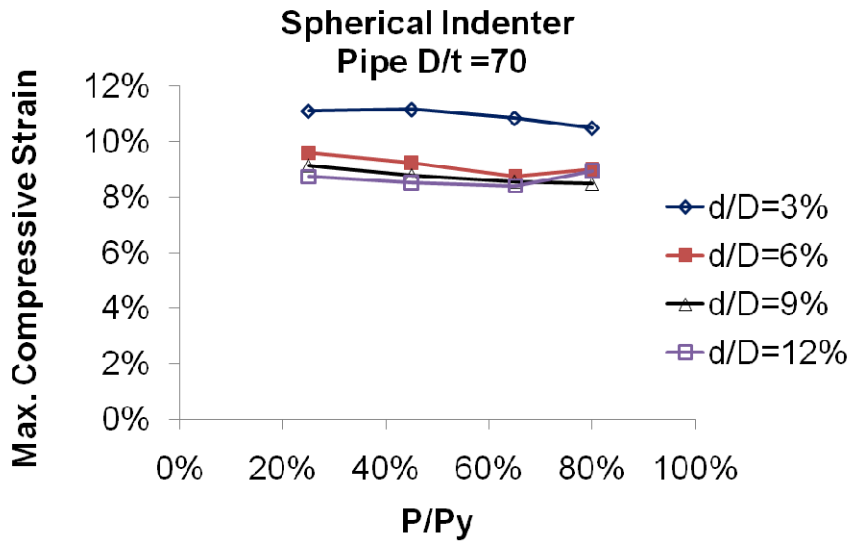


Figure 6.20(h): Effect of internal pressure on the maximum longitudinal compressive strain for spherical indenter and pipe with D/t of 70

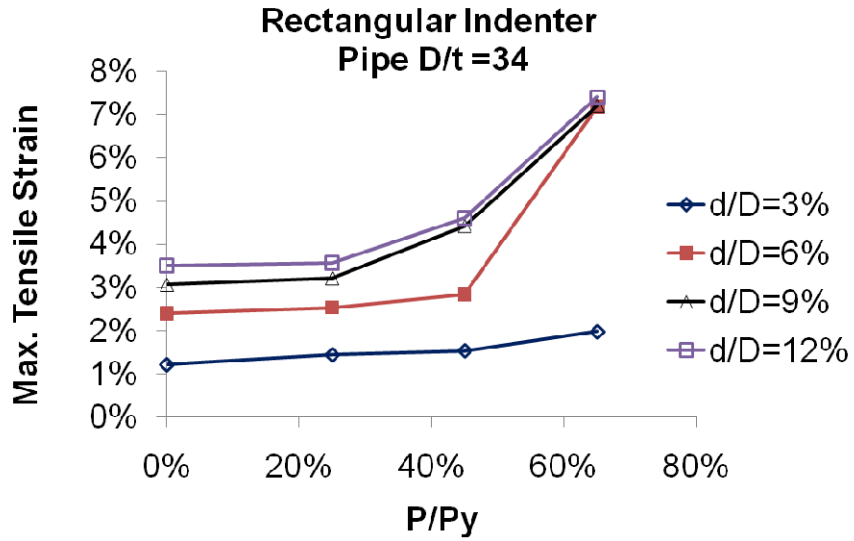


Figure 6.20(i): Effect of internal pressure on the maximum circumferential tensile strain for rectangular indenter and pipe with D/t of 34

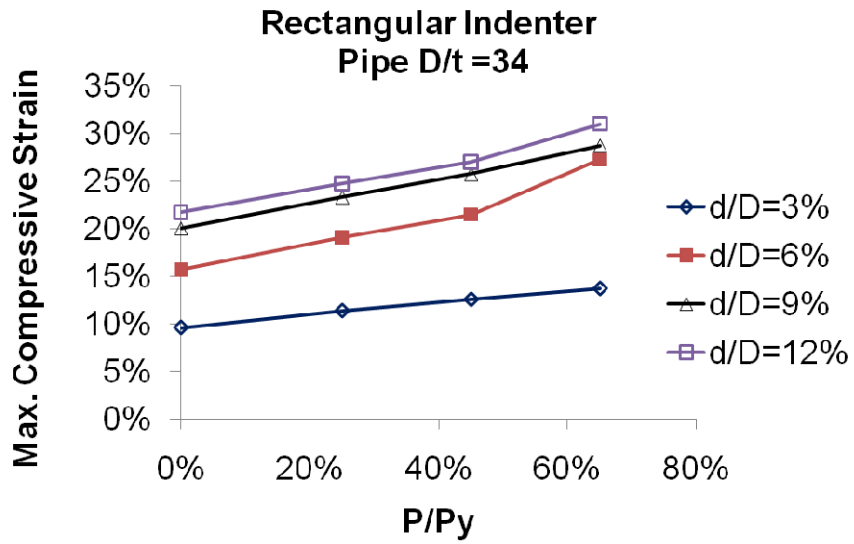


Figure 6.20(j): Effect of internal pressure on the maximum circumferential compressive strain for rectangular indenter and pipe with D/t of 34

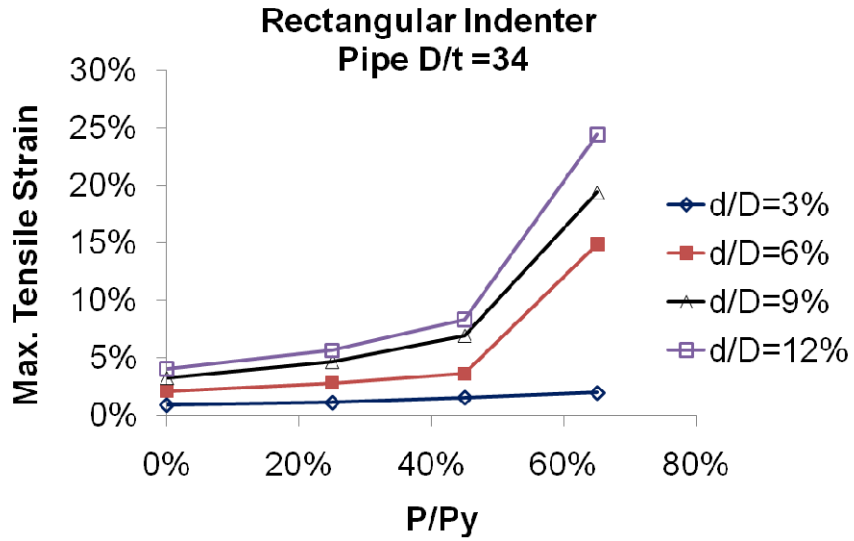


Figure 6.20(k): Effect of internal pressure on the maximum longitudinal tensile strain for rectangular indenter and pipe with D/t of 34

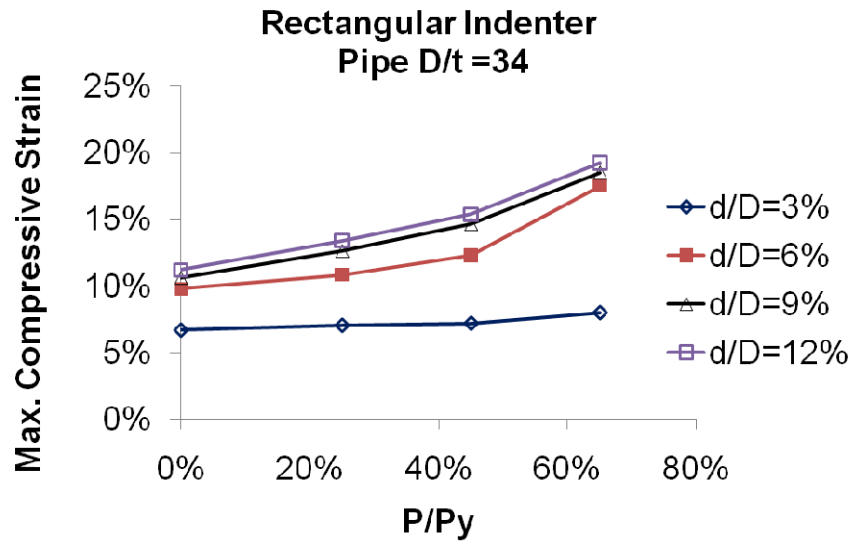


Figure 6.20(l): Effect of internal pressure on the maximum longitudinal compressive strain for rectangular indenter and pipe with D/t of 34

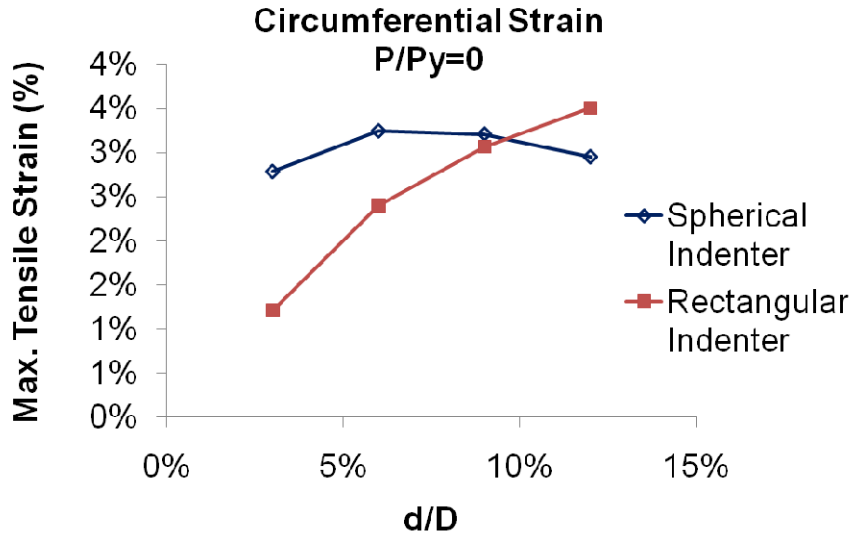


Figure 6.21(a): Effect of indenter shape on the maximum circumferential tensile strain at 0 internal pressure and pipe with D/t of 34

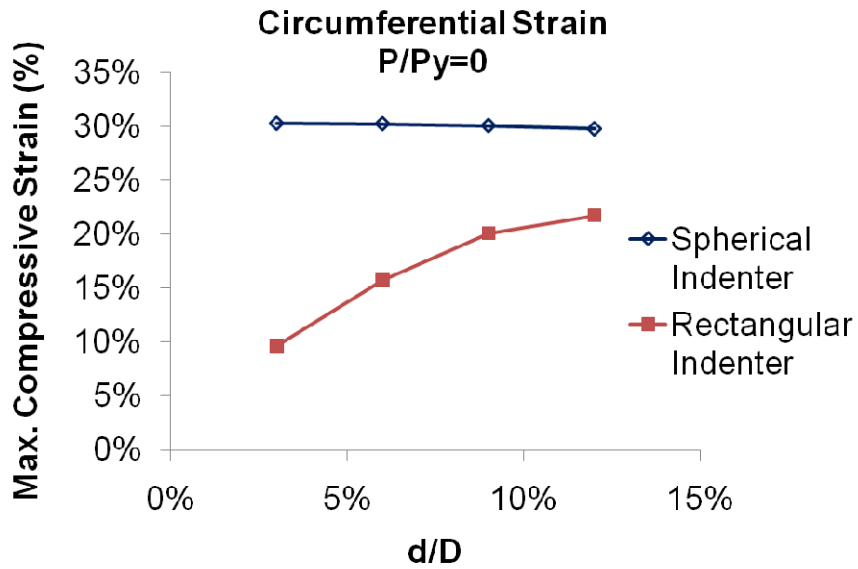


Figure 6.21(b): Effect of indenter shape on the maximum circumferential compressive strain at 0 internal pressure and pipe with D/t of 34

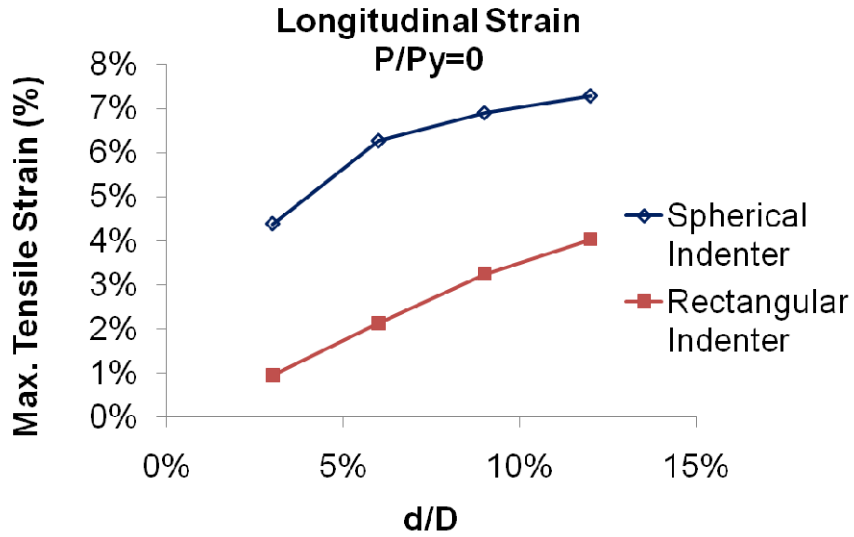


Figure 6.21(c): Effect of indenter shape on the maximum longitudinal tensile strain at 0 internal pressure and pipe with D/t of 34

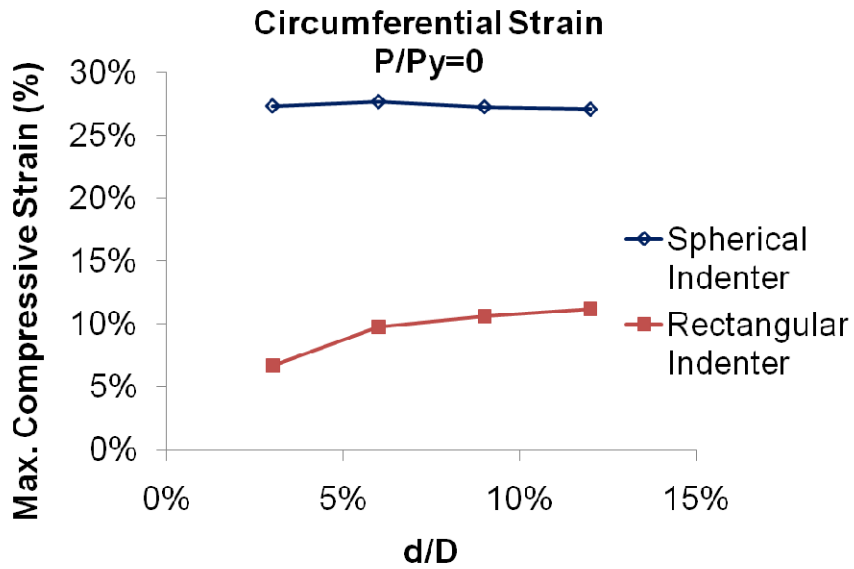


Figure 6.21(d): Effect of indenter shape on the maximum longitudinal compressive strain at 0 internal pressure and pipe with D/t of 34

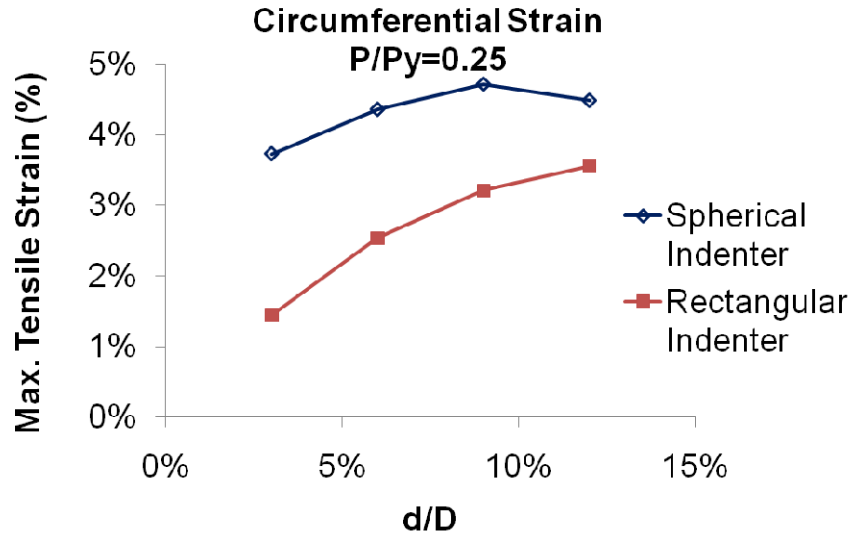


Figure 6.21(e): Effect of indenter shape on the maximum circumferential tensile strain at 0 internal pressure and pipe with D/t of 34

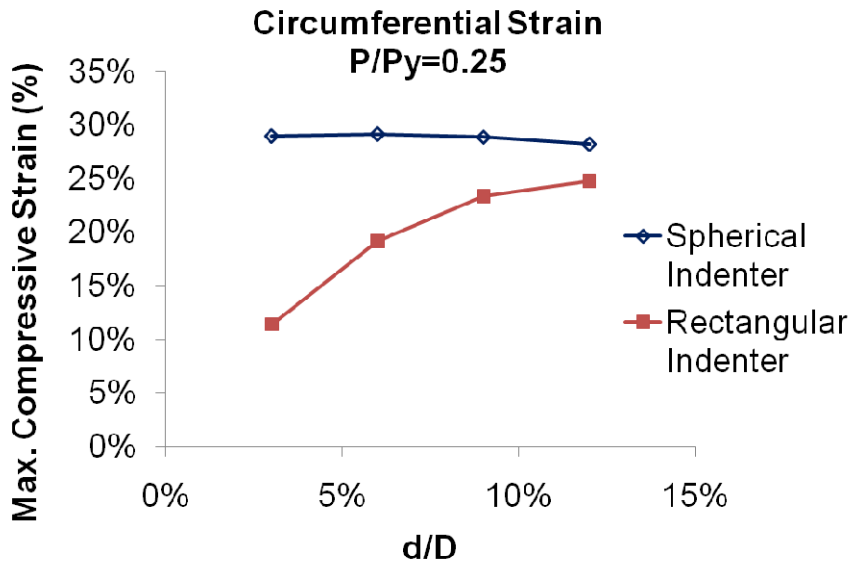


Figure 6.21(f): Effect of indenter shape on the maximum circumferential compressive strain at $0.25p_y$ internal pressure and pipe with D/t of 34

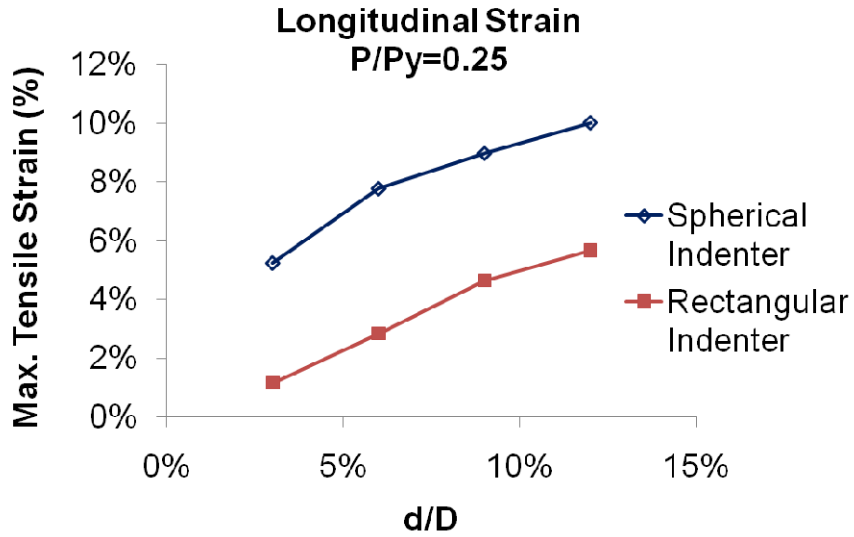


Figure 6.21(g): Effect of indenter shape on the maximum longitudinal tensile strain at 0.25 p_y internal pressure and pipe with D/t of 34

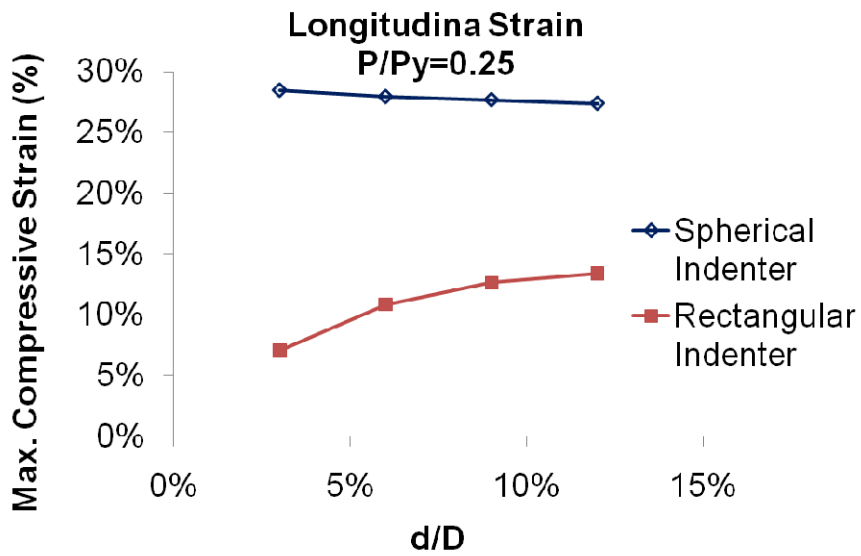


Figure 6.21(h): Effect of indenter shape on the maximum longitudinal compressive strain at 0.25 p_y internal pressure and pipe with D/t of 34

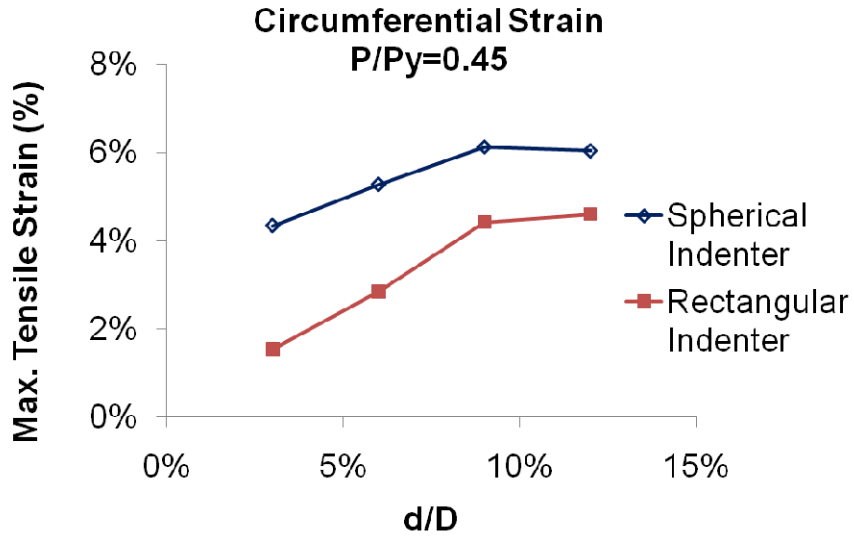


Figure 6.21(i): Effect of indenter shape on the maximum circumferential tensile strain at $0.45p_y$ internal pressure and pipe with D/t of 34

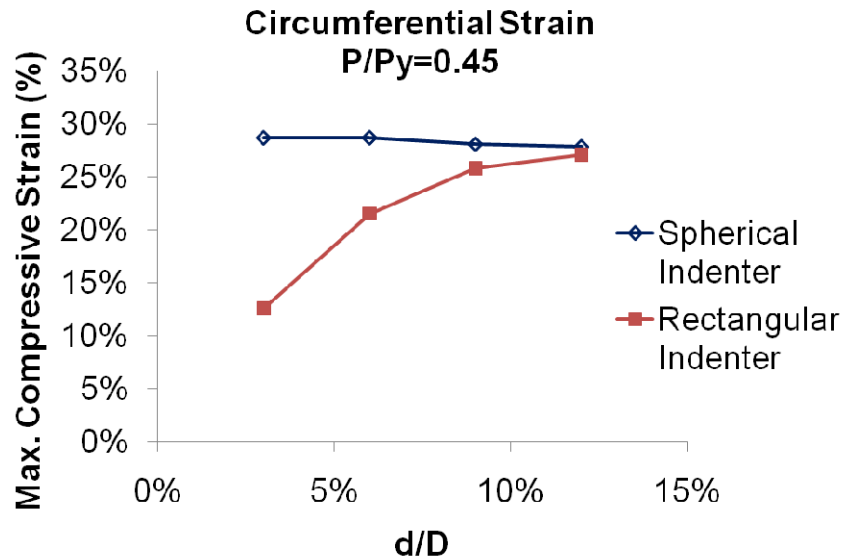


Figure 6.21(j): Effect of indenter shape on the maximum circumferential compressive strain at $0.45p_y$ internal pressure and pipe with D/t of 34

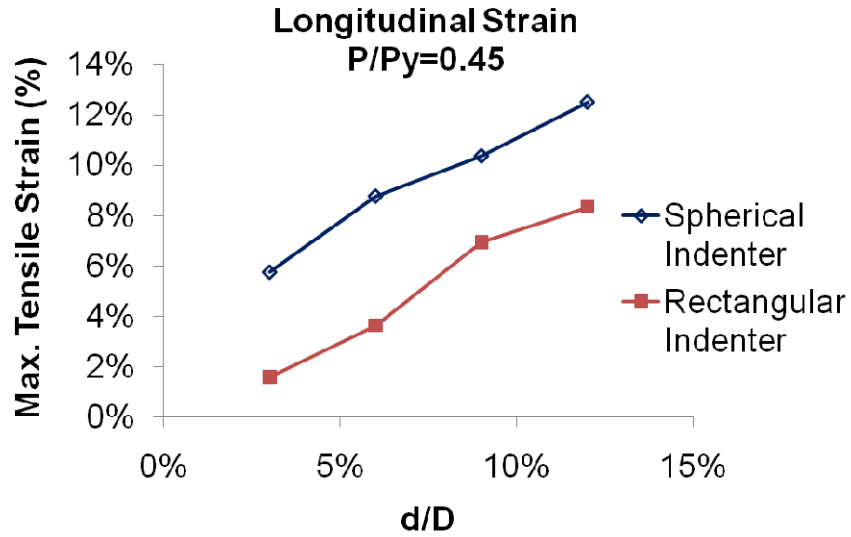


Figure 6.21(k): Effect of indenter shape on the maximum longitudinal tensile strain at 0.45 p_y internal pressure and pipe with D/t of 34

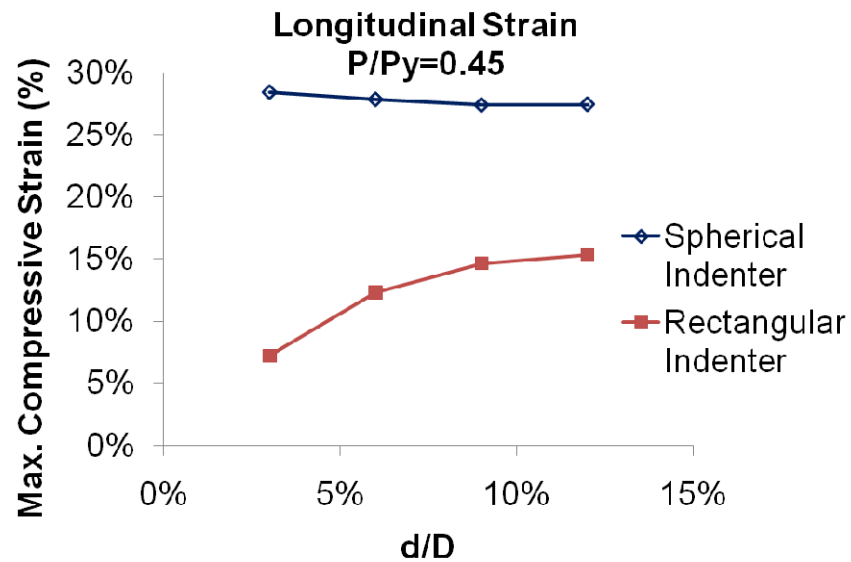


Figure 6.21(l): Effect of indenter shape on the maximum longitudinal compressive strain at 0.45 p_y internal pressure and pipe with D/t of 34

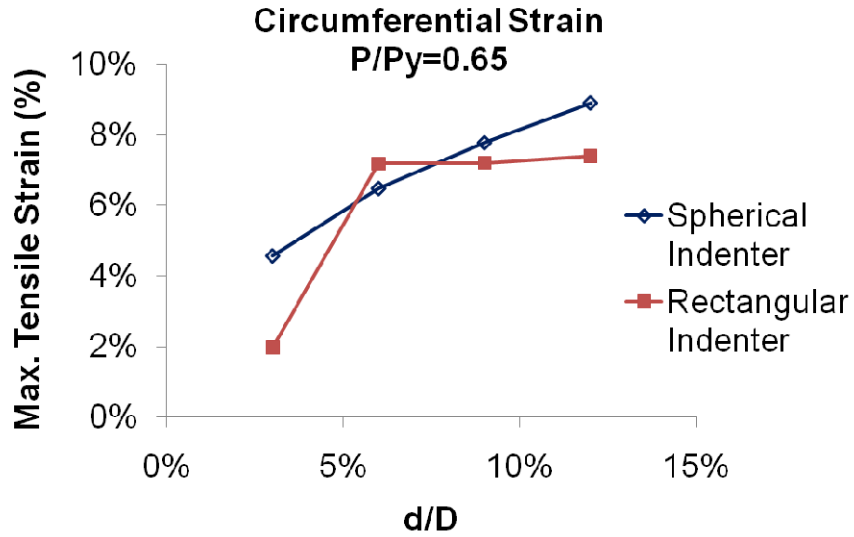


Figure 6.21(m): Effect of indenter shape on the maximum circumferential tensile strain at $0.65p_y$ internal pressure and pipe with D/t of 34

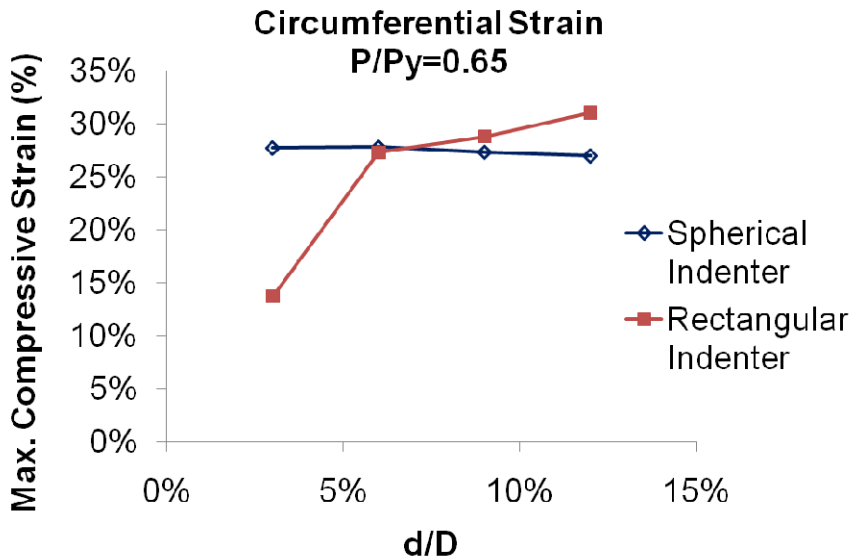


Figure 6.21(n): Effect of indenter shape on the maximum circumferential compressive strain at $0.65p_y$ internal pressure and pipe with D/t of 34

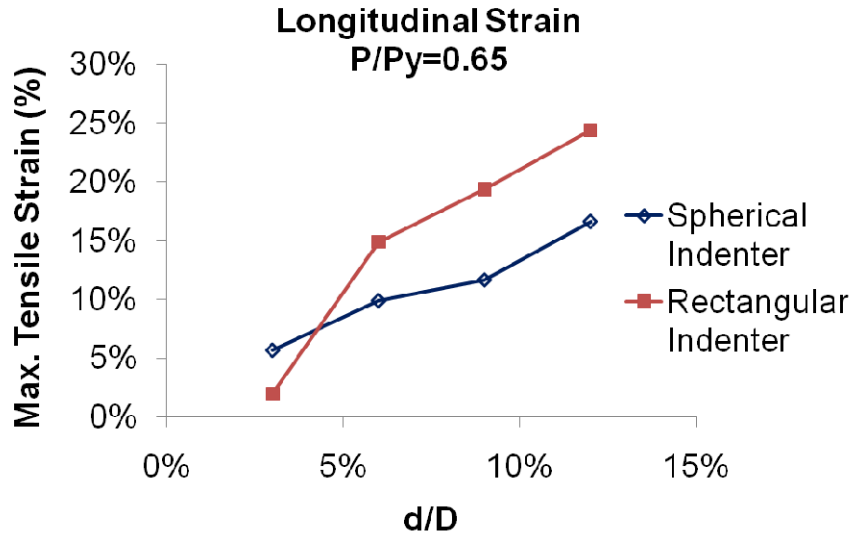


Figure 6.21(o): Effect of indenter shape on the maximum longitudinal tensile strain at $0.65 p_y$ internal pressure and pipe with D/t of 34

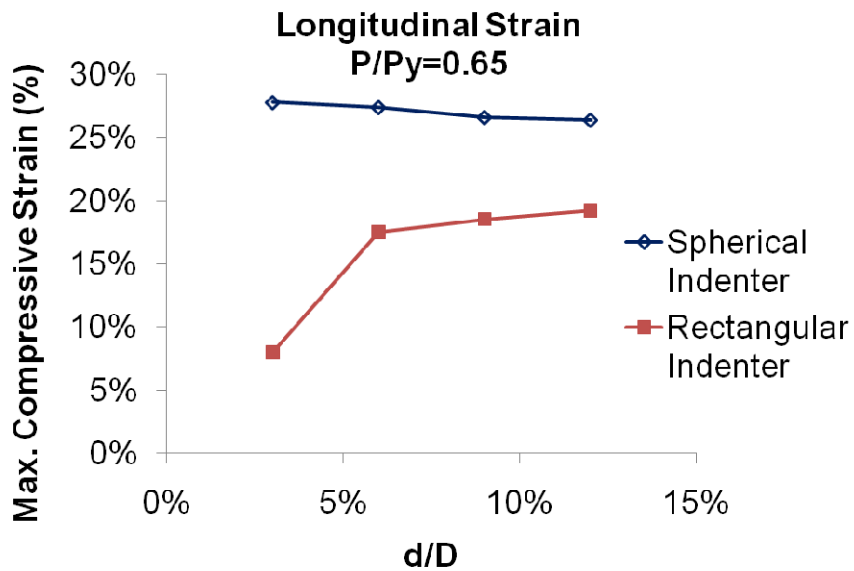


Figure 6.21(p): Effect of indenter shape on the maximum longitudinal compressive strain at $0.65 p_y$ internal pressure and pipe with D/t of 34

CHAPTER 7

ASME DENT STRAIN EQUATIONS

7.1 General

Dent depth as a percentage of outer diameter of the pipe is the only geometric parameter which is most commonly used by the different codes, standards, and manuals for determining the severity and acceptability of a dent in the field pipeline. Dent depth can be a possible threat to the operational and structural integrity of a pipeline. However, depth is not always the most useful parameter for identifying whether or not a dent is threat to the structural integrity of pipeline. The use of depth alone can result in unnecessary excavations required for the repair of many dents those do not necessarily pose any threat to the structural integrity of pipeline. On the other hand a dent with a small depth can be much severe if the shape is such that it creates creating large stress or strain concentrations (Gao et al., 2008). In case of flaws like dents which are mainly characterized as deformation, the local strain in the material could be a more appropriate criterion for judging its severity (Baker, 2004). The previous edition of ASME B31.8 (ASME 2003) acknowledges this concept and hence offers an option for using strain based criterion for determining severity of dents. It also provides non mandatory formulas for calculating the strain associated with a dent. In the current edition of ASME B31.8 (ASME2007), some corrections to the equations are provided. The main purpose of this chapter is to review the assumptions and equations presented in ASME B31.8 (2007) and indentify the shortcomings and strength of these equations. Then based on the current study, new suggestions are made to improve these equations.

7.2 Dent Strain

The strain in a dent can be divided in two main components: longitudinal and circumferential strains. Both the longitudinal and circumferential strains can be further divided into bending and membrane strains. The bending strain is proportional to the curvature of the dent and the thickness of the pipe wall. It changes linearly from outer surface to inner surface of the pipe wall and attains a maximum value at the surfaces. Bending strain is compressive on the inside of a bend and tensile on the outside of a bend. Membrane strain is uniform through the material thickness and occurs where the pipe wall is stretched or contracted (Rosenfeld et al. 1998 and Lukasiewicz et al. 2006).

7.3 ASME B31.8 Equations

The 2003 edition of ASME B31.8 (ASME 2003) recognized the fact that evaluation of dent should consider the strain values in the dent. Hence this edition of ASME B31.8 (ASME 2003) provided relationships for the calculation dent strain. According to the ASME B31.8 (2003) the estimation of the maximum strain in a dent is performed by first evaluating separately the following three strain components.

1. Bending strain in circumferential direction
2. Bending strain in longitudinal direction, and
3. Membrane strain in longitudinal direction

The relationships presented in ASME B31.8 (ASME 2003) are as follows.

1. Bending strain in circumferential direction

$$\varepsilon_1 = t \left(\frac{1}{R_0} - \frac{1}{R_1} \right) \quad (7.1)$$

2. Bending strain in longitudinal direction

$$\varepsilon_2 = -\left(\frac{t}{R_2}\right) \quad (7.2)$$

3. Membrane strain in longitudinal direction

$$\varepsilon_3 = \left(\frac{1}{2}\right) \left(\frac{d}{L}\right)^2 \quad (7.3)$$

In these equations, R_0 is the radius of curvature of undeformed pipe surface, which is half of the nominal outside diameter of the pipe and t , d , L correspond respectively to the wall thickness, dent depth and dent length in longitudinal direction respectively (Figure 7.2). The R_1, R_2 are the external surface radii of curvature and are measured respectively, in the transverse and longitudinal planes through the dent respectively. The value of R_1 is positive when dent partially flattens the pipe, in such case, the curvature of the pipe surface in the transverse plane is in the same direction as the original surface radius of curvature. Otherwise, if the dent is reentrant, value of R_1 is negative. Value of R_2 is generally negative.

Noronha et al. (2005) identified that equations provided by 2003 edition of ASME B31.8 overestimates the longitudinal and circumferential bending strain by a factor of two. The latest edition of ASME B31.8 (2007) acknowledges this correction and incorporated the correction factor suggested by Noronha et al. (2005). The corrected equations for the calculation of circumferential and longitudinal bending strain are as follows.

1. Bending strain in circumferential direction

$$\varepsilon_1 = \frac{t}{2} \left(\frac{1}{R_0} - \frac{1}{R_1} \right) \quad (7.1a)$$

2. Bending strain in longitudinal direction

$$\varepsilon_2 = -\left(\frac{t}{2}\right) \left(\frac{1}{R_2}\right) \quad (7.2a)$$

The strain components are then combined by assuming that each of the components occurs coincidentally at dent apex. Both editions of ASME B 31.8 assume that the membrane strain in the circumferential direction is negligible (Noronha et al 2010). All of the strain components are combined according to the following equations to calculate the total/effective strain acting on the inside and outside pipe surfaces and these two strain are denoted by ε_i and ε_o respectively.

$$\varepsilon_i = \sqrt{\varepsilon_1^2 - \varepsilon_1(\varepsilon_2 + \varepsilon_3) + (\varepsilon_2 + \varepsilon_3)^2} \quad (7.4)$$

$$\varepsilon_o = \sqrt{\varepsilon_1^2 + \varepsilon_1(-\varepsilon_2 + \varepsilon_3) + (-\varepsilon_2 + \varepsilon_3)^2} \quad (7.5)$$

The dent is considered acceptable when the larger of the values ε_i and ε_o is lower than the allowable strain limits of 6% strain. It should again be noted that, membrane strain in circumferential direction (ε_4) is ignored in the total/effective strain calculation.

7.4 Finite Element Analysis

A series of non linear finite element analysis (FEA) was performed using ABAQUS (SIMULIA 2008) to verify the assumptions and equations presented in ASME B31.8 (ASME 2007). The analysis was performed using the finite element (FE) models developed using ABAQUS and validated with to a large number test data as described

earlier in Chapters 5 and 6. Influence of various parameters on the distributions of strain in the dented region of a 274 mm nominal outside diameter (OD) pipe with 8.2 mm wall thickness was studied. Hence, the diameter-to-thickness ratio of the pipe was ~ 34 . The actual yield strength of the pipe material was found to be 400 MPa. The different parameters used in this study were

Dent depth: 3%, 6%, 9%, and 12% of pipes outer nominal diameter

Internal pressure during indentation: 0%, 25%, 45%, and 65% of the yield pressure

Shape of indenter: spherical and rectangular

Table 1 shows the description of the FE models and various parameters and their ranges used to study their effect on the distributions of strain in the dented region. Name of a FE model is chosen such that it describes most important attributes of the specimen and this was discussed in chapter 6.

7.5. Review of ASME B31.8 Equations and Assumptions

ASME B31.8 (ASME-2007) provides relationships for calculating bending strain in the circumferential and longitudinal directions and membrane strain in the longitudinal direction. It does not provide any relationship for calculating membrane strain in the circumferential direction and this code, in fact, assumes that membrane strain in the circumferential direction is always negligible.

7.5.1 Membrane Strain in Circumferential Direction

Membrane strain, which is uniform through the material thickness, occurs where the pipe wall is stretched or contracted. During indentation of a pipe, both of the bending and elongation and/or contraction of the pipe wall takes place. A series of finite element

analysis was performed as described earlier to determine the extent of elongation and/or contraction occurs due to the formation of a dent in the pipe wall. As shown in Table 7.1, dent of four different depths (3%, 6%, 9% and 12% of the nominal OD) were used in the study. Indenter of two different shapes (spherical and rectangular) was used. The shapes of the dent produced by a spherical indenter found from the test and FEA model are shown in Figure 7.3. The shapes of the dent produced by a rectangular indenter found from the test and FEA model are shown in Figure 7.4. Each dent depth was created under four different internal pressures and these were 0%, 25%, 45% and 65% of yield pressure p_y , to evaluate the effect of internal pressure in the membrane strain.

The values of maximum membrane strain in the circumferential direction obtained from the FE analysis are shown in Table 7.2. Figures 7.5(a) and 7.5(b) represent graphically the effect of dent depth and internal pressure on the maximum membrane strain in the circumferential direction for dent created with rectangular indenter. In these figures dent depth is normalized by the nominal outer diameter (D) of the pipe and applied pressure is normalized by yield pressure (p_y) of the pipe. Similar plots for spherical indenter are shown in Figure 7.6 (a) and 7.6 (b). From these figures it is evident that with the increase in dent depth membrane strain in the circumferential direction increases for both dent shapes. It was also observed that, for dents created at a relatively low internal pressure level, the increase in membrane strain with depth, for dent created with spherical indenter was higher as compared to the dent created with rectangular indenter (see Figure 7.5(a), 7.6 (a) and Table 7.3). For example, for an increase in dent depth from 3% to 12% at an internal pressure of $0.25p_y$, an increase in maximum circumferential membrane strain from 0.23% to 6.47% for dent created with rectangular shape indenter was observed

(Figure 7.5 (a)). On the other hand for a similar increase in dent depth at the same internal pressure level the increase in maximum circumferential membrane strain for the dent created with spherical indenter was from 0.74% to 15.2% (Figure 7.6(a)). Similar trend was observed for dents created at internal pressure levels of $0p_y$, and $0.45p_y$ (Table 7.3). For dents created at a high internal pressure level ($0.65p_y$) it was observed that the increase in circumferential membrane strain with depth for dent created with spherical indenter is lower as compared to the dent created with rectangular indenter (Table 7.3). For example for an increase in dent depth from 3% to 12% at an internal pressure of $0.65p_y$, an increase in maximum circumferential membrane strain from 1.18% to 20.06% for dent created with rectangular shape indenter was observed, while under same condition the increase in maximum circumferential membrane was from 1.71% to 17.07% for dent created with a spherical indenter.

The value of maximum membrane strain in circumferential direction at a particular dent depth is also greatly influenced by the level of internal pressure applied during indentation. For example, for the 6% dent depth created with a rectangular indenter, the maximum circumferential membrane strains recorded are 0.07%, 1.19%, 3.27%, and 16.04% for denting under internal pressure level of $0p_y$, $0.25p_y$, $0.45p_y$, $0.65p_y$ respectively (Figure 7.5(b) and Table 7.4). It was also observed that with the increase in dent depth the effect of internal pressure on the tensile membrane strain in circumferential direction has increased significantly (Figure 7.5(b)). For example for a dent depth of 9% created with a rectangular indenter, maximum circumferential membrane strain recorded are 0.73%, 4.45%, 8.94%, and 18.4% for denting under internal pressure level of $0p_y$, $0.25p_y$, $0.45p_y$, $0.65p_y$ respectively (Figure 7.5(b) and Table

7.4). The similar trend was also observed in dent created with spherical indenter (Figure 7.6(b) and Table 7.4).

From the comparison of both shapes of the dent, it can be observed that for a particular dent depth, the effect of internal pressure on the circumferential membrane strain is higher in case of dent created with rectangular indenter as compared to dent created with spherical indenter (Table 7.4). For example in case of rectangular indenter for a dent of depth 6% the increase in membrane strain was from 0.07% to 16.4% for an increase internal pressure from $0p_y$ to $0.65p_y$. On the hand in case of spherical indenter for a dent of same depth the increase in membrane strain was from 3.27% to 9.62% for the same amount of increase in internal pressure (Table 7.4).

From the analyses, it can be observed that for a very shallow dent (3% dent depth) membrane strain in the circumferential direction is not significant and hence it may be neglected as recommended in ASME B31.8 (ASME 2007). Also for dents introduced in the pipe wall with a rectangular indenter at zero internal pressure, membrane in the circumferential direction is low for dent depths up to 6% and hence, in this case the effect of membrane strain in circumferential direction can possibly be ignored as well. However, in all other cases, the value of maximum membrane strain in circumferential direction is very high and hence, effect of circumferential membrane strain should not be ignores while computing the total/effective strains (Equations 7.4 and 7.5)

Again it should be taken into consideration that the chance of a dent formation in an operating pipeline, while the pipeline is in a state of zero internal pressure is very unlikely. This is possible only if dent is created during the transportation or fabrication

of the pipe or during construction or the pipeline is in shut-down condition. The most likely scenario is formation of a dent in the pipeline under operating pressure, which could be in the range of $0.2p_y$ to $0.8p_y$. From Tables 7.3 and 7.4, and Figures 7.5(a), 7.5 (b), 7.6 (a) and 7.6 (b) it is obvious that the value of membrane strain in circumferential direction is very high if dent develops under operating condition. This study shows that in that case, effect of membrane strain in circumferential direction cannot be neglected.

As mentioned earlier, ASME B31.8 (ASME 2007) does not provide any guideline for calculating membrane strain in circumferential direction and it assumes that the value of membrane strain in circumferential direction is negligible. It provides relationships for calculating effective/total strain (Equations 7.4 and 7.5) in the dented region without considering the effect of circumferential membrane strain. The current study found that membrane strain in the circumferential direction is rather substantial. Therefore the assumption of membrane strain in circumferential direction being negligible is not justified. Therefore, the effective/total strain calculated without incorporating circumferential membrane strain components will result in underestimation of effective strains in the dent.

7.5.2 Membrane Strain in Longitudinal Direction

ASME B 31.8 (ASME 2007) provides the equation (Equation 7.3) for calculating membrane strain in the longitudinal direction as a function of dent depth and dent length. It does not consider the effect of other parameters such as internal pressure. However, the results of finite element analysis show that for a dent with same depth and created with same indenter, the value of longitudinal membrane strain is highly influenced by the level

of internal pressure. Figure 7.7 shows the effect of internal pressure on the longitudinal membrane strain for a dent created by the rectangular indenter and Figure 7.8 shows the effect of internal pressure for dent created with spherical indenter. For example for a 6% dent depth, for an increase in internal pressure from $0p_y$ to $0.65p_y$, an increase in longitudinal membrane strain from 0.46% to 21.64% was observed for rectangular indenter (Figure 7.7 and Table 7.5), and for spherical indenter the increase in longitudinal membrane strain was from 4.90% to 10.86% (Figure 7.8 and Table 7.5). Similar trend was observed for other cases except for a very shallow dent of depth 3% (Table 7.5). Hence it can be concluded that the determination of longitudinal membrane strain based only on dent depth and dent length without considering internal pressure level is unrealistic.

7.5.3 Review of the ASME Equations for Calculating Effective Strain

ASME B31.8 (ASME 2007) code requires that after calculation of all of the strain components according to the Equations 7.1, 7.2 and 7.3, these strain values need to be combined according to Equations 7.4 and 7.5, by assuming that all of the strain components are acting simultaneously at the dent apex (Rosenfeld et al. 1998). It seems that these equations were recommended based on the original equations suggested by the Rosenfeld et al (1998). However the ASME equations appear in different format. Following are the equations suggested by Rosenfeld et al. (1998) for calculating the total/effective strain on the outer and inner surfaces of the pipe wall at the dent.

$$\varepsilon_i = \sqrt{\varepsilon_{ci}^2 - \varepsilon_{ct}\varepsilon_{xi} + \varepsilon_{xi}^2} \quad (7.6)$$

$$\varepsilon_o = \sqrt{\varepsilon_{co}^2 - \varepsilon_{co}\varepsilon_{xo} + \varepsilon_{xo}^2} \quad (7.7)$$

Here ε_{co} and ε_{ci} are net circumferential strains on the outside and inside surfaces respectively, and, ε_{xo} and ε_{xi} are the net longitudinal strain in the outside and inside surfaces respectively. Net strain is the algebraic summation of all the strain components acting on a particular direction (either circumferential or longitudinal) of the dent. Both Rosenfeld et al. (1998) and ASME B31.8 (ASME 2007) assumes that the membrane strain in circumferential direction is negligible, and hence so net strain at the inside pipe surface in circumferential and longitudinal direction are as follows

$$\varepsilon_{ci} = \varepsilon_1 \quad (7.8)$$

$$\varepsilon_{xi} = \varepsilon_2 + \varepsilon_3 \quad (7.9)$$

Equation 7.4 is obtained when these values are substituted in Equation 7.6. As discussed earlier bending strain in the pipe wall changes linearly from outer surface to inner surface. Hence, the value of bending strain in outer pipe surface will be exactly same as inner surface, with the difference in sign. Therefore, net strain at the outside pipe surface in circumferential and longitudinal directions are as follows.

$$\varepsilon_{co} = -\varepsilon_1 \quad (7.10)$$

$$\varepsilon_{xo} = -\varepsilon_2 + \varepsilon_3 \quad (7.11)$$

Equation 7.5 is obtained when these values are substituted in Equation 7.7.

7.5.4 Incorporation of Circumferential Membrane Strain

This study shows that membrane strains in circumferential direction can be significant depending on dent shape and internal pressure during indentation. Circumferential membrane strain component needs to be incorporated into the equations for calculating effective strains in inner and outer pipe surfaces. Circumferential membrane strain component can be denoted as ε_4 . As a result the equations for calculation of net strain in inside and outside pipe surface, in circumferential direction will be as follows:

$$\varepsilon_{ci} = \varepsilon_1 + \varepsilon_4 \quad (7.12)$$

$$\varepsilon_{co} = -\varepsilon_1 + \varepsilon_4 \quad (7.13)$$

Substitution of these values along with the values for net strain in longitudinal direction from Equations 7.9 and 7.11, into the Equations 7.7 and 7.8 the following relationships are developed and these can be used for calculation of the effective/total strain in inside and outside pipe surfaces accurately.

Effective/total strain at inner pipe surface

$$\varepsilon_i = \sqrt{(\varepsilon_1 + \varepsilon_4)^2 - (\varepsilon_1 + \varepsilon_4)(\varepsilon_2 + \varepsilon_3) + (\varepsilon_2 + \varepsilon_3)^2} \quad (7.14)$$

Effective/total strain at outer pipe surface

$$\varepsilon_o = \sqrt{(-\varepsilon_1 + \varepsilon_4)^2 - (-\varepsilon_1 + \varepsilon_4)(-\varepsilon_2 + \varepsilon_3) + (-\varepsilon_2 + \varepsilon_3)^2} \quad (7.15)$$

7.5.5 Comparison between the Effective Strains Calculated Using Different Equations

The different relationships presented in the previous sections for calculating the effective/total strains are compared in this section using results of finite element analysis. Maximum circumferential and longitudinal strain components obtained for dent with different depth and introduced under different internal pressure is shown in Table 7.6.

Table 7.7 compares the effective/total strain at inner and outer surface of the pipe wall; obtained using equations presented in ASME B31.8 (ASME 2007) (Equations 7.4 and 7.5) and modified equations that incorporate circumferential membrane strain component (Equations 7.14 and 7.15). From the results it can be observed that there is a mentionable difference between the effective/total strains calculates using ASME equations and modified equations (Equation 7.14 and 7.15). From the result presented in Table 7.7 it can be observed that in case of inside pipe surface ASME equations underestimated the effective strain, while in case of outer pipe surface ASME equations overestimated the effective strain in the dent.

Figure 7.9 shows the difference between the effective/total strain values at inner pipe surface calculated using ASME equation (Equation 4) and modified equation (Equation 14) for a dent created with a rectangular indenter. From the observation of the Figure 7.9 it can be concluded that for a particular dent depth, with the increase in internal pressure the discrepancy between the effective/total strains calculated using Equation 7.4 and Equation 7.14 increases. Figure 7.10 shows the difference between the effective/total strain values at outer pipe surface calculated using ASME equation (Equation 5) and modified equation (Equation 15) for a dent created with a rectangular indenter. From the observation of Figure 7.10 it can be concluded that ASME equation overestimates the effective/total strain component. The discrepancy between the calculations increases with the increase in internal pressure level. Similar trend was observed for the dent created with a spherical indenter (Figure 7.11 and 7.12)

7.6 Conclusions

From the discussions presented in this chapter following conclusions can be drawn.

1. ASME B31.8 (ASME 2007) code neglected the effect of circumferential membrane strain in a dent. This study showed that circumferential membrane strain cannot be neglected.
2. ASME B31.8 (ASME 2007) provides the relationship for estimating the longitudinal membrane strain as a function of dent depth and length and ignores the effect of internal pressure. This study showed that longitudinal membrane strain is significantly influenced by the internal pressure level during indentation.
3. ASME B31.8 (ASME 2007) provides relationships for calculating effective/total strain at the inner and outer surface of dent without considering the effect of circumferential membrane strain. This study showed that the ignorance of circumferential membrane strain results in the underestimation of the effective strain in case of inner surface, while an overestimation of effective strain occurs in case of outer surface.

Table 7.1: Parameters Used for FEA Analysis

FE model	Indenter shape	Dent depth, d/D (%)	Internal pressure p/p _y (%)
SP0D3	Spherical	3	0%
SP0D6		6	
SP0D9		9	
SP0D12		12	
SP25D3		3	25%
SP25D6		6	
SP25D9		9	
SP25D12		12	
SP45D3		3	45%
SP45D6		6	
SP45D9		9	
SP45D12		12	
SP65D3		3	65%
SP65D6		6	
SP65D9		9	
SP65D12		12	
SP80D3		3	80%
SP80D6		6	
SP80D9		9	
SP80D12		12	
RP0D3	Rectangular	3	0%
RP0D6		6	
RP0D9		9	
RP0D12		12	
RP25D3		3	25%
RP25D6		6	
RP25D9		9	
RP25D12		12	
RP45D3		3	45%
RP45D6		6	
RP45D9		9	
RP45D12		12	
RP65D3		3	65%
RP65D6		6	
RP65D9		9	
RP65D12		12	

Table 7.2: Maximum circumferential tensile membrane strain

FE Model	Circumferential membrane strain
SP0D3	0.05%
SP0D6	3.27%
SP0D9	8.84%
SP0D12	11.00%
SP25D3	0.74%
SP25D6	5.25%
SP25D9	12.36%
SP25D12	15.20%
SP45D3	1.56%
SP45D6	7.11%
SP45D9	14.93%
SP45D12	15.10%
SP65D3	1.71%
SP65D6	9.62%
SP65D9	15.43%
SP65D12	17.07%
SP80D3	2.84%
SP80D6	10.88%
SP80D9	15.63%
SP80D12	18.07%
RP0D3	0.11%
RP0D6	0.07%
RP0D9	0.73%
RP0D12	2.45%
RP25D3	0.23%
RP25D6	1.19%
RP25D9	4.45%
RP25D12	6.47%
RP45D3	0.40%
RP45D6	3.27%
RP45D9	8.94%
RP45D12	11.19%
RP65D3	1.18%
RP65D6	16.04%
RP65D9	18.10%
RP65D12	20.06%

Table 7.3: Effect of dent depth and indenter shape on the circumferential membrane strain

Internal pressure p/p_y	Dent depth, d/D (%)	Maximum circumferential membrane strain	
		Rectangular Indenter	Spherical Indenter
0	3	0.11%	0.05%
	6	0.07%	3.27%
	9	0.73%	8.84%
	12	2.45%	11.00%
0.25	3	0.23%	0.74%
	6	1.19%	5.25%
	9	4.45%	12.36%
	12	6.47%	15.20%
0.45	3	0.40%	1.56%
	6	3.27%	7.11%
	9	8.94%	14.93%
	12	11.19%	15.10%
0.65	3	1.18%	1.71%
	6	16.04%	9.62%
	9	18.10%	15.43%
	12	20.06%	17.07%

Table 7.4: Effect of pressure on circumferential membrane strain

Dent depth, d/D (%)	Internal pressure p/p _y	Maximum circumferential membrane strain	
		Rectangular indenter	Spherical indenter
3	0	0.11%	0.05%
	0.25	0.23%	0.74%
	0.45	0.40%	1.56%
	0.65	1.18%	1.71%
6	0	0.07%	3.27%
	0.25	1.19%	5.25%
	0.45	3.27%	7.11%
	0.65	16.04%	9.62%
9	0	0.73%	8.84%
	0.25	4.45%	12.36%
	0.45	8.94%	14.93%
	0.65	18.10%	15.43%
12	0	2.45%	11.00%
	0.25	6.47%	15.20%
	0.45	11.19%	15.10%
	0.65	20.06%	17.07%

Table 7.5: Effect of pressure on longitudinal membrane strain

Dent depth, d/D (%)	Internal pressure p/p _y	Maximum circumferential membrane strain	
		Rectangular indenter	Spherical indenter
3	0	0.27%	1.33%
	0.25	0.23%	2.04%
	0.45	0.18%	2.62%
	0.65	0.26%	2.65%
6	0	0.46%	4.90%
	0.25	2.42%	7.37%
	0.45	4.92%	8.80%
	0.65	21.64%	10.86%
9	0	4.13%	8.48%
	0.25	7.93%	12.18%
	0.45	13.04%	14.83%
	0.65	24.94%	17.11%
12	0	6.66%	9.74%
	0.25	10.59%	14.65%
	0.45	15.99%	18.48%
	0.65	28.47%	22.21%

Table 7.6: Maximum strain components in dent

FE Model	Max. Circ. Bending Strain ε_1	Max. Circ. Membrane Strain ε_4	Max. Long. Bending Strain ε_2	Max Long. Membrane Strain ε_3
RP0D3	8.90%	0.11%	5.27%	0.27%
RP0D6	15.20%	0.07%	9.73%	0.46%
RP0D9	20.03%	0.73%	14.00%	4.13%
RP0D12	22.06%	2.45%	15.97%	6.66%
RP25D3	11.16%	0.23%	6.48%	0.23%
RP25D6	19.29%	1.19%	12.33%	2.42%
RP25D9	24.18%	4.45%	17.64%	7.93%
RP25D12	26.06%	6.47%	19.36%	10.59%
RP45D3	12.56%	0.40%	7.39%	0.18%
RP45D6	22.14%	3.27%	14.80%	4.92%
RP45D9	27.52%	8.94%	21.63%	13.04%
RP45D12	30.52%	11.19%	23.29%	15.99%
RP65D3	14.02%	1.18%	8.28%	0.26%
RP65D6	34.25%	16.04%	27.35%	21.64%
RP65D9	37.14%	18.10%	28.66%	24.94%
RP65D12	40.13%	20.06%	29.23%	28.47%
SP0D3	0.05%	0.05%	28%	1%
SP0D6	3.27%	3.27%	29.26%	4.90%
SP0D9	8.84%	8.84%	28.83%	8.48%
SP0D12	11.00%	11.00%	28.80%	9.74%
SP25D3	0.74%	0.74%	30.36%	2.04%
SP25D6	5.25%	5.25%	29.95%	7.37%
SP25D9	12.36%	12.36%	29.48%	12.18%
SP25D12	15.20%	15.20%	29.17%	14.65%
SP45D3	1.56%	1.56%	30.44%	2.62%
SP45D6	7.11%	7.11%	29.98%	8.80%
SP45D9	14.93%	14.93%	29.59%	14.83%
SP45D12	15.10%	15.10%	29.69%	18.48%
SP65D3	1.71%	1.71%	30.16%	2.65%
SP65D6	9.62%	9.62%	29.64%	10.86%
SP65D9	15.43%	15.43%	29.01%	17.11%
SP65D12	17.07%	17.07%	28.63%	22.21%
SP80D3	2.84%	2.84%	30.04%	3.53%
SP80D6	10.88%	10.88%	29.41%	11.56%
SP80D9	15.63%	15.63%	29.27%	19.95%
SP80D12	18.07%	18.07%	29.12%	23.17%

Table 7.7: Effect of Circumferential membrane strain in the calculation of effective strain

FE Model	Equation 7.4	Equation 7.14	% Variation	Equation 7.5	Equation 7.15	% Variation
RP0D3	7.78%	7.87%	1.11%	7.73%	7.64%	-1.17%
RP0D6	13.42%	13.47%	0.42%	13.27%	13.21%	-0.44%
RP0D9	19.15%	19.57%	2.22%	17.34%	16.71%	-3.63%
RP0D12	22.35%	23.63%	5.71%	19.18%	16.99%	-11.43%
RP25D3	9.73%	9.92%	1.92%	0.096855	8.88%	-8.28%
RP25D6	17.47%	18.30%	4.75%	0.167054	14.91%	-10.75%
RP25D9	24.90%	27.23%	9.34%	0.210726	18.29%	-13.21%
RP25D12	28.21%	31.32%	11.04%	0.22971	19.90%	-13.38%
RP45D3	10.95%	11.27%	2.92%	10.92%	9.79%	-10.32%
RP45D6	21.04%	23.10%	9.79%	19.21%	16.64%	-13.39%
RP45D9	31.71%	35.60%	12.28%	24.39%	21.12%	-13.40%
RP45D12	35.72%	40.55%	13.54%	27.60%	23.91%	-13.39%
RP65D3	12.24%	13.20%	7.87%	12.18%	10.70%	-12.17%
RP65D6	43.54%	49.65%	14.06%	31.79%	27.59%	-13.20%
RP65D9	47.56%	54.44%	14.47%	35.43%	30.86%	-12.91%
RP65D12	51.23%	58.98%	15.14%	39.75%	34.75%	-12.58%
SP0D3	29.16%	29.19%	0.09%	27.90%	27.88%	-0.11%
SP0D6	31.97%	33.34%	4.30%	27.10%	25.17%	-7.09%
SP0D9	33.95%	37.61%	10.79%	25.83%	20.29%	-21.47%
SP0D12	34.70%	39.16%	12.87%	25.35%	18.45%	-27.22%
SP25D3	30.80%	31.11%	1.02%	28.61%	28.23%	-1.31%
SP25D6	34.06%	36.07%	5.89%	26.67%	23.42%	-12.20%
SP25D9	37.04%	41.61%	12.34%	25.43%	17.08%	-32.85%
SP25D12	38.53%	43.79%	13.67%	24.74%	13.98%	-43.51%
SP45D3	31.25%	31.90%	2.10%	28.45%	27.65%	-2.80%
SP45D6	35.05%	37.71%	7.58%	26.29%	21.77%	-17.21%
SP45D9	39.04%	44.13%	13.03%	25.05%	14.39%	-42.54%
SP45D12	41.98%	46.19%	10.01%	25.15%	12.64%	-49.73%
SP65D3	30.90%	31.62%	2.30%	28.04%	27.18%	-3.08%
SP65D6	36.15%	39.60%	9.54%	25.49%	19.09%	-25.09%
SP65D9	40.34%	45.17%	11.97%	24.99%	12.65%	-49.37%
SP65D12	44.12%	48.33%	9.53%	25.68%	9.74%	-62.05%
SP80D3	31.27%	32.43%	3.69%	27.46%	26.01%	-5.27%
SP80D6	36.41%	40.29%	10.65%	25.10%	17.84%	-28.95%
SP80D9	42.78%	46.79%	9.37%	24.96%	11.36%	-54.50%
SP80D12	45.32%	49.49%	9.20%	25.59%	8.68%	-66.07%

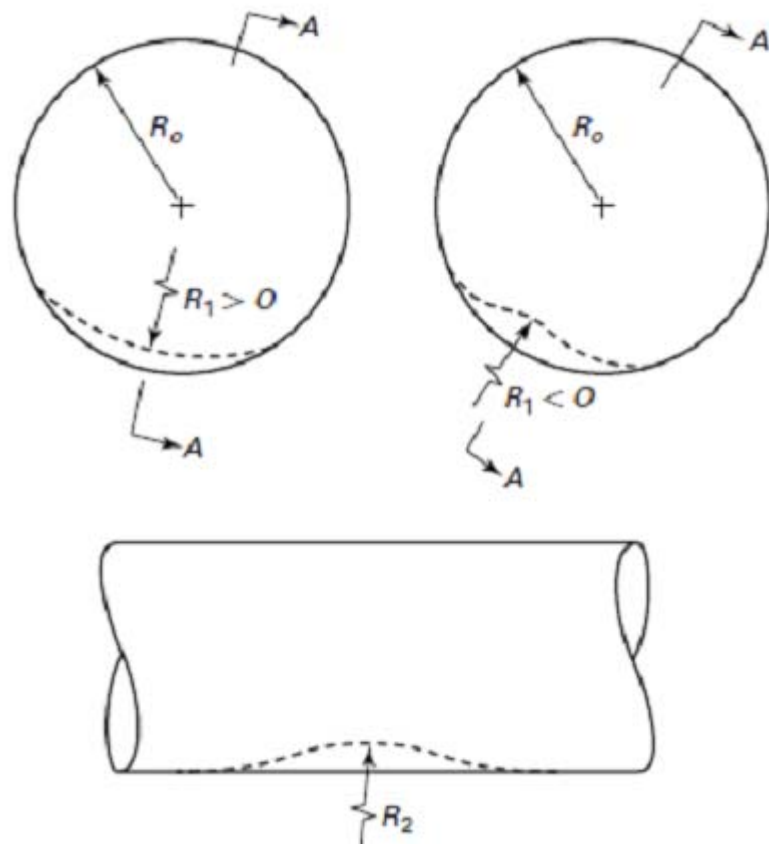


Figure 7.1: Geometric parameter of a dent (ASME B31.8-2007)



Figure 7.2(a): Photograph of a dent created by a spherical indenter

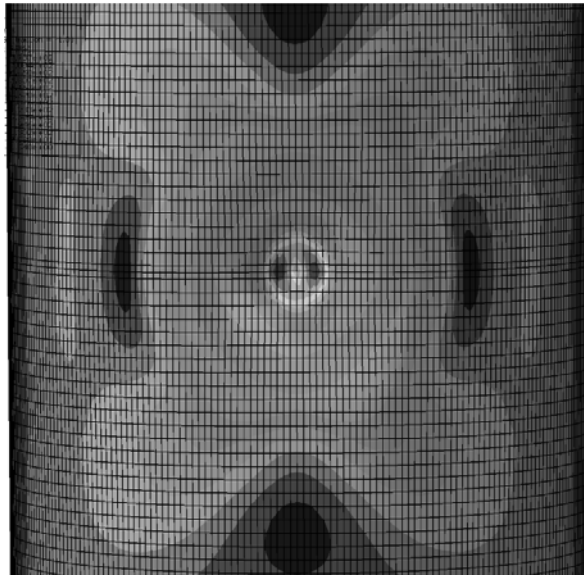


Figure 7.2 (b): FEA simulation of a spherical dent.

Figure 7.2: Experimental and FEA dent shapes simulated by spherical indenter



Figure 7.3(a): Photograph of a dent produced by rectangular indenter

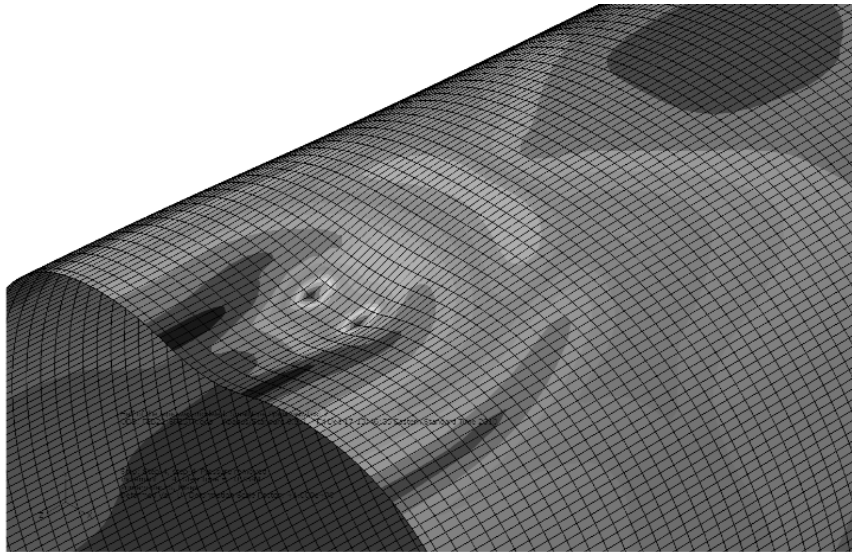


Figure 7.3(b). FEA simulation of a rectangular dent

Figure 7.3: Experimental and FEA dent shapes simulated by rectangular indenter

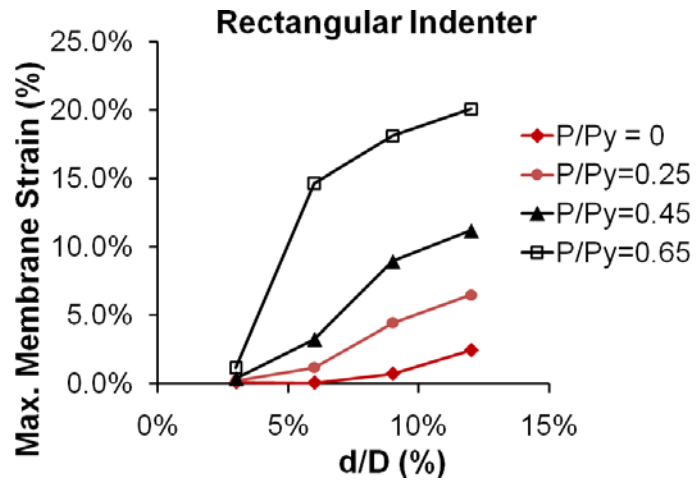


Figure 7.4 (a): Effect of dent depth on circumferential membrane strain for rectangular indenter

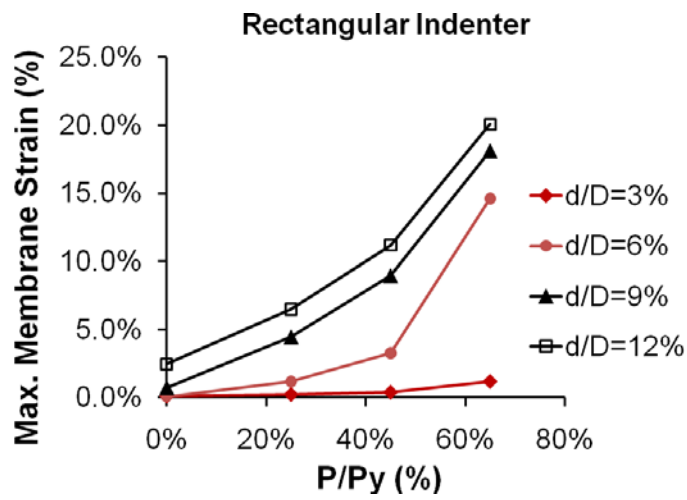


Figure 7.4 (b): Effect of internal pressure on circumferential membrane strain for rectangular indenter

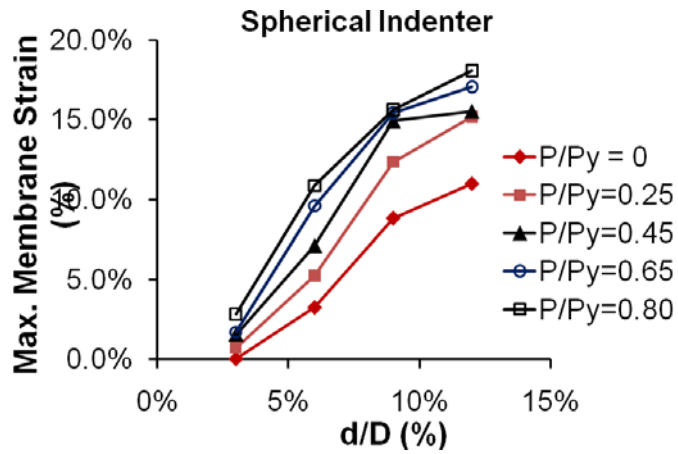


Figure 7.5 (a): Effect of dent depth on circumferential membrane strain for spherical indenter

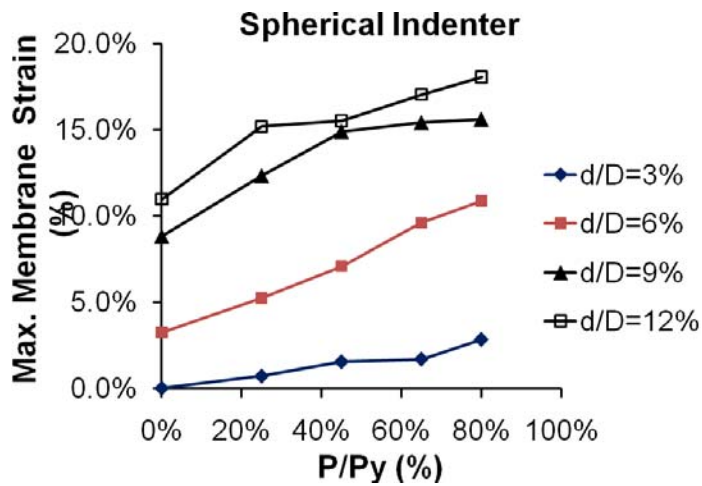


Figure 7.5 (b): Effect of internal pressure on circumferential membrane strain for spherical indenter

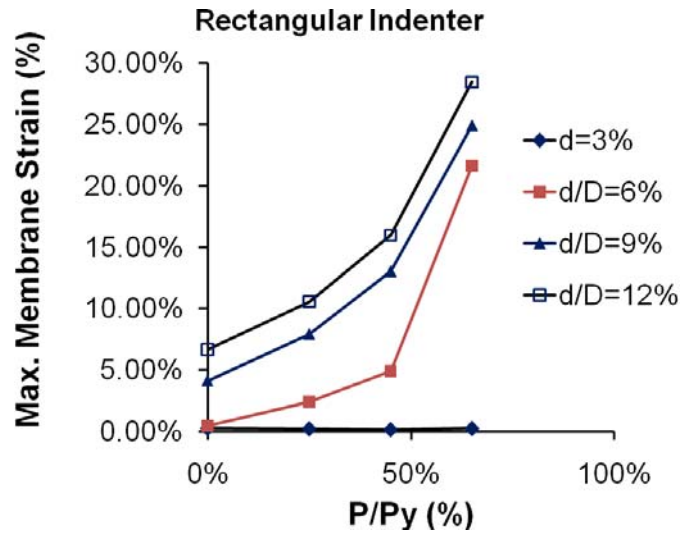


Figure 7.6: Effect of internal pressure on longitudinal membrane strain for rectangular indenter

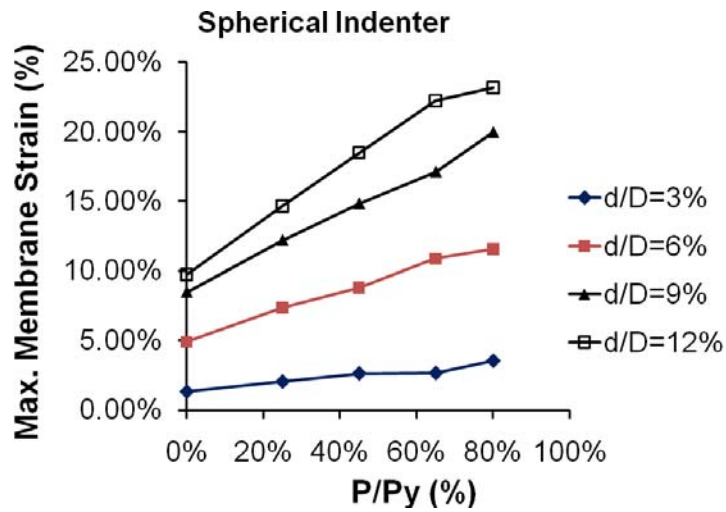
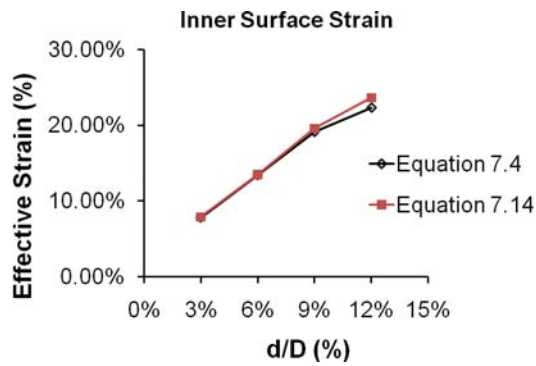
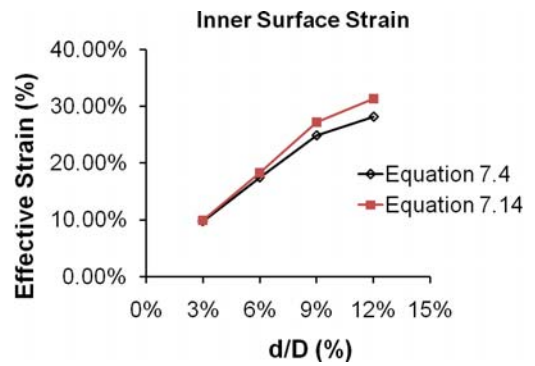


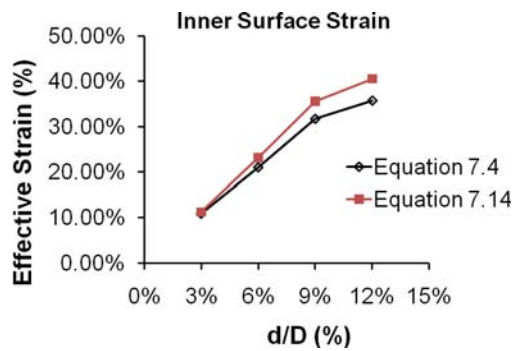
Figure 7.7: Effect of internal pressure on longitudinal membrane strain for spherical indenter.



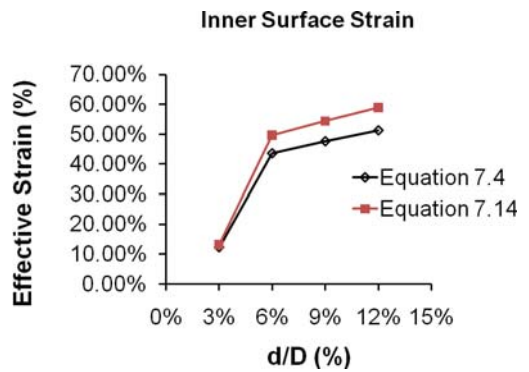
(a) 0% Internal Pressure



(b) 25% Internal Pressure

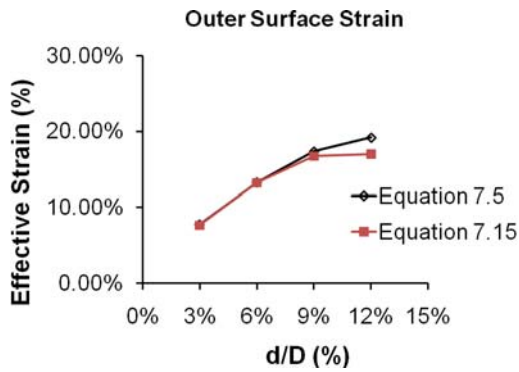


(c) 45% Internal Pressure

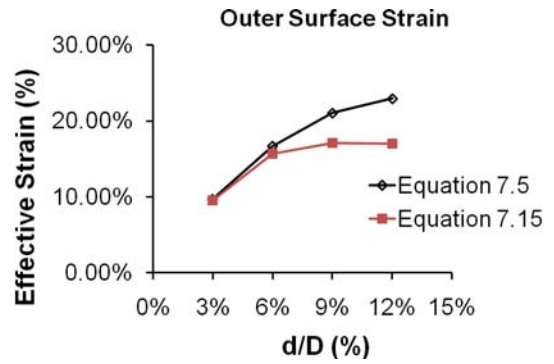


(d) 65% Internal Pressure

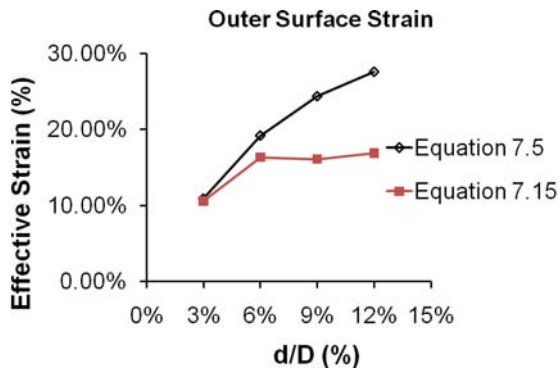
Figure 7.8: Effect of circumferential membrane strain on the inner surface effective strain calculation for dent created with rectangular indenter under different internal pressure level



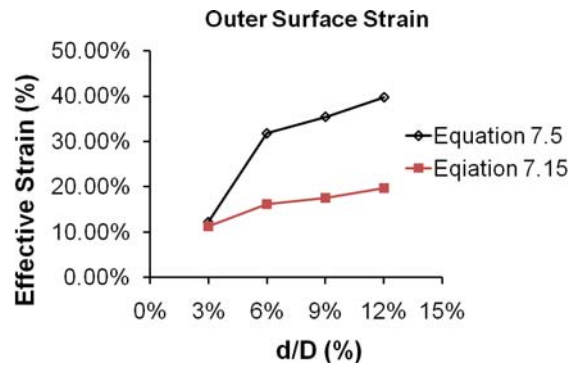
(a) 0% Internal Pressure



(b) 25% Internal Pressure

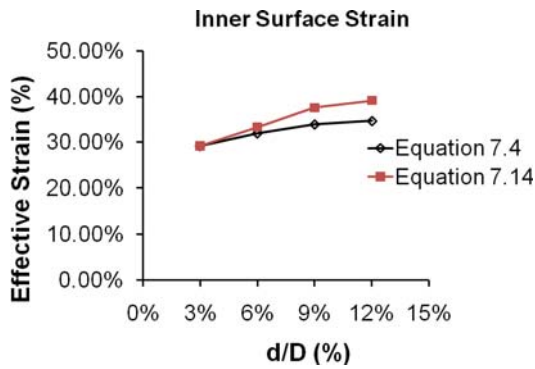


(c) 45% Internal Pressure

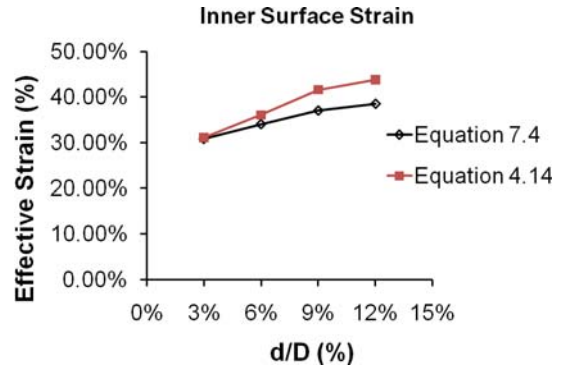


(d) 65% Internal Pressure

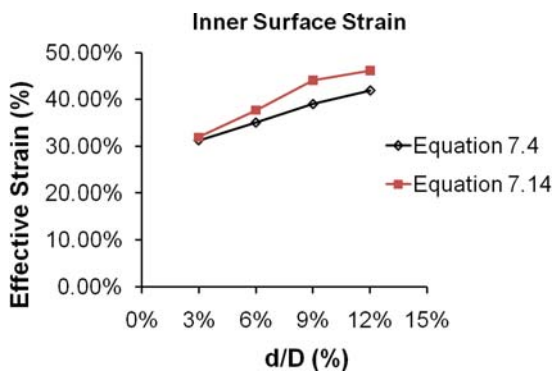
Figure 7.9: Effect of circumferential membrane strain on the outer surface effective strain calculation for dent created with rectangular indenter under different internal pressure level



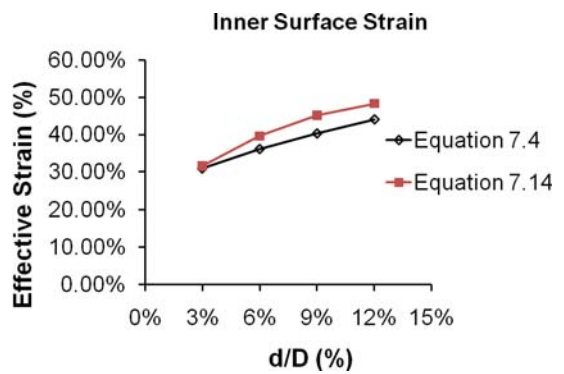
(a) 0% Internal Pressure



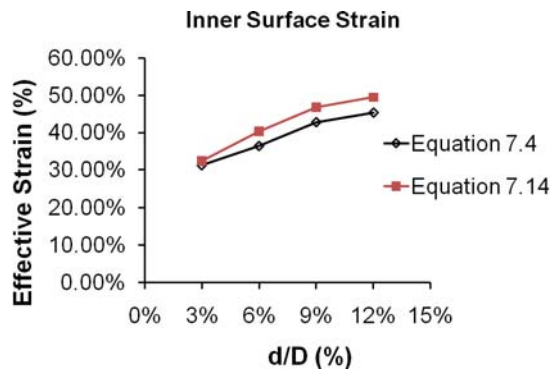
(b) 25% Internal Pressure



(c) 45% Internal Pressure

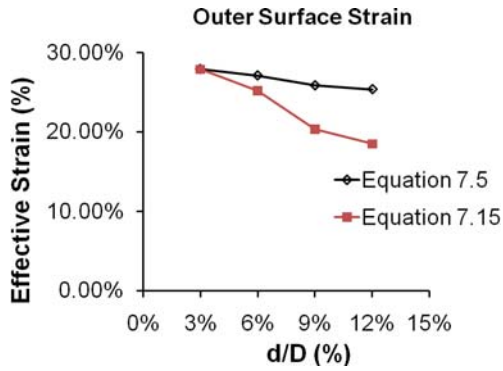


(d) 65% Internal Pressure

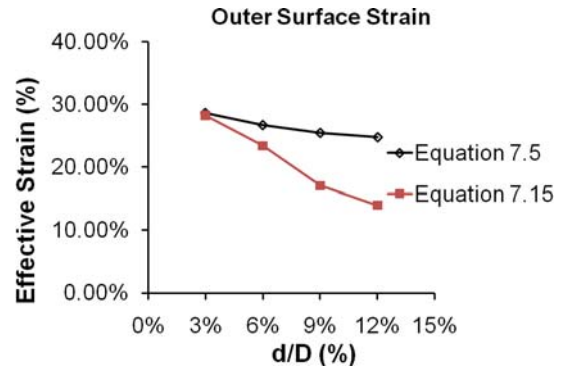


(e) 80% Internal Pressure

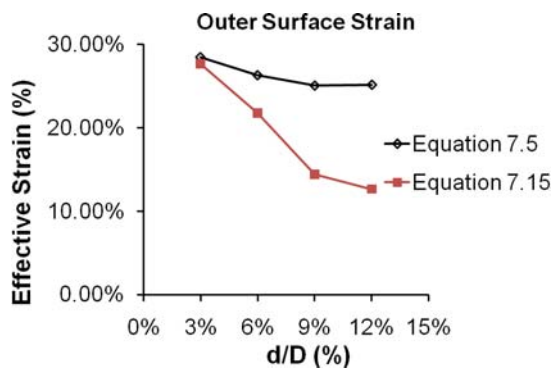
Figure 7.10: Effect of circumferential membrane strain on the inner surface effective strain calculation for dent created with spherical indenter under different internal pressure level



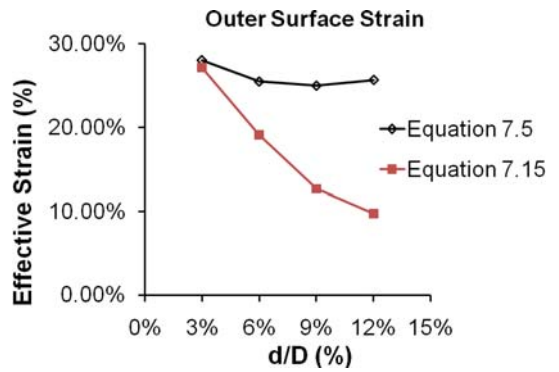
(a) 0% Internal Pressure



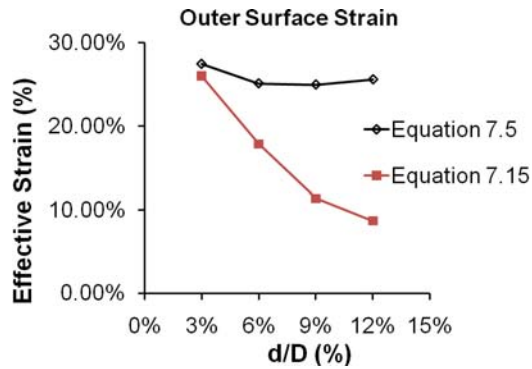
(b) 25% Internal Pressure



(c) 45% Internal Pressure



(d) 65% Internal Pressure



(e) 80% Internal Pressure

Figure 7.11: Effect of circumferential membrane strain on the outer surface effective strain calculation for dent created with spherical indenter under different internal pressure level

CHAPTER 8

SUMMARY, CONCLUSIONS AND RECOMMENDATIONS

8.1 General

This Chapter summarizes the research and findings, provides conclusions on the work completed under the scope of the thesis, and recommends further work that is necessary and can be undertaken in future researches.

8.2 Summary

The project has three primary objectives and these are as follows.

1. To study the overall structural behavior of the pipe under internal pressure and concentrated lateral (denting) loading.
2. To investigate the effect of internal pressure during denting, dent depth, and dent shapes on the strain values in a dent.
3. To review and revisit the ASME strain-based dent evaluation criterion and provide recommendations for improvement of the criterion.

To accomplish these objectives, nine full-scale laboratory tests were completed. In the experimental program effect of dent depth, dent shape, and internal pressure on the overall structural behavior of the pipe under lateral denting load and on the strain distributions around a dent of pipe was studied. However, it is not possible to obtain all the information required for a thorough understanding of structural behavior of dented

pipes from the experimental data. For example, the information about the strains in the region underneath the indenter was impossible to obtain from the tests as the strain gauges under the indenter fail as soon as the load is applied. At the same time, experimental testing is expensive and time consuming. Hence, it is not viable to consider full-scale tests for a wide range of test parameters. Consequently, finite element (FE) models were developed using the commercially available general purpose finite element analysis software code, ABAQUS/Standard version 6.9.1 distributed by SIMULIA (SIMULIA, 2008). The FE models were validated using the laboratory test data. Then, a detailed parametric study using the FE models was performed to investigate the effect of internal pressure during denting, dent depth, and dent shapes on complete strain distributions and the strain values in a dent. These information could not be obtained from the test data. In addition, the dent strain criterion of ASME B 31.8 code (2007) was reviewed using the results of the finite element analysis.

8.3 Conclusions

Based on this study, a number of conclusions are drawn and these are as follows.

1. The load-deformation behavior of pipe subjected to denting load is significantly influenced by the internal pressure. The increase in internal pressure results in a significant increase in the denting load required to produce same amount of deformation.
2. The load-deformation behavior of pipe under lateral denting load is dependent on the size of the contact area between the pipe surface and the indenter. Higher load is required for rectangular indenter which has higher contact area.

3. The shape of the dent has a significant influence on the maximum strain values in a dent. Maximum strain concentration is found in dent created with spherical indenter. Strain concentration for dent created with dome shaped indenter is lowest.
4. Values of maximum tensile strains on the outer surface in the circumferential and longitudinal directions increase with the increase in dent depth. The rate of increase is influenced by the level of internal pressure during indentation. At high internal pressure the rate of increase of maximum tensile strain with the dent depth is higher as compared to that at low internal pressure. This is true for both indenters.
5. Value of maximum compressive strain on the outer surface in the circumferential direction decreases with the increase in dent depth when dent was created with spherical indenter. However, for longitudinal compressive strain no definite pattern was observed. For rectangular indenter, maximum compressive strains in both circumferential and longitudinal directions increase with the increase in dent depth.
6. Values of maximum tensile strain in the circumferential and longitudinal direction increase with the increase in internal pressure during indentation. This is true for both indenters.
7. For spherical indenter, the maximum compressive strain in circumferential direction decreases with the increase in internal pressure and no definite pattern was observed in the maximum compressive strain in the longitudinal direction. However, for rectangular indenter, both maximum compressive strains increase with the increase in internal pressure.
8. ASME B31.8 code (2007) provides the equations for estimating the longitudinal membrane strain as a function of dent depth and dent length. However, these

- equations ignore the effect of internal pressure. This study showed that the membrane strains are significantly influenced by the internal pressure level during indentation.
9. ASME B31.8 code (2007) provides equations for calculating total (critical) strain at the inner and outer surfaces of dent without considering the effect of circumferential membrane strain. This study shows this assumption results in the underestimation of the total strain in the inner surface and overestimation at the outer surface. Hence, this study shows that circumferential membrane strain cannot always be neglected.

8.4 Recommendations

This study provided a number of significant contributions in the area of structural behavior of dented pipes. In order to develop a detailed guideline for the assessment of the dent, more researches are recommended and these recommendations are as follow.

1. Every code and standards other than ASME B31.4 code (2007) considers the dent depth as the only parameter for the assessment of severity and acceptability of dents. Future study is required for the development of a comprehensive dent evaluation criterion based on the strain level in the dent. This criterion should include all the parameters those influence the strain values in a dent.
2. Future works is required on the methods for calculation of circumferential membrane strain.

REFERENCES

Alexander, C.R., Kiefner, J.F., 1997, "Effect of Smooth and Rock Dents on Liquid Petroleum Pipelines," Final Report to the American Petroleum Institute, Stress Engineering Services, Inc., and Kiefner and Associates, Inc. API Publication 1156.

API: American Petroleum Institute, 2008. "API 5L- Specifications for line pipe." Washington DC, USA.

ASME (2006), "B31.4-2006: Pipeline Transportation Systems for Liquid Hydrocarbons and Other Liquids", ASME International, New York, NY, USA

ASME (2007), "B31.8-2007: Gas Transmission Distribution Piping Systems", ASME International, New York, NY, USA

ASTM (2008), "ASTM Specification A 370-94: Standard Testing Method for Tension Testing of Metallic Material."

Baker, M. 2004. Department of Transportation, Office of Pipeline Safety, TTO Number 10, Integrity Management Program- Dent Study. Report: Delivery Number DTRS56-02-D-70036, Final report submitted to the Department of Transportation, USA.

Belonos, P., and Ryan, R.S., 1958, "Dents in Pipe," The Oil and Gas Journal, pp. 155-160

Bjornoy, O. H., Rengard, O., Fredheim, S., and Bruce P., 2000, "Residual Strength of Dented Pipelines, DNV Test Results," Proceedings of the Tenth (2000) international Offshore and Polar engineering Conference, Seattle.

Bolton, B., Semiga, V., Dinovitzer, A. Tiku, S., Alexander, C. 2008, ASME 7th International Pipeline Conference, Calgary, Alberta, Canada.

Cosham, A., and Hopkins, P. 2003. The Effect of Dent in Pipelines-Guidance in the Pipeline Defect Assessment Manual. International Journal of Pressure Vessels and Piping, ELSEVIER, 81: 127-139

CSA (2007), “Z662-07: Oil and Gas Pipeline Systems”, Canadian Standard Association. Mississauga, ON, Canada.

DNV-OS-F101 (2007), “Submarine Pipeline Systems”. Det Norkse Veritas.

Eiber, R.J., Maxey, W.A., Bert, C.W., McClure, G.M., 1981, “The effects of dents on the failure characteristics of linepipe,” Battele ColumbasLaboratories, NG18, Report No.125.

Fowler, J.R., Alexander, C.R., Kovach, P.J, and Connelly, L.M., 1995, “Fatigue Life of Pipelines with Dents and Gouges Subjected to Cyclic Internal Pressure,” in Petroleum Division (Publication) PD69, ASME, pp. 17–35.

Gao, M. McNealy, R., and Krishnamurthy, R., 2008, Strain-Based Models for Dent Assessment- a Review. ASME 7th International Pipeline Conference, Calgary, Alberta, Canada.

Gresnigt, A.M. Karamanos, S.A., Andreadakis, K.P., 2007, “Lateral Loading of Internally Pressurised Steel Pipes,” Journal of Pressure Vessel Technology, ASME, 129: 630-638

Hopkins, P., 2009, “Assessment of Pipeline Defects and Appropriate Repair Methodologies” WTIA/APIA Welded Pipeline Symposium, Sydney, Australia.

Hopkins, P., Jones, D.G., Clyne, A.C., 1989, "The Significance of Dents and Defects in Transmission Pipelines," Proceedings of International Conference of Pipework, Engineering and Operation, London, Paper C376/049.

Hopkins, P., Corder. I., Corbin. P., 1992, "The Resistance of Gas Transmission Pipeline to Mechanical Damage," International Conference on Pipeline Reliability, Calgary, Canada, Paper VIII-3.

Hertz-Clements, S., 2006, "Experimental and Numerical Modeling of Pipeline Denting" International Pipeline Conference, 2996, Calgary, Alberta, Canada, Paper No. IPC2006-10138.

Hopkins, P., 2009, "Assessment of Pipeline Defect and Appropriate Repair Methodologies," WTIA/APIA Welded Pipeline Symposium, Sydney, Australia.

Karamanos, S.A., Andreadakis, K.P., 2006, "Denting of Internally Pressurized Tubes under Lateral Loads," International Journal of Mechanical Science, ELSEVIER, 48:1080-1094.

Keating, P.B. and Hoffmann, R.L., 1997, "Fatigue Behavior of Dented Petroleum Pipelines," Final report, Texas Transportation Institute, Texas A&M University, for Office of Pipeline Safety, U.S. Dept. of Transportation, College Station, TX.

Kiefner, J.F., Kolovich, C., Kolovich, k., 2006, "Pipeline Incidents Caused by Mechanical Damage," Presentation at the Mechanical Damage Technical Workshop, Houston, USA

Kiefner JF, Alexander CR, Fowler JR, “1996, Repair of Dents Containing Minor Scratches,” Ninth Symposium of Line Pipe Research, Houston, Texas, Paper 9.

Lancaster, E.R., and Palmer S.C., 1996, “Strain Concentrations in Pressurized Dented Pipes,” Journal of Process Mechanical Engineering, Part E, pp. 19-27.

Lukasiewicz, S.A., Czyz, J. A., Sun, C., Adeeb, S., 2006, “Calculation of Strains in Dents Based in High Resolution In-Line Caliper Survey,” ASME 6th International Pipeline Conference, Calgary, Alberta, Canada.

Noronha, D.B., Martins, R.R., Jacob, B.P., and Souza, E., 2005, “The Use of B-Splines in the Assessment of Strain Levels Associated with Plain Dents,” Proceedings of the Rio Pipeline Conference & Exposition 2005, Rio de Janeiro, Brazil, Paper No. IBP 1245_05.

Noronha, D.B., Martins, R.R., Jacob, B.P., Souza, E., 2010, “Procedures for the Strain Based Assessment of Pipeline Dents,” International Journal of Pressure Vessels and Piping, ELSEVIER, 87: 254-269.

Ong, L. S., Soh, A. K., and Ong, J. K., 1992, “Experimental and Finite Element Investigation of a Local Dent on a Pressurized Pipe,” Journal of Strain Analysis, 27(3), pp. 177-185.

Rinehart, A.J., Keating, P.B., 2002, Predicting Fatigue Life of Long Dents in Petroleum Pipeline,” 21st International Pipeline Conference of on Offshore Mechanics and Artic Engineering, 2002, Oslo, Norway, Paper No. OMAE 2002-28015.

Roovers, P., Bood, R., Galli, M., Marewski, U., Stainer, M., and Zarea M., 2000, “EPRG methods for assessing the tolerance and resistance of pipeline to external damage,” In:

Denys R, editor. Pipeline Technology Proceedings of the Third International Pipeline Technology Conference, Brugge, Belgium, vol. II. Amsterdam: Elsevier; 2000.pp.405-425

Rosenfeld, M. J., Porter, P.C., Cox., J.A., 1998, "Strain Estimation Using Vector Deformation Tool Data," ASME 2nd International Pipeline Conference, Calgary, Alberta, Canada.

Rosenfeld, M. J., Pepper, J. W., Lewis, K., 2002, "Basis of the New Criteria in ASME B31.8 for Prioritization and Repair of Mechanical Damage," ASME 4th International Pipeline Conference, Calgary, Alberta, Canada.

SIMULIA (2008), "ABAQUS user's manuals," SIMULIA, RISING Sun Mills, Providence, RI, USA.

Wang, K. C., and Smith, E. D., 1982, "The Effect of Mechanical Damage in the Fracture Initiation of Linepipes: Part I- Dents," an internal report submitted to Physical Metallurgical Research laboratories of CANMET, Ottawa, Canada, Report No. ERP/PMRL 82-11(TR)

Yukon Government. 2011. "Frequently Asked Questions," Oil and Gas Information, <http://www.emr.gov.yk.ca/oilandgas/faq.html#pipe1>, updated on November 10, 2009, viewed on 1 April 2011.

APPENDIX

1. Permission from Elsevier for Figure 2.2 and 2.3

ELSEVIER LICENSE TERMS AND CONDITIONS

Apr 29, 2011

This is a License Agreement between Abu Naim Md Rafi ("You") and Elsevier ("Elsevier") provided by Copyright Clearance Center ("CCC"). The license consists of your order details, the terms and conditions provided by Elsevier, and the payment terms and conditions.

All payments must be made in full to CCC. For payment instructions, please see information listed at the bottom of this form.

Supplier	Elsevier Limited The Boulevard, Langford Lane Kidlington, Oxford, OX5 1GB, UK
Registered Company Number	1982084
Customer name	Abu Naim Md Rafi
Customer address	Apt # 302, 3187 Peter St Windsor, ON N9C 1H4
License number	2651681173596

License date	Apr 17, 2011
Licensed content publisher	Elsevier
Licensed content publication	Engineering Failure Analysis
Licensed content title	Assessing mechanical damage in offshore pipelines – Two case studies
Licensed content author	K.A. Macdonald, A. Cosham, C.R. Alexander, P. Hopkins
Licensed content date	December 2007
Licensed content volume number	14
Licensed content issue number	8
Number of pages	13
Start Page	1667
End Page	1679
Type of Use	reuse in a thesis/dissertation
Portion	figures/tables/illustrations
Number of figures/tables/illustrations	2
Format	both print and electronic
Are you the author of this Elsevier article?	No
Will you be translating?	No
Order reference number	
Title of your thesis/dissertation	Structural Behavior of Dented Pipelines
Expected completion date	Apr 2011
Estimated size (number	300

of pages)

Elsevier VAT number	GB 494 6272 12
Permissions price	0.00 USD
VAT/Local Sales Tax	0.0 USD / 0.0 GBP
Total	0.00 USD
Terms and Conditions	

INTRODUCTION

1. The publisher for this copyrighted material is Elsevier. By clicking "accept" in connection with completing this licensing transaction, you agree that the following terms and conditions apply to this transaction (along with the Billing and Payment terms and conditions established by Copyright Clearance Center, Inc. ("CCC"), at the time that you opened your Rightslink account and that are available at any time at <http://myaccount.copyright.com>).

GENERAL TERMS

2. Elsevier hereby grants you permission to reproduce the aforementioned material subject to the terms and conditions indicated.

3. Acknowledgement: If any part of the material to be used (for example, figures) has appeared in our publication with credit or acknowledgement to another source, permission must also be sought from that source. If such permission is not obtained then that material may not be included in your publication/copies. Suitable acknowledgement to the source must be made, either as a footnote or in a reference list at the end of your publication, as

follows:

“Reprinted from Publication title, Vol /edition number, Author(s), Title of article / title of chapter, Pages No., Copyright (Year), with permission from Elsevier [OR APPLICABLE SOCIETY COPYRIGHT OWNER].” Also Lancet special credit - “Reprinted from The Lancet, Vol. number, Author(s), Title of article, Pages No., Copyright (Year), with permission from Elsevier.”

4. Reproduction of this material is confined to the purpose and/or media for which permission is hereby given.

5. Altering/Modifying Material: Not Permitted. However figures and illustrations may be altered/adapted minimally to serve your work. Any other abbreviations, additions, deletions and/or any other alterations shall be made only with prior written authorization of Elsevier Ltd. (Please contact Elsevier at permissions@elsevier.com)

6. If the permission fee for the requested use of our material is waived in this instance, please be advised that your future requests for Elsevier materials may attract a fee.

7. Reservation of Rights: Publisher reserves all rights not specifically granted in the combination of (i) the license details provided by you and accepted in the course of this licensing transaction, (ii) these terms and conditions and (iii) CCC's Billing and Payment terms and conditions.

8. License Contingent Upon Payment: While you may exercise the rights licensed immediately upon issuance of the license at the end of the licensing process for the

transaction, provided that you have disclosed complete and accurate details of your proposed use, no license is finally effective unless and until full payment is received from you (either by publisher or by CCC) as provided in CCC's Billing and Payment terms and conditions. If full payment is not received on a timely basis, then any license preliminarily granted shall be deemed automatically revoked and shall be void as if never granted. Further, in the event that you breach any of these terms and conditions or any of CCC's Billing and Payment terms and conditions, the license is automatically revoked and shall be void as if never granted. Use of materials as described in a revoked license, as well as any use of the materials beyond the scope of an unrevoked license, may constitute copyright infringement and publisher reserves the right to take any and all action to protect its copyright in the materials.

9. Warranties: Publisher makes no representations or warranties with respect to the licensed material.

10. Indemnity: You hereby indemnify and agree to hold harmless publisher and CCC, and their respective officers, directors, employees and agents, from and against any and all claims arising out of your use of the licensed material other than as specifically authorized pursuant to this license.

11. No Transfer of License: This license is personal to you and may not be sublicensed, assigned, or transferred by you to any other person without publisher's written permission.

12. No Amendment Except in Writing: This license may not be amended except in a

writing signed by both parties (or, in the case of publisher, by CCC on publisher's behalf).

13. **Objection to Contrary Terms:** Publisher hereby objects to any terms contained in any purchase order, acknowledgment, check endorsement or other writing prepared by you, which terms are inconsistent with these terms and conditions or CCC's Billing and Payment terms and conditions. These terms and conditions, together with CCC's Billing and Payment terms and conditions (which are incorporated herein), comprise the entire agreement between you and publisher (and CCC) concerning this licensing transaction. In the event of any conflict between your obligations established by these terms and conditions and those established by CCC's Billing and Payment terms and conditions, these terms and conditions shall control.

14. **Revocation:** Elsevier or Copyright Clearance Center may deny the permissions described in this License at their sole discretion, for any reason or no reason, with a full refund payable to you. Notice of such denial will be made using the contact information provided by you. Failure to receive such notice will not alter or invalidate the denial. In no event will Elsevier or Copyright Clearance Center be responsible or liable for any costs, expenses or damage incurred by you as a result of a denial of your permission request, other than a refund of the amount(s) paid by you to Elsevier and/or Copyright Clearance Center for denied permissions.

LIMITED LICENSE

The following terms and conditions apply only to specific license types:

15. **Translation:** This permission is granted for non-exclusive world **English** rights only unless your license was granted for translation rights. If you licensed translation rights you may only translate this content into the languages you requested. A professional translator must perform all translations and reproduce the content word for word preserving the integrity of the article. If this license is to re-use 1 or 2 figures then permission is granted for non-exclusive world rights in all languages.

16. **Website:** The following terms and conditions apply to electronic reserve and author websites:

Electronic reserve: If licensed material is to be posted to website, the web site is to be password-protected and made available only to bona fide students registered on a relevant course if:

This license was made in connection with a course,
This permission is granted for 1 year only. You may obtain a license for future website posting,

All content posted to the web site must maintain the copyright information line on the bottom of each image,

A hyper-text must be included to the Homepage of the journal from which you are licensing at <http://www.sciencedirect.com/science/journal/xxxxx> or the Elsevier homepage for books at <http://www.elsevier.com> , and

Central Storage: This license does not include permission for a scanned version of the material to be stored in a central repository such as that provided by Heron/XanEdu.

17. **Author website** for journals with the following additional clauses:

All content posted to the web site must maintain the copyright information line on the bottom of each image, and the permission granted is limited to the personal version of your paper. You are not allowed to download and post the published electronic version of your article (whether PDF or HTML, proof or final version), nor may you scan the printed edition to create an electronic version,

A hyper-text must be included to the Homepage of the journal from which you are licensing at <http://www.sciencedirect.com/science/journal/xxxxx> , As part of our normal production process, you will receive an e-mail notice when your article appears on Elsevier's online service ScienceDirect (www.sciencedirect.com). That e-mail will include the article's Digital Object Identifier (DOI). This number provides the electronic link to the published article and should be included in the posting of your personal version.

We ask that you wait until you receive this e-mail and have the DOI to do any posting.

Central Storage: This license does not include permission for a scanned version of the material to be stored in a central repository such as that provided by Heron/XanEdu.

18. **Author website** for books with the following additional clauses:

Authors are permitted to place a brief summary of their work online only.

A hyper-text must be included to the Elsevier homepage at <http://www.elsevier.com>

All content posted to the web site must maintain the copyright information line on the bottom of each image

You are not allowed to download and post the published electronic version of your chapter, nor may you scan the printed edition to create an electronic version. Central Storage: This license does not include permission for a scanned version of the material to be stored in a central repository such as that provided by Heron/XanEdu.

19. **Website** (regular and for author): A hyper-text must be included to the Homepage of the journal from which you are licensing at <http://www.sciencedirect.com/science/journal/xxxxx>. or for books to the Elsevier homepage at <http://www.elsevier.com>

20. **Thesis/Dissertation**: If your license is for use in a thesis/dissertation your thesis may be submitted to your institution in either print or electronic form. Should your thesis be published commercially, please reapply for permission. These requirements include permission for the Library and Archives of Canada to supply single copies, on demand, of the complete thesis and include permission for UMI to supply single copies, on demand, of the complete thesis. Should your thesis be published commercially, please reapply for permission.

21. **Other Conditions**:

v1.6

Gratis licenses (referencing \$0 in the Total field) are free. Please retain this printable license for your reference. No payment is required.

If you would like to pay for this license now, please remit this license along with your payment made payable to "COPYRIGHT CLEARANCE CENTER" otherwise you will be invoiced within 48 hours of the license date. Payment should be in the form of a check or money order referencing your account number and this invoice number RLNK10971365. Once you receive your invoice for this order, you may pay your invoice by credit card. Please follow instructions provided at that time.

Make Payment To:
Copyright Clearance Center
Dept 001
P.O. Box 843006
Boston, MA 02284-3006

For suggestions or comments regarding this order, contact Rightslink Customer Support: customercare@copyright.com or +1-877-622-5543 (toll free in the US) or +1-978-646-2777.

2. Permission from Elsevier for Figure 2.7

**ELSEVIER LICENSE
TERMS AND CONDITIONS**

Apr 29, 2011

This is a License Agreement between Abu Naim Md Rafi ("You") and Elsevier ("Elsevier") provided by Copyright Clearance Center ("CCC"). The license consists of your order details, the terms and conditions provided by Elsevier, and the payment terms and conditions.

All payments must be made in full to CCC. For payment instructions, please see information listed at the bottom of this form.

Supplier	Elsevier Limited The Boulevard, Langford Lane Kidlington, Oxford, OX5 1GB, UK
Registered Company Number	1982084
Customer name	Abu Naim Md Rafi
Customer address	Apt # 302, 3187 Peter St Windsor, ON N9C 1H4
License number	2651690124127
License date	Apr 17, 2011
Licensed content publisher	Elsevier
Licensed content publication	International Journal of Pressure Vessels and Piping
Licensed content title	Procedures for the strain based assessment of pipeline dents

Licensed content author	Dauro Braga Noronha Jr., Ricardo Rodrigues Martins, Breno Pinheiro Jacob, Eduardo de Souza
Licensed content date	May 2010
Licensed content volume number	87
Licensed content issue number	5
Number of pages	12
Start Page	254
End Page	265
Type of Use	reuse in a thesis/dissertation
Intended publisher of new work	other
Portion	figures/tables/illustrations
Number of figures/tables/illustrations	1
Format	both print and electronic
Are you the author of this Elsevier article?	No
Will you be translating?	No
Order reference number	
Title of your thesis/dissertation	Structural Behavior of Dented Pipelines
Expected completion date	Apr 2011
Estimated size (number of pages)	300
Elsevier VAT number	GB 494 6272 12
Permissions price	0.00 USD
VAT/Local Sales Tax	0.0 USD / 0.0 GBP

Total 0.00 USD

Terms and Conditions

INTRODUCTION

1. The publisher for this copyrighted material is Elsevier. By clicking "accept" in connection with completing this licensing transaction, you agree that the following terms and conditions apply to this transaction (along with the Billing and Payment terms and conditions established by Copyright Clearance Center, Inc. ("CCC"), at the time that you opened your Rightslink account and that are available at any time at <http://myaccount.copyright.com>).

GENERAL TERMS

2. Elsevier hereby grants you permission to reproduce the aforementioned material subject to the terms and conditions indicated.

3. Acknowledgement: If any part of the material to be used (for example, figures) has appeared in our publication with credit or acknowledgement to another source, permission must also be sought from that source. If such permission is not obtained then that material may not be included in your publication/copies. Suitable acknowledgement to the source must be made, either as a footnote or in a reference list at the end of your publication, as follows:

“Reprinted from Publication title, Vol /edition number, Author(s), Title of article / title of chapter, Pages No., Copyright (Year), with permission from Elsevier [OR APPLICABLE

SOCIETY COPYRIGHT OWNER].” Also Lancet special credit - “Reprinted from The Lancet, Vol. number, Author(s), Title of article, Pages No., Copyright (Year), with permission from Elsevier.”

4. Reproduction of this material is confined to the purpose and/or media for which permission is hereby given.

5. Altering/Modifying Material: Not Permitted. However figures and illustrations may be altered/adapted minimally to serve your work. Any other abbreviations, additions, deletions and/or any other alterations shall be made only with prior written authorization of Elsevier Ltd. (Please contact Elsevier at permissions@elsevier.com)

6. If the permission fee for the requested use of our material is waived in this instance, please be advised that your future requests for Elsevier materials may attract a fee.

7. Reservation of Rights: Publisher reserves all rights not specifically granted in the combination of (i) the license details provided by you and accepted in the course of this licensing transaction, (ii) these terms and conditions and (iii) CCC's Billing and Payment terms and conditions.

8. License Contingent Upon Payment: While you may exercise the rights licensed immediately upon issuance of the license at the end of the licensing process for the transaction, provided that you have disclosed complete and accurate details of your proposed use, no license is finally effective unless and until full payment is received from you (either by publisher or by CCC) as provided in CCC's Billing and Payment terms and

conditions. If full payment is not received on a timely basis, then any license preliminarily granted shall be deemed automatically revoked and shall be void as if never granted. Further, in the event that you breach any of these terms and conditions or any of CCC's Billing and Payment terms and conditions, the license is automatically revoked and shall be void as if never granted. Use of materials as described in a revoked license, as well as any use of the materials beyond the scope of an unrevoked license, may constitute copyright infringement and publisher reserves the right to take any and all action to protect its copyright in the materials.

9. Warranties: Publisher makes no representations or warranties with respect to the licensed material.

10. Indemnity: You hereby indemnify and agree to hold harmless publisher and CCC, and their respective officers, directors, employees and agents, from and against any and all claims arising out of your use of the licensed material other than as specifically authorized pursuant to this license.

11. No Transfer of License: This license is personal to you and may not be sublicensed, assigned, or transferred by you to any other person without publisher's written permission.

12. No Amendment Except in Writing: This license may not be amended except in a writing signed by both parties (or, in the case of publisher, by CCC on publisher's behalf).

13. Objection to Contrary Terms: Publisher hereby objects to any terms contained in any purchase order, acknowledgment, check endorsement or other writing prepared by you,

which terms are inconsistent with these terms and conditions or CCC's Billing and Payment terms and conditions. These terms and conditions, together with CCC's Billing and Payment terms and conditions (which are incorporated herein), comprise the entire agreement between you and publisher (and CCC) concerning this licensing transaction. In the event of any conflict between your obligations established by these terms and conditions and those established by CCC's Billing and Payment terms and conditions, these terms and conditions shall control.

14. **Revocation:** Elsevier or Copyright Clearance Center may deny the permissions described in this License at their sole discretion, for any reason or no reason, with a full refund payable to you. Notice of such denial will be made using the contact information provided by you. Failure to receive such notice will not alter or invalidate the denial. In no event will Elsevier or Copyright Clearance Center be responsible or liable for any costs, expenses or damage incurred by you as a result of a denial of your permission request, other than a refund of the amount(s) paid by you to Elsevier and/or Copyright Clearance Center for denied permissions.

LIMITED LICENSE

The following terms and conditions apply only to specific license types:

15. **Translation:** This permission is granted for non-exclusive world **English** rights only unless your license was granted for translation rights. If you licensed translation rights you may only translate this content into the languages you requested. A professional translator must perform all translations and reproduce the content word for word preserving the

integrity of the article. If this license is to re-use 1 or 2 figures then permission is granted for non-exclusive world rights in all languages.

16. **Website:** The following terms and conditions apply to electronic reserve and author websites:

Electronic reserve: If licensed material is to be posted to website, the web site is to be password-protected and made available only to bona fide students registered on a relevant course if:

This license was made in connection with a course,
This permission is granted for 1 year only. You may obtain a license for future website posting,

All content posted to the web site must maintain the copyright information line on the bottom of each image,

A hyper-text must be included to the Homepage of the journal from which you are licensing at <http://www.sciencedirect.com/science/journal/xxxxx> or the Elsevier homepage for books at <http://www.elsevier.com> , and

Central Storage: This license does not include permission for a scanned version of the material to be stored in a central repository such as that provided by Heron/XanEdu.

17. **Author website** for journals with the following additional clauses:

All content posted to the web site must maintain the copyright information line on the bottom of each image, and the permission granted is limited to the personal version of your paper. You are not allowed

to download and post the published electronic version of your article (whether PDF or HTML, proof or final version), nor may you scan the printed edition to create an electronic version,

A hyper-text must be included to the Homepage of the journal from which you are licensing at <http://www.sciencedirect.com/science/journal/xxxxx> , As part of our normal production process, you will receive an e-mail notice when your article appears on Elsevier's online service ScienceDirect (www.sciencedirect.com). That e-mail will include the article's Digital Object Identifier (DOI). This number provides the electronic link to the published article and should be included in the posting of your personal version. We ask that you wait until you receive this e-mail and have the DOI to do any posting.

Central Storage: This license does not include permission for a scanned version of the material to be stored in a central repository such as that provided by Heron/XanEdu.

18. **Author website** for books with the following additional clauses:
Authors are permitted to place a brief summary of their work online only.
A hyper-text must be included to the Elsevier homepage at <http://www.elsevier.com>

All content posted to the web site must maintain the copyright information line on the bottom of each image

You are not allowed to download and post the published electronic version of your chapter, nor may you scan the printed edition to create an electronic version.
Central Storage: This license does not include permission for a scanned version of the material to be stored in a central repository such as that provided by Heron/XanEdu.

19. **Website** (regular and for author): A hyper-text must be included to the Homepage of the journal from which you are licensing at <http://www.sciencedirect.com/science/journal/xxxxx>. or for books to the Elsevier homepage at <http://www.elsevier.com>

20. **Thesis/Dissertation**: If your license is for use in a thesis/dissertation your thesis may be submitted to your institution in either print or electronic form. Should your thesis be published commercially, please reapply for permission. These requirements include permission for the Library and Archives of Canada to supply single copies, on demand, of the complete thesis and include permission for UMI to supply single copies, on demand, of the complete thesis. Should your thesis be published commercially, please reapply for permission.

21. **Other Conditions**:

v1.6

Gratis licenses (referencing \$0 in the Total field) are free. Please retain this printable license for your reference. No payment is required.

If you would like to pay for this license now, please remit this license along with your payment made payable to "COPYRIGHT CLEARANCE CENTER" otherwise you will be invoiced within 48 hours of the license date. Payment should be in the form of a check or money order referencing your account number and this invoice number RLNK10971367. Once you receive your invoice for this order, you may pay

your invoice by credit card. Please follow instructions provided at that time.

**Make Payment To:
Copyright Clearance Center
Dept 001
P.O. Box 843006
Boston, MA 02284-3006**

For suggestions or comments regarding this order, contact Rightslink Customer Support: customercare@copyright.com or +1-877-622-5543 (toll free in the US) or +1-978-646-2777.

VITA AUCTORIS

Name: Abu Naim Md Rafi

Place of Birth: Sylhet, Bangladesh

Year of Birth: 1985

Education Bangladesh University of Engineering and Technology (BUET),
Dhaka, Bangladesh, 2004-2009, BSc, Civil Engineering.